MECHANICAL BEHAVIOR OF MULTI-ROW BOLTED CONNECTIONS OF WOVEN FABRIC GFRP STRUCTURAL MEMBERS

by

Mohammad Abdul Kader

September 2015

A Dissertation
Submitted in Fulfillment of the Requirements
for the Degree of Doctor of Philosophy
Graduate School of Engineering
Nagoya University
Nagoya, Japan

To

my wife

and

my daughter

ABSTRACT

Although high strength-to-weight ratio, high stiffness-to-weight ratio, high durability, and corrosion resisting capacity make fiber reinforced polymer (FRP) composite materials extremely attractive to structural engineers, there are some factors that prevent the materials from being widely accepted as a structural material in civil engineering structures, which include a lack of standards and design guidelines, and a lack of experience of designing structures, especially connections, using these materials.

Bearing-type bolted connections are usually used to connect FRP structural members because friction-type bolted connections are difficult to design due to creep of FRP. In a bearing-type multi-row bolted connection, the load does not distribute uniformly among the bolt rows due to the relative displacement of the cover plates to the main plate; therefore, relative stiffness of the cover plates to the main plate is a vital factor of the load distribution. To understand mechanical behavior of a bearing-type multi-row bolted connection of FRP members, experimental and numerical investigations were conducted at Nagoya University. This study is focused on the effect of cover plate stiffness and connection geometry on the load distribution among the bolt rows as well as strength of connections made of woven fabric glass fiber reinforced composite material.

A series of 3D elastic finite element analyses of multi-row bolted connections were performed to determine the effect of cover plate stiffness on the load distribution among the bolt rows. Results showed that the load distribution in bearing-type multi-row bolted connections is significantly affected by the relative stiffness of the cover plate to the main plate. A connection with a higher cover plate stiffness tends to show lower efficiency. For a connection with steel cover plates, to increase the number of bolt rows more than three does not lead to a higher capacity of a connection. The results also indicate that the effect of geometric parameters of a connection on the load distribution is not significant.

In order to evaluate strength of a multi-row bolted connection accurately in a numerical simulation, a progressive damage model of FRP materials was implemented in a commercial finite element analysis software by using a user subroutine. A series of 3D non-linear finite element analyses based on the progressive damage material model were performed to evaluate behavior of multi-row bolted connections after the damage initiation. Based on the results, the effect of cover plate stiffness on the connection strength was examined. Results showed that a connection with FRP cover plates could resist a larger load than a connection with steel cover plates by about 6%, 19%, and 35%, for the two, three, and four-row bolted connections, respectively. In addition, it was found that a multi-row bolted connection with FRP cover plates needs a larger end distance than that with steel cover plates in order to avoid an end shear failure. Although current design codes specify different end distances for single and multi-row bolted connections with FRP cover plates, the same end distance may be required for both single and multi-row bolted connections to avoid the end shear failure.

An experimental program was conducted to understand the behavior of bolted connection. First, a series of material tests were performed to obtain material properties of GFRP laminates with thicknesses of 6, 9, and 12 mm which were used in the connection test. Then, single bolted connections were tested to failure. Three basic failure modes of net-tension, shear, and bearing failures were observed in the single bolted connections. Among the failure modes, only the net-tension failure mode was a catastrophic failure. The connection with bolt axial force that is equivalent to a finger- tight condition had 93% larger bearing strength and 30% larger shear strength than the connection without bolt axial force. The strength decreased by about 26% for the bearing failure and by about 8% for shear failure when the 6-mm steel cover plate was changed to 6-mm GFRP cover plate because cover plates would fail first; therefore, connections with a cover plate thickness half of the main plate may not be appropriate if the bearing failure is a desired mode, and a thicker cover plate may be required. For a single bolted connection with a w/d ratio of 4 and e/d ratio of 4

showed a bearing failure. Therefore, w/d = 4 and e/d = 4 are recommended as minimum requirements for the bearing failure.

A series of multi-row bolted connections were tested to failure. Three basic failure modes of net-tension, shear, and bearing failures were also observed in the multi-row bolted connections. The effect of w/d, p/d, and e/d on the ultimate strength of the connection is significant. The strength is linearly increased with w/d ratio for the case of net-tension failure, and p/d and e/d ratios for the case of shear failure. The net-tension failure switches to the bearing failure when the w/d ratio is changed from 3 to 6 for the two-row bolted connection and from 5 to 9 for three-row bolted connection. The shear failure switches to the bearing failure when the p/d ratio is changed from 3 to 5. The strength is linearly increased with number of bolt rows for the case of bearing failure. The results also showed that ultimate strength is not affected by cover plate stiffness for any failure modes, although the load distribution among the bolt rows is different in the elastic range. A connection with GFRP cover plates having a half of the main plate thickness showed lower ultimate strength than that with a higher stiffness of cover plate, although numerical results showed that the connection with FRP cover plates having a half of the main plate thickness has a more uniform load distribution and can have a larger strength than those with the other cover plates. The difference between the experiment and numerical analysis indicates limitations of the numerical model tha is proposed in this study. One of the limitations is a lack of consideration of the confinement effect in the thickness direction of FRP plates.

The connections that satisfy the minimum requirements of ASCE LRFD Pre-standard failed in either net-tension or shear failure rather than bearing failure. Therefore, the minimum requirement of multi-row bolted connection would be e/d = 4, p/d = 5, and w/d = 6 for two-row and 9 for three-row bolted connection. The ultimate bearing strength is proportional to the number of bolt rows regardless of connection geometries and cover plate types.

Therefore, the ultimate bearing strength of a multi-row bolted connection can be evaluated by multiplying the strength of a single bolted connection by the number of bolt rows.

Simple design equations to evaluate strength of a connection for different failure modes were proposed based on the experimental results. It was proved that the proposed formulae could predict the ultimate strength and failure mode of multi-row bolted connections examined in the experimental program with high accuracy.

ACKNOWLEDGEMENTS

The author wishes to express his deepest sense of gratitude of Associate Prof. Dr. Yasuo Kitane for his guidance, continuous encouragement and invaluable supports and dynamic support throughout the course of this research work. His tireless devotion, unfailing support and dynamic leadership in the pursuit to excellence have earned the author's highest respect. The author will remain ever grateful to him for giving the opportunity to undertake graduate studies under his supervision and inspiring to work hard in research activities.

The author also wishes to express his sincerest thank to Prof. Dr. Yoshito Itoh for valuable suggestions and comments throughout the course of this research work.

The author would like to thank to the member of his dissertation examining committee Prof. Dr. Kazuo Tateishi and Prof. Dr. Hitoshi Nakamura for going through the text of this dissertation carefully and for making enlightening suggestion and comments.

The author thanks to Assistant Prof. Dr. Mikihito HIROHATA for his support and valuable information during the research work.

The author would also like to thank to Mr. Masahiro Myoga, masters student for his valuable help during the experimental work. Without his help, it was difficult to complete the experimental work successfully. My gratitude goes out to Hibi Inc., an FRP manufacture who helped me for the manufacture of the glass fiber reinforced polymer laminates and for the fabrication of connection plates.

The research work has been carried out in the Department of Civil Engineering, Nagoya University, Japan during 2012-2015, on leave from Dhaka University of Engineering and Technology, Gazipur, Bangladesh. The financial support given by the Ministry of Education, Culture, Sports, Science, and Technology (MEXT) of Japan is gratefully appreciated.

Finally I wish to express sincere thanks to my family for their moral support, tolerance and understanding while preparing this dissertation.

TABLE OF CONTENTS

LIST OF FIGURES

LIST OF TABLES

CHAPTER 1 INTRODUCTION

1.1 Background

Nowadays, design of high-performance civil structures is becoming increasingly important in view of its large impact on economics. According to the Civil Engineering Research Foundation (1994), high-performance denotes one or more attributes, such as greater strength, improved durability and easier placement or fabrication, with their implication for reducing life cycle costs.

Construction materials play a vital role in the design of high-performance civil structures. Recently steel and concrete are widely used over the world for the construction of civil structures which are required to carry loads for long periods of time, often in harsh environmental conditions. The materials would be deteriorating with that environment in course of time due to various reasons. The corrosion is the most common cause of deterioration of steel and concrete.

Upon the structural deterioration, a condition of a bridge can be classified as deficient or not deficient. Deficient bridges are in two categories: structurally deficient and functionally obsolete. The number of deficient bridges is the most common indicator of the overall condition of bridges in a country. Figure 1.1 and Figure 1.2 show the bridge condition for the last twenty years in the United State of America. According to the U.S. Department of Transportation, of 607,751 bridges across the country as of December 2013, 63,522 (10.5%) were categorized as structurally deficient and 84,348 (13.9%) were categorized as functionally obsolete, and most of the bridges are constructed of steel and concrete.

The percentage of bridges that are either functionally obsolete or structurally deficient has been decreasing slowly over the last decade as states and cities have increased efforts to prioritize repairs and replacements. The investment backlog of the nation’s bridges is

estimated to be $121 billion, according to the Federal Highway Administration (FHWA). The FHWA estimates that to eliminate the bridge backlog by 2028, the nation would need to invest $20.5 billion annually; however, currently only $12.8 billion is being spent annually on the nation's bridges.

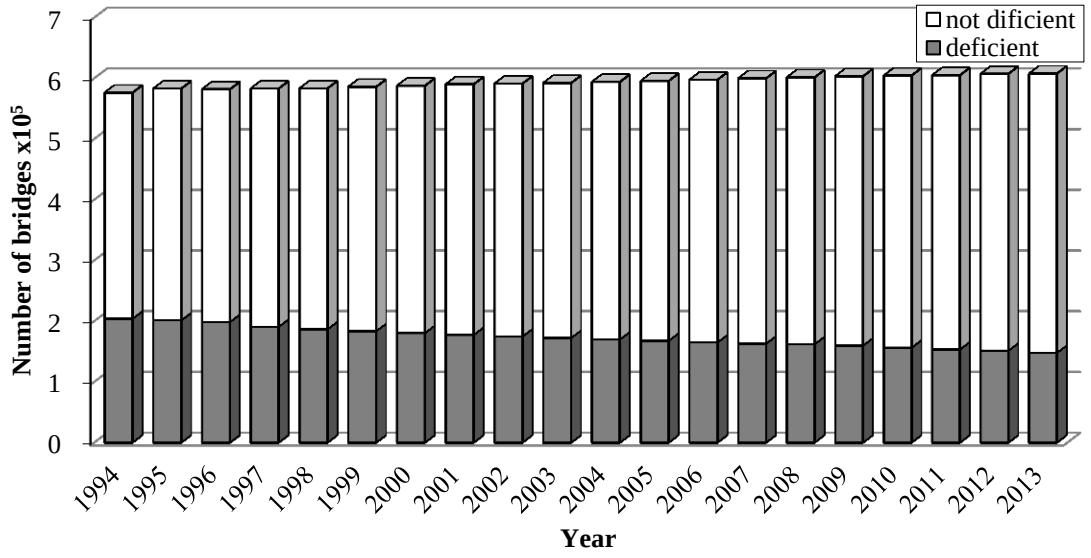

Figure 1.1: Number of deficient bridges in the United States of America (Data source: National Bridge Inventory)

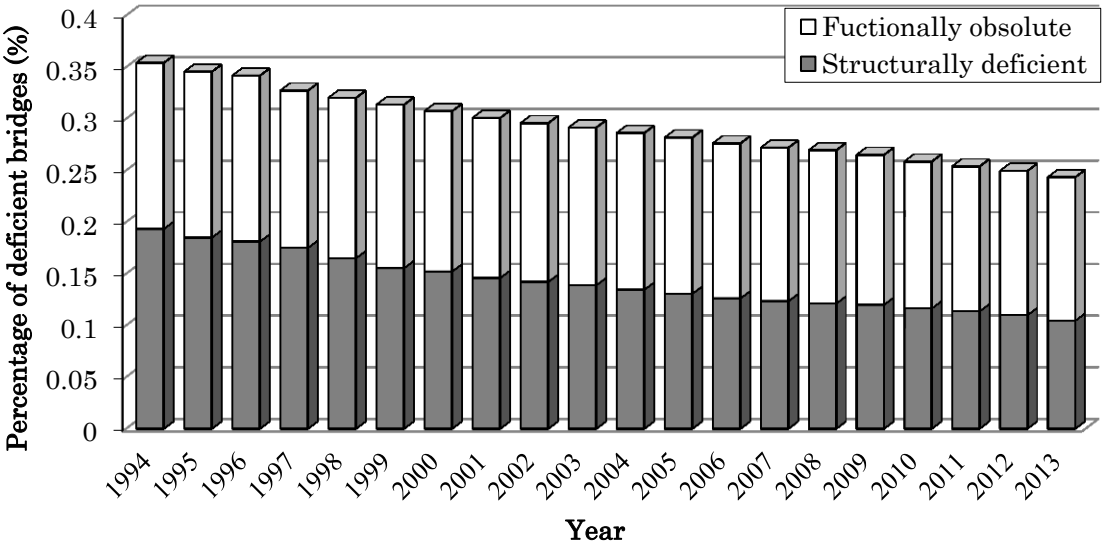

Figure 1.2: Percentage of deficient bridges in the United States of America (Data source: National Bridge Inventory)

In order to prevent the deterioration and reduce the life-cycle cost of a structure, an introduction of new materials may be one of the solutions. Applications of fiber reinforced polymer (FRP) composite materials for a structure in the harsh environment is one of such options. The FRP composite materials do not corrode in the severe environment, and the materials have other advantages in the context of structural applications such as high specific strength and stiffness, light weights, tailored properties, and fatigue resisting capacity.

1.2 Fiber Reinforced Polymer Composite

The development of composite materials represents a milestone in the history of our civilization. Composite materials were first innovated the date back to the ancient Egyptians who used straw to strengthen mud bricks which were used to make strong and durable buildings. They used different rearrangement of straw and wood to achieve superior strength and resistance to thermal expansion as well as to swell. Later, in 1200 AD, the Mongols invented the first composite bow. Using a combination of wood, bamboo, bone, and animal glue, bows were pressed and wrapped with birch bark. These bows were extremely powerful and extremely accurate. The development of modern composite, that is, FRP composite materials started in the early 1940's when glass fiber reinforced polymer (GFRP) were used in radar domes. The FRP composites were rapidly developed and applied during the World War II. During the World War II, there was scarcity of materials, especially in the military applications due to constraint impositions on various nations for crossing boundaries as well as importing and exporting the materials. During this period the fighter planes were the most advanced instruments of war. The lightweight, strong materials have been yet in high demand.

The composite materials consist of two or more constituent materials that differ in shape and chemical composition and are insoluble to each other. Although each constituent maintains its unique material properties and characteristics, they together produce a material having properties which cannot be achieved by each constituent material alone. FRP

composite materials consist of fibers and matrix. The fibers are usually glass, carbon, basalt or aramid, and the matrix is polymers usually epoxy, vinylester or polyester thermosetting plastic, and phenol formaldehyde resins. The fibers are the principal constituent in an FRP composite material, which provide strength and stiffness of the material. On the other hand, the matrix keeps the fibers in the desired location and orientation, transfers load between the fibers, and protects the fibers from the environment.

The most common form of FRP composites are used in structural applications is called a laminate, which is made by stacking a number of thin layers of fibers and matrix and consolidating them into a desired thickness. Fiber orientation in each layer as well as the stacking sequence of various layers in a composite laminate can be controlled to generate a wide range of physical and mechanical properties for the composite laminate. According to Karbhari and Zhao (2000), some of the important advantages of the FRP composites are:

(a) High specific strength and stiffness

(b) Enhanced fatigue life

(c) Corrosion resistance

(d) Controllable thermal properties

(e) Parts integration

(f) Tailored properties

(g) Non-magnetic properties

(h) Lower life-cycle costs

These advantages of FRP composites make suitable structural materials. Therefore, it is extensively used in aerospace, automotive, defense, marine, electronics industries, and sports, kitchen and toiletry products over a few decades. In civil engineering structures, FRP composite members have been gaining their acceptance as structural members due to their attractive properties such as corrosion resistance. FRP may offer solutions to overcome the corrosion problems of steel structures and the deterioration of reinforced concrete members

due to salt. A high strength-to-weight ratio makes them also extremely attractive as a building material for civil engineering applications. Weight reduction could result in enhancement in seismic resistance, increased speed of erection and a dramatic reduction in time for fabrication of large structures. The lightweight structure can be installed handle and installation generally more easily and can greatly reduce the cost of assembly. Further, as in offshore applications, weight savings accrued in the superstructure translate into multiple levels of savings in the supporting and substructure elements.

Structural applications of FRP composite materials can be classified as shown in Figure 1.3. In the civil structures, FRP composite materials are mostly used for rehabilitation of existing structures. The use of FRP composites appears to be an excellent solution. Strengthening and retrofitting of existing structures using externally bonded FRP composites are one of the first applications of FRP in civil engineering. The technique is simple, rapid, and effective. FRP used for strengthening and retrofitting can be in the forms of FRP sheet or strip, depending on their application. Externally bonded FRP composites have also been used for increasing both flexural and shear capacity of concrete elements, including girders, beams and slabs. Therefore, FRP composites are popular materials for repair, strengthening and retrofit of a structure.

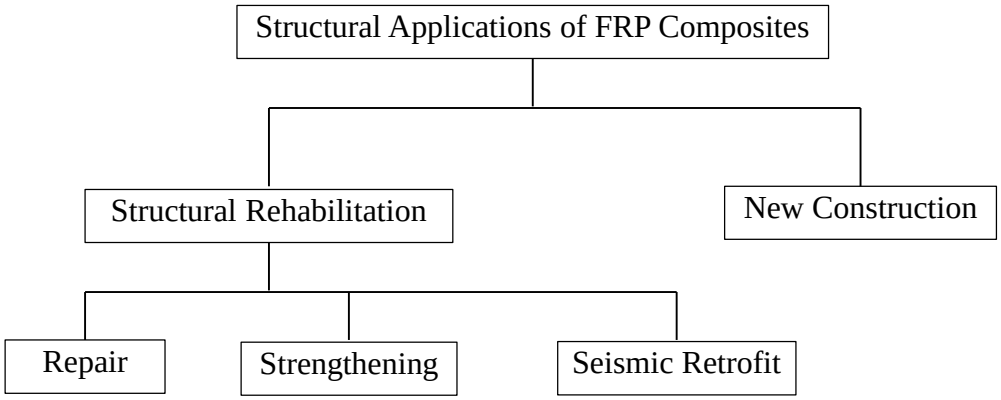

Figure 1.3: Types of structural applications of FRP composites

FRP composites can be used in seismic retrofitting of reinforced concrete bridges in the form of wrapped column. Conventional methods used for seismic retrofit of reinforced concrete columns include the use of steel shells or casings, the use of steel cables wound helically around the columns, and the use of external reinforced concrete section. However, these methods introduce additional stiffness to the structural system due to the isotropic nature of the retrofitting material and, therefore, higher seismic force can be transferred to adjacent elements. In addition, traffic disruption is a major problem during retrofitting operation. With the use of FRP composite, on the other hand, FRP can provide only in the direction hoop stress, hence no additional stiffness. It also causes no or little traffic disruption.

Figure 1.4: Aberfeldy pedestrian bridge, Scotland
(http://www.nce.co.uk/features/nce-40-years/no13-aberfeldy-footbridge/8630564.article)

The FRP composite materials have been used in new constructions due to light weight, good durability, low life cycle costs and easy and rapid installation with short time. The first pedestrian bridge was built by the Israelis in 1975. Many other pedestrian bridges as well as vehicular bridges have been built over the world since then. The construction of FRP bridges

has been increased. The first all-FRP composite pedestrian bridge was opened for public in 1992 in Aberfeldy, Scotland (Figure 1.4). The bridge is a three-span cable-stayed bridge with a 63 m main span and 25 m side spans. The width of the walkway is 2.3 m. Pillars and deck were manufactured by pultruded GFRP sections strengthened with carbon sheets in some areas. The longitudinal girders are supported by transverse beams, which in turn are supported by CFRP cable stays. The Japanese first all-FRP composite pedestrian bridge in Okinawa Prefecture, Japan was opened in 2000 (Figure 1.5). The first vehicular bridge was the Miyun Bridge completed in September 1982 near Beijing, which carries full highway traffic. It has a span of 20.7 m and consists of six hand-laminated glass fiber/polyester sandwich girders, whereas the first application of FRP composites in Japan for road bridge was the Shinmiya Bridge, Ishikawa Prefecture in 1988 and in the USA the first application for road bridge was the Kansas in 1996.

Figure 1.5: FRP pedestrian bridge, Okinawa, Japan (Courtesy: Dr. Itaru Nishizaki)

1.3 Bolted Connection

In typical structures, structural components are connected together. However, the connections between components contribute to an excess weight, may become a source of failure and cause manufacturing problems. Therefore, a designer will avoid using them whenever it is possible. Unfortunately, it is rarely possible to make a structure without connections due to limitations of member size, convenience in manufacture or transportation, and the need for access.

For the FRP composite members, three types of connections are commonly used: (a) mechanically fastened connections, (b) adhesively bonded connections, and (c) combined connections as shown in Figure 1.6

Mechanically fastened or combined connections are the dominant connection types in connecting primary structural members made of FRP in civil structures. The bolted connection offers several advantages over the bonded connection, and they are listed as follows.

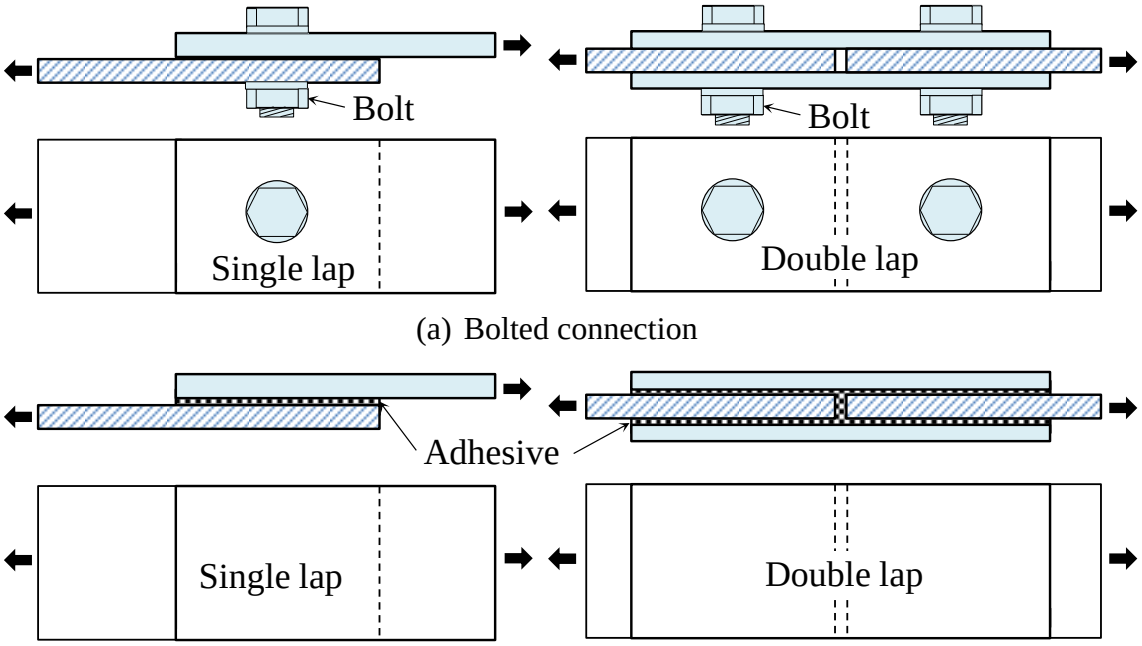

(a) Bolted connection

(b) Bonded connection

Figure 1.6: Connection of FRP members

1) It is not sensitive to surface preparation, service temperature, or humidity
2) It is easy to assemble, and allows component disassembly for repair or replacement
3) It can be easily inspected for connection quality
4) Its strength does not scatter as much as bonded connections

Bolted connections can be classified as shear connections and tension connections. The shear connections can be further classified as either bearing type or friction type based on the load transfer mechanism. In the bearing type connection, the connection load is assumed to be transferred only by the bearing of the bolt to the plate hole. It is assumed that the load will not transferred by the friction between the plates. The design ultimate load should not exceed the design shear resistance calculated from the equations specified in the codes.

The design of friction type connection can be either slip-resistant in the serviceability limit state or slip-resistant in the ultimate limit state. When a connection is designed as slip-resistant in the serviceability limit state, the connection load is assumed to be transferred by the friction between the plates up to the service load level. Axial force is introduced in the bolt so that slip will not occur in the serviceability limit state. The design ultimate load is resisted by the design shear resistance or the design bearing resistance of the connection.

When a connection is designed as slip-resistant in the ultimate limit state, the connection load is assumed to be transferred by the friction between the plates up to the ultimate load level. Axial force is introduced in the bolt so that slip will not occur in the ultimate limit state. The design ultimate load should not exceed the design slip resistance.

The load transfer mechanism of a bolted connection is illustrated in Figure 1.7 and Figure 1.8. The bearing type of connections, the plates are in firm contact with each other but may slip under loading until the hole surface bears against the bolt. The load transmitted from plate to bolt is therefore by bearing and the bolt is in shear. The free body diagram of the shear force transfer in a bearing type bolted connection is shown in Figure 1.7.

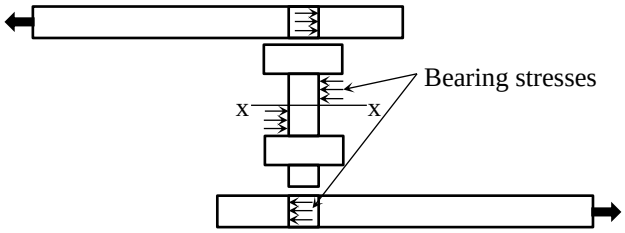

Figure 1.7: Load transfer mechanism of bearing-type bolted connection

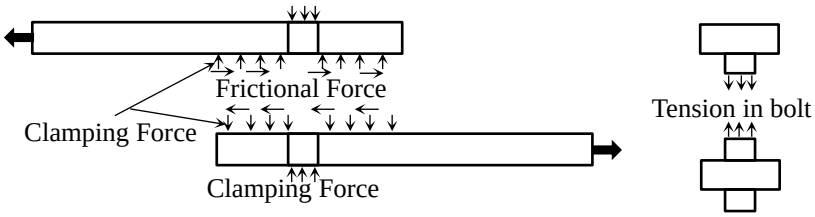

Figure 1.8: Load transfer mechanism of friction-type bolted connection

The free body diagram of a friction-type connection is shown in Figure 1.8. The pretension in the bolt causes clamping forces within the plates even before the external load is applied. When the external load is applied, the tendency of two plates to slip against each other is resisted by the friction between the plates. The frictional resistance is equal to the coefficient of friction multiplied by the normal clamping load between the plates. Until the externally applied force exceeds this frictional resistance, the relative slip between the plates is prevented. The friction-type connections are designed such that under service load the force does not exceed the frictional resistance so that the relative slip is avoided during the service. When the external load exceeds the frictional resistance, the plates slip until the bolts come into contact with the plate and start bearing against the hole. Beyond this point the external load is resisted by the combined action of the frictional resistance and the bearing resistance.

Friction-type multi-row bolted connection is popular in steel structures. Designers usually rely much on the friction-type connection due to the characteristic behavior of creep and friction of steel is well defined. However, creep and friction of FRP composite is not well defined. The creep and friction largely depend on the constituent materials, and environmental conditions such as temperature and humidity. Due to the creep, the bolt clamping force

reduces and it is reported that re-tightening of the bolt after the relaxation period does not recover the bolt strain to its initial value (Mottram, 2005). It is therefore, the current design code (Clarke, 1996) recommended to design a bearing type connection where bolt bearing is assumed to be the only mechanism for the load transfer in bolted plate-to-plate connections.

In the bearing-type bolted connection, failure modes depend on connection geometry, fiber orientation, stacking sequence, friction, bolt torque, and so on. There are following failure modes in bolted connections: (a) bearing failure of the material as in the elongated bolt hole, (b) net-tension failure of the material in the reduced cross section through the bolt hole, (c) shear out failure, (d) cleavage failure of the material (actually transverse tension failure of the material), (e) cleavage-tension failure, and (f) bolt failure. These failure modes are shown in Figure 1.9. In addition, a failure may consist of their combination. Among the failure modes, the bearing failure mode is less catastrophic than other failure modes and facilitates the highest capacity.

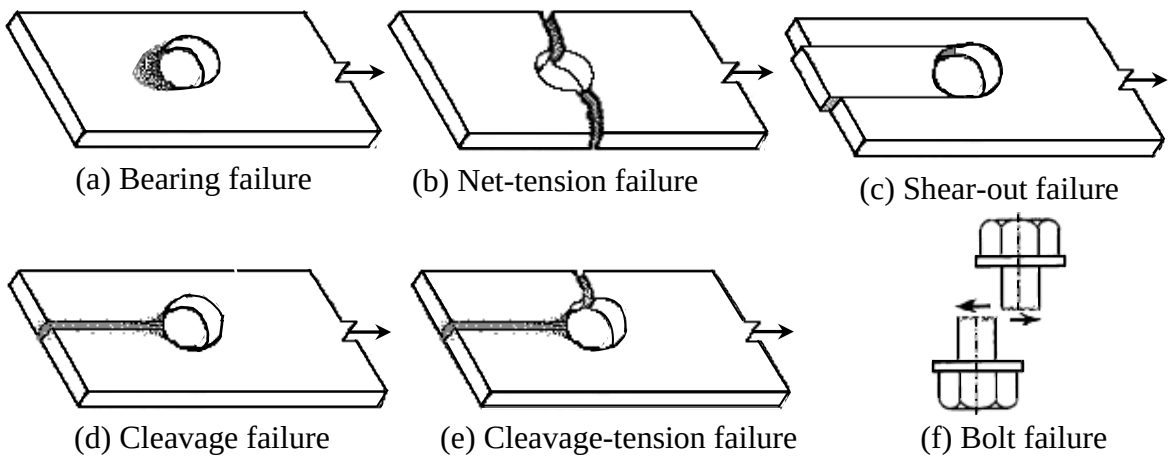

Figure 1.9: Failure modes of bolted connection in shear

Since FRP composites are generally orthotropic and heterogeneous, the design of structural connections is much more complex than with conventional isotropic and homogenous structural materials such as steel. The material could lead to a larger stress concentration in a connection, without possible redistribution of the stresses before failure due

to the lack of yielding characterization. Capacity of bolted connections could be severely reduced due to the discontinuity of fibers at bolt holes. Since the capacity of FRP structure is often limited the capacity of its connections, understanding the mechanical behavior of connections in FRP is particularly important. Several experimental and numerical studies have been conducted to understand the mechanical behavior as well as the ultimate strength of the connections of FRP members. In the following, past studies on the bolted connection of FRP members by different researchers are summarized.

The experimental work conducted by Rosnar (1992) on 102 single-bolt double-lap connections using pultruded GFRP plate to investigate different parameters including the effects of geometric parameters: connection width to bolt diameter ratio, *w/d*, and edge distance to bolt diameter ratio, *e/d*, plate thickness, and fiber orientation. Based on his findings a design procedure was introduced which accounts for material orthotropic, pseudo-yielding capability, and other factors that influenced the connection behavior. The results were also used to correlate and refine a proposed analytical model introduced to describe the behavior of single-bolted connections in composite materials.

Cooper and Turvay (1995) also investigated 81 double-lap single bolted connections using 6.35-mm thick pultruded GFRP plate to investigate the effects of geometric parameters: connection width to bolt diameter ratio, *w/d*, and edge distance to bolt diameter ratio, *e/d*, and bolt clamping torque on the failure load, failure mode and stiffness of a single bolt connection. The results show that the bearing failure loads of the 3 N-m and 30 N-m bolt torque connections increased by 45% and 80%, respectively, when compared with pin connections where no axial force is introduced in the bolt. It was also observed that by increasing the bolt torque the critical *e/d* and critical *w/d* ratios increased significantly. They proposed design charts based on damage load and critical connection geometry. The damage load is defined as a load at which the connection stiffness has been reduced in load-bolt displacement curve.

A failure load of a connection is defined in several ways in the literature. Mottram and

Zafari (2011) explained seven ways of defining failure load using a load-extension relationship based on research by Johnson and Matthews (1979). They reported that the failure load at which the bolt hole elongation becomes 4% of its initial diameter is dependent on the length of gauge used to measure hole elongation and at 4% (defined in ASTM D 953-02) the elongation can be too large for pultruded materials. Johnson and Matthews reported that significant damage occurs when the permanent hole elongates by about 0.4% of the original diameter. DiNicola and Fantle (1993) investigated the bearing strength of clearance-fit fastener holes in woven laminates with quasi-isotropic and ±45° lay-ups. They measured hole deformation, and calculated 4% hole elongation strength and maximum bearing strength. The test method followed ASTM D 953. The results indicated that the 4% hole deformation strength is reduced by up to 30% due to hole oversize. Thoppul et al. (2009) explained the procedure to determine the 4% hole elongation strength and 2% offset bearing strength according to ASTM D 953 and the ASTM D 5961 respectively. McCarthy et al. (2002) performed an experimental study to investigate the effects of bolt-hole clearance on the strength of single bolted connection of FRP composite laminate. The test was performed according to ASTM D 5961 to obtain the connection stiffness, 2% offset bearing strength, ultimate bearing strength and ultimate bearing strain.

Khashaba et al. (2006) performed experiments to determine the effect of washer size and tightening torque on the strength of bolted connections of glass fiber reinforced epoxy laminate. They used the tightening torque of T = 0, 5, 10 and 15 Nm and the washer outer diameter size of D_{wo} = 14, 18, 22 and 27 mm. Diameter of bolt is 6 mm. The results illustrate that the stiffness of the connections increase with decreasing washer size under a constant tightening torque, T=15 N-m. The bolted connection with 18 mm washer size has the maximum bearing strength with the torque. For larger washer size than 18 mm with the constant tightening torque, the bearing strength decreases with increasing the washer size. It should be noted that the contact pressure of the washer decreases with increasing clamping

area. However, Abd-El-Naby and Hollaway (1993) and Stockdate and Matthews (1976) observed that the failure load would increase with an increase in the clamping area at a constant clamping pressure.

Khashaba et al. (2013) investigated the effect of stacking sequence on the failure strength and failure modes of pinned connections of glass-fiber reinforced epoxy composite laminates. They investigated specimens with different stacking sequences $[0/90]_{2S}$, $[15/-75]_{2S}$, $[30/-60]_{2S}$ and $[45/-45]_{2S}$ experimentally and numerically. The results showed that the $[0/90]_{2S}$ laminate has the highest ultimate strength and the $[30/-60]_{2S}$ laminate has the minimum ultimate strength. The failure mode of the connections with stacking sequences $[0/90]_{2S}$, $[15/-75]_{2S}$ and $[30/-60]_{2S}$ was shear-out failure, while connections with $[45/-45]_{2S}$ was bearing failure mode.

Godwin and Matthews (1980) provided a review paper on the strength of bolted connections. The review involves a detailed summary of various materials, fasteners, and design parameters of bolted connections. In general their findings showed that with increasing bolt torque, the bearing strength of the connection would increase provided that the bolts are not over tightened and do not crush the material. It was found that to achieve bearing failure the end distance to bolt diameter ratio, *e/d*, must be within a range of 3 to 5 depending on the laminate lay-up. The review indicated that the minimum width to bolt diameter ratio, *w/d*, recommended by various researchers ranged between 3 to 8. The effect of bolt diameter to plate thickness, *d/t*, was shown to be negligible in the presence of lateral constraint. For pin-loaded plates, the *d/t* ratio should be less than 1 to achieve full bearing strength. It was also found that the direction of load bearing with respect to the fibers could have a great influence on the bearing strength of the material. In general, generous edge distances and widths and adequately tightened bolts will provide the maximum bearing strength possible for composite bolted connections.

Hassan (1995) conducted an experimental study on 115 multi-row bolted connections

with double lap of five different connection configurations to investigate the effects of various geometrical parameters, including width of the member, edge distance, fiber orientation, number of bolts and bolts pattern, on the behavior of these connections. Based on the stress concentration factor presented by Hart-Smith (1980), an analytical model is developed to determine the strength and failure modes of the FRP multi-bolted connections. The model accounts for material orthotropy, pseudo-yielding capability and other factors that influence the connection behavior. The model is able to predict the ultimate load capacity of the connection and its mode of failure.

The present study focuses on the bearing-type multi-row bolted connections with a double-lap configuration of FRP members. Load is not distributed equally among rows of bolts in the bearing-type multi-row bolted connection and how the load is distributed among the bolts depends on relative stiffness of cover plate to the main plate, bolt position, bolt-hole clearance, bolt-torque or tightening of the bolt, friction between member plates and at washer-plate interface. For a ductile material, the load distribution among the bolt rows does not affect the ultimate strength of the connection since the load would be re-distributed among the bolt rows due to the plastic deformation (Vasarhelyi and Chang, 1965). However, the load distribution in a connection of a brittle material like FRP affects its ultimate strength because the load does not re-distribute among the bolts. Feo et al. (2012) investigated the load distribution among bolt rows up to four rows in pultruded FRP structural members, where each cover plate has a half of the main plate stiffness. Pre-Standard for Load and Resistance Factor Design of Pultruded Fiber Reinforced Polymer Structures (ASCE, 2010) specifies the load distribution up to three rows of bolts for FRP and steel cover plates, and EUROCOMP (Clarke, 1996) and Guide for the Design and Construction of Structures Made of FRP Pultruded Elements (National Research Council, 2007) specify the load distribution among the rows of bolts up to four rows for FRP and steel cover plate. However, how a relative stiffness of the cover plate to the main plate will affect the load distribution in the multi-row

bolted connection is not explicitly described in these design codes and guidelines.

1.4 Statement of Problem

In bearing-type multi-bolted connections, the load distribution among bolts is greatly dependent on the relative stiffness of cover plate to the main plate. The ultimate strength and failure modes of bolted connections depend on the load distribution among the bolts. It means that the stiffness of the cover plate affects not only the load distribution but also the strength and failure mode of a connection. Current design guidelines specify the load distribution among rows in multi-row bolted connections with FRP and steel cover plates where FRP cover plates have a half of the main plate thickness. How the different stiffness of cover plate will affect load distribution and strength is not specified in the design codes. Furthermore, the current design guidelines specify the strength of a bolted connection where axial force in the bolt is not considered; therefore the obtained strength may be conservative. In the practical application, a certain amount of axial force is introduced in the bolt that provides lateral restraint resulting in an increase of the capacity of a connection. In addition, the current design guidelines are in the preliminary stage and need to be developed. Therefore, the mechanical behavior of bearing-type multi-row bolted connection should be examined, and their ultimate strength and typical failure modes should be understood to further develop the design guidelines.

1.5 Objectives of the Study

The principal objectives of the present study are:

(a) To determine the effect of cover plate stiffness on load distribution among the bolts of bearing type multi-row bolted connections.

(b) To evaluate efficiency and capacity of the connections based on the load distribution.

(c) To develop a three dimensional finite element model that can obtain the failure mode and ultimate strength of a bolted connection of FRP structural members.

(d) To evaluate the effect of cover plate stiffness on ultimate strength and failure modes of bearing-type multi-row bolted connections by the three dimensional finite element analysis and experimental investigation.

(e) To determine how to influence geometric parameters on ultimate strength, load distribution among the bolts, and failure modes of bolted connections for varying the cover plate stiffness.

(f) To determine the relationship between ultimate strength of single and multi-row bolted connections.

(g) To provide design guidelines for the multi-row bolted connections of FRP structural members.

1.6 Scope of the Work

The study focused on the behavior of bearing-type multi-row bolted connection with a double-lap configuration fabricated from a woven fabric GFRP. Therefore, comprehensive experimental and numerical investigations have been conducted at the Nagoya University to study the behavior of bearing-type bolted connections in FRP composite materials for civil engineering applications. In the investigation, effect of cover plate stiffness on the connection strength has been studied with various geometric parameters including the width to bolt diameter ratio, *w/d*, pitch distance to diameter ratio, *p/d*, and edge distance to bolt diameter ratio, *e/d*. The ultimate strength, failure modes, and load distribution among the bolts are determined experimentally as well as numerically. A series of test coupons were tested of 6, 9, and 12-mm thick GFRP plates to determine the material properties. In this investigation, 20 sets of single bolted connection and 41 sets multi-row bolted connections were also tested to

examine the behavior of bolted connection. A progressive damage model is developed based on failure criteria and material stiffnesses degradation to determine the ultimate strength and failure modes of a connection. The progressive damage mode is implemented through user subroutine UMAT in Abaqus. Based on the research findings, a design procedure for bearing-type multi-row bolted connections has been developed.

1.7 Outline of the Thesis

In this research, an experimental and numerical investigation have been conducted to determine the effect of relative stiffness of cover plate on ultimate strength, failure modes and load distribution among the bolts in bolted connections fabricated from GFRP. The thesis consists of seven chapters and the content of each chapter is described in the following:

(a) Chapter 1: Introduction to the research work, composite material, and applications of composite structures in general, and in civil engineering structures in particular, are described. Current research activities in the field of bolted connections are also presented in this chapter. The objectives and scope of the work are also presented in this chapter.

(b) Chapter 2: In this chapter focuses on load distribution among the bolt rows of bearing-type multi-row bolted connections of FRP members. A series of 3D elastic finite element analyses were performed of two to four-row bolted connections to determine the effect of cover plate stiffness on the load distribution among the bolt rows. The finite element analysis results were critically analyzed and presented in this chapter. Based on the load distribution among the bolt rows, efficiency and capacity of connections were evaluated with respect to a single bolt connection and shown in this chapter.

(c) Chapter 3: The chapter focuses on strength and failure modes of bearing-type multi-row bolted connections of FRP members with different geometric parameters

and stiffness of cover plates. A series of 3D non-linear finite element analyses based on the progressive damage model were performed two to four-row bolted connections to evaluate behavior of multi-row bolted connections at the damage stage. In order to evaluate behavior of a multi-row bolted connection accurately, a progressive damage model of FRP materials was implemented in a commercial finite element analysis software by using a user subroutine. Based on the finite element analysis, the effects of cover plate stiffness on the connection strength and failure modes were shown. The effect of geometric parameters were also shown in this chapter

(d) Chapter 4: An experimental program was conducted in the study. A series of test coupon were tested to determine the material properties of 6, 9, and 12-mm thick GFRP plate. Tests procedure and material properties are shown in chapter. A series of single bolted connections with different geometric parameters were also tested. The ultimate strength and failure modes were found and presented in this chapter. The results were critically analyzed and minimum requirements of geometric parameters for GFRP plate are proposed.

(e) Chapter 5: In this chapter, an experimental program was conducted to determine the ultimate strength and failure modes of multi-row bolted connections. A series of two to four-row bolted connections with different geometric parameters and cover plate stiffness were tested. The ultimate strength and failure modes are presented in this chapter. The minimum requirements of ASCE LRFD Pre-standard were also investigated and results are presented.

(f) Chapter 6: Based on the experimental results, simple equations were developed to predict the ultimate strength and failure modes of a connection. The experimental and predicted ultimate strength and failure modes are compared to justify the accuracy of the equations which is presented in this chapter.

(g) Chapter 7: The conclusions and design recommendations, as well as, identification of the areas which need further investigation are presented in this chapter.

CHAPTER 2 LOAD DISTRIBUTION IN MULTI-ROW BOLTED CONNECTIONS

2.1 Introduction

This study focuses on bearing-type multi-row bolted connections of FRP members. The load is not distributed equally among rows of bolts, and the load distribution profile depends on different factors including relative stiffness of cover plate, varying bolt position, and bolt-hole clearance. LRFD Pre-Standard (ASCE, 2010) specifies the load distribution among the bolts for the bolted connections with rows up to three and CNR-DT 205/2007 (National Research council, 2007) and Eurocomp (Clarke, 1996) specify the load distribution among the bolts for the bolted connections with rows up to four where a steel cover plate or an FRP cover plate having a half of the main plate thickness is used. However, how the cover plate stiffness affects the load distribution among the bolts of the multi-row connection has not yet been studied.

The aim of this chapter is to examine the effect of cover plate stiffness on the load distribution among rows of bolts in multi-row bolted connections of FRP structural members. The study also includes the influence of connection geometry on the load distribution. Based on the load distribution, efficiency and capacity of connections are evaluated with respect to a single bolt connection.

2.2 Methods of Approach

2.2.1 Connection Geometry

Finite element analysis is performed to examine the load distribution among the bolts of multi-row bolted connections with a double-lap configuration. In this study, one line of two, three, and four rows of bolted connections are examined, which are shown in Figure 2.1. The

thickness of FRP main plate, t_m, is 12 mm and the diameter of steel bolts, d, is 16 mm. The diameter of bolt hole, d_h, of 17.6 mm is used in this study. Therefore, the clearance of bolt hole is 1.6 mm (1/16 in.). Two types of cover plate are used: FRP and steel. To change the cover plate stiffness, thicknesses of cover plates are changed. For FRP cover plates 6, 9 and 12 mm are used, and for steel cover plates 3, 4.5, and 6 mm are used. Therefore, stiffness ratios of two cover plates to the main plate are 1.0, 1.5, and 2.0 for FRP cover plates, and 7.35, 11.0, and 14.7 for steel cover plates. The stiffness ratio, r_k, is defined as the ratio of the stiffness of two cover plates to the main plate as follows.:

$$r_k = \frac{2k_c}{k_m} \tag{2.1}$$

where, k_c= stiffness of each cover plate in the loading direction, and k_m= stiffness of the main plate in the loading direction.

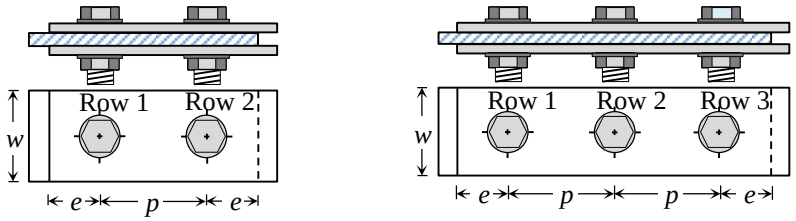

(a) Two-row bolted connection (b) Three-row bolted connection

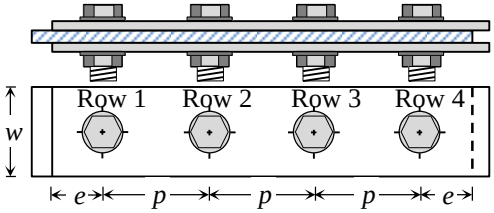

(c) Four-row bolted connection

Figure 2.1: Geometry of connections

In addition to the stiffness ratio, r_k, different geometric parameters of bolted connections of plate width to bolt diameter ratio, *w/d*, pitch distance to bolt diameter ratio, *p/d*, and edge distance to bolt diameter ratio, *e/d*, are also examined. Geometric parameters of connections examine in in the study are shown in Table 2.1. A connection type represents a

set of geometric parameters, and seven types from Type A to Type G are considered in this study. A connection ID is used in this study to designate each of the connection geometry. A connection ID consists of a number of bolt rows, connection type, cover plate material, and cover plate thickness as shown in Figure 2.2.

Table 2.1: Geometric parameter of connections

Type	A	B	C	D	E	F	G
w/d	4.0	4.0	4.0	3.0	5.0	4.0	4.0
p/d	3.0	4.0	5.0	4.0	4.0	4.0	4.0
e/d	2.0	2.0	2.0	2.0	2.0	1.5	2.5

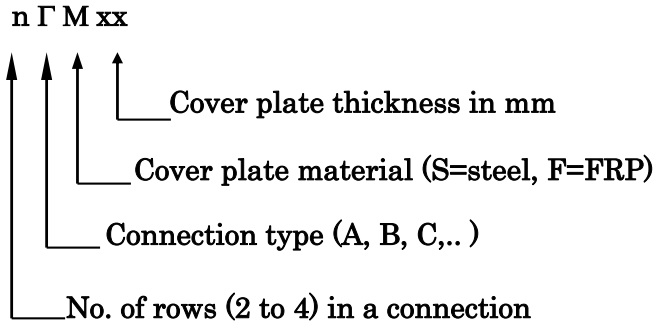

Figure 2.2: Definition of connection ID

2.2.2 Material Properties

Glass fiber reinforced polymer (GFRP) composite is used in this study. Quasi-isotropic glass-fiber laminates are considered for the connection plates. A thickness of each ply is 0.375 mm, and a stacking sequence is symmetric in each laminate. Material properties of unidirectional lamina are given in Table 2.2 (Khashaba at al., 2013). E_{11} and E_{22} are moduli of elasticity of the lamina in fiber and transverse to the fiber directions, respectively, and ν_{12} and G_{12} are Poisson's ratio and shear modulus in the 12 plane, respectively.

Table 2.2: Material properties of unidirectional lamina

E_{11} (GPa)	E_{22} (GPa)	ν_{12}	G_{12} (GPa)
32.1	5.74	0.33	1.24

To obtain a complete set of material properties, other material properties are determined according to the relations of transverse isotropic materials, i.e., $E_{33} = E_{22}$, $G_{13} = G_{12}$ $\nu_{13} = \nu_{12}$. The following approximations (Kriz and Stinchcomb, 1979) are also considered: $G_{23} \approx G_{12} \approx G_{13}$ and $\nu_{23} \approx \nu_{12} \approx \nu_{13}$. Material properties of steel for bolt and cover plate are as follows: Young's modulus $E = 200$ GPa and Poisson's ratio $\nu = 0.3$.

2.2.3 Finite Element Model

Finite element models of the connections are created using the general purpose finite element software, Abaqus 6.11. A one eighth of a connection is modelled by taking advantage of symmetry conditions. An example of finite element model and boundary conditions are shown in Figure 2.3. At the end of main and cover plates are considered free, at the center of cover plate x-symmetric boundary conditions are applied, and a displacement is applied at the continuous edge of the main plate. Three dimensional solid eight-nodded elements are used to model FRP plates, steel plates, and steel bolts and washers. A set of a washer and a bolt is modelled together as a single part. Surface to surface contact definition is employed where different parts may contact each other. In the contact definition, the Coulomb friction model with a coefficient of frictional of 0.2 is used (Mottram et al., 2004; Hyer et al., 1987), and the penalty method is utilized. Finger-tighten torque (≤ 3 N-m) (Mottram and Turvey, 2003), that is equivalent to an axial pre-tension force of 500 N, is assumed and applied to bolt shank. The analysis includes geometrical nonlinearity, but materials are assumed to be elastic.

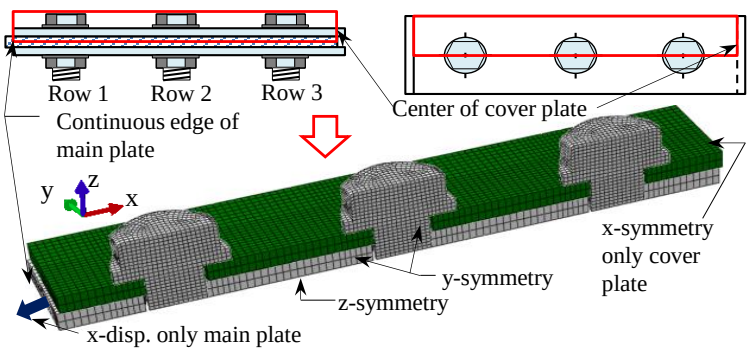

Figure 2.3: Finite element model

2.3 Results and Discussions

Load distribution coefficients among the bolts in the connections are evaluated from the analysis results. The load distribution coefficient for a bolt can be defined as the ratio of load transferred by the bolt to the total load transferred by the connection as expressed in Eq. (2.2):

$$C_i = \frac{P_i}{\sum_{i=1}^{n} P_i}, \quad \text{for } i = 1,2,...,n \tag{2.2}$$

where, C_i = load distribution coefficient of the ith row, n = number of rows in the connection, P_i = load transferred by the bolt in the ith row, which is a sum of contact forces at the bolt hole in the loading direction. The summation of load transferred by the bolts in Eq. (2.2) is assumed to be the total load because the load transferred by the friction between the main plate and cover plates are found to be only 1 to 2% of the total load in this study, and the amount of the load transferred by the friction depends on the assumed coefficient of friction, the assumed axial force in bolts, and the total applied load.

2.3.1 Model Validation

The load distribution coefficients obtained from the analysis for the connection Type B with an FRP cover plate having half the thickness of an FRP main plate are given in Table 2.3 along with those found in the literature. Geometrical parameters of Type B are set to satisfy the minimum requirements specified by LRFD Pre-Standard. Load distribution coefficients from the present finite element analysis are in very good agreement with previously reported studies (Feo et al., 2012, ASCE, 2010, Clarke, 1996, National Research Council, 2007). The load distribution coefficients are the same as those of EUROCOMP (Clarke, 1979) and close to the others. Therefore, the finite element model of the present study is validated.

Table 2.3: Load distribution coefficients of FRP/FRP (r_k = 1) bolted connection

	Three rows of connection		
	Row 1	Row 2	Row 3
FEA of this study	0.37	0.26	0.37
Feo et al. (2012)	0.36	0.28	0.36
ASCE (2010)	0.40	0.20	0.40
EUROCOMP (Clarke,1996)	0.37	0.26	0.37
CNR DT 205/2007 (National Research Council, 2007)	0.41	0.17	0.41

2.3.2 Load Distribution

Figure 2.4 shows load distribution coefficients of each row in the three-row bolted connection for different stiffness ratios. It can be seen that the load distribution coefficient increases in the first row and decreases in the last row with an increase in the cover plate stiffness. For the intermediate row, the load distribution coefficient is not much affected by the stiffness ratio. In this study, the farthest bolt to the end of the main plate is designated as first bolt as shown in Figure 2.4. The rate of change of the load distribution coefficient decreases with an increase in the stiffness ratio. Therefore, the load distribution does not change significantly for the connections with steel cover plates when the cover plate thickness is changed. The same trend is also found in two and four-row bolted connections.

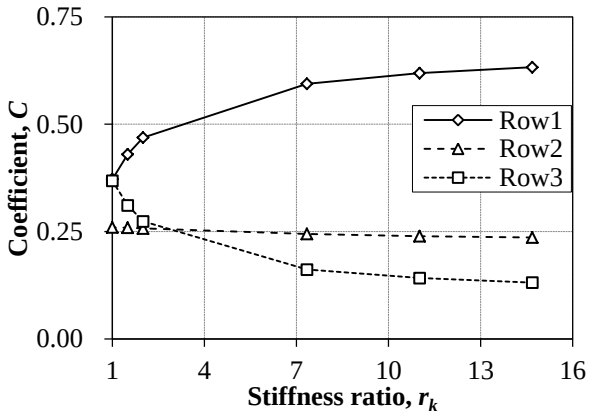

Figure 2.4: Effect of stiffness ratio on load distribution for the three-row bolted connections (Type B)

Figure 2.5 shows the load distribution coefficients for the connection Type B with different thicknesses of steel and FRP cover plates. It is observed that the load distribution among the bolts depends on the material and thickness of cover plate. The loads distribution coefficients are more uniform for the connection with FRP cover plates than that with steel cover plates. The load distribution coefficients in connections with steel cover plates are very different from those in connections with FRP cover plates, which is caused by the difference in the stiffness of cover plates. The load distribution coefficients in the first row of two, three, and four-row bolted connections are 0.50, 0.37, 0.32 for 6 mm FRP cover plates and 0.69, 0.63, 0.62 for 6 mm steel cover plates, respectively. It means that just by changing the cover plate material FRP to steel and keeping the same thickness, the load distribution coefficients in the first row of two, three, and four-row bolted connections will be increased by as much as 38%, 70%, and 93%, respectively.

It should be noted that capacity of a connection depends on the largest load distribution coefficient in the connection. The load distribution coefficients do not result in a significant change for changing thickness of steel cover plates from 3 mm to 6 mm. On the other hand, a significant change in the load distribution is observed when the thickness of FRP cover plate is changed from 6 mm to 12 mm. By changing the thickness of FRP cover plates from 6 mm to 12 mm for the 12 mm main plate, the load distribution coefficient in the first row of the two, three, and four-row bolted connections is increased from 0.50 to 0.57, from 0.37 to 0.47, and from 0.32 to 0.43, respectively.

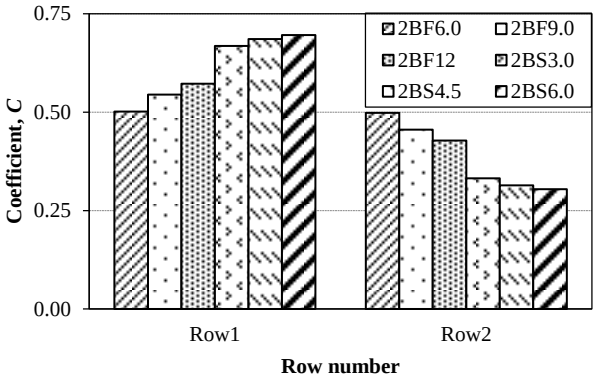

(a) Two-row bolted connections

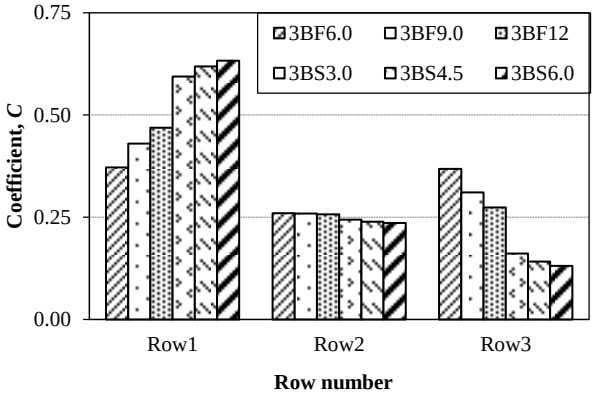

(b) Three-row bolted connections

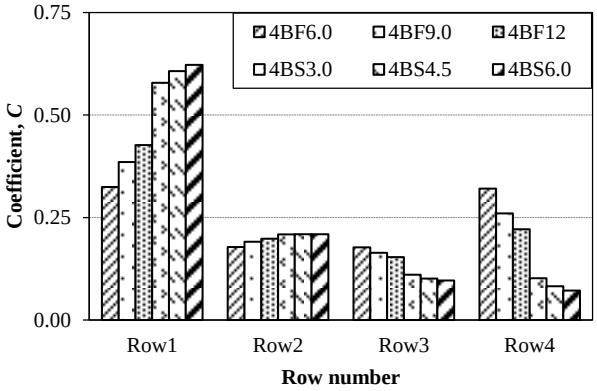

(c) Four-row bolted connections

Figure 2.5: Load distribution coefficients of Type B connections with differents cover plates

Figure 2.6 shows the effect of the *w/d* ratio on the load distribution among the bolts. It can be observed that the effect of the *w/d* ratio on load distribution is not significant although the load distribution is slightly changed for a larger stiffness of cover plate. The load distribution coefficients of the two, three, and four-row bolted connection with 6 mm steel

cover plates in first bolt are increased by 0.06, 0.06, and 0.08, respectively to decrease the *w/d* ratio 4 to 3. The load distribution coefficient increases in the first row and decreases in the other rows for a connection with a lower *w/d* ratio than the others.

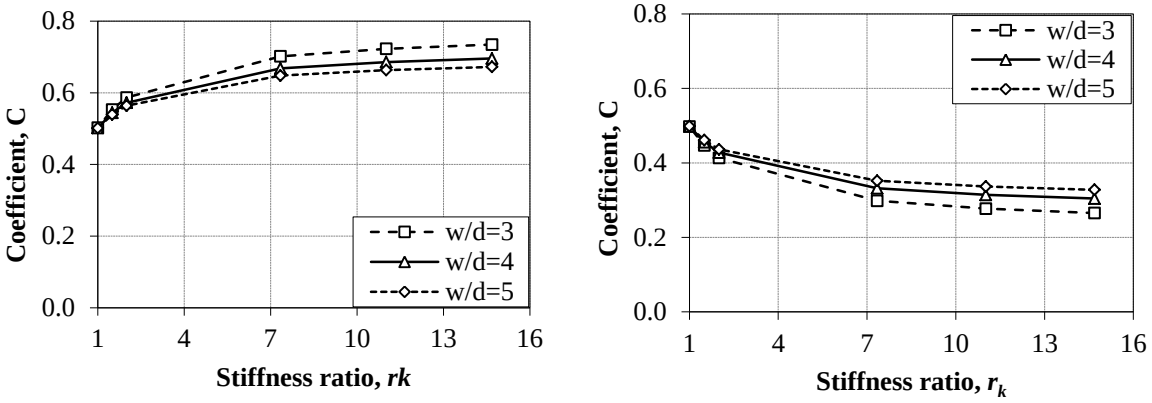

i) Row 1 ii) Row 2

(a) Two-row bolted connections

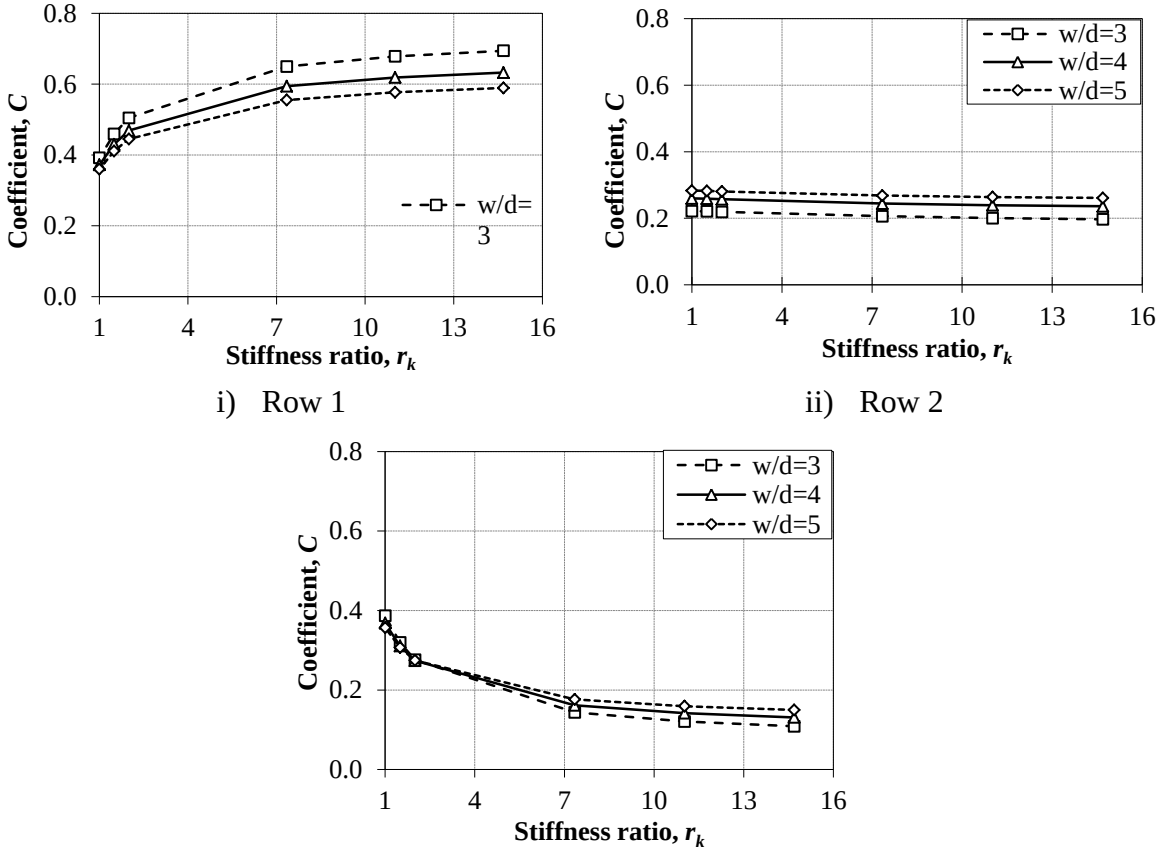

i) Row 1 ii) Row 2

iii) Row 3

(b) Three-row bolted connections

Figure 2.6: Effect of *w/d* ratio on load distribution

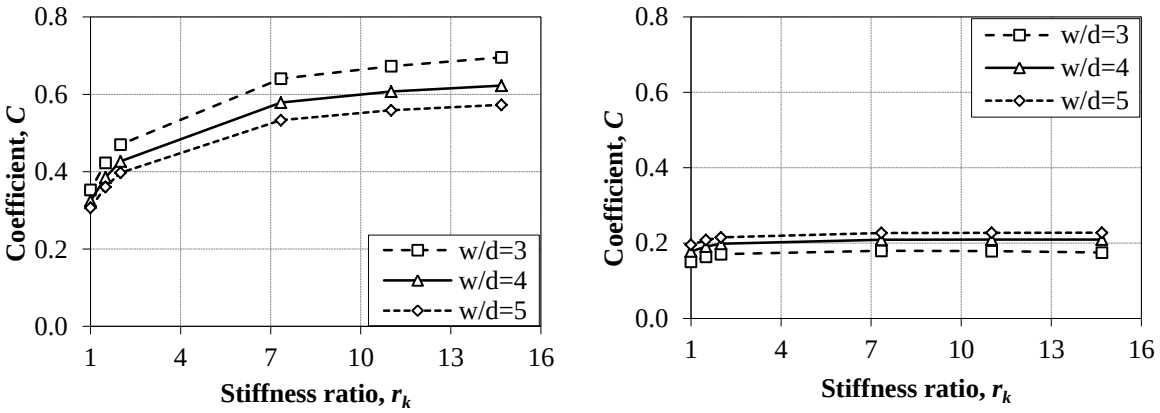

i) Row 1 ii) Row 2

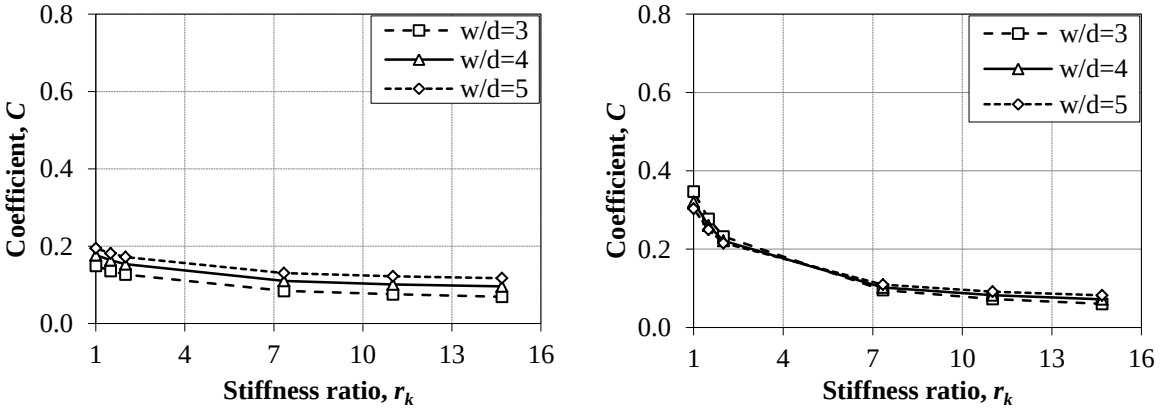

iii) Row 3 iv) Row 4

(c) Four-row bolted connections

Figure 2.6: Effect of *w/d* ratio on load distribution (cont'd)

Figure 2.7 shows the effect of the *p/d* ratio on the load distribution among the bolts. It can also be observed that the effect of the *p/d* ratio on load distribution is not significant. The load distribution is slightly changed for a larger stiffness of cover plate. The load distribution coefficient increases in the first row and decreases in the other rows for a connection with a larger *p/d* ratio, which is an opposite trend to the *w/d* ratio. The load distribution coefficients of the two, three, and four-row bolted connection with 6 mm steel cover plates in first bolt are decreased by 0.04, 0.04, and 0.04, respectively to increase the *p/d* ratio 3 to 4.

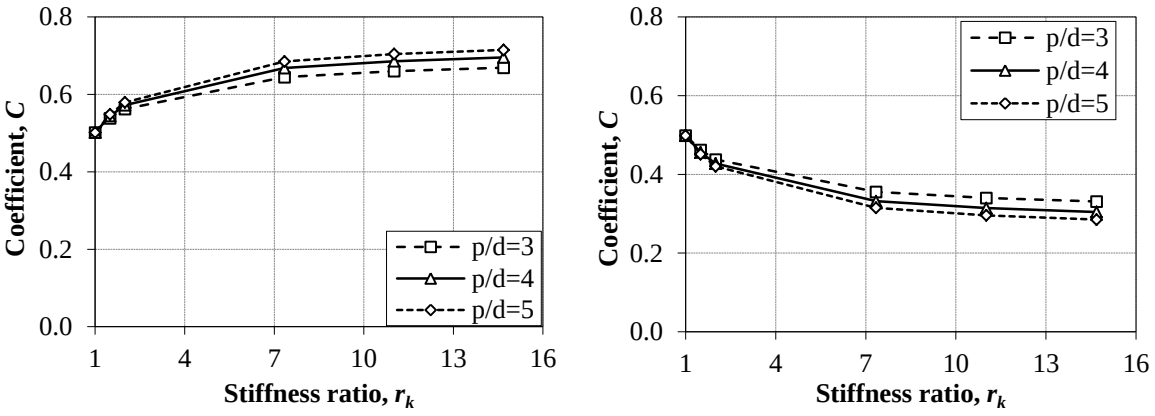

i) Row 1 ii) Row 2

(a) Two-row bolted connections

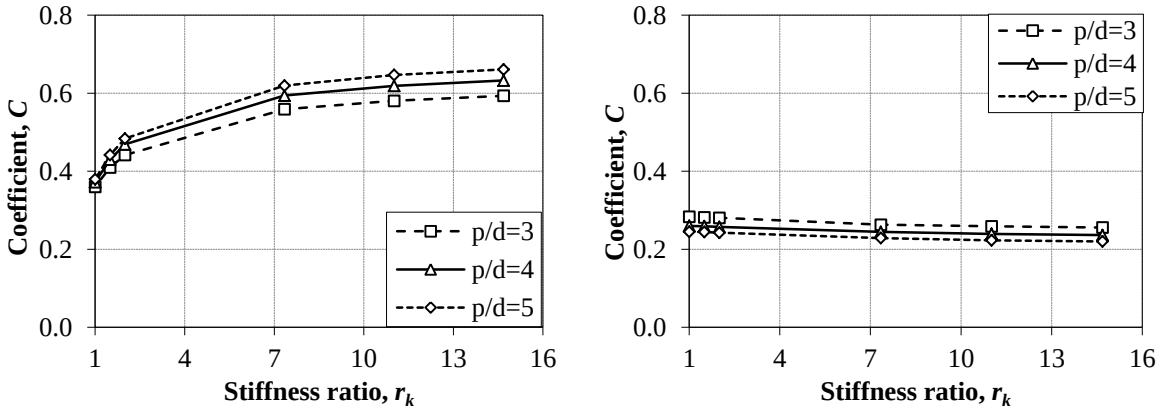

i) Row 1 ii) Row 2

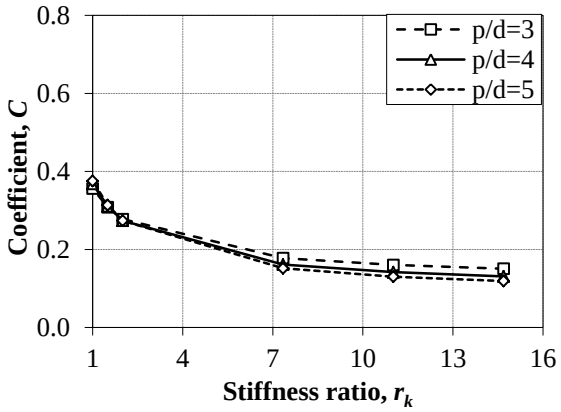

iii) Row 3

(b) Three-row bolted connections

Figure 2.7: Effect of *p/d* ratio on load distribution

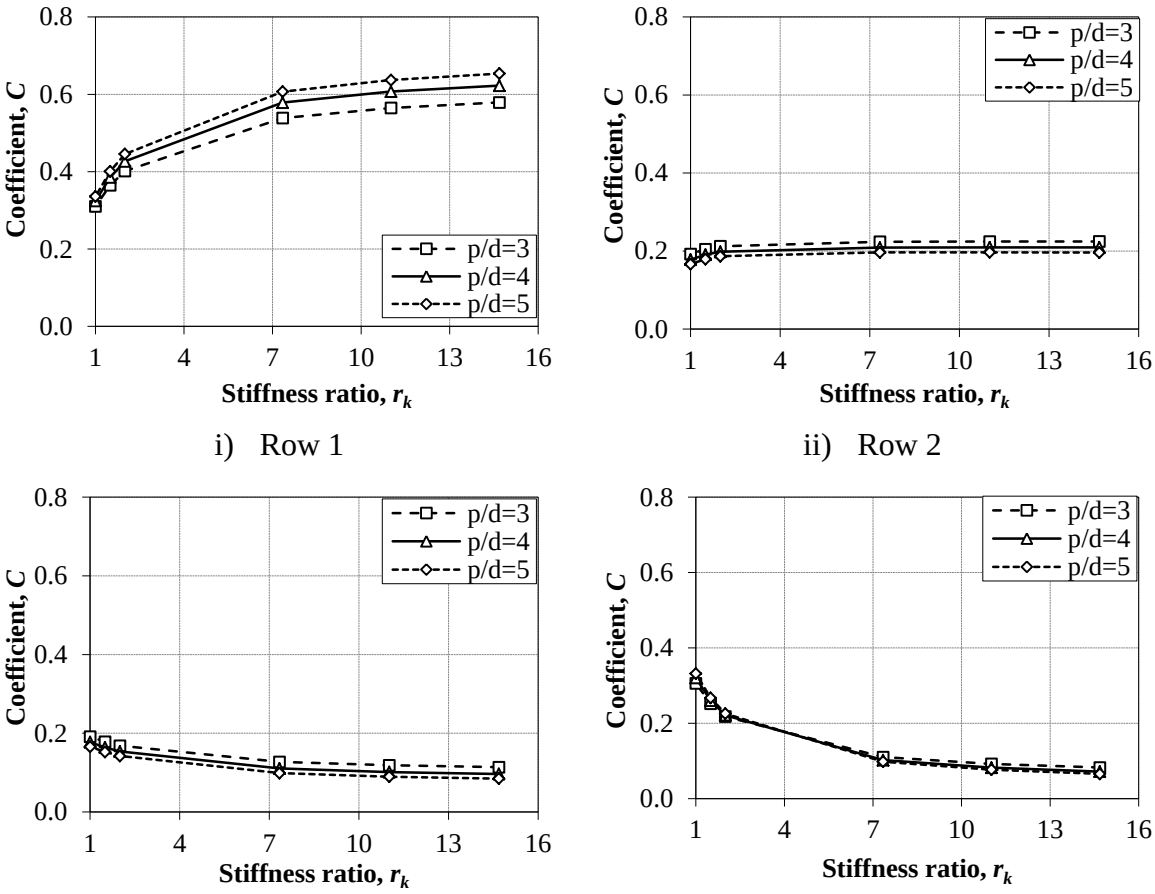

i) Row 1 ii) Row 2

iii) Row 3 iv) Row 4

c) Four-row bolted connections

Figure 2.7: Effect of *p/d* ratio on load distribution (cont'd)

Figure 2.8 shows the effect of the *e/d* ratio on the load distribution among the bolts. It can be observed that the effect of the *e/d* ratio on load distribution is not significant either. For two-row bolted connection, the effect of the *e/d* ratio on the load distribution increases with the increase of stiffness of cover plate, whereas, for three and four-row bolted connections, the effect of the *e/d* ratio on the load distribution increases with the decrease of stiffness of cover plate in the intermediate rows. It is because the last and first rows release some load, which is taken by the intermediate rows.

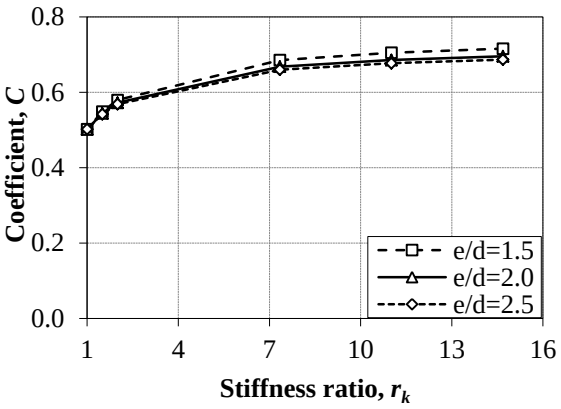

i) Row 1

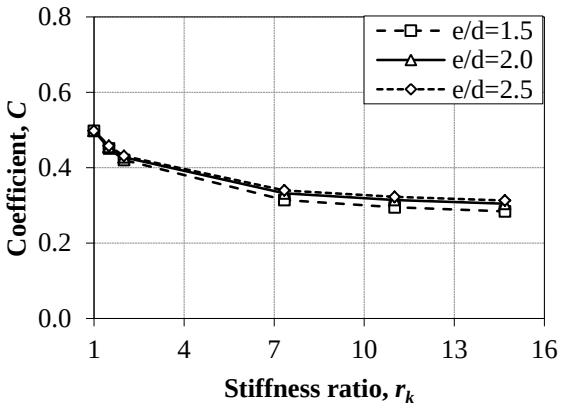

ii) Row 2

(a) Two-row bolted connections

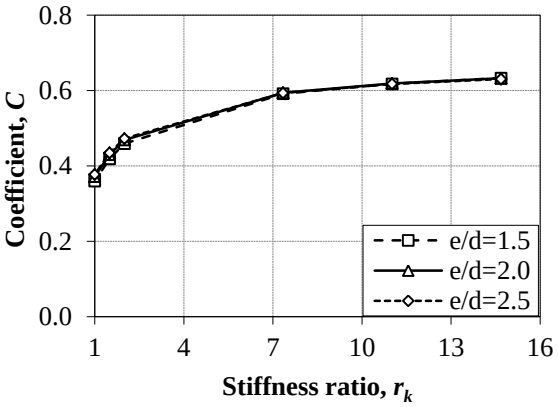

i) Row 1

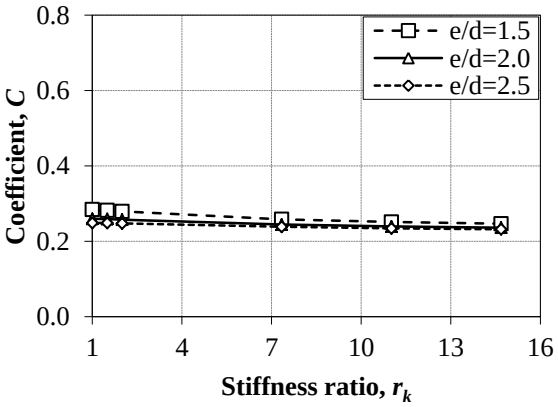

ii) Row 2

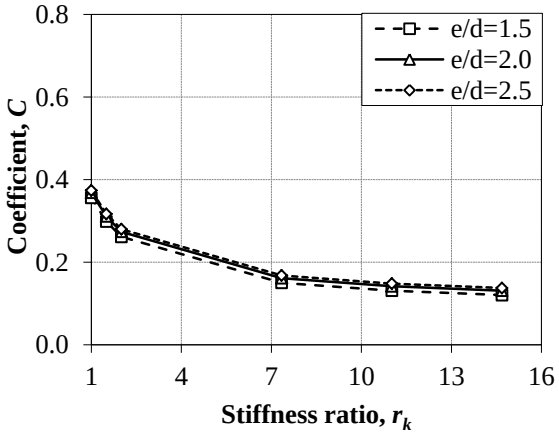

iii) Row 3

(b) Three-row bolted connections

Figure 2.8 : Effect of *e/d* ratio on load distribution

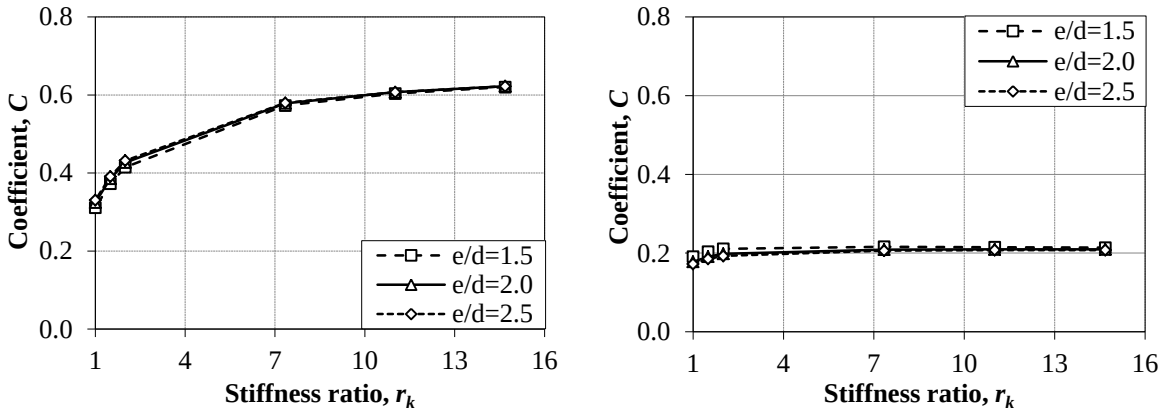

iii) Row 1 iv) Row 2

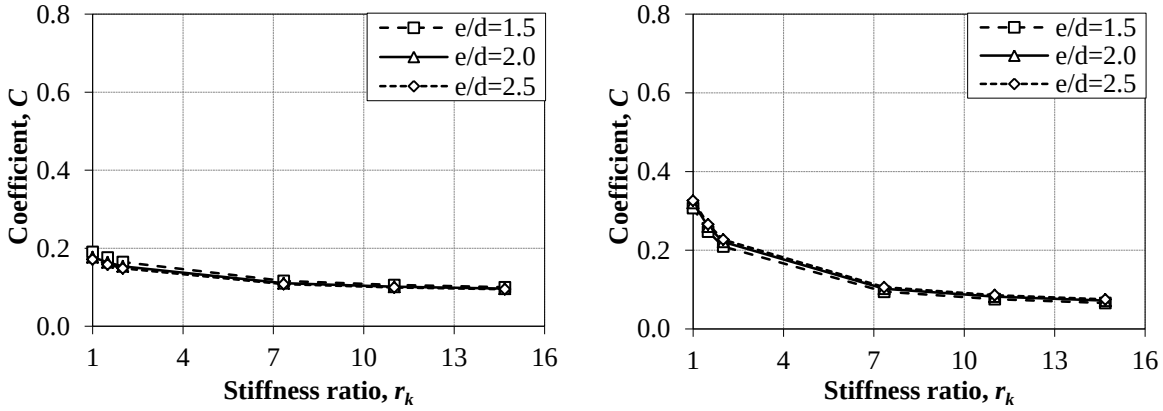

iii) Row 3 iv) Row 4

(c) Four-row bolted connections

Figure 2.8: Effect of *e/d* ratio on load distribution (cont'd)

2.3.3 Efficiency and Capacity

In a bearing-type multi-row bolted connection of FRP composite structures, efficiency of a connection depends on the load distribution among the rows of bolts. Because FRP composite materials are brittle in nature, the row of bolt that takes the largest load determines the strength of a connection. Therefore, the more uniform the distribution among rows of bolts is the larger strength of connection becomes. In the study, the FRP composite material is assumed to be linearly elastic until failure. The efficiency on a connection is defined as the ratio of the sum of load distribution coefficients among bolt rows to the maximum load distribution coefficient in the connection multiplied by the number of rows as expressed in Eq. (2.3):

$$\eta = \frac{\sum_{i=1}^{n} C_i}{nC_{\max}}, \text{ for } i = 1,2,...,n \tag{2.3}$$

where η = efficiency of a connection, C_i = load distribution coefficient of the ith row, C_{Max} = the maximum load distribution coefficient among the rows of bolts, and n = the number of bolt rows in the connection. Note that the sum of load distribution coefficients is equal to unity. Therefore, Eq. (2.3) can be reduced to

$$\eta = \frac{1}{nC_{\max}} \tag{2.4}$$

Eq. (2.4), shows that the efficiency of a connection depends on the maximum load distribution coefficient in a connection.

Figure 2.9 shows the efficiency of Type B connections for varying stiffness ratio of cover plates to the main plate. It can be observed that the efficiency of the connections decreases with an increase of the stiffness ratio and also with the number of rows. The connection with an FRP cover plate having a thickness of 6 mm attains the largest efficiency among others. Connections with FRP cover plates having a half of the main plate thickness, which translates to a stiffness ratio of 1.0, are found to be the largest efficiency among connections with different stiffness ratios, and efficiencies for the two, three, and four-row connections are 1.00, 0.90 and 0.77, respectively. On the other hand, the efficiency of the two, three and four-row bolted connections with steel cover plates that have a half of the main plate thickness are equal to 0.72, 0.53 and 0.40, respectively. Therefore, in terms of efficiency, it is better to make the stiffness of cover plate be the same as that of the main plate.

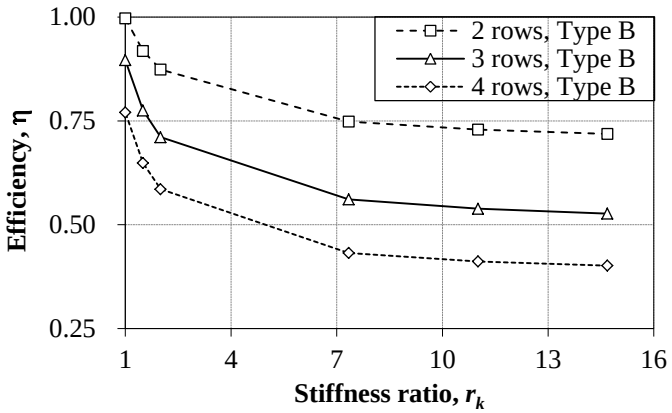

Figure 2.9: Effect of stiffness ratio on efficiency

To determine the effect of different geometry on the strength of connection, efficiency is compared. Figure 2.10 shows the efficiency ratio vs. the stiffness ratio for connections with different geometric parameters. The efficiency ratio, r_η, is defined by the following equation:

$$r_\eta = \eta / \eta_{nBMxx} \tag{2.5}$$

where η is efficiency of a connection, and η_{nBMxx} is efficiency of Type B connection with the same number of rows and the same cover plate.

It is observed from Figure 2.10 that the efficiency is affected by the geometric parameter of a connection. The efficiency increases with the increasing *w/d* ratio or the decreasing *p/d* ratio. It means that the efficiency increases with an increase in the connection stiffness, where the connection stiffness can be defined as the ratio of connection load to connection displacement within an elastic range. However, the efficiency is very not sensitive to the *e/d* ratio. It is also observed that the efficiency ratio does not change significantly with the change of stiffness ratio. The change of efficiency in percentage for changing a *w/d* ratio or a *p/d* ratio is given in Table 2.4.

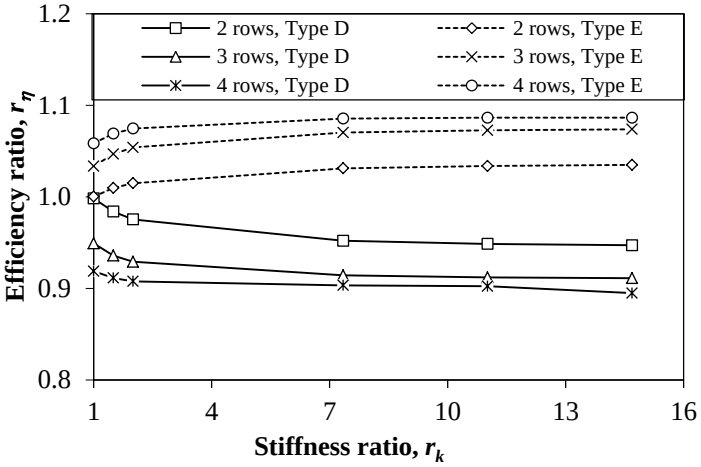

(a) Type D and Type E (Different *w/d* ratio)

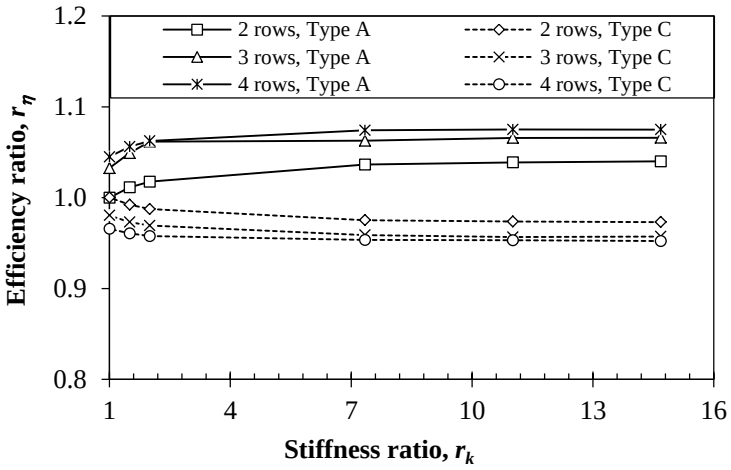

(b) Type A and Type C (Different *p/d* ratio)

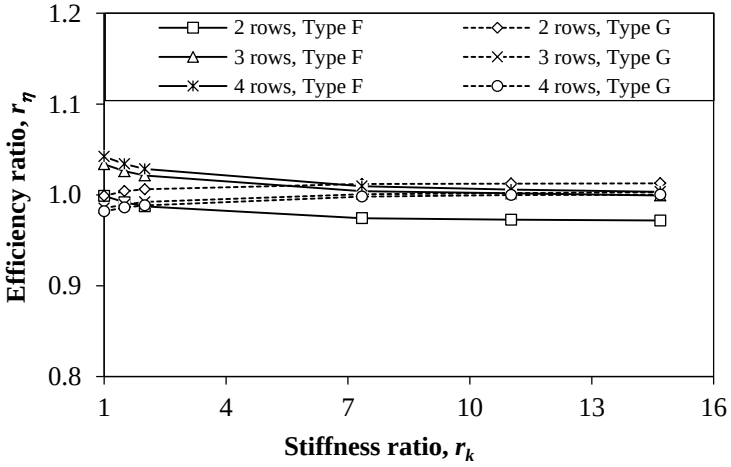

(c) Type F and Type G (Different *e/d* ratio)

Figure 2.10: Effect of geometric parameters on efficiency

Table 2.4: Change of efficiency Δη (%) with the change of geometric parameters

Number of rows		n=2		n=3		n=4	
Cover plate		FRP	Steel	FRP	Steel	FRP	Steel
Δ(*w/d*)	+1	0~2	3	3~5	7	6	9
	-1	0~-1	-5	-5~-7	-9	-9	-11
Δ(*p/d*)	+1	0~-1	-3	-3	-4	-4	-5
	-1	0~2	4	3~6	7	4~6	7

By using the efficiency, the capacity of a connection is examined. It is assumed that the capacity of a multi-row bolted connection is reached when a load on the bolt row that has the maximum load distribution coefficient among rows reaches the capacity of a single bolt connection. Again, a linear elastic behavior of the connection is assumed. In this case, the capacity can be evaluated as the efficiency of a connection multiplied by the number of bolt rows in the connection as shown in Eq. (2.6):

$$Q = n\eta \tag{2.6}$$

where Q = capacity of a connection with respect to a single bolt connection. Therefore, the capacity can be directly evaluated from the efficiency, and they have the same physical meaning. Substituting Eq. (2.4) into Eq. (2.6) and with some arrangements, Eq. (2.6) can be rewritten as:

$$Q = \frac{1}{C_{\max}} \tag{2.7}$$

Figure 2.11 shows the capacity in relation with the stiffness ratio for Type B connections. It can be observed that the capacity of the connections in the range of a low stiffness ratio, i.e., connections with FRP cover plates, decreases sharply with the increase of stiffness ratio, whereas the capacity of the connections for a higher stiffness ratio, i.e., those with steel cover plates, does not change with the change of the stiffness ratio. It is also observed that increasing the number of rows, more than three, in a connection with steel cover plates does not increase its capacity significantly. On the other hand, the number of rows can

be increased to increase the capacity in a connection with FRP cover plates. The capacity of two, three and four-row bolted connections with FRP cover plates having a half of the main plate thickness are equal to 2.0, 2.69, and 3.08, respectively.

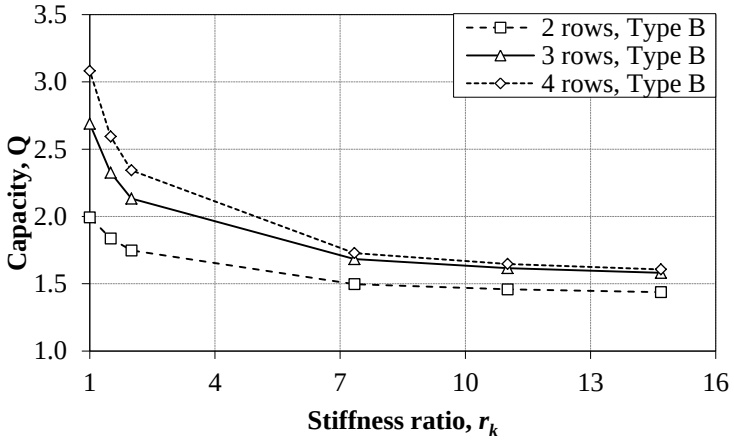

Figure 2.11: Effect of stiffness ratio on capacity

2.4 Summary

The present study investigates the effect of different thicknesses of steel and FRP cover plates on the load distribution among bolt rows of bearing-type multi-row bolted connections for FRP composite structures. The study also includes the influence of connection geometry on the load distribution as well as the efficiency and capacity of connections. Connections with a double-lap configuration up to four rows of bolts subjected to tensile loads have been studied numerically. The following remarks can be made based on the results from the analysis of the connection with a 12 mm thick FRP main plate and the FRP material is assumed to be perfectly brittle.

In bearing-type multi-row bolted connections of FRP structural members, load distribution coefficients are affected by cover plate stiffness. The coefficients of the first and the last rows are affected significantly with the change of cover plate stiffness, while those of intermediate rows are insensitive. However, load distribution coefficients do not change much when the stiffness ratio of cover plates to the main plate becomes greater than 7. Therefore,

the load distribution is insensitive to the cover plate thickness when a connection has steel cover plates.

Efficiency as well as capacity of a connection is significantly affected by the cover plate stiffness. The efficiency of the connection with FRP cover plates is larger than that with steel cover plates. The efficiency of two, three and four-row bolted connections with the FRP cover plate having a half of the main plate thickness are equal to 1.00, 0.90 and 0.77, respectively, whereas the efficiency of those connections with the same thickness of steel cover plate are equal to 0.72, 0.53 and 0.40, respectively.

The capacity of a connection is largely affected by the cover plate thickness. However, the capacity does not change much when the stiffness ratio increases at a large stiffness ratio. Moreover, the capacity cannot be increased by increasing the number of rows when the number of rows is more than three in a connection with steel cover plates.

CHAPTER 3 PROGRESSIVE DAMAGE ANALYSIS OF MULTI-ROW BOLTED CONNECTIONS

3.1 Background

The aim of this chapter is to determine the effect of cover plate stiffness on the strength and failure mode of bearing type multi-row bolted connection. The study also includes the effect of bolt-hole position error on the ultimate strength and failure mode. The bearing-type multi-row bolted connections where load does not distribute uniformly among the bolts due to the relative displacement of the cover plates to the main plate. The load distribution among the bolt rows may change due to the bolt-hole position error. In a bearing-type bolted connection, the load would be re-distributed among the bolts due to the plastic deformation of a ductile material. Therefore, the load distribution does not affect the ultimate strength of the connection with the ductile material. However, for a connection of brittle of the material like FRP, the ultimate strength is significantly affected by the load distribution among the bolts.

Since FRP composites are generally orthotropic and heterogenous, the design of structural components and connections is much more complex than with conventional structural materials such as steel which are isotropic and homogenous. A number of parameters for a bolted connection need to be investigated to understand the mechanical behavior of bolted connection of FRP composite structural members. The parametric study through experiments can be very costly to understand the mechanical behavior of the connection. As a result, a numerical investigation is needed. Several researches were carried out to develop a finite element model of progressive damage with different failure criteria FRP bolted connections (Dano et al., 2000; Olmedo and Santiuste, 2012; Chang and Lessard, 1991; Hassan, 1995; Zhang et al., 2014; Camanho and Matthews, 1999; Kishore et al., 2009). Most of current finite element models are in two dimensions where the third directional effect

is neglected. Numerous researchers have proposed material property degradation rules where the stiffness of material is rapidly reduced after the material failure. Those degradation rules would lead to numerical problems since the elements that have failed to lose their stiffness abruptly, and the analysis stops before the ultimate strength. In practice, finite element analyses often stop before the ultimate strength is reached due to large deformation. In the present study, an implicit 3D finite element model is developed to analyze progressive damage of a bolted connection. To overcome convergence, a progressive material model is specified to gradually decrease the stiffness after the failure of the material. In addition, a viscous regularization is included to further reduce a convergence problem in the analysis.

3.2 Materials and Methods

3.2.1 Connection Geometry

The finite element model of a bolted connection is described in the Section 2.2.3. Thicknesses of the FRP main plate and cover plates are the same as those described in Section 2.2.2. Diameters of a steel bolt and bolt hole are also the same as those described in Section 2.2.1. The thickness of steel cover plate is 6 mm used in the analysis.

The geometric parameters examined in this study are shown in Table 3.1. Based on the geometric parameters, the connections are classified into seven types: Type B, Type E, Type H, Type I, Type J, Type K, and Type L. Type B satisfies the minimum requirements by LRFD Pre-standard (ASCE, 2010).

Table 3.1: Geometric parameters

Type	B	E	H	I	J	K	L
w/d	4.0	5.0	6.0	6.0	6.0	6.0	6.0
p/d	4.0	4.0	4.0	3.0	5.0	4.0	4.0
e/d	2.0	2.0	2.0	2.0	2.0	2.5	1.5

3.2.2 Material Properties

Quasi-isotropic glass-fiber laminates are assumed. A thickness of each ply is 0.375 mm, and a stacking sequence is symmetric in each laminate. Material properties of unidirectional lamina are given in Table 3.2.

Table 3.2: Material properties of FRP unidirectional lamina (Kishore et al., 2009)

E_{11} (MPa)	E_{22} (MPa)	E_{33} (MPa)	ν_{12}	ν_{13}	ν_{23}	G_{12} (MPa)	G_{13} (MPa)	G_{23} (MPa)
26000	6000	6000	0.3	0.3	0.49	3120	3120	2000
X_T (MPa)	X_C (MPa)	Y_T (MPa)	Y_C (MPa)	Z_T (MPa)	Z_C (MPa)	S_{12} (MPa)	S_{13} (MPa)	S_{23} (MPa)
500	300	22.5	60	22.5	60	45	45	30

Steel bolts and plates are assumed to be stainless steel properties of which are shown in Table 3.3. A stress-stain relationship of the stainless steel used in this study is the one specified by the following equation (BSI, 2006):

$$\varepsilon = \begin{cases} \dfrac{\sigma}{E} + 0.002\left(\dfrac{\sigma}{f_y}\right) & \text{for } \sigma \le f_y \\ 0.002 + \dfrac{f_y}{E} + \dfrac{\sigma - f_y}{E_y} + \varepsilon_u\left(\dfrac{\sigma - f_y}{f_u - f_y}\right)^{\mathrm{m}} & \text{for } \sigma > f_y \end{cases} \tag{3.1}$$

where *n* is coefficient defined as $n = \dfrac{\ln(20)}{\left(f_y / R_{p0.01}\right)}$, in which $R_{p0.01}$ is the 0.01% proof stress, E_y is a tangent modulus of the stress-strain curve at the yield strength defined as $E_y = \dfrac{E}{1 + 0.002nE / f_y}$, ε_u is the ultimate strain, corresponding to the tensile strength f_u which may be approximated by equation $1 - \dfrac{f_y}{f_u}$, but $\varepsilon_u \le A$ where A is the elongation after facture defined EN 10088, and *m* may be determined as $m = 1 + 3.5\dfrac{f_y}{f_u}$.

The initial part of the curve is assumed to be linear up to 0.01% proof stress ($R_{0.01}$). The stress-strain curve of the stainless steel is shown Figure 3.1.

Table 3.3: Material properties of stainless steel

Component	E (GPa)	ν	$R_{0.01}$ (MPa)	f_y (MPa)	f_u (MPa)	n
Plate	200	0.3	125	205	520	6
Bolt	200	0.3	250	450	700	5

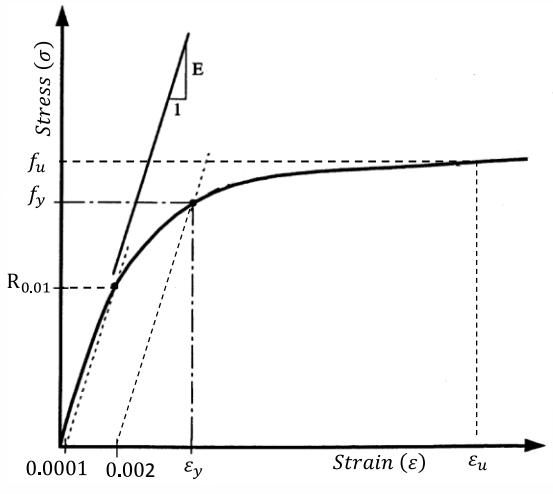

Figure 3.1: Stress-strain curve of stainless steel

3.2.3 Sampling

Effect of bolt-hole position errors on the strength of bolted connections was studied. Latin Hypercube sampling technique is adopted to generate the bolt-hole position error for simplicity and accuracy. The Latin Hypercube sampling was first proposed by McKay et al. (1979). The Latin Hypercube sampling technique can be described as the cumulative probability distribution functions (CPDF) for all random variables are divided into *N* intervals of equal probability and then centroids of intervals are used in the simulation process. The samples can be determined by using the formula

$$x_{i,k} = F_i^{-1}\left(\frac{k-0.5}{N}\right) \tag{3.2}$$

where $x_{i,k}$ is the *k*-th sample of the *i*-th variable X_i , and F_i^{-1} is the inverse CPDF for variable X_i.

The representative parameters of variables are selected randomly based on random

permutations of integers 1, 2, ... N. Every interval of each variable will be used only once during the simulation. Fifty simulations are performed for each connection in this study. The bolt-hole position errors are assumed to be normally distributed with a mean value of 0.00 mm and a standard deviation of 0.17 mm for all bolt holes. In the Latin Hypercube sampling, 50 intervals are used.

3.3 Damage Growth

3.3.1 Failure Criteria

Many failure criteria such as the Hashin (1980) failure criterion, the Chang and Lessard (1991) failure criterion, the Tsai-Wu (1971) tensor failure criterion, and the Hill (1948) failure criterion have been proposed to date to judge the damage of FRP composites. In this study, the failure criterion by Chang and Lessard (1991) is modified to propose a set of failure criteria. Two principal failures are considered: a) fiber failure and b) matrix failure. A fiber failure criterion is specified differently depending on compression or tension. The failure modes are predicted by the following criteria:

a) Fiber failure criterion:

Fiber failure occurs when the failure index, $F_{ft,}$ reaches 1.0.

For the fiber tension $\left(\hat{\sigma} \geq 0\right)$,

$$F_{ft} = \left(\frac{\hat{\sigma}_{11}}{X_T}\right)^2 + \frac{\frac{\hat{\tau}_{12}^2}{2G_{12}^2} + \frac{3}{4}\alpha\hat{\tau}_{12}^4}{\frac{S_{12}^2}{2G_{12}^2} + \frac{3}{4}\alpha S_{12}^4} + \frac{\frac{\hat{\tau}_{13}^2}{2G_{13}^2} + \frac{3}{4}\alpha\hat{\tau}_{13}^4}{\frac{S_{13}^2}{2G_{13}^2} + \frac{3}{4}\alpha S_{13}^4} \tag{3.3}$$

For the fiber compression $\left(\hat{\sigma} < 0\right)$

$$F_{ft} = \left(\frac{\hat{\sigma}_{11}}{X_C}\right)^2 \tag{3.4}$$

X_T and X_C denote tensile strength and compressive strengths in the 11 and 22 direction, respectively. S_{ij} and G_{ij} are shear strength and shear modulus in the *ij* plane, respectively. α is a parameter representing the nonlinear relationship of the shear strain and shear stress, the value of 1.9×10^{-6} is used in this study (Khashaba at al., 2013). $\hat{\sigma}_{ii}$ is the effective stress defined as $\hat{\sigma}_{ii}=\sigma_{ii}/(1-d_I)$, and $\hat{\tau}_{ij}$ is the effective shear stress defined as $\hat{\tau}_{ij}=\tau_{ij}/(1-d_{ij})$.

b) Matrix failure criterion:

Matrix failure occurs when the failure index, $F_{m,}$ reaches 1.0.

$$F_m=\left(\frac{\hat{\sigma}_{22}}{Y}\right)^2-\frac{\hat{\sigma}_{22}\hat{\sigma}_{33}}{YZ}+\left(\frac{\hat{\sigma}_{33}}{Z}\right)^2+\frac{\frac{\hat{\tau}_{12}^2}{2G_{12}^2}+\frac{3}{4}\alpha\hat{\tau}_{12}^4}{\frac{S_{12}^2}{2G_{12}^2}+\frac{3}{4}\alpha S_{12}^4}+\frac{\frac{\hat{\tau}_{13}^2}{2G_{13}^2}+\frac{3}{4}\alpha\hat{\tau}_{13}^4}{\frac{S_{13}^2}{2G_{13}^2}+\frac{3}{4}\alpha S_{13}^4}+\frac{\frac{\hat{\tau}_{23}^2}{2G_{23}^2}+\frac{3}{4}\alpha\hat{\tau}_{23}^4}{\frac{S_{23}^2}{2G_{23}^2}+\frac{3}{4}\alpha S_{23}^4} \tag{3.5}$$

where

$$Y=\begin{cases}Y_T & \text{for } \sigma_{22}\geq 0\\ Y_C & \text{otherwise}\end{cases} \quad \text{and} \quad Z=\begin{cases}Z_T & \text{for } \sigma_{33}\geq 0\\ Z_C & \text{otherwise}\end{cases}$$

Y_T and Z_T denote tensile strengths, and Y_C and Z_C denote compressive strengths in the respective directions.

3.3.2 Damaged Material Response

In the progressive damage theory, material degradation is defined as the development of voids, defects or micro cracks, which reduce the effective volume of the material. Subsequently, the material reduces its strength. In this study, the effect of damage is taken into account by reducing the values of stiffness coefficients. In the model, the relationship between the stress, σ, and the strain, ε, is postulated to have the form:

$$\varepsilon=MC_0\sigma \tag{3.6}$$

where C_0 is the compliance matrix without damage, and *M* is the damage operator suggested by Matzenmiller et al. (1995) to compute degraded coefficients of the compliance matrix. The damage operator can be expressed by the following equation:

$$M = \begin{bmatrix} \frac{1}{(1-d_f)} & 0 & 0 & 0 & 0 & 0 \\ 0 & \frac{1}{(1-d_m)} & 0 & 0 & 0 & 0 \\ 0 & 0 & \frac{1}{(1-d_m)} & 0 & 0 & 0 \\ 0 & 0 & 0 & \frac{1}{(1-d_{12})} & 0 & 0 \\ 0 & 0 & 0 & 0 & \frac{1}{(1-d_{13})} & 0 \\ 0 & 0 & 0 & 0 & 0 & \frac{1}{(1-d_{23})} \end{bmatrix} \tag{3.7}$$

where, d_f is fiber damage index, d_m is matrix damage index and d_{12}, d_{13}, and d_{23} are shear damage indices with respective planes. Van Der Meer and Sluys (2009) proposed the matrix damage index equal to the shear damage index. It means that shear properties are not affected by the fiber damage. Lapczyk and Hurtado (2007) proposed the shear damage index, d_{12}, which is equal to $1-(1-d_f)(1-d_m)$ as a combination of matrix damage and fiber damage. In the present study, the shear damage index is taken as larger value of the fiber and matrix damage indices. Moreover, the maximum shear damage is considered to be 80% for the case of d_{13} and d_{23} to avoid a convergence problem in the analysis. The fiber and matrix damage indices are described in Section 2.3.1 in detail.

3.3.3 Damage Evaluation

Once a failure criterion is satisfied, further loading will cause degradation of material stiffness coefficients. The reduction of the stiffness coefficients is controlled by damage indices that have a value between zero and one. This growth law is a generalization of the approach by Camanho and Dávila (2002) that was originally proposed to model interlaminar delamination using cohesive elements.

Each damage index is evaluated by using an equivalent strain. Equivalent strains and stresses for different failure modes are listed in Table 3.4. The damage index d_I for each failure mode *I* can be expressed by the following relation:

$$d_I = \frac{\varepsilon_{I,eq}^F\left(\varepsilon_{I,eq}^{\max} - \varepsilon_{I,eq}^0\right)}{\varepsilon_{I,eq}^{\max}\left(\varepsilon_{I,eq}^F - \varepsilon_{I,eq}^0\right)};\ \ \varepsilon_{I,eq}^0 \le \varepsilon_{I,eq}^{\max} \le \varepsilon_{I,eq}^F;\ \ \varepsilon_{I,eq}^{\max} = \max\left(\varepsilon_{I,eq}^{\max}, \varepsilon_{I,eq}\right);\ \ I \in \{ft, fc, m\} \qquad (3.8)$$

where $\varepsilon_{I,eq}^0$ is the equivalent strain at which the failure criterion becomes 1.0 the damage initiates for the failure mode *I* and $\varepsilon_{I,eq}^F$ is the equivalent strain at which the damage index becomes 1.0. Lapczyk and Hurtado (2007) proposes $\varepsilon_{I,eq}^F$ that is a function of fracture energy and equivalent stress. In the present study, $\varepsilon_{I,eq}^F$ is assumed to be $10^{10}\varepsilon_{I,eq}^0 / L_c$ to keep the constant equivalent stress equal to the equivalent stress, $\sigma_{I,eq}^0$, of the damage initiation in order to avoid a severe convergence problem in finite element analysis. A characteristic length, L_c, is used to eliminate the mesh dependency on the damage index and it can be calculated as the cubic root of the volume of an element. The equivalent stress-strain relationship is explained in Figure 3.2. The equivalent stress-strain relationship is linear up to the damage initiation point A. After Point A, the equivalent stress is constant up to Point C where the damage index is 0.95, and that the damage index is assumed to be 1.0. In the case of unloading and loading at a partially damaged state, such as Point B in Figure 3.2, the equivalent stress-strain follows a linear path toward the origin O, and the same path is followed back to Point B upon reloading as shown in the figure. Lapczyk and Hurtado (2007) indicate that the equivalent stress and strain will follow the equivalent stress-strain curve shown in Figure 3.2 in the case of one dimensional problem. However, for the three dimensional stress and strain states, the equivalent stress after the damage initiation at Point A may not remain constant at $\sigma_{I,eq}^0$, except for the case that the strain components proportionally increase or decrease from those at Point A.

Table 3.4: Definition of equivalent strain and stress

Failure mode	Equivalent strain ($\varepsilon_{I,eq}$)	Equivalent stress ($\sigma_{I,eq}$)
Fiber failure	$\sqrt{(\varepsilon_{11})^2 + (\gamma_{12})^2 + (\gamma_{13})^2}$	$\frac{\sigma_{11}\varepsilon_{11} + \tau_{12}\gamma_{12} + \tau_{13}\gamma_{13}}{\varepsilon_{ft \text{ or } fc,eq}}$
Matrix failure	$\sqrt{(\varepsilon_{22})^2 + (\varepsilon_{33})^2 + (\gamma_{12})^2 + (\gamma_{13})^2 + (\gamma_{23})^2}$	$\frac{\sigma_{22}\varepsilon_{22} + \sigma_{33}\varepsilon_{33} + \tau_{12}\gamma_{12} + \tau_{13}\gamma_{13} + \tau_{23}\gamma_{23}}{\varepsilon_{m,eq}}$

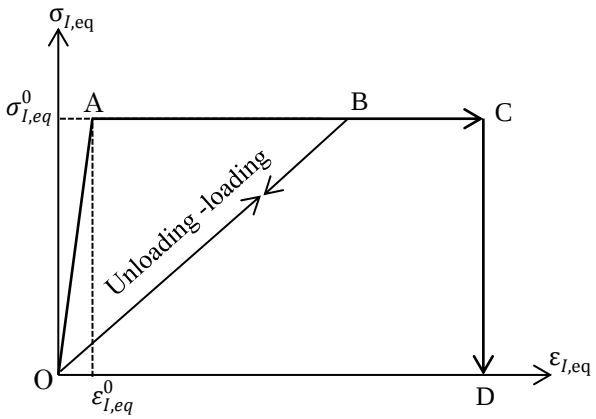

Figure 3.2: Equivalent stress-strain curve

3.3.4 Mesh Dependency

When the material shows strain-softening behavior, leading to strain localization, then the amount of dissipated energy depends on the element size in the finite element analysis, and it approaches zero for infinitesimally small elements. In the current model, the characteristic length is introduced at a material point, which is equal to the cubic root of the volume associated with it. Although, it does not solve completely the mesh dependency, this approach can reduce the effect.

3.3.5 Viscous Regularization

A generalized viscous regularization scheme (Duvaut and Lions 1976) is introduced to overcome convergence difficulties led by material softening behavior and stiffness degradation in an implicit analysis. In the regularization scheme, a viscous damage variable is

defined as

$$\dot{d}_{i,eq}^{\nu} = \frac{1}{\eta_i}\left(d_i - d_i^{\nu}\right) \tag{3.9}$$

η_i is the viscosity coefficient representing the viscous system relaxation time, and d_i is the damage variable evaluated in the inviscid backbone model. In the present analysis, the viscosity coefficient, η_i, for fiber damage is used 0.001 and for matrix damage is 0.005 (Lapczyk and Hurtado, 2007). The regularized damage variable is updated as:

$$d_i^{\nu}\Big|_{t_0+\Delta t} = \frac{\Delta t}{\eta_i + \Delta t} d_i\Big|_{t_0+\Delta t} + \frac{\Delta t}{\eta_i + \Delta t} d^{\nu}\Big|_{t_o} \tag{3.10}$$

The damaged response of the viscous material is given as $\sigma = D\left(d^{\nu}\right)\varepsilon$. A small viscosity parameter usually helps improve the rate of convergence of the model in a softening scheme without compromising results.

3.3.6 Model Implementation

The progressive model is implemented in Abaqus (Dassault Systèmes, 2011), through a user subroutine UMAT. The failure criteria, material degradation model, and stress updating procedure are contained in the subroutine. Figure 3.3 shows a flow chart of the subroutine UMAT.

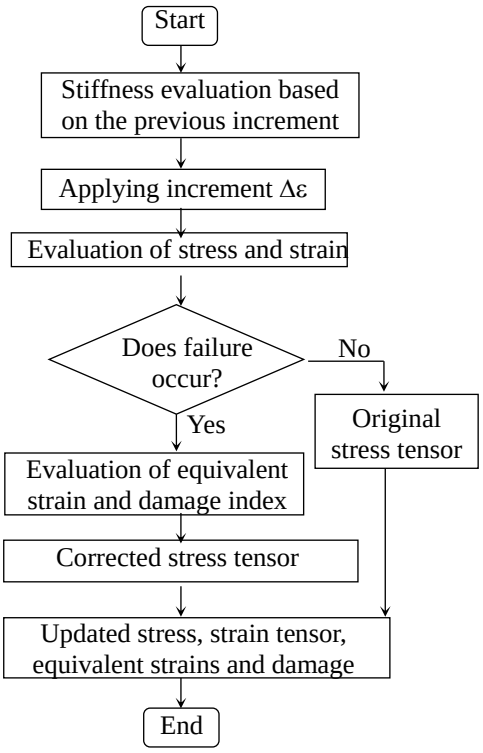

Figure 3.3: Flow chart of the subroutine UMAT

A strain increment is passed into the subroutine, and stresses are evaluated based on stiffness to be used in the failure criteria. Once a failure occurs, then, the damage index is evaluated to correct stress tensor. Damage propagation in an increment is absent, the damaged elasticity matrix does not change at the increment, and therefore the response of the material is linearly elastic. In general, however, the values of damage indices will change in an increment, and the contribution of these terms must be taken into account. The equivalent strains $\varepsilon_{I,eq}^{0}$ at the onset of damage are computed only once when the failure criteria are first satisfied; their values are stored and reused in subsequent iterations. Finally, the stress and strain tensors, equivalent strains and damage indices are updated.

3.3.7 Model Validation

In order to verify the progressive model and failure criteria, single pin connections of GFRP members tested by Khashaba et al. (2013) under a tensile loading have been analyzed. The connections were pin-bearing connections. Figure 3.4 shows the geometry of a GFRP

plate. Material properties are given in Table 3.5. The thickness of each lamina is 0.4 mm and stacking sequences examined are $[0^o/90^o]_{2s}$, $[15^o/-75^o]_{2s}$, $[30^o/-60^o]_{2s}$, and $[45^o/-45^o]_{2s}$. Steel pin and steel cover plates are used, and they are considered to be an elastic material with Young's modulus E of 200 GPa and Poisson's ratio ν of 0.3.

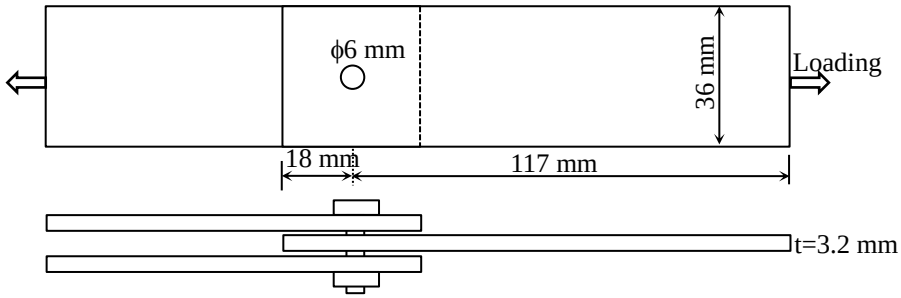

Figure 3.4: Geometry of the connections

Table 3.5: Material properties of unidirectional FRP lamina

E_{11} (MPa)	E_{22} (MPa)	E_{33} (MPa)	ν_{12}	ν_{13}	ν_{23}	G_{12} (MPa)	G_{13} (MPa)	G_{23} (MPa)
32,100	5,740	5,740*	0.33	0.33*	0.33*	1,240	1,240*	1,240*
X_T (MPa)	X_C (MPa)	Y_T (MPa)	Y_C (MPa)	Z_T (MPa)	Z_C (MPa)	S_{12} (MPa)	S_{13} (MPa)	S_{23} (MPa)
722.0	230.0	14.0	34.0	14.0*	34.0*	54.6	54.6*	54.6*

* assumed value

Three-dimensional finite element models of connections are created in Abaqus. Frictionless contact is used between the FRP main plate and steel cover plates. However, a friction coefficient of 0.1 is considered at bolt holes between FRP and bolt (Khashaba et al., 2013).

Figure 3.5 shows the predicted failure modes for different stacking sequences. The red color indicates failure of elements by their respective failure mode. The shear-out failure mode appears the connection with $[0^o/90^o]_{2s}$ stacking sequence. The staking sequence $[30^o/-60^o]_{2s}$ also shows the shear-out failure mode but with a different angle. The shear out failure mode also appears at layer 15^o due to fiber failure in the laminate $[15^o/-75^o]_{2s}$

but the other layers seem to be a cleavage failure. Bearing failure mode is found in the laminate $[45^o/-45^o]_{2s}$ at layer 0^o and 90^o with a tendency to net tension. From the finite element analysis, failure mode of the connection with stacking sequence $[45^o/-45^o]_{2s}$ is found to be bearing whereas the connection with stacking sequences $[0^o/90^o]_{2s}$, $[15^o/-75^o]_{2s}$, and $[30^o/-60^o]_{2s}$ are found to be shear-out, and these failure modes are in good agreement with those found in the experiment.

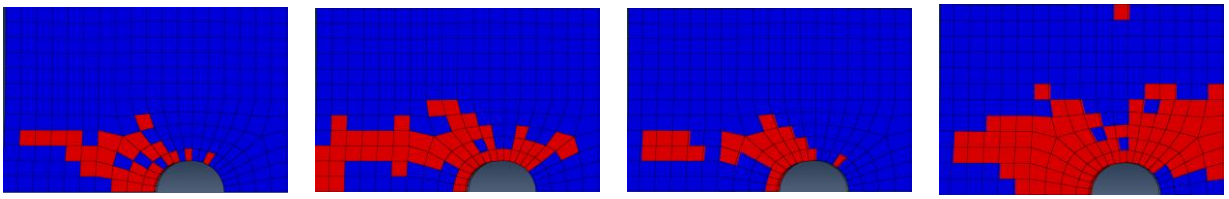

i) Fiber failure in 0^o layer ii) Matrix failure in 0^o layer iii)Fiber failure in 90^o layer iv)Matrix failure in 90^o layer

(a) $[0^o/90^o]_{2s}$

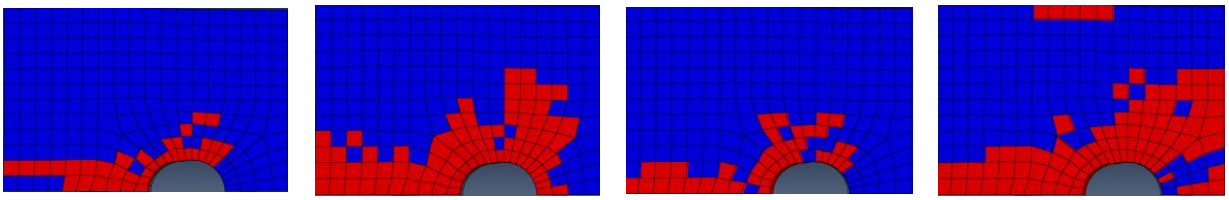

i) Fiber failure in 15^o layer ii) Matrix failure in 15^o layer iii)Fiber failure in -75^o layer iv)Matrix failure in -75^o layer

(b) $[15^o/-75^o]_{2s}$

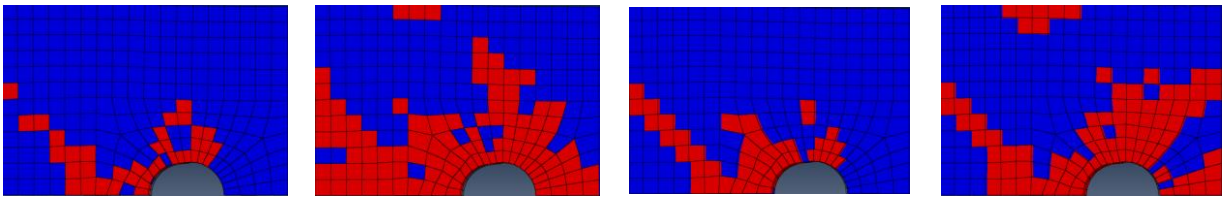

i) Fiber failure in 30^o layer ii) Matrix failure in 30^o layer iii)Fiber failure in -60^o layer iv)Matrix failure in -60^o layer

(c) $[30^o/-60^o]_{2s}$

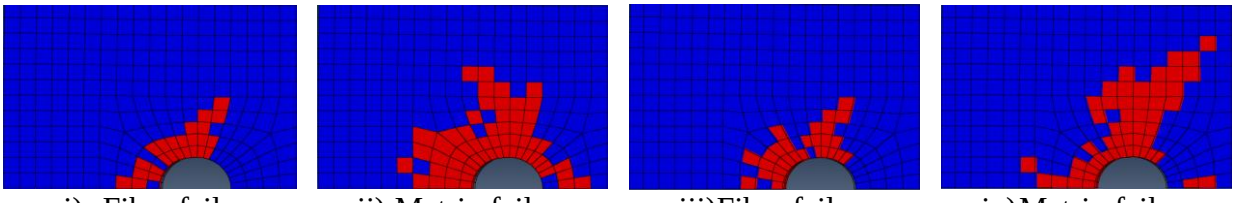

i) Fiber failure in 45^o layer ii) Matrix failure in 45^o layer iii)Fiber failure in -45^o layer iv)Matrix failure in -45^o layer

(d) $[45^o/-45^o]_{2s}$

Figure 3.5: Predicted failure modes for connections with different stacking sequences

The load-displacement relationships of connections for different stacking sequences are compared with experimental results in Figure 3.6. From the figure, it is observed that initial stiffness and ultimate strength are in good agreement with experimental results for the connection with stacking sequence $[45^o/-45^o]_{2s}$. The error in ultimate strength is about 2.0%. However, initial stiffnesses in the cases of $[0^o/90^o]_{2s}$, $[15^o/-75^o]_{2s}$, and $[30^o/-60^o]_{2s}$ are very different from the experimental results. Causes of this difference have not yet been determined. However, the initial damage is predicted at similar loading level to those of the experiment, and the ultimate strengths are predicted relatively well. The maximum difference between the experimental and the analytical ultimate strengths is about of 12% among four different stacking sequences.

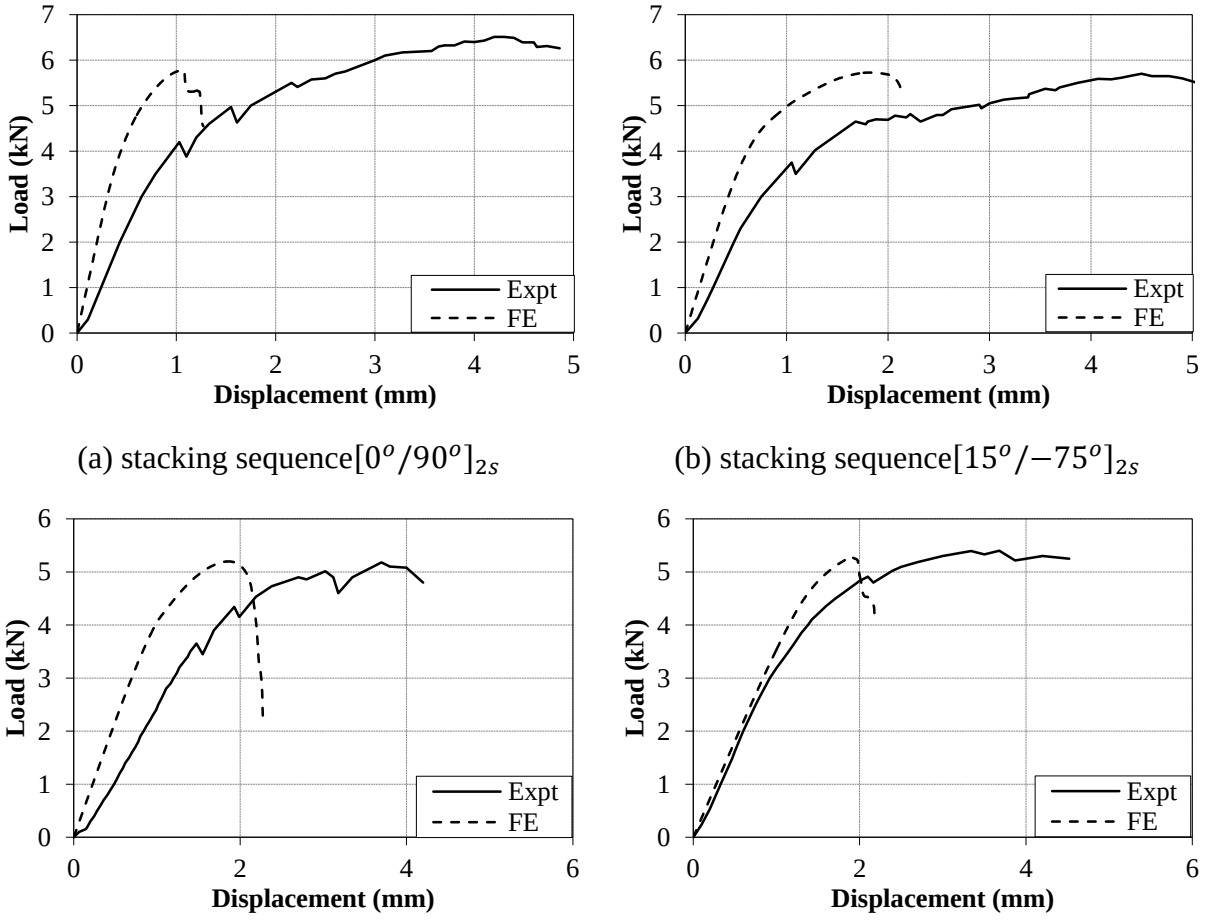

(a) stacking sequence$[0^o/90^o]_{2s}$ (b) stacking sequence$[15^o/-75^o]_{2s}$

(c) stacking sequence$[30^o/-60^o]_{2s}$ (d) stacking sequence$[45^o/-45^o]_{2s}$

Figure 3.6: Load-displacement relationship of the connections

3.4 Results and Discussions

3.4.1 Load Displacement

Progressive damage analyses are performed to determine the effect of cover plate stiffness on the strength of multi-row bolted connection of FRP structural members. Different geometric parameters examined in this study are shown in Table 3.1. The load-displacement relationships of the connection Type H for 2 to 4 rows are shown in Figure 3.7. Relative displacement of the cover plate to the main plate is measured between the ends, load and displacement values shown in the figure are those for a whole connection, and they are obtained by multiplying the values of load and displacement of the one eighth model by 4 and 2, respectively. Load begins to increase at the displacement of 2 mm due to the initial clearance of the holes.

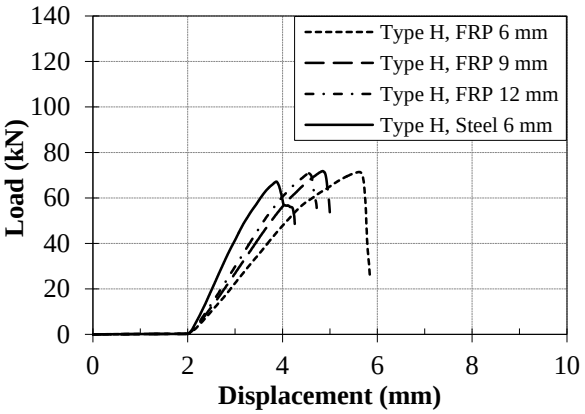

(a) Two-row bolted connections

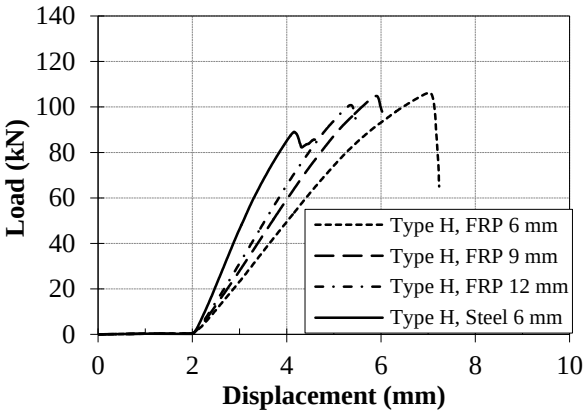

(b) Three-row bolted connections

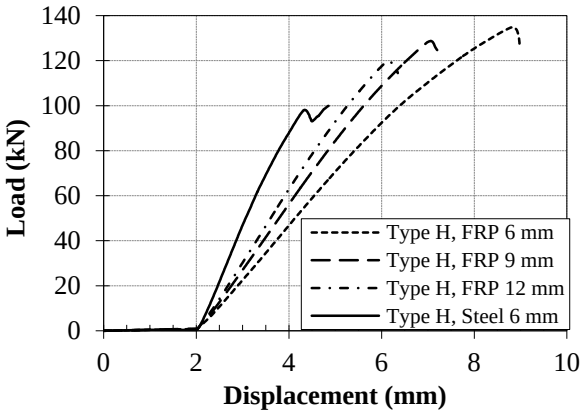

(c) Four-row bolted connections

Figure 3.7: Load-displacement relationship of Type H connections

It is observed from Figure 3.7 that the stiffness of a connection increases with of FRP cover plate thickness and that the connections with steel cover plates has larger stiffness than those with FRP cover plates. It is also observed that the connection with 6 mm FRP cover plates has the largest ultimate load among different plates. It is because the load in the first row is larger than the other rows as shown in Figure 3.8 (b), and the first row sheds the load to the other rows after ultimate load of the first row. The ultimate load of a bolt is that load when load is decreased with displacement of the connection. However, the trend is different for the connections with FRP cover plates, because the load in the first row and the last row are close to each other, and these rows fail at almost the same time as shown in Figure 3.8 (a). Bearing failure started at the load of 22 kN as these rows, and the hole is completely damaged at the load of 32 kN. It can be observed that the bearing failure is initiated at the load of 76 kN in the connection with 6 mm FRP cover plates while it is at 48 kN in the connection with 6 mm steel cover plates. Bolted connections of two and three row with steel cover plates also showed bearing failure initiation earlier than those with FRP cover plates.

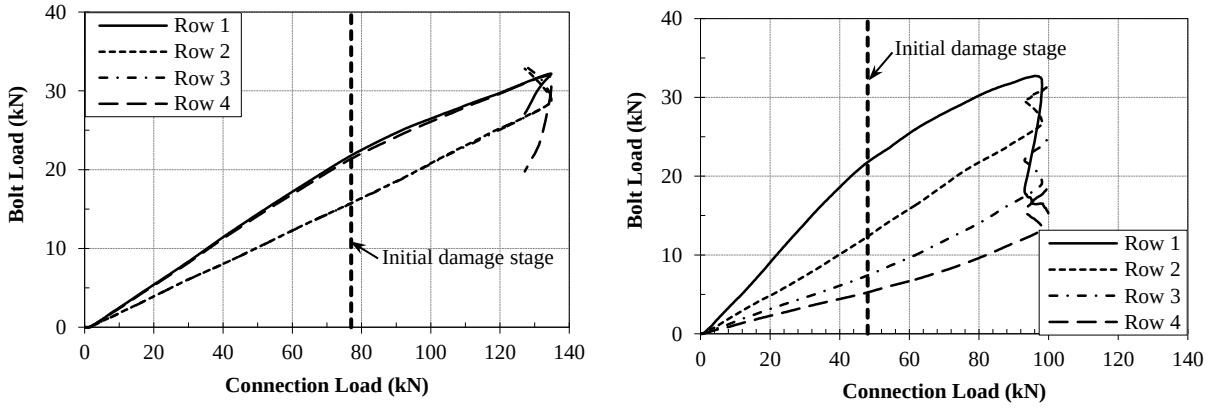

(a) 6 mm FRP cover plate (b) 6 mm steel cover plate

Figure 3.8: Bolt load distribution of four-row bolted connections (Type H)

3.4.2 Failure Mode

Table 3.6 shows the failure modes obtained in the numerical analysis of this study. Two basic failure modes are observed in the analysis: bearing and net-tension. Shear failure was

not observed in the analysis because the 45^{o} fiber used in the laminate increases the shear capacity of the material. Cleavage failure occurred at the end of some connections. The failure modes are judged according to locations of the damaged elements in the connection plates.

Table 3.6: Failure mode of connections

# of rows	Cover plate	Connection type						
		B	E	H	I	J	K	L
1	FRP 6 mm	BF	BF	BF	-	-	BF	EF
	Steel 6 mm	BF	BF	BF	-	-	BF	EF
2	FRP 6 mm	BF	BF	BF	BF	BF	BF	BF, EF
	FRP 12 mm	BF	BF	BF	BF	BF	BF	BF, EF
	Steel 6 mm	BF	BF	BF	BF	BF	BF	BF, EF
3	FRP 6 mm	TF	BF	BF	BF	BF	BF	BF, EF
	FRP 12 mm	TF	BF	BF	BF	BF	BF	BF, EF
	Steel 6 mm	BF	BF	BF	BF	BF	BF	BF, EF
4	FRP 6 mm	TF	TF	BF	BF	BF	BF	BF, EF
	FRP 12 mm	TF	BF	BF	BF	BF	BF	BF, EF
	Steel 6 mm	BF	BF	BF	BF	BF	BF	BF

Note: BF = bearing failure; TF = net-tension failure; EF = end failure (cleavage)

It is observed that the failure mode depends not only on the geometric parameters but also on the stiffness of the cover plate. Failure mode changes from bearing to net-tension failure when the cover plate is changed from 6 mm steel cover plate to 6 mm FRP cover plate for the connection Type B with three and four rows, and the connection Type E with four rows. The same change of failure mode is observed for the four-row connection of Type E when the FRP cover plate thickness is changed from 12 mm to 6 mm. These results imply that a larger stiffness ratio of the bolted connections would lead to a lower ultimate load.

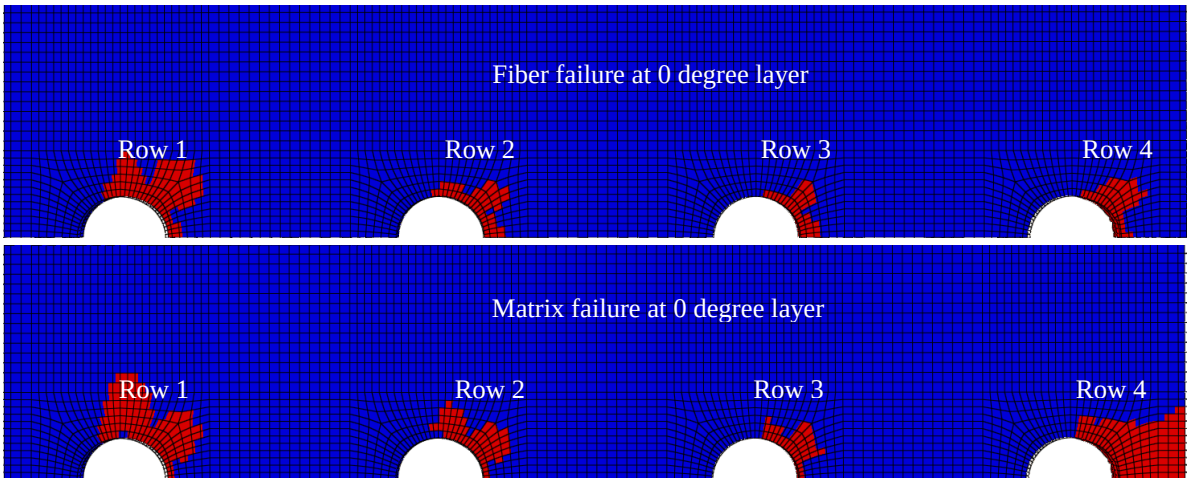

(a) FRP cover plate

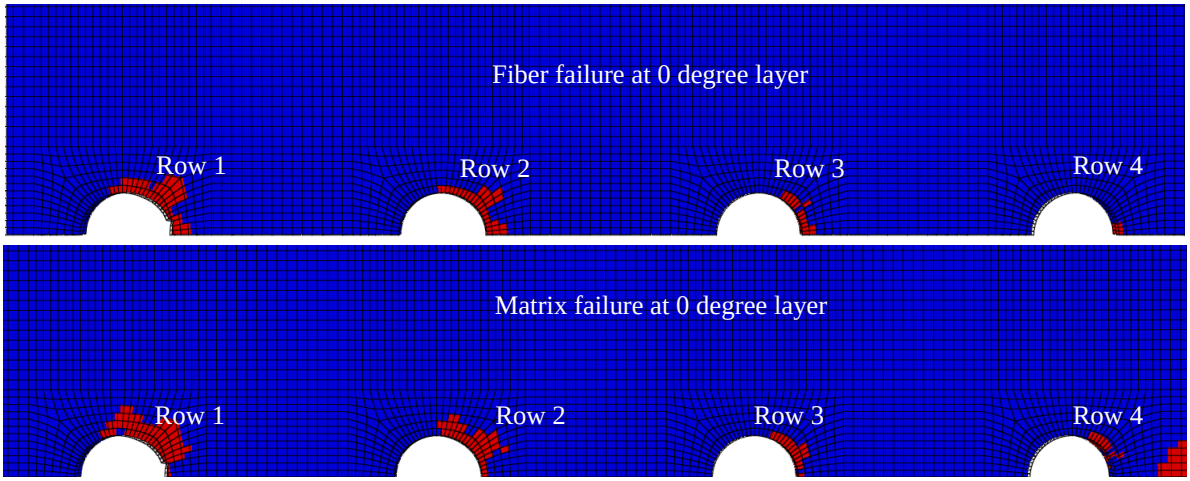

(b) Steel cover plate

Figure 3.9: Failure of four row bolted connections (Type L)

The connection Type L which has a small end distance (e/d =1.5) a showed cleavage failure at the ends of all Type L connections except the four-row bolted connection with steel cover plates. The cleavage failure occurred because a lower load transfer by the last row of bolt compared with the other rows in a multi-row bolted connection with a larger stiffness ratio, which is depicted Figure 3.8. The failed elements in the 0^o layer for each failure mode is indicated by the red color in Figure 3.9. A significant damage occurs at the first and last rows of the connection with FRP cover plates, whereas the connection with steel cover plates showed a significant damage at the first row and successive rows sustained the reduced damage. As a result, a connection with FRP cover plates having a half of the main thickness

needs a larger end distance than a connection with steel cover plates, and the required end distance should be equal to that of a single bolted connection to avoid the end failure. This is reasonable the bearing load at last row of connection with FRP cover plates having a half of the main plate thickness is equal to the bearing load of single bolted connection.

3.4.3 Ultimate Strength

The ultimate strength of a connection is examined according to the stiffness ratio of cover plates to the main plate by using a strength ratio. Strength ratio, r_s, can be defined as the ratio of the strength of a connection to that of a connection with the same geometry and 6 mm FRP cover plates, as shown in the following equation.

$$r_s = \frac{F}{F_{F6.0}} \tag{3.11}$$

where,

F = ultimate strength of a connection,

$F_{F6.0}$ = ultimate strength of the connection with the same geometry and 6-mm FRP cover plates.

The strength ratio of Type H connections for the varying stiffness ratio of cover plates to the main plate is shown in Figure 3.10. It is seen that the strength ratio of a connection decreases with an increase of the stiffness ratio as well as with the number of rows. The change of strength ratio due to the stiffness ratio is not significant for the connections with a stiffness ratio more than 14. For the two, three, and four-row bolted connections with 6-mm steel cover plates, the strength is lower than that of connections with 6 mm FRP cover plates by 6%, 16%, and 26%, respectively. As a result, in terms of the strength, it is better to make the stiffness of two cover plates the same as that of the main plate.

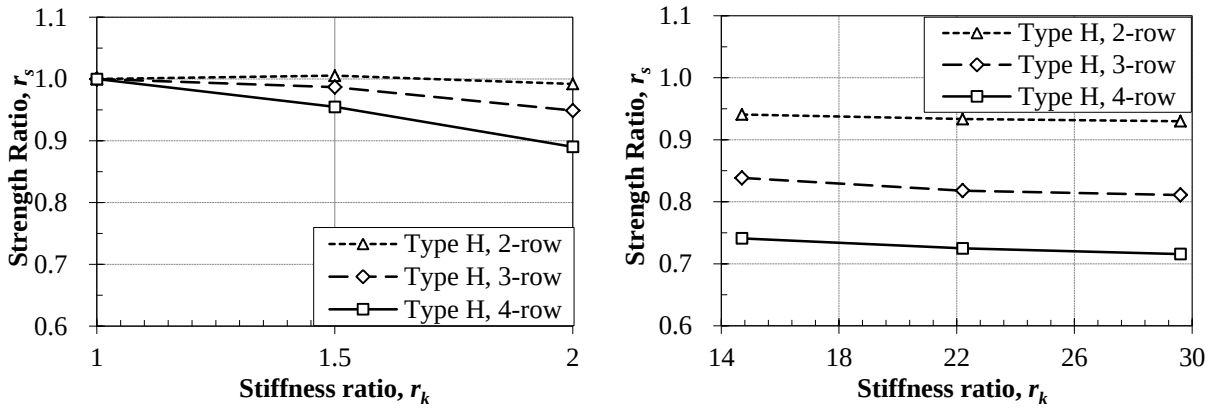

(a) FRP cover plates (b) Steel cover plates

Figure 3.10: Effect of stiffness ratio on ultimate strength

Ultimate capacity, Q_u, is calculated to evaluate the effect of cover plate stiffness on the strength. The ultimate capacity, is defined as a ratio of the ultimate strength of a connection to that of a single bolted connection as expressed in Eq. (3.11):

$$Q_u = \frac{F}{F_{Single}} \tag{3.12}$$

where F_{Single} is the ultimate strength of a single bolted connection with the same main plate thickness.

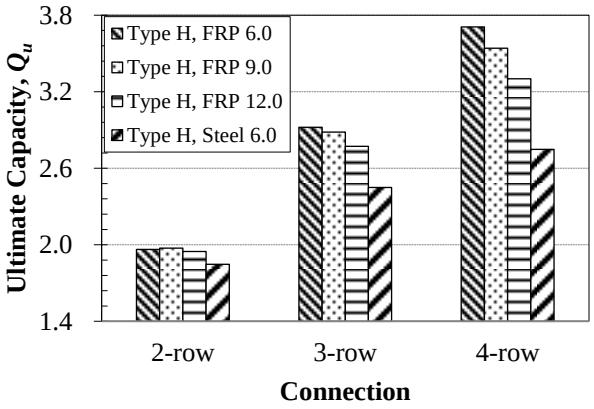

Figure 3.11: Effect of cover plates on ultimate capacity (Type H)

Ultimate capacities of the Type H connections with different cover plates are shown in Figure 3.11. It can be observed that the ultimate capacity of the connections with 6 mm steel

cover plates is lower than the ultimate capacity of the connections with 6 mm FRP cover plates. The difference between the ultimate capacities of connection with steel and FRP cover plates increases with the number of bolt rows. The ultimate capacity of the connections with FRP cover plates having a half thickness of the main plate is increased by about 0.96, 0.96, and 0.75 by increasing a number of rows from 1 to 2, from 2 to 3, and from 3 to 4, respectively, whereas the capacity is increased by about 0.85, 0.60, and 0.30 for the connections with 6 mm thicknesses of steel cover plates. When connections with FRP cover plates of different cover plate thicknesses are compared, the ultimate capacity decreases with the increase of cover plate thickness for three and four-row bolted connections.

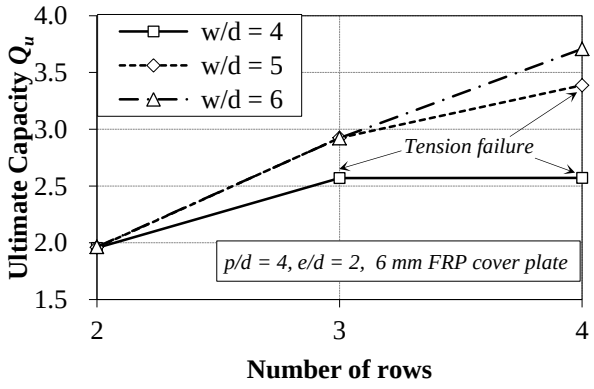

(a) Different *w/d* ratios for FRP cover plates

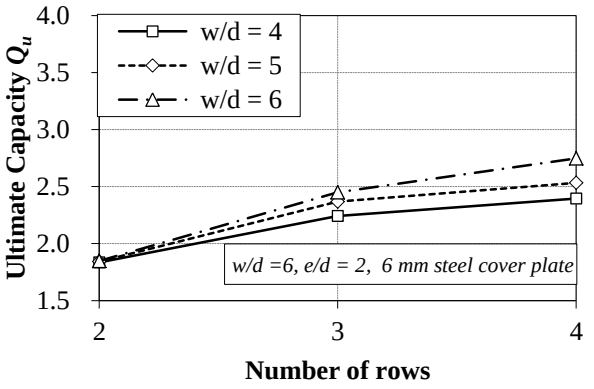

(b) Different *w/d* ratios for steel cover plates

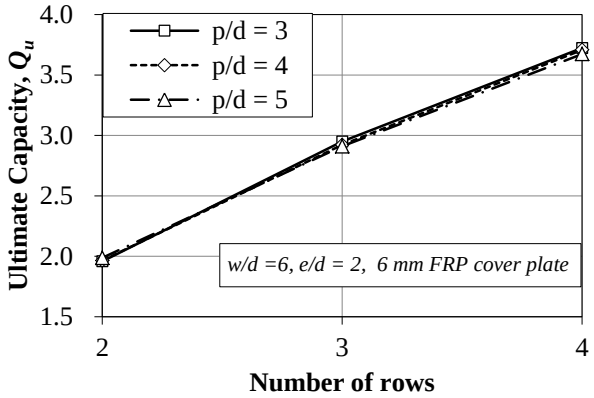

(c) Different *p/d* ratios for FRP cover plates

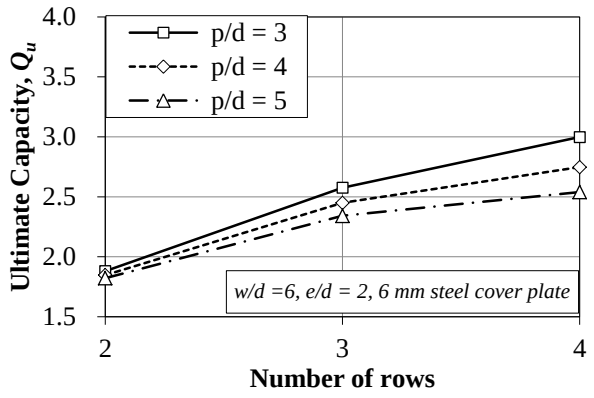

(d) Different *p/d* ratios for steel cover plates

Figure 3.12: Effect of geometry on ultimate capacity

Figure 3.12 shows the ultimate capacities of two, three, and four-row bolted connections

with 6 mm FRP and steel cover plates for different *w/d* ratios and *p/d* ratios to understand how different connection geometries affect the ultimate capacity. It is observed that the effect of *w/d* ratio and *p/d* ratio on the ultimate capacity is significant for the connections with steel cover plates, and that the ultimate capacity is larger for a larger *w/d* ratio and a lower *p/d* ratio. However, the effect of *w/d* ratio and *p/d* ratio on the ultimate capacity in the connections with FRP cover plates is much smaller than those with steel cover plates. It is because the load distribution among the bolts is more uniform for the connection with FRP cover plates than that with steel cover plates. For two, three, and four-row bolted connections with steel cover plates, the ultimate capacity decreases by 0.03, 0.13, and 0.25, respectively, when the *p/d* ratio increases from 3 to 4. On the other hand, for two, three, and four-row bolted connections with steel cover plates, by increasing the *w/d* ratio from 4 to 5, the ultimate capacity increases by 0.01, 0.13, and 0.22 respectively. These comparisons are made based only on the connections with the bearing failure mode. It can be seen in Figure 3.12(a), the three-row connection with *w/d* = 4 and four-row connections with *w/d* = 4 and 5 show much smaller ultimate capacities than corresponding connections with *w/d* = 6 because tension failure occurs in those connections.

3.4.4 Effect of Bolt-Hole Position Error

(a) Load Distribution Among the Bolt Rows

Load distribution among the bolts of the three-row bolted connections with steel and FRP cover plates where there is no error in bolt-hole positions shown in Figure 3.13. To describe the load distribution among the bolts, load of the bolts is shown by the thicker line and bolt load ratios are shown by the thinner line in the figure. The bolt load ratio is defined as a ratio of a bolt load, P_b, to the bolted connection load, P. All bolts in the connections start to carry load at the same time. In the bolted connection with steel cover plates, every bolt carries different loads, where the first bolt takes a higher load than other bolts. However, in

the bolted connection with FRP cover plates, the first and last bolts carry the same load which is higher than that of the intermediate bolt. The closest and farthest bolts to the end of a main plate are designated as the last and first bolts, respectively.

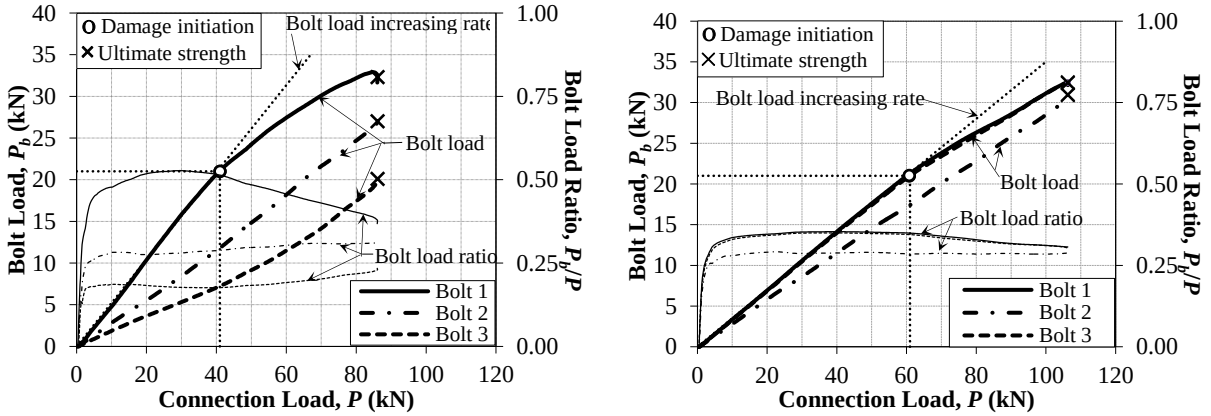

(a) Three-row bolted connection with steel cover plates

(b) Three-row bolted connection with FRP cover plates

Figure 3.13: Load distribution among the bolts with a perfect bolt-hole position

In Figure 3.13, the load increasing rate of the largest bolt load in the bolted connections within the elastic limit is indicated by using a dotted line. In the bolted connection with steel cover plates, the first bolt has the higher load increasing rate and reaches earlier at the damage initiation stage than the other bolts and then the bolt begin shed the load to the others bolts. The damage initiation strength is defined as a load of a connection at which the load increasing rate of the largest bolt load reduces with the connection load due to the damage of the hole. It is seen in Figure 3.13, the damage begins at the bolt load about 21 kN where cover plates are steel or FRP. The first bolt also fails at first in the connection. However, the first and last bolts have the higher load increasing rate then the intermediate bolt of the bolted connection with FRP cover plates and reach at a time to those stages. The load of intermediate bolt is not very smaller than the load of the first and last bolts. It indicates that the load distribution among the bolts of the connection with FRP cover plates is more uniform than the bolted connection with steel cover plates. For this reason, the bolted connection with the FRP

cover plates carries a larger load about 23% than that with steel cover plates. The same results are also found in the two and four-row bolted connections. It means that the strength of a connection is affected by the load distribution among the bolts. A bolted connection will be tolerated the maximum load when the load distribution among the bolts is uniform.

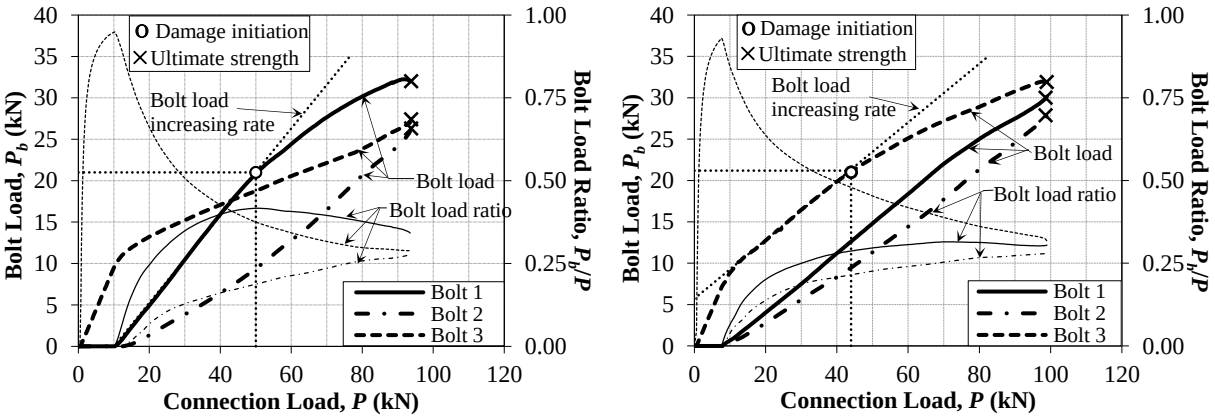

(a) Three-row bolted connection with steel cover plates

(b) Three-row bolted connection with FRP cover plates

Figure 3.14: Load distribution among the bolts with the bolt-hole position error

The load distribution among the bolts depends on the stiffness of the cover plate, and the number of bolt rows. However, the load distribution among bolt rows is affected significantly when there are errors in bolt-hole positions. Figure 3.14 shows the load distribution among the bolts of the three-row bolted connection with bolt-hole position errors in the first and second holes of the cover plates along to the loading direction. Figure 3.15 describes the bolt-hole position error. It can be observed that the last bolt of the connection contact with the cover plates and the main plate and begins to carry the load, and the other bolts are not in contact with the cover plates. At the connection load of about 10 kN, the first and second bolts also begin to carry loads. After that the load increasing rates of bolt loads in the elastic limit of the material do not change, but the bolt load ratio is changed with the change of connection load. Therefore, the first bolt picks up the largest load and reaches the damage initiation stage earlier than the other bolts for the bolted connection with steel cover

plates. However, in the bolted connection with FRP cover plates, the last bolt keeps the largest load and reaches those stages first because the load increasing rates of the first and last bolts are the same after all bolts in contact with cover plates. It is found that the connection with steel cover plates shows a larger ultimate load 8.8% when compared to the strength of that with bolt-hole positions perfectly aligned (see Figs.3 and 4), although the ultimate strength of the connection with FRP cover plates is decreased to about 7%. It is because the load distribution among the bolts becomes more uniform for the connection with steel cover plates and less uniform for the connection with FRP cover plates due to the bolt-hole errors when compared that with a perfect bolt hole aligned.

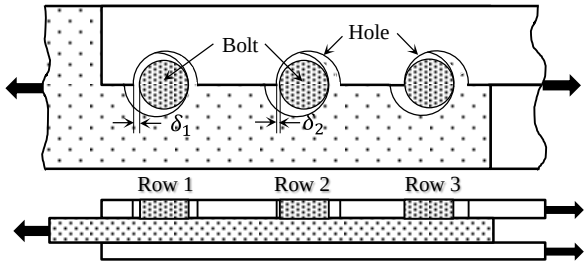

Figure 3.15: Three-row bolted connection with bolt-hole position error

Based on the observation above, the strength of a connection will be increased when the bolt with a lower load increasing rate in the connection begins to carry load early and all the bolts reach almost the same time at the ultimate strength of the connection and failed at a time. On the other hand, the strength of a connection will be decreased when the bolt with a larger load increasing rate in the connection begins to carry load early and the bolts are failed in different interval of the connection load.

(b) Strength

The damage initiation strength and ultimate strength are determined for each bolted connection. The statistical parameters of these strengths of 50 connections with bolt-hole position errors are show in Figure 3.16 and Figure 3.17. The strengths of the connections with

perfect alignment of bolt holes also in the figures by using bar.

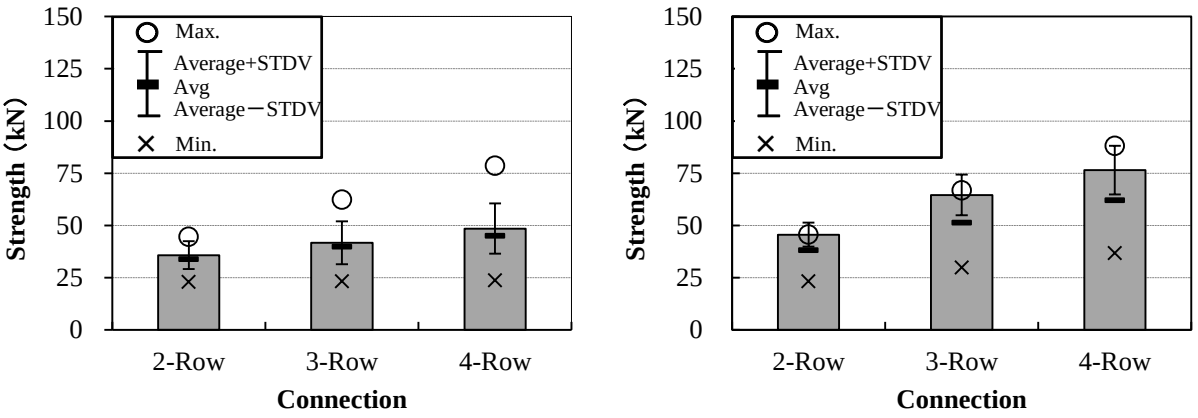

(a) Three-row bolted connection with steel cover plates

(b) Three-row bolted connection with FRP cover plates

Figure 3.16: Statistical parameters of the damage initiation strengths

It is observed in Figure 3.16 that that the effect of bolt-hole error on the damage initiation strength is significant for the connection with either steel or FRP cover plates. In contrast, the variations of damage initiation strength are larger for the connections with steel cover plates than those with FRP cover plates. The coefficients of variation of the damage initiation strength for two, three, and four-row bolted connections are 14.9, 18.9, and 18.7% for FRP cover plates and 20.5, 25.0, and 26.7% for steel cover plates, respectively. The average damage initiation strength is always lower than those with bolt-hole position perfectly aligned. It is about 7% lower for steel cover plates and about 20% lower for FRP cover plates than that with bolt-hole position perfectly aligned. Due to the error in the first and last bolt hole, the connection with FRP cover plates shows the more non-uniform load distribution a larger number of cases. For this reason, the connection with FRP cover plates shows lower average damage initiation strength than that with steel cover plates.

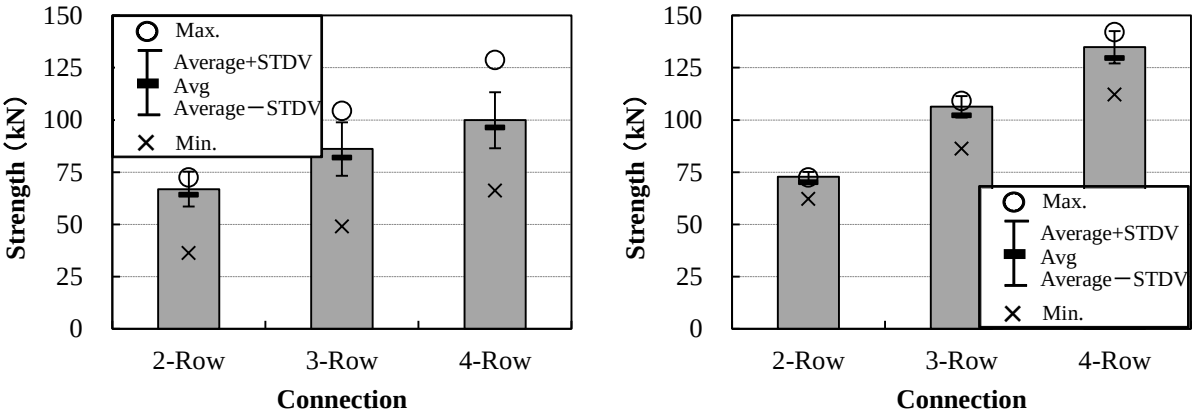

(a) Three-row bolted connection with steel cover plates

(b) Three-row bolted connection with FRP cover plates

Figure 3.17: Statistical parameters of the ultimate strengths

It can be observed in Figure 3.17 that the connections with steel cover plates are more sensitive to the bolt-hole position errors than those with FRP cover plates because the change of load distribution is larger for the connections with steel cover plates than those with FRP cover plates due to the larger stiffness. The ultimate strength of the two, three, and four-row bolted connections with steel cover plates decreases by about 46%, 43%, and 34% and increases by about 8%, 21%, and 29% respectively for the bolt-hole position errors. Whereas the connection with FRP cover plates of the two-row bolted connections, the strength does not increase anymore, but decreases by about 14%. For the three and four-row bolted connections, the strength decreases by 18% and 17% and increases by about 3% and 5%, respectively. The variation of the strengths is larger for the connections with steel cover plates than those with FRP cover plates. The coefficients of variation for the ultimate strengths are less than 6% for the connections with FRP cover plates. While they are greater than 13% for the connections with steel cover plates. The average ultimate strength is about 4% lower than that of a connection with bolt-hole position perfectly aligned for any type of connections examined in this study.

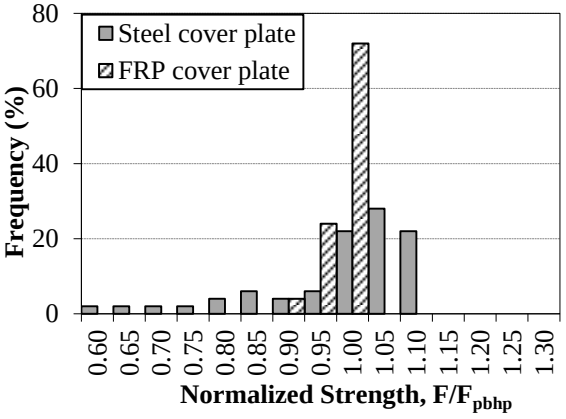

(a) Two-row bolted connections

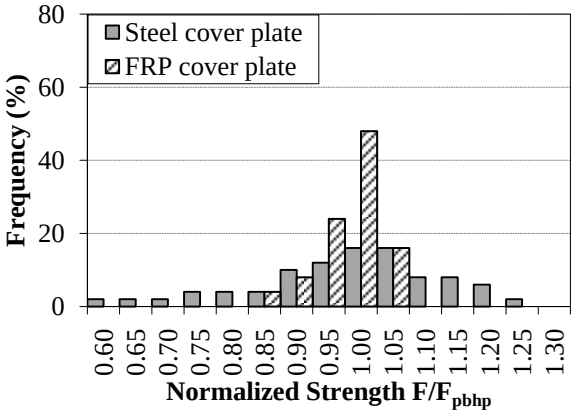

(b) Three-row bolted connections

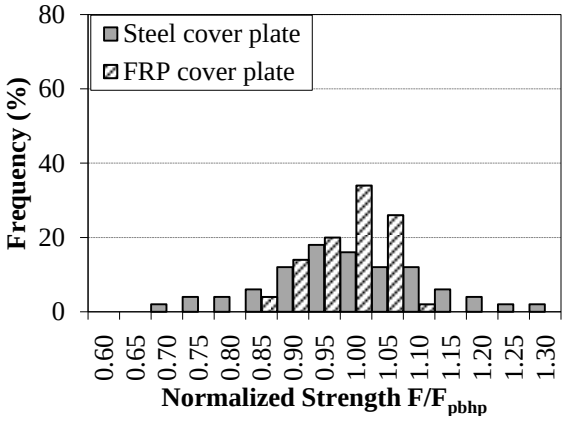

(c) Four-row bolted connections

Figure 3.18: Frequency distribution of the ultimate strength

To describe the effect of bolt-hole position error on the ultimate strength of connections, *F*, the strengths are normalized by the strength of a connection with bolt-hole position perfectly aligned, F_{pbhp}. Frequency distribution of the normalized strength of the connections is shown in Figure 3.18. The frequency is considered in terms of percentage. The interval of the normalized strength is assumed to be 0.05. It is observed that the strengths of the connections with steel cover plates have spread in a wider range than those with FRP cover plates. The frequencies are larger around the normalized strength of 1.0 for the connections with steel cover plates and FRP cover plates. It is because the bolt-hole errors are normally distributed.

3.5 Summary

Progressive damage analyses are performed to determine the effect of cover plate stiffness on the ultimate strength and failure mode of the bearing type multi-row bolted connection. The connections were a double-lap configuration having a 12-mm FRP main plate. Steel and FRP cover plates are used to change the cover plate stiffness. Three dimensional finite element models were developed for bolted connection of FRP composite members. The analysis can consider progressive damage of material by including a three dimensional failure criterion and stiffness degradation due to damage which are implemented through a user subroutine UMAT in Abaqus. The stiffnesses are gradually decreased after failure of material and a viscous regularization is included in the model. In order to reduce the convergence problem significantly and prevent the analysis from stopping prematurely, so that the analysis can predict failure mode and strength of bolted connection. The following remarks can be made as conclusions of this chapter:

(a) For a multi-row bolted connection of FRP members, FRP cover plates can give a more even distribution of load among bolt rows when compared to steel cover plates.

(b) A connection with FRP cover plates offers a larger strength than that with steel cover plates. For the two, three, and four-row bolted connections, the strength will be increased, by 6%, 19%, and 35%, respectively by using FRP cover plates instead of steel cover plates having a half of the main plate thickness.

(c) When the number of bolt rows is increased an additional strength obtained by the increase of bolt rows is larger in a connection with FRP cover plates than that with steel cover plates. By increasing a number of bolt rows from 1 to 2, from 2 to 3, and from 3 to 4, FRP cover plates will increase more ultimate capacity than steel cover plates by 0.11, 0.36, and 0.45, respectively.

(d) A multi-row bolted connection with FRP cover plates requires a larger end distance than steel cover plates. It is almost the same as that of a single bolted connection to avoid the cleavage failure at the end, although current design codes specify a smaller end distance for multi-row bolted connections with FRP cover plates than that for single bolted connections.

(e) Effect of bolt-hole error on the damage initiation strength is significant for type of connections examined in this study. Variations of the damage initiation strength due to bolt-hole errors are larger for the connections with steel cover plates than those with FRP cover plates. The coefficients of variation of the damage initiation strength for two, three, and four-row bolted connections are 20.5, 25.0, and 26.7% for steel cover plates and 14.9, 18.9, and 18.7% for FRP cover plates, respectively. The average damage initiation strength is about 7% lower for steel cover plates and about 20% lower for FRP cover plates than that with perfect bolt-hole position.

(f) The ultimate strength of bolted connections is also affected by the bolt-hole errors. The effect of bolt-hole error of the connection on the ultimate strength is larger for the bolted connection with steel cover plates than that with FRP cover plates. The coefficients of variation of the ultimate strength of the two, three, and four-row bolted connections with steel cover plates are 13.0, 15.6, and 13.9%, respectively, whereas those of bolted connections with FRP cover plates are 3.2, 5.0, and 5.9%, respectively. The strength can either increase or decrease with a larger probability to decrease. The average ultimate strength is about 4% lower than that of a connection with perfect bolt-hole position for any type of connections examined in this study.

CHAPTER 4 EXPERIMENTAL STUDY ON SINGLE BOLTED CONNECTIONS

4.1 Background

This chapter presents an experimental program undertaken to examine the behavior of single bolted connections fabricated from woven fabric GFRP composite material members. Connection configurations, test setup, instrumentation, the various parameters considered in this program, and test results are presented in detail. Various material tests are conducted to determine the material properties of woven fabric GFRP and the test results are also described.

4.2 Material Properties

The GFRP composite material used in the investigation is produced by a hand layup. The reinforcement is woven fabric glass fiber and the matrix is unsaturated polyster resin. The same amount of glass fiber is oriented in the 0° and 90° of the loading directions. The woven fabric GFRP plate is produced in the form of 0.9 m x 3.0 m plates and manufactured in three

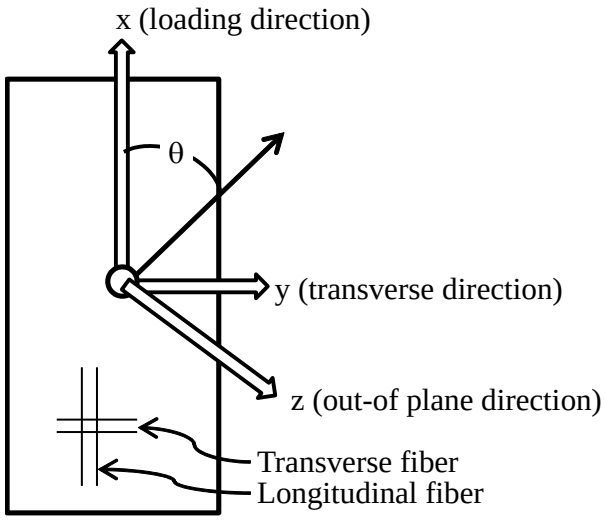

Figure 4.1: Loading axes of FRP plate

different thicknesses: 6.0 mm, 9.0 mm, and 12.0 mm. Material test coupons and connection plates of different dimensions are cut out from these 0.9 m x 3.0 m plate.

Table 4.1: List of test specimens with different test standards

Specimen ID	Thickness (mm)	Direction	Test type	Test standard
T0006	6	0°	Tension test	JIS K7164
T0009	9			
T0012	12			
T9006	6	90°		
T9009	9			
T9012	12			
C0006	6	0°	Compression test	JIS K7018
C0009	9			
C0012	12			
C9006	6	90°		
C9009	9			
C9012	12			
Z12	12	z-axis direction (Thickness direction)	Compressive test	JIS K7181
S4506	6	45°	Shear test	JIS K7019
S4509	9			
S4512	12			
B0012	12	0°	Bending test	JIS K7057
B9012		90°		

To determine the material properties, tension tests, compression tests, and shear tests are conducted for laminates with three different thicknesses. The tension and compression tests are conducted in the directions parallel (0°) and transverse (90°) to the loading direction. In-plane shear tests are conducted as a 45^{o} tensile test. To determine out-of-plane compression and shear properties, short block compression test and bending test are also conducted. The directions of fibers and loading are illustrated in Figure 4.1. Table 4.1 shows list of material test specimens according to different test standards. In the test specimen identification (ID), the alphabet indicates a test type, two-digit number indicates an angle between the direction of material property and loading direction, and the last two-digit number indicates the thickness of the specimen, respectively. This rule does not apply to the out-of-plane

compression test.

4.2.1 Tension Test

In-plane tensile properties of the laminate were determined experimentally according to JIS K7164. The test was carried out using an MTS material testing machine (maximum load of 500 kN) shown in Figure 4.2. Dimensions of a tensile test specimen are shown in Figure 4.3. In the grip portion, 2-mm thick aluminium tabs are bonded on both sides of the specimen to reduce the stress concentration. Six strain gauges are mounted in each test coupon for laminates with a thickness of 6 mm or 9 mm: two in the longitudinal direction and one in the transverse direction on each side. Eight strain gauges are mounted in each test coupon for laminates with a thickness of 12.0 mm: two in the longitudinal direction, one in the transverse direction on each side, and one in the thickness direction on each side. The tension test method allows determination of the following properties for the laminates.

E_x^{T} : Tensile modulus of elasticity in the loading direction

E_y^{T} : Tensile modulus of elasticity in the transverse of the loading direction

υ_{xy} : Poisson's ratio determined by a tensile test in the loading direction

υ_{yx} : Poisson's ratio determined by a tensile test in the transverse of the loading direction

υ_{xz} : Poisson's ratio determined by a tensile test in the loading direction

υ_{yz} : Poisson's ratio determined by a tensile test in the transverse of the loading direction

X_T : Ultimate tensile strength in the loading direction, and

Y_T : Ultimate tensile strength in the transverse of the loading direction

Figure 4.2: Setup of tension test specimen

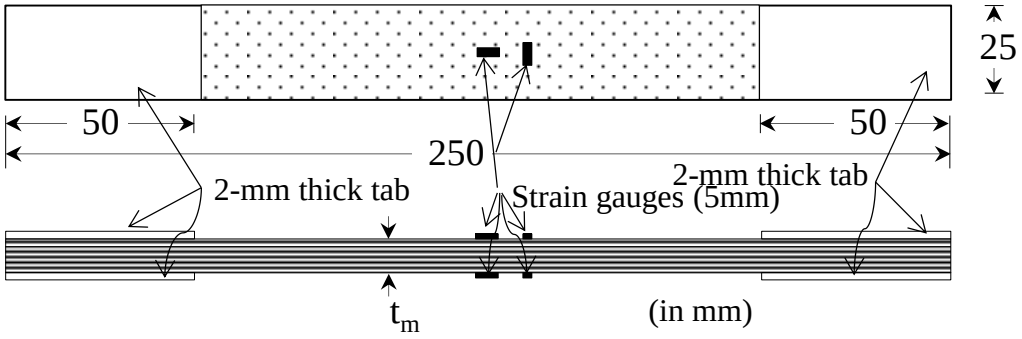

Figure 4.3: Dimension of test specimen

Five coupons were tested for each direction and thickness. Table 4.2 shows the obtained tensile properties of the laminates, and Figure 4.4 shows the typical stress-strain curves in the 0^o direction and 90^o direction. A tensile modulus of elasticity is determined by the chord modulus method. The chord modulus of elasticity is defined by Eq. (4.1).

$$E^{\text{T-chord}} = \frac{\Delta\sigma}{\Delta\varepsilon} \tag{4.1}$$

where,

$E^{\text{T-chord}}$: Tensile chord modulus of elasticity

$\Delta\sigma$: Difference between the tensile stresses at two strain points of 0.0005 and 0.0025

$\Delta\varepsilon$: Difference between two strain points of 0.0005 and 0.0025 (0.002)

Table 4.2: In-plane tensile properties

Specimen name	Direction	In plane tensile strength, X_T or Y_T			In plane modulus of elasticity, E		
		σ_{avg} (MPa)	STD (MPa)	COV (%)	E_{avg} (GPa)	STD (MPa)	COV (%)
T0006	0^o	358	30.2	8.4	25.5	0.5	2.0
T0009		321	16.2	5.0	26.6	0.4	1.5
T0012		353	14.8	4.2	26.2	0.21	0.8
T9006	90^o	382	11.8	3.1	25.9	1.08	4.2
T9009		376	9.0	2.4	26.4	0.13	0.5
T9012		335	6.51	1.9	25.1	0.42	1.7

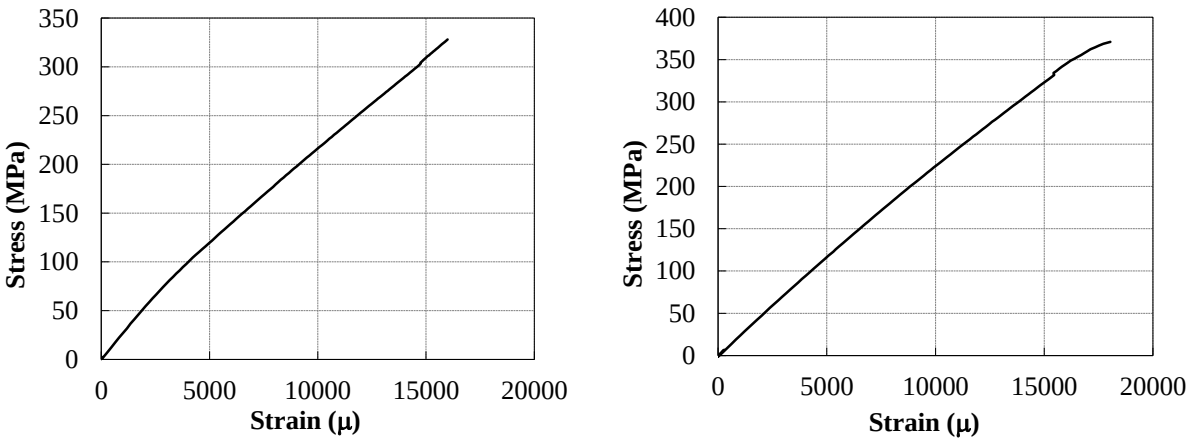

(a) T0012 (b) T9012

Figure 4.4: Stress-strain curve of tension test specimen

Poisson's ratio is also determined by the chord method.

$$\upsilon = \frac{\Delta\varepsilon_T}{\Delta\varepsilon_L} \tag{4.2}$$

where, υ : Poisson's ratio

$\Delta\varepsilon_T$: Difference between lateral strains the two longitudinal strain points of 0.0005 and 0.0025

$\Delta\varepsilon_L$: Difference between the two longitudinal strain points of 0.0005 and 0.0025.

4.2.2 Compression Test

Compressive test was conducted according to JIS K7018. The test was carried out using an MTS material testing machine (maximum load of 500 kN) as shown in Figure 4.5. Dimensions of test coupon are shown in Figure 4.6. In the same way as the tensile test coupon, 2-mm thick aluminum tabs were attached at both ends of coupon to secure the grip portion. Two strain gauges are mounted in the loading direction, one on each side of the test coupon to determine the modulus of elasticity of the laminates. The compression test method allows determination of the following properties for the laminates:

E_x^C : Compressive modulus of elasticity in the loading direction

E_y^C : Compressive modulus of elasticity in the transverse direction

Figure 4.5: Setup of compression test specimen

X_C : Ultimate tensile strength in the loading direction

Y_C : Ultimate tensile strength in the transverse direction

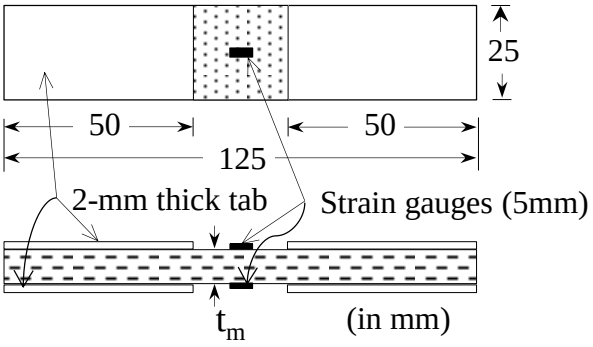

Figure 4.6: Dimension of compression test coupon

Five specimens were tested in each direction and thickness of the laminates. Table 4.3 shows the obtained compressive properties of the laminates, and Figure 4.7 shows the typical stress-strain curves in the 0^o and 90^o directions. A compressive modulus of elasticity is determined by the chord modulus method. The chord modulus of elasticity is determined by using two points at strains of 0.0005 and 0.0025.

Table 4.3: In-plane compressive properties

Specimen name	In plane compressive strength, X_C or Y_C			In plane compressive modulus of elasticity, E		
	σ_{avg} (MPa)	STD (MPa)	COV (%)	E_{avg} (GPa)	STD (MPa)	COV (%)
C0006	274	20.7	7.5	28.3	1.2	4.1
C0009	294	13.6	4.6	27.5	0.9	3.4
C0012	267	17.9	6.7	26.1	1.9	7.2
C9006	356	9.9	2.8	28.9	0.9	3.3
C9009	307	17.2	5.6	27.1	1.6	5.8
C9012	288	6.3	2.2	26.2	0.8	3.1

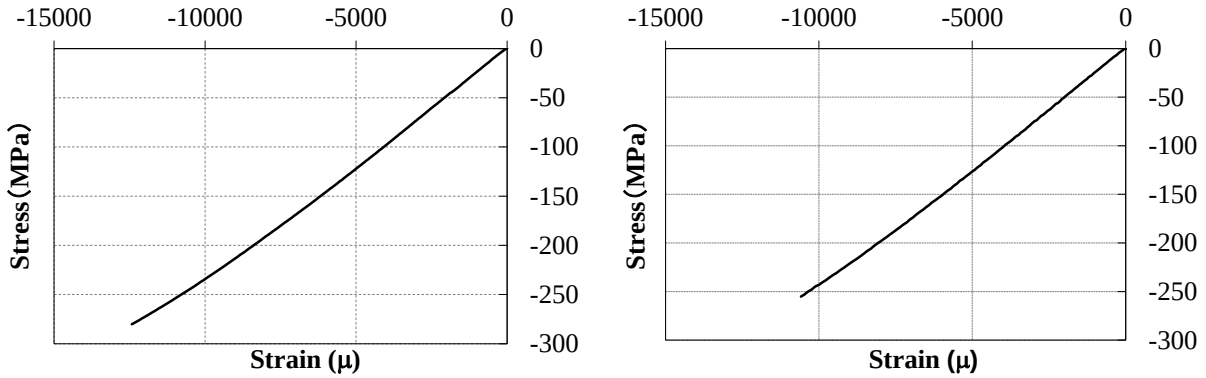

(a) C0012 (b) C9012

Figure 4.7: Stress-strain curve of in-plane compression test coupon

To determine the compressive properties in out-of-plane, a short block test was performed. The test was performed only for the 12-mm thick GFRP laminate. The test was carried out by using the Maekawa universal testing machine in accordance with JIS K7181. Figure 4.8 shows the test setup of the out-of-plane compression test. The dimension of the specimen is 6 × 6 × 12 mm as shown in Figure 4.9. Four stain gauges are mounted on the four sides of the specimen.

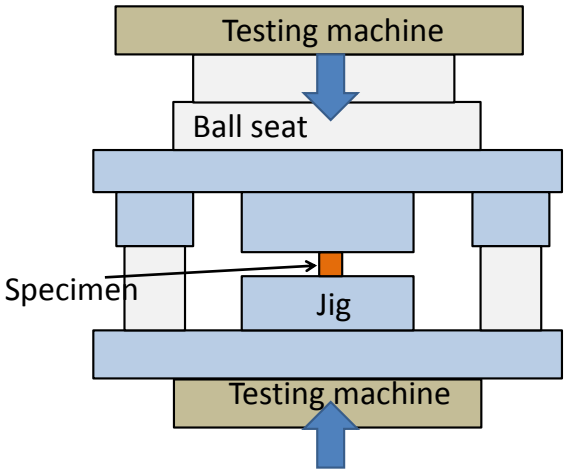

Figure 4.8: Experimental setup of out-of-plane compression test

Five coupons were tested. Table 4.4 shows the obtained out-of-plane compressive properties. A compressive modulus of elasticity was determined by the chord modulus method.

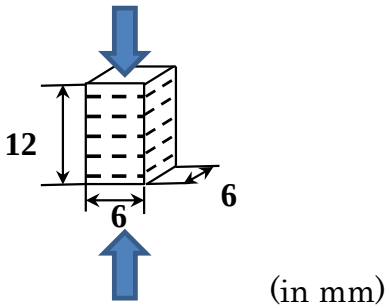

Figure 4.9: Dimensions of short block test coupon

Table 4.4: Out-of-plane compressive properties

coupon name	Out-of-pane compressive strength, X_T or Y_T			Out-of-pane compressive modulus of elasticity, E		
	σ_{avg} (MPa)	STD (MPa)	COV (%)	E_{avg} (GPa)	STD (MPa)	COV (%)
CZ12	339	6.15	1.9	13.2	0.71	5.4

4.2.3 Shear Test

The in-plane shear test was carried out using the MTS material testing machine in accordance with JIS K7019. The test was performed to obtain the in-plane shear properties of the 6 mm, 9 mm, and 12 mm composite laminates. The test procedure is similar to the tension test while the fiber orientation is $+45^o$ to the loading direction. Dimension of the coupons are the same of the as those tensile test coupon as shown in Figure 4.10. Four strain gauges are attached on the each specimen of the front and back surfaces of the test specimen to obtain the shear modulus of the laminates.

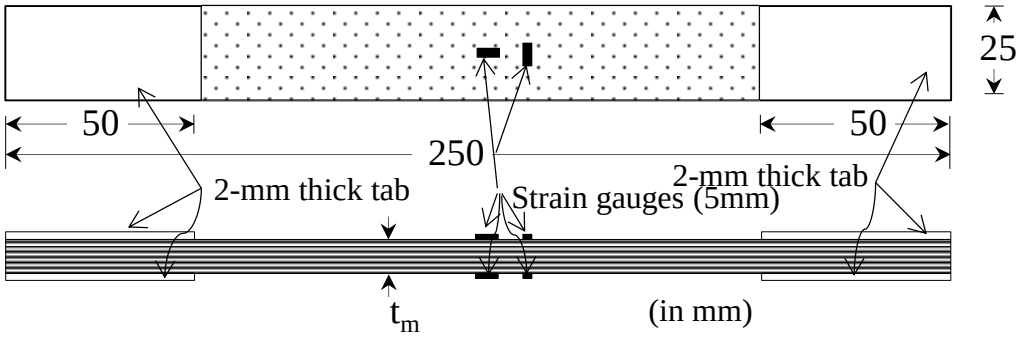

Figure 4.10: Dimensions of in-plane shear test specimen

Shear stress and strain can be determined according to the following equations:

$$\tau_{xy} = -\frac{\sigma_x}{2} \tag{4.3}$$

$$\gamma_{xy} = \varepsilon_y - \varepsilon_x \tag{4.4}$$

Hence, the shear modulus can be found by:

$$G_{xy} = \frac{\tau_{xy}}{\gamma_{xy}}$$

$$G_{xy} = \frac{\sigma_x}{2\left(\varepsilon_x - \varepsilon_y\right)} \tag{4.5}$$

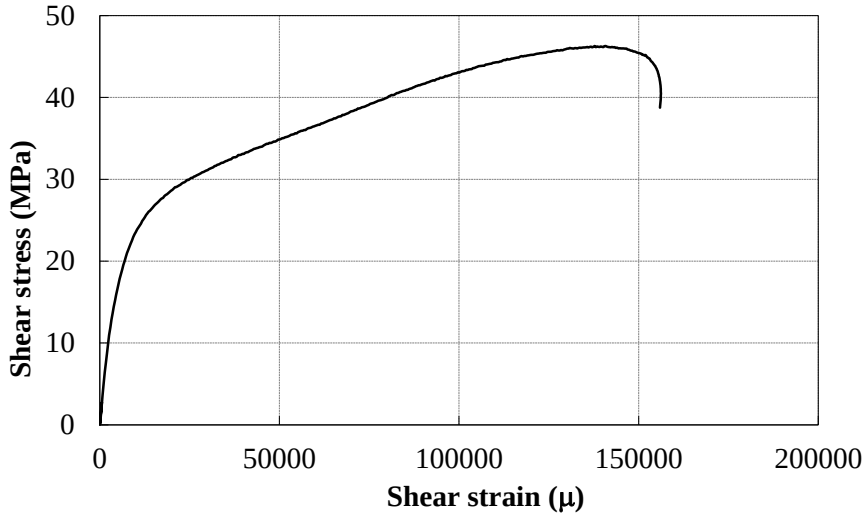

Figure 4.11: Shear stress-strain curve of S4512 test specimen

Shear properties and stress-strain curves obtained in the test are shown in Table 4.5 and Figure 4.11. The shear modulus was determined by using the shear strain points of 0.001 and 0.005.

Table 4.5: In-plane shear properties

Specimen name	In plane shear strength, S_{xy}			In plane shear modulus, G_{xy}		
	τ_{avg} (MPa)	STD (MPa)	COV (%)	G_{avg} (GPa)	STD (MPa)	COV (%)
S4506	46.3	1.35	0.029	3.06	0.12	0.040
S4509	53.4	1.33	0.025	3.01	0.29	0.095
S4512	47.9	0.69	0.014	2.98	0.06	0.020

To obtain the out-of-plane shear strength and shear modulus of the composite material, a short beam test was performed according to JIS K7057. The test is carried out by using the Maekawa universal testing machine. The short beam shear test setup is shown in Figure 4.13. Dimension of test coupons are shown in Figure 4.12. The short beam shear test was performed for only 12-mm thick laminate. Two strain gauges were attached at a 45^o angle with the horizontal axis on the coupon sides as shown in Figure 4.12.

The maximum shear stress on the neutral axis is calculated by Eq. (4.6).

$$\tau_{xz} = \frac{3P}{4A} \tag{4.6}$$

where, A is the cross-sectional area, and P is the applied force.

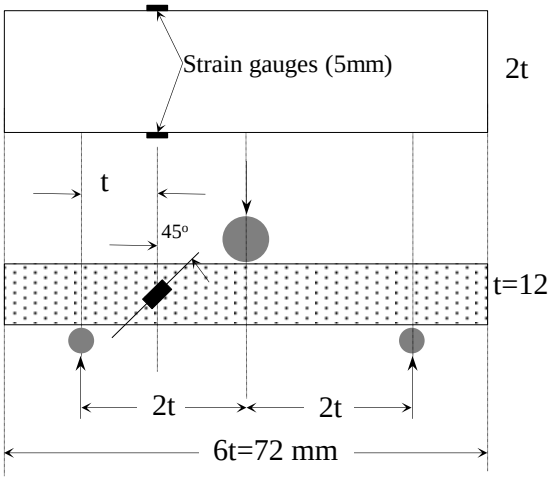

Figure 4.12: Dimension of short beam shear test specimen

The out-of-plane shear modulus can be calculated by using Eq. (4.7).

$$G_{xz} = \frac{\tau_{xz}}{\gamma_{xz}} \tag{4.7}$$

where γ_{xz} is the shear strain calculated by Eq. (4.8).

$$\gamma_{xz} = 2\varepsilon \tag{4.8}$$

where, ε is the strain.

Figure 4.13: Setup of short bean test specimen

Shear failure occurred in the specimens with shear failure line at a 45° angle from the beam axis as shown in Figure 4.14. The obtained shear properties and stress-strain curves are shown in Table 4.6 and Figure 4.15. The shear modulus was determined by using the shear strain points of 0.0005 and 0.0025.

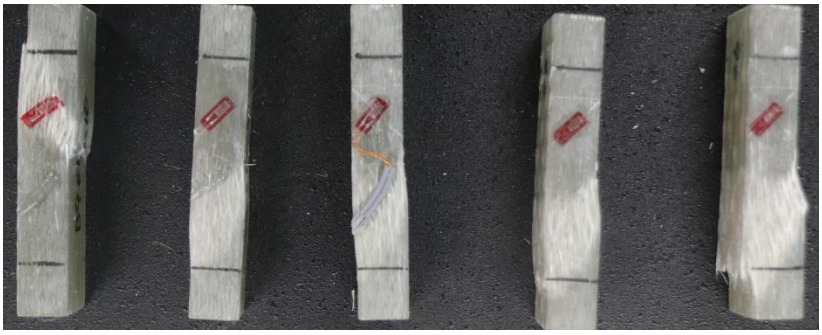

Figure 4.14: Failure mode of short beam test specimen

Table 4.6: Out-of-plane shear properties

Specimen name	Out-of-plane shear strength, S_{xz} or S_{yz}			Out-of-plane shear modulus, G_{xz} or G_{xz}		
	τ_{avg} (MPa)	STD (MPa)	COV (%)	G_{avg} (GPa)	STD (MPa)	COV (%)
B0012	34.3	0.421	0.012	4.44	0.191	0.043
B9012	34.0	0.875	0.026	4.64	0.365	0.079

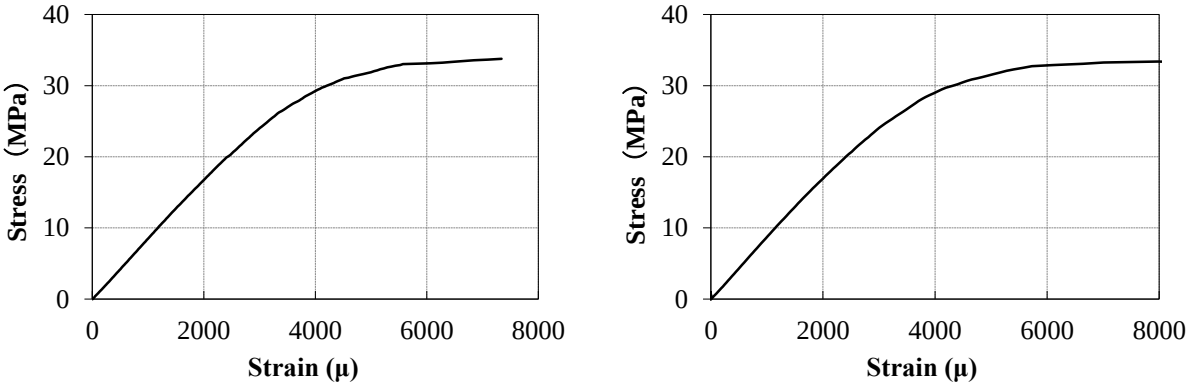

(a) B0012 (b) B9012

Figure 4.15: Shear stress-strain curve of short beam test specimen

4.2.4 Tension Test of Stainless Steel

Tensile test of stainless steel was conducted according to JIS Z 2241. The test was carried out using an universal testing machine (maximum load of 500 kN). Dimensions of test coupon are shown in Figure 4.16 and Table 4.7. Four strain gauges are mounted on the test coupon to determine the stress-strain characteristic of the material.

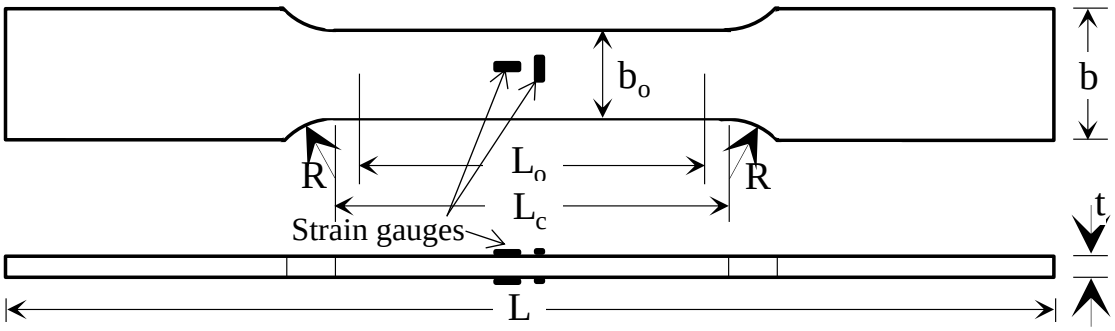

Figure 4.16: Dimension of tensile test coupon of stainless steel

Table 4.7: Dimensions of the test coupon (mm)

t	L	L_c	L_o	b	b_o	R
6	300	60	50	45	25	25

Three coupons were tested of the stainless steel. Table 4.8 shows the obtained tensile properties of the laminates, and Figure 4.17 shows one of stress-strain curves obtained from the tensile test of the stainless steel. The modulus of elasticity was determined by using the

strain points of 0.0001 and 0.001.

Table 4.8: Tensile properties of stainless steel

	Average	STD	COV(%)
2% offset strength of yield strength (MPa)	358.8	6.2	1.9
Tensile strength (MPa)	658.5	8.8	1.3
Modulus of elasticity (GPa)	208.3	4.4	1.9
Poisson's ratio	0.308	0.027	8.8

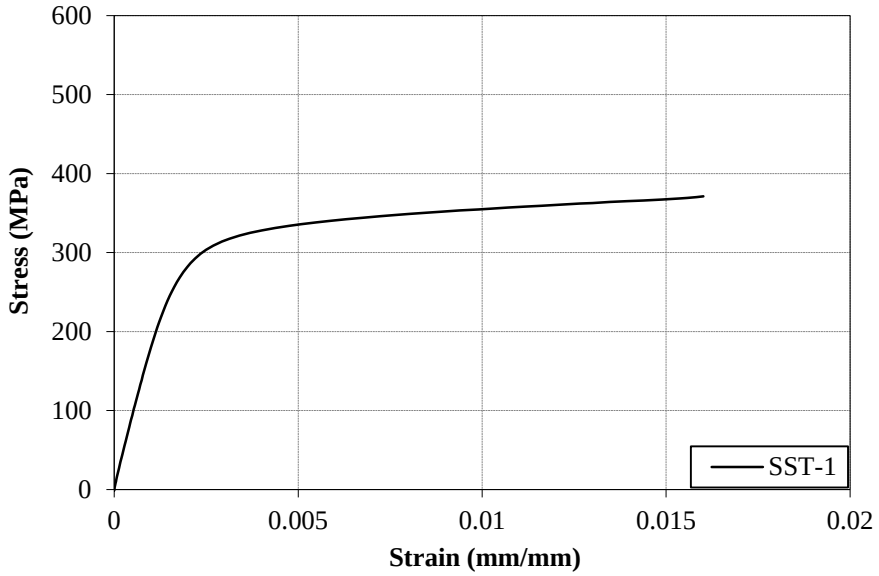

Figure 4.17: Stress-strain curve of stainless steel test specimen

4.2.5 Bolt and Washer

A2-72 stainless steel (SUS 304) bolts with a diameter of 16 mm are used in this study. The material properties of the bolt are shown in Table 4.9, which are catalog values. Washer is also of stainless steel (SUS 304). Inner and outer diameters of the washers are 17 mm and 32 mm, respectively, and the thickness of the washers is 2.5 mm.

Table 4.9: Material properties of stainless steel bolt

E (GPa)	ν	f_y (MPa)	f_u (MPa)
200	0.3	450	700

4.3 Single Bolted Connection Specimens

4.3.1 Parameters

An experimental study was conducted to examine mechanical behavior of single bolted connections of a double-lap configuration with one to four rows of bolts. The main plate is made of GFRP with a thickness, t_m, of 12 mm. Three different cover plates were used in this investigation, which may influence the ultimate strength of a single bolted connection, and they are 6-mm and 12-mm thick GFRP cover plates, and 6 mm for steel cover plates, which corresponds to stiffness ratios of two cover plates to the main plate of about 1 and 2 for GFRP cover plates and about 8 for steel cover plates, respectively. The stiffness ratio was defined by Eq. (2.1) in Section 2.2.1.

Table 4.10: List of single bolted connections with parameters

ID	*w/d*	*e/d*	*Torque*	Main plate	Cover plate	ID	*w/d*	*e/d*	*Torque*	Main plate	Cover plate
J1	3.0	4.0	3 N-m	GFRP 12 mm	Steel 6 mm	J11	2.0	4.0	3 N-m	GFRP 12 mm	Steel 6 mm
J2	4.0	3.0	3 N-m	GFRP 12 mm	Steel 6 mm	J12	2.0	4.0	3 N-m	GFRP 12 mm	GFRP 12 mm
J3	4.0	4.0	3 N-m	GFRP 12 mm	Steel 6 mm	J13	4.0	1.5	3 N-m	GFRP 12 mm	GFRP 12 mm
J4	2.0	4.0	Pin-bearing	GFRP 12 mm	Steel 6 mm	J14	4.0	4.0	3 N-m	GFRP 12 mm	GFRP 12 mm
J5	4.0	4.0	Pin-bearing	GFRP 12 mm	Steel 6 mm	J15	2.0	4.0	Pin-bearing	GFRP 12 mm	Steel 6 mm
J6	4.0	2.0	Pin-bearing	GFRP 12 mm	Steel 6 mm	J16	4.0	1.5	Pin-bearing	GFRP 12 mm	Steel 6 mm
J7	4.0	2.0	3 N-m	GFRP 12 mm	Steel 6 mm	J17	4.0	4.0	Pin-bearing	GFRP 12 mm	Steel 6 mm
J8	4.0	1.5	3 N-m	GFRP 12 mm	Steel 6 mm	J18	2.0	4.0	3 N-m	GFRP 12 mm	FRP 6 mm
J9	2.5	4.0	3 N-m	GFRP 12 mm	Steel 6 mm	J19	4.0	1.5	3 N-m	GFRP 12 mm	FRP 6 mm
J10	5.0	4.0	Pin-bearing	GFRP 12 mm	Steel 6 mm	J20	4.0	4.0	3 N-m	GFRP 12 mm	FRP 6 mm

The two basic geometric parameters were also studied in this investigation: the width of the member and the edge distance. The effects of the width and the edge distance are effectively described in terms of the dimensionless ratios with respect to the bolt diameter. In this investigation the steel bolt diameter was kept constant at 16 mm for all the tested connections. The width and edge distance were varied to obtain different values for the width to bolt diameter ratio, *w/d*, and the edge distance to bolt diameter ratio, *e/d*. The values of *w/d* and *e/d* are selected so that different failure modes could be obtained. The dimensions of specimen used in this study are listed in Table 4.10. To designate each connection geometry, a connection ID is used in this study. In the investigation, 20 sets of single bolted connections were tested. There were three specimens in each set.

To determine the influence of the members thickness on the behavior of a connection, two different thicknesses were used: 6 mm and 12 mm as given in Table 4.10. These thicknesses were selected to understand the behavior of a cover and a main plate.

In this investigation, standard washers were used. The diameter the diameter of a bolt hole, d_h, is 17 mm, resulting in a clearance of 1 mm. This clearance was chosen according to CNR DT 205/2007 (National Research Council, 2007). To prepare bolted connections, two cases of bolt torque were considered: finger tight and pin-bearing (no torque). Finger tight torque was set to 3 N-m according to Mottram and Turvey (2003).

4.3.2 Connection Fabrication

In this study, steel and GFRP plates were used to assemble the connections. The GFRP plate was used to make the main and cover plates, while the steel plate was used only for cover plates. Main and cover plates have different dimensions as shown in Figure 4.18. In the main plate L_1= 150 mm was considered for the grip and free space of the connection.

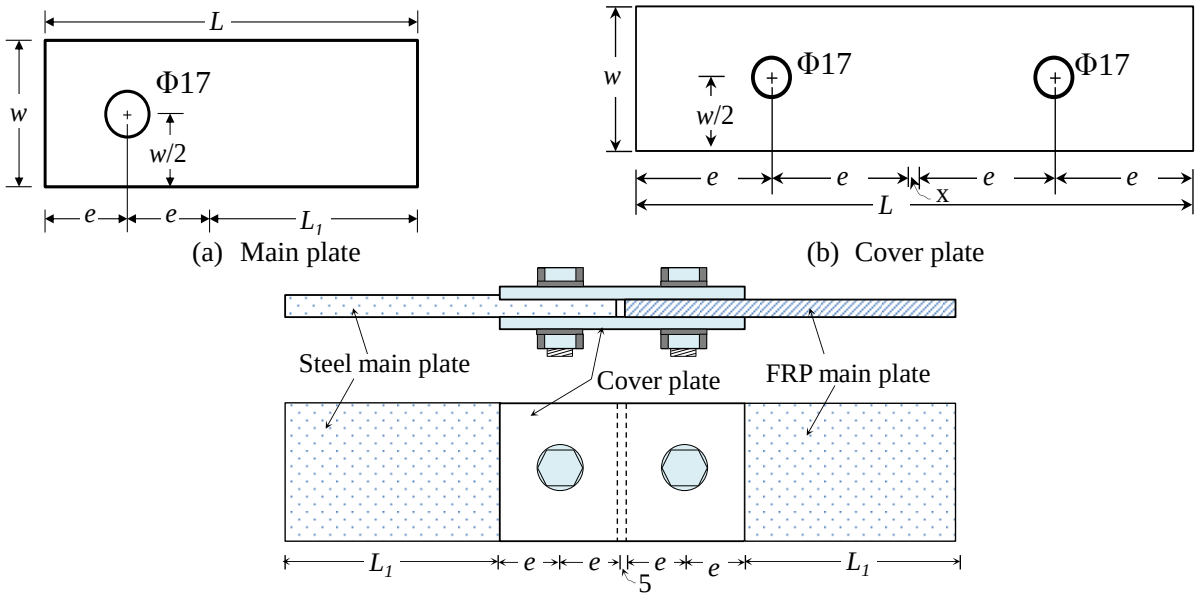

Figure 4.18: Specimen of single bolted connection

A2-72 stainless steel bolt with a diameter of 16 mm. The finger tightening torque, 3 N-m, is applied to the bolts by the torque wrench for clamping the connection plates through the standard washers of 17-mm inner and 32-mm outer diameters, and 2.5-mm thick. For the pin-bearing connection, about 5-mm gap is provided between the main and the cover plate.

4.4 Test Set-up

Tensile load was applied to the specimen by a 500 kN capacity universal testing machine. The test setup of the single bolted connection is shown in Figure 4.19. The main plates, where one is GFRP and another one is steel, were gripped by the universal testing machine.

For each test, load displacement relationships were obtained. Displacements were measured by using four transducers. The setting of the transducers is illustrated in Figure 4.19. The displacement transducer, D1, was used to measure the connection displacement between the center of cover plate to the main plate, the clip type transducer, D2, is used to measure the relative displacement of the main plate to the cover plate at the edge of the cover plate, and the transducers D3 and D4 were used to measure the displacement of a bolt and the

displacement of the main plate at a bolt hole location, and they determined the bolt hole elongation.

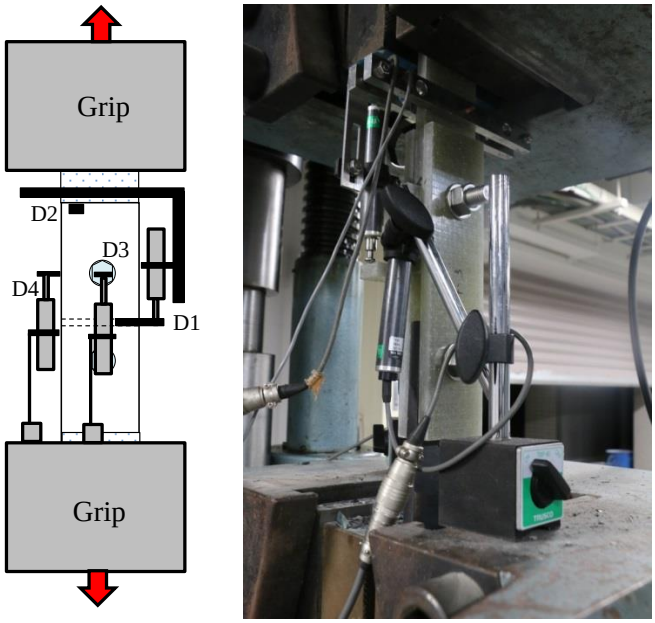

Figure 4.19: Set-up of single bolted connection

4.5 Results and Discussions

The ultimate loads and failure modes of all the single bolted connections measured from the experiments are summarized in Table 4.11. The ultimate strength is maximum load in the test of a connection. The coefficient of variation of ultimate load each set of connections is below 7% which is within the range of material strength variability. The ultimate strengths are also given in the table. The ultimate strength is calculated with respect to the failure mode, and described in Section 5.4.3.

Table 4.11: Ultimate strengths and failure modes of single bolted connections

ID	Failure mode	Average ultimate strength (kN)	COV (%)	Average ultimate strength (MPa)	ID	Failure mode	Average ultimate strength (kN)	COV (%)	Average ultimate strength (MPa)
J1	B	84.2	5.1	448	J11	NT	56.8	3.0	322
J2	S	76.3	4.0	68	J12	NT	57.4	2.9	325
J3	B	93.1	0.3	495	J13	S	44.2	2.0	78
J4	NT	45.7	6.4	259	J14	B	90.7	1.0	482
J5	B	48.2	2.7	256	J15	B	20.0	1.0	216
J6	S	45.7	6.4	61	J16	S	17.4	1.3	61
J7	S	59.2	2.0	79	J17	B	17.9	2.0	190
J8	S	44.5	3.9	79	J18	NT	59.3	3.1	335
J9	NT	75.5	6.0	279	J19	S	41.0	2.4	72
J10	B	52.1	1.1	277	J20	B	69.2	6.8	368

Note: NT= Net-tension failure, B = Bearing failure, S = Shear Failure

4.5.1 Failure Mode

Three basic failure modes were observed in the single bolted connection tests: net-tension, shear, and bearing failure modes. The net-tension failure occurred in J4, J9, J11, J12, and J18 connections, and the shear failure occurred in J2, J6, J7, J8, J13, J16, and J19 connections, whereas the bearing failure occurred in J1, J3, J5, J10, J14, J15 J17 and J20 connections. The three failure modes of typical specimens tested are shown in Figure 4.20 for cases with bolt torque and in Figure 4.21 for those without torque. Net tension failure is characterized by fracture through the section with a bolt hole. Bearing failure is characterized by crushing of the material in the area of the bolt-to-hole interface. After the bearing failure, the bolt hole elongates excessively, and the connection plates finally would fail in either tension of shear-out (see Figure 4.20(c)). Shear failure occurs in matrix through the section parallel to the loading direction at first and then bearing damage occurs in the vicinity of the bolt-to-hole interface and finally shear fracture occurs through the sections at 45^{o} angle to the direction parallel to the loading direction. The 45^{o} angle of the failure line is due to an

existence of fibers in the 90^o direction (see Figure 4.20(b)). In the connection with 3 N-m torque, the axial force in the bolt provides lateral restraint on the main plate by the cover plates. However, in the pin-bearing connections shown in Figure 4.21, material expands through thickness direction because no lateral restraint is provided.

Figure 4.22 shows the failure modes of connections that failed in cover plates (J18 to J20). Tension failure mode is similar to that of the main plate. However, in the bearing and shear failure cases, material expend in the through thickness direction outside of washer and the washer penetrates into the cover plate.

Since there exists the same amount of fibers in the transverse direction as longitudinal direction the cleavage failure was not observed in any specimens.

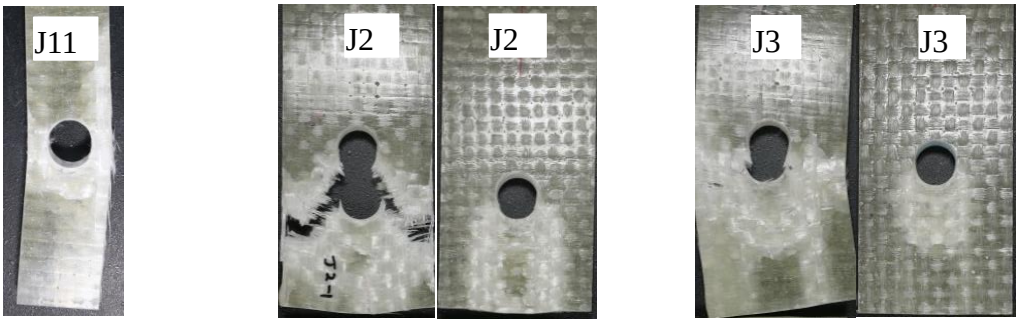

(a) Net-tension failure (b) Shear failure (c) Bearing failure

Figure 4.20: Failure modes of single bolted connections with bolt torque

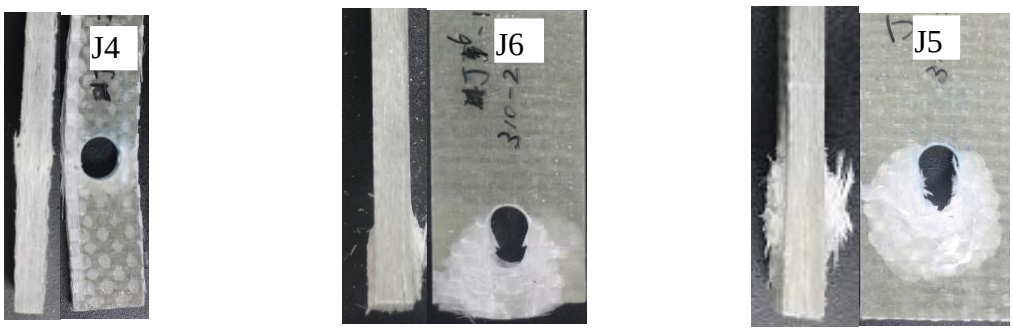

(a) Net-tension failure (b) Shear failure (c) Bearing failure

Figure 4.21: Failure modes of single bolted connections without bolt torque

(a) Net-tension failure (b) Shear failure (c) Bearing failure

Figure 4.22: Failure modes in cover plate of single bolted connections with bolt torque

4.5.2 Load-displacement Relationship

Figure 4.23 and Figure 4.24 show the load-relative displacement relationships of the three basic failure modes of the connections with the bolt torque and without bolt torque. The relative displacement of main plate to cover plate was measured at the end of the cover plate, which was indicated D2 in Figure 4.19. At the initial stage of the experiment, the main plate slips due to the bolt-hole clearance. A frictional force due to the clamping force of the bolt lower than 1 kN. The relative displacement in the figure is the measured relative displacement minus the initial slip. Therefore, curves start from zero relative displacement.

Figure 4.23 shows the load-relative displacement relationship of the connection without bolt torque in the bolt. The load-relative displacement characteristic is linear before onset of the material nonlinearity shown in Figure 4.23(a). After that the slope decreases slightly due to the material nonlinearity and then suddenly net-tension failure occurred in the connection. There was no sufficient warning before net-tension failure of the connection, and the net-tension failure is a catastrophic failure.

For the bearing failure case, the load-relative displacement relationship is linear before the onset of bearing damage in the connection as shown in Figure 4.23(c). The slope decreases slightly and then load suddenly drop by about 2/3 of ultimate strength. After the drop of load, displacement is increased without any increase of load, and a large deformation

is observed in the connection before failure.

For the shear failure case, the load-relative displacement relationship is also linear before the onset of shear damage in the connection as shown in Figure 4.23(b). The slope of the curve gradually decreases after the initiation of the shear damage and reaches at the ultimate level and then gradually decreases. The shear failure mode did not show any sudden load drop like bearing failure mode in the load-displacement relationship. The shear failure mode shows large displacement before failure. Therefore, the shear failure mode is not a catastrophic failure like net-tension.

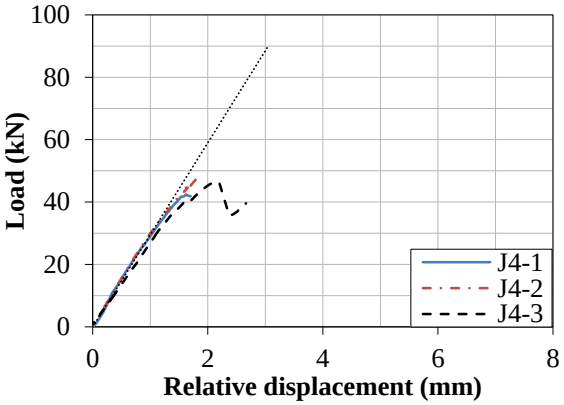

(a) Net-tensile failure

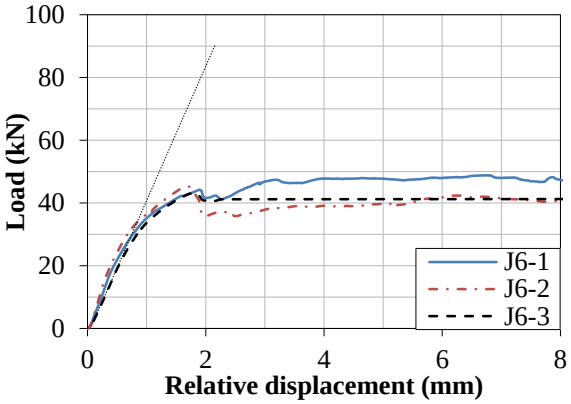

(b) Shear failure

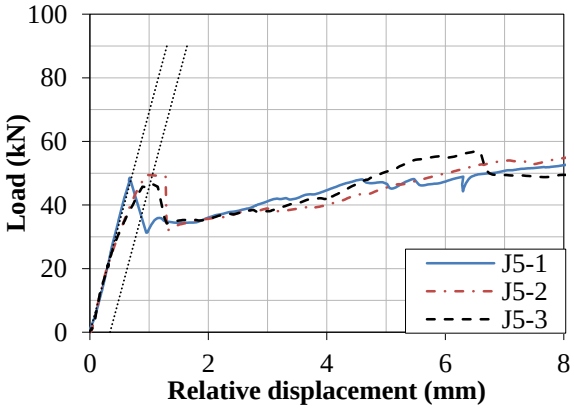

(c) Bearing failure

Figure 4.23: Load-relative displacement of single bolted connections without bolt torque

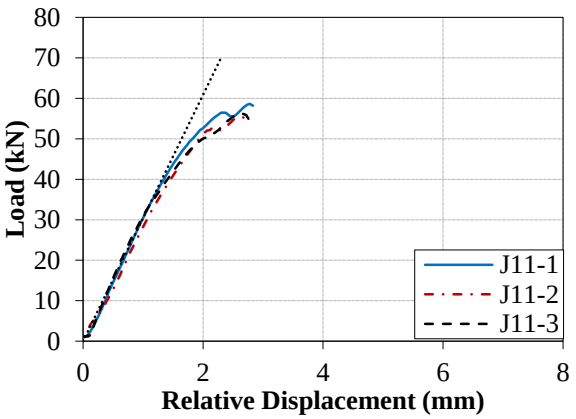

(a) Net-tensile failure

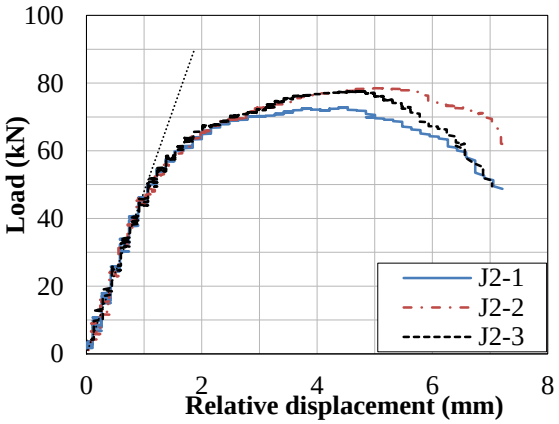

(b) Shear failure

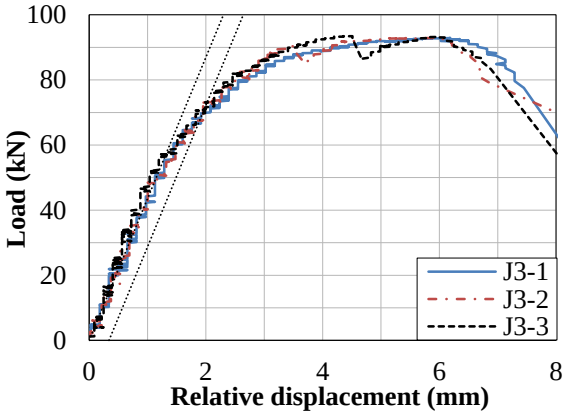

(c) Bearing failure

Figure 4.24: Load-relative displacement of single bolted connections with bolt torque

Figure 4.24 shows the load-relative displacement relationship of the connection with bolt torque in the bolt. The load-relative displacement characteristic of net-tension failure is shown in Figure 4.24(a). There is no significant difference between the net-tension failure connections with and without bolt torque in load-displacement relationship. However, a significant difference is observed in the load-relative displacement relationship of the bearing failure connection with bolt torque, which does not have any load drop in the connection. The load gradually increases with the increase of displacement up to the ultimate strength, and then the load gradually decreases and finally connection would fail. The confinement effect on the main plate is increased with deformation of material in the thicknes direction caused by damage of material, resulting in an increase of the material strength. At the ultimate stage, the shear damage occurred at a 45° angle with the loading direction from the first bolt hole,

resulting in the reduction of resisting force in the connection. In addition, the ultimate strength of bearing failure connection with bolt torque is larger than that of the connection without bolt torque. It is because the connection with bolt torque provides lateral restraint by the washers through the cover plates. The ultimate strength of shear failure connection with bolt torque is larger than that of the connection without bolt torque.

4.5.3 Ultimate Strength

The ultimate strength of a connection is calculated by using the following equations.

$$\text{Bearing strength } = \frac{P_u}{td} \tag{4.9}$$

$$\text{Tensile strength } = \frac{P_u}{(w-d_h)t} \tag{4.10}$$

$$\text{and shear strength } = \frac{P_u}{2et} \tag{4.11}$$

In Eqs. (4.9), (4.10), and (4.11), P_u is the ultimate failure load of the connection and d, t, w, and d_h are the bolt diameter, thickness of plate, width of a plate, and diameter of hole, respectively. The ultimate strength of the connections is shown in Table 4.11 with respect to the failure mode.

In this study, 2% offset strength is also calculated. At first, the stiffness of a connection is calculated between two specific load or relative displacement points corresponding to the linear portion of the curve using the relation: $E_c = \Delta_L/\Delta_{rd}$, where Δ_L and Δ_{rd} are the changes in the load and the relative displacement over the chord stiffness range, respectively. Then a 2% offset line is drawn with respect to the stiffness line. The 2% offset strength is defined as the load where the offset line interests of the load-relative displacement curve before the ultimate load. Therefore, the 2% offset strengths are not considered strength of pin bearing connections. The 2% offset strengths are calculated only for the bearing failure cases.

Damage initiation strength is also calculated and summarized with 2% offset load in Table 4.12. The damage initiation strength is defined as the load corresponding to the point

where the slope of the curve is reduced by 30% from the initial stiffness.

A variation of the damage initiation strength is relatively large when compared with the ultimate strength because the load is fluctuated at the initiation of damage due to brittleness of the material. The average variation of the damage initiation is about 10 %.

Strengths of the connections are also calculated according to the current design guidelines of ASCE LRFD Pre-standard (ASCE, 2010) and CNR-DT 205/2007 (National Research Council, 2007) and presented in Table 4.12. It is observed that the difference of ultimate strengths between the experimental and predict by the design guidelines is very large. In the most of the connection cases, the difference is more than 30%.

Failure modes of the connections are also predicted by the design guidelines. Failure modes are predicted correctly in 11 cases out of the 20 cases for ultimate failure and 10 out of 20 for damage initiation by the ASCE LRFD Pre-standard. CNR-DT 205/2007 predicts correct failure modes in 15 cases out of the 20 cases for both the ultimate failure and the damage initiation. It should be mentioned that these design guidelines specify equations of strength evaluation for the pultruded FRP composite material.

Table 4.12: Strengths and failure modes of single bolted connections

ID	Experimental results								ASCE				CNR			
	Bolt torque (N-m)	Ultimate strength			Damage initiation strength			2% offset	Failure mode	Strength (kN)	% Difference (US)	% Difference (DIS)	Failure mode	Strength (kN)	% Difference (US)	% Difference (DIS)
		Failure mode	Average (kN)	COV (%)	Failure mode	Average (kN)	COV (%)									
J1	3	B	84.2	5.1	B	48.7	5.0	68.0	S	43.2	-49	-11	B	51.2	-39	5
J2	3	S	76.3	4.0	B	49.0	3.0	-	S	30.7	-60	-37	S	44.5	-42	-9
J3	3	B	93.1	0.3	B	51.7	6.2	66.7	S	43.2	-54	-16	B	51.2	-45	-1
J4	0	NT	45.7	6.4	NT	37.2	2.6	-	NT	39.7	-13	7	B	51.2	12	38
J5	0	B	48.2	2.7	B	25.1	60.0	-	S	43.2	-10	72	B	51.2	6	104
J6	0	S	45.7	6.4	S	21.66	5.3	-	S	18.3	-60	-16	S	26.7	-42	23
J7	3	S	59.2	2.0	S	35.0	14.8	-	S	18.3	-69	-48	S	26.7	-55	-24
J8	3	S	44.5	3.9	S	21.7	6.7	-	S	12.1	-73	-44	S	17.8	-60	-18
J9	3	NT	75.5	6.0	B	47.3	4.9	-	S	43.2	-43	-9	B	51.2	-32	8
J10	0	B	52.1	1.1	B	35.5	6.9	-	S	43.2	-17	22	B	51.2	-2	44

Note: NT= Net-tension failure, B = Bearing failure, S = Shear Failure，US = ultimate strength, DIS = damage initiation strength

Table 4.12: Strengths and failure modes of single bolted connections (cont'd)

ID	Experimental results								ASCE				CNR			
	Bolt torque (N-m)	Ultimate strength			Damage initiation strength			2% offset failure strength (kN)	Failure mode	Strength (kN)	% Difference (US)	% Difference (DIS)	Failure mode	Strength (kN)	% Difference (US)	% Difference (DIS)
		Failure mode	Average (kN)	COV	Mode of damage initiation	Damage initiation strength	COV									
J11	3	NT	56.8	3.0	NT	38.8	6.0	-	NT	39.7	-30	2	B	51.2	-10	32
J12	3	NT	57.4	2.9	NT	47.1	9.9	-	NT	39.7	-31	-16	B	51.2	-11	9
J13	3	S	44.2	2.0	S	19.2	14.7	-	S	12.1	-73	-37	S	17.8	-60	-7
J14	3	B	90.7	1.0	B	51.2	2.2	60.7	S	43.2	-52	-16	B	51.2	-44	0
J15	0	B	20.0	1.0	B	15.3	13.5	-	NT	20.1	1	31	B	26.3	32	72
J16	0	S	17.4	1.3	S	11.7	8.3	-	S	6.2	-64	-47	S	9.2	-47	-21
J17	0	B	17.9	2.0	B	15.4	6.3	-	S	22.3	25	45	B	26.3	47	71
J18	3	NT	59.3	3.1	NT	43.0	2.9	-	NT	40.3	-32	-6	B	51.2	-14	19
J19	3	S	41.0	2.4	S	23.4	4.5	-	S	12.5	-70	-47	S	18.4	-55	-21
J20	3	B	69.2	6.8	B	38.2	10.2	-	S	43.2	-38	13	B	51.2	-26	34

Note: NT= Net-tension failure, B = Bearing failure, S = Shear Failure , US = ultimate strength, DIS = damage initiation strength

4.5.4 Effect of Width and Bolt Torque

The ultimate bearing strength with respect to the width to bolt diameter ratio, *w/d*, is given in Figure 4.25 for the connections with and without bolt torque. The various failure modes are represented as “NT” for net tension failure and "B" for bearing failure, and the combined failure of them are represented by hyphenated letters. It can be observed that the failure modes change as the *w/d* ratios change. The net-tension failure changes to the bearing failure when the *w/d* ratio is increased from 2 to 4. The combined failure, where bearing damage occurred first and then net-tension failure occurs, as observed for of the connections for the *w/d* ratios of 2.5 and 3.0. In these cases, net-tension failure occurs in the connection before the ultimate strength for bearing is reached. It can also be observed that the ultimate strength with the bolt torque is larger than that without bolt torque. The ultimate bearing strength increases by about 93% for the connection with a *w/d* ratio of 4 due to the bolt torque. The bearing strength of the material is also shown in the figure. The bearing strength of the pin-bearing connection is almost equal to the compressive strength of material found from the compressive test in this study.

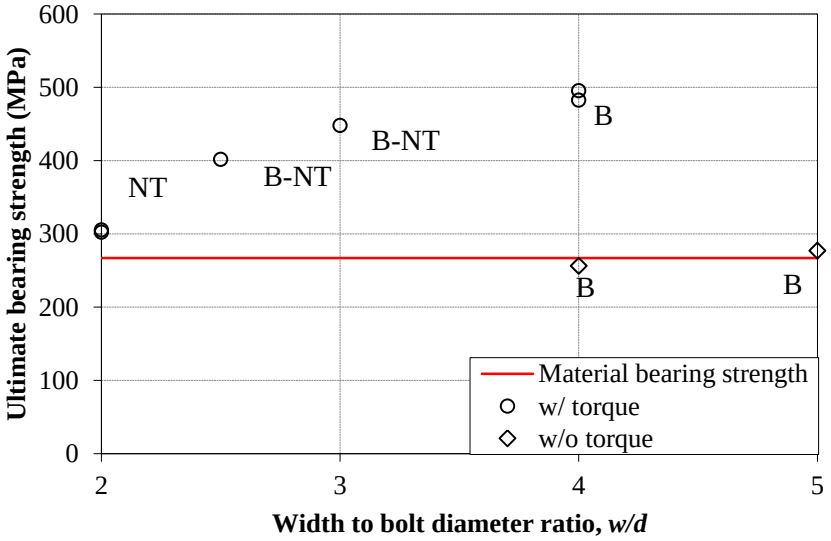

Figure 4.25: Effect of width to bolt diameter ratio, *w/d*

4.5.5 Effect of Edge Distance and Bolt Torque

The ultimate bearing strengths are plotted with respect to the edge distance to bolt diameter ratio, *e/d*, in Figure 4.26 for the connections with and without bolt torque. The various failure modes are represented as “S” for shear failure and "B" for bearing failure, and the combined failure of them are represented by hyphenated letters. It can be observed that the failure mode changes with as the *e/d* ratio changes. The shear failure switch to bearing failure when the *e/d* ratio is increased from 1.5 to 4. The combined failure, where bearing damage occurs first and then shear failure occurs, was observed for the connections with the *w/d* ratios of 2.0 and 3.0. In these cases, the shear failure occurs in the connection before the ultimate strength for bearing is reached. It can also be observed that the ultimate strength increases due to bolt torque. The ultimate shear strength increases by about 30% for the connection with an *e/d* ratio of 2 by using bolt torque.

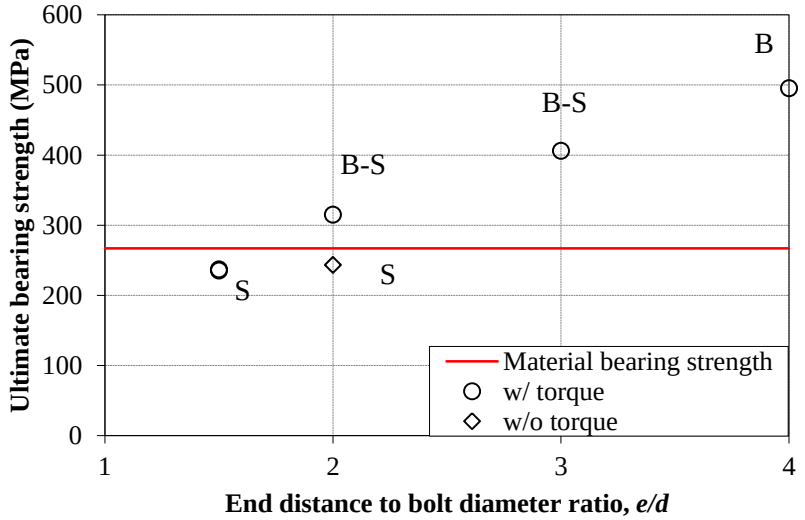

Figure 4.26: Effect of end distance to bolt diameter ratio, *e/d*.

4.5.6 Effect of Cover Plate

Figure 4.27 illustrates the effect of different cover plates on the strength of connections. It can be observed that strengths are almost the same for connections with 6-mm steel and 12-mm GFRP cover plate for each failure mode. However, for the bearing and shear failure

cases, the strength of the connection with the 6-mm GFRP cover plates is lower than those with other cover plates, and the cover plate would fail. Using 6-mm GFRP cover plate in the connection leads to about 26% lower strength for the bearing failure case and about 8% lower strength for the shear failure case than the connection with 6-mm steel cover plates. This reduction in the strength can be explained by the following reason: (a) confinement effect is better for connections with 6-mm steel and 12-GFRP cover plates than the connection with 6-mm GFRP cover plates, (b) the 6-mm GFRP cover plate fails, (c) bending effect act on the cover plate shown in Figure 4.28.

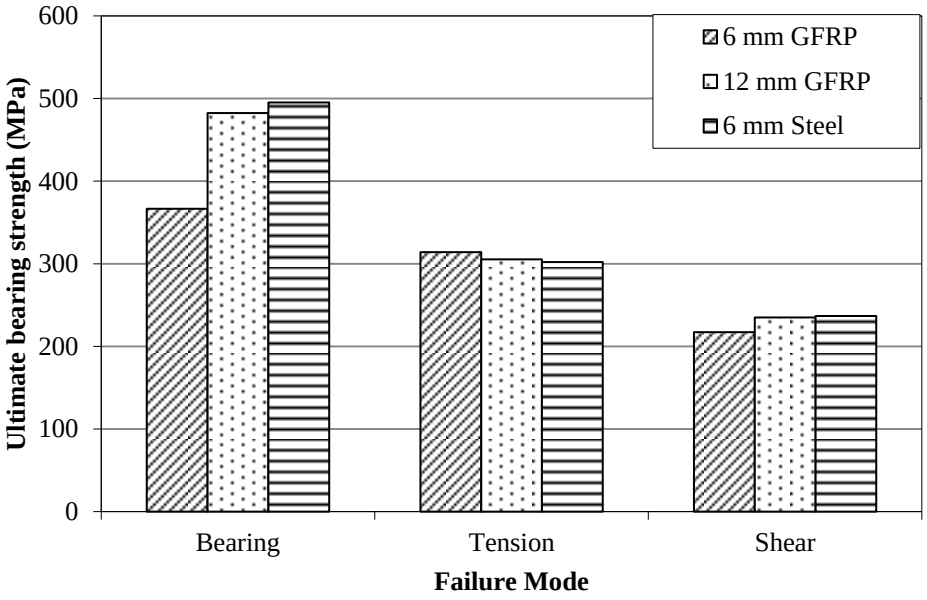

Figure 4.27: Effect of cover plate

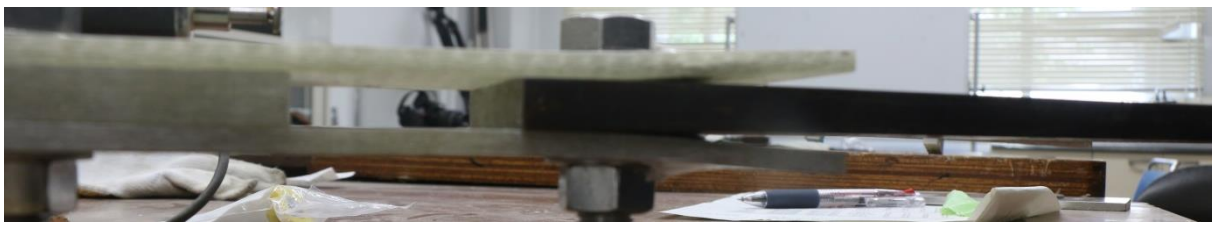

Figure 4.28: Bending effect in cover plate

4.5.7 Effect of Confinement by Washers

To see the effect of confinement by washers on the cover plate, cases of no confinement

by washers (J16, J17) are compared with cases with confinement (J19, J20). The effect of washer is shown in Figure 4.29. The strength increases by about 18% in the shear failure case and by about 93% in the bearing failure case due to the confinement by washers.

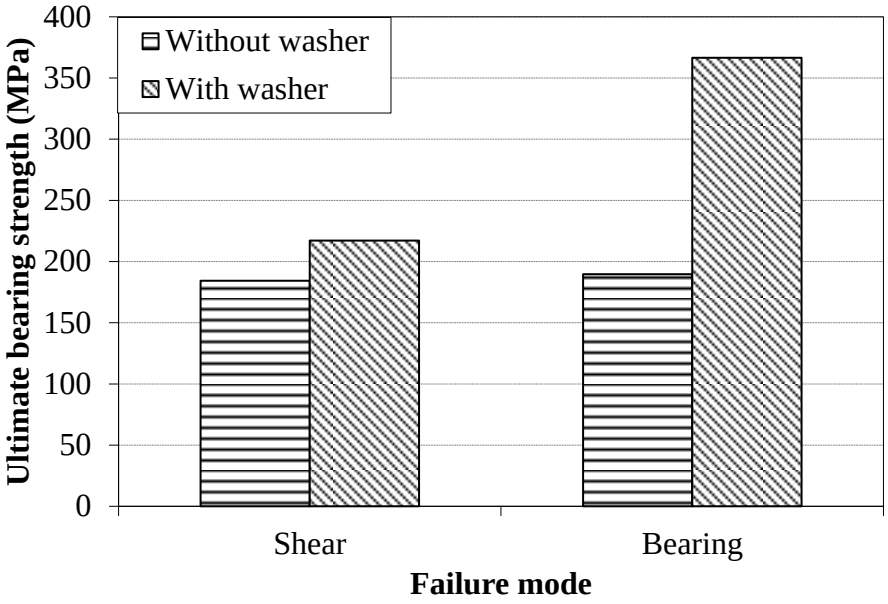

Figure 4.29: Effect of washer

4.5.8 Analysis of Experimental Strength and Strength Predicted by Design Codes

Using the current design guidelines of ASCE LRFD Pre-standard (ASCE, 2010) and CNR-DT 205/2007 (National Research Council, 2007) strengths of the connections are calculated with respect to the experimental failure mode. The ultimate strength ratio, experimental strength to the strength calculated by the codes, is also determined and presented in Figure 4.30 and Figure 4.31.

Figure 4.30 shows the ratio of the damage initiation strength to the strength calculated by the design codes, r_i. It is observed that for the ASCE LRFD Pre-standard, the strength ratios are closer to 1.0 for the net-tension and bearing failure cases. However, the strength ratio of shear failure is too large, the range of values about 1.2 to 1.9. On the other hand, for the CNR –DT 205/2007, the strength ratios are closer to 1.0 for the bearing and shear failure cases, but the strength ratio of net-tension is too low, the range of values about 0.5 to 0.8.

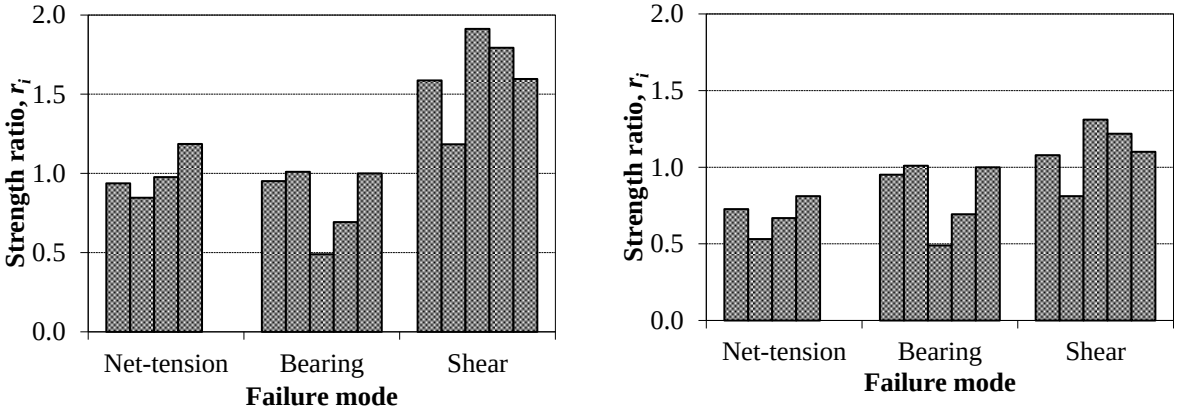

(a) ASCE LRFD Pre-Standard (b) CNR-DT 205/2007

Figure 4.30: Damage initiation strength to predicted strength

Figure 4.31 shows the ratio of the ultimate strength from the experiment to the strength calculated by the design codes, r_u. It is observed that for the ASCE LRFD Pre-standard, the strength ratios are mere than 1.0 for all cases except the two in bearing failure mode where those connections are pin-bearing. On the other hand, for the CNR –DT 205/2007, the strength ratios are closer to 1.0 for net-tension failure cases. However, the strength ratios are too large for the bearing and shear failure.

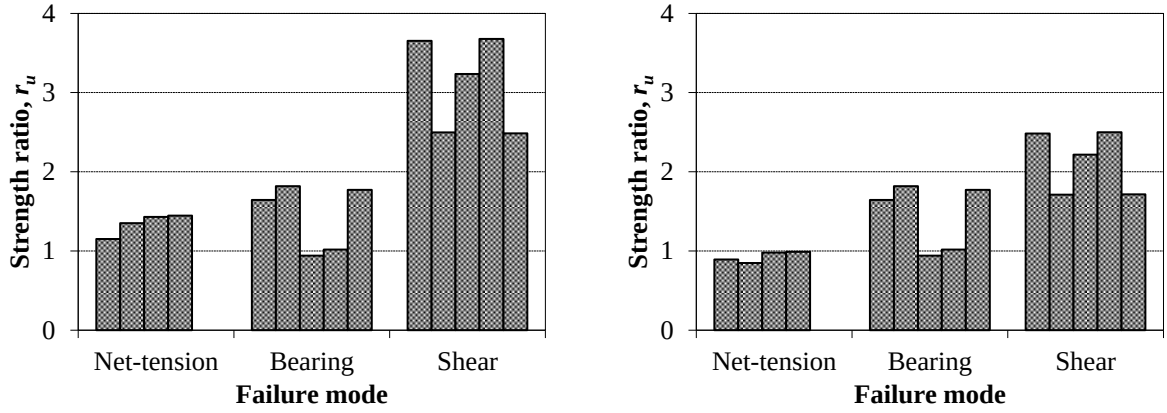

(a) ASCE LRFD Pre-Standard (b) CNR-DT 205/2007

Figure 4.31: Ultimate strength to predicted strength

4.5.9 Comparison of Numerical Analysis of a Connection and Experiment

Experimental results for the single bolted connections are compared with results from the numerical analysis described in Chapter 3. The material properties described in Section

4.2 are used in the analysis. From the numerical analysis, strength, failure modes, and load displacement characteristics were found and those were compared with experimental results.

Figure 4.32 shows the failure modes from the numerical analyses and experiments of Connection J1, J2, and J3. Contour in the figure shows the damage of the connection plates. It can be observed that failure modes are predicted well by the numerical model. The connections J1 and J3 are bearing failure, and the connection J2 is bearing failure.

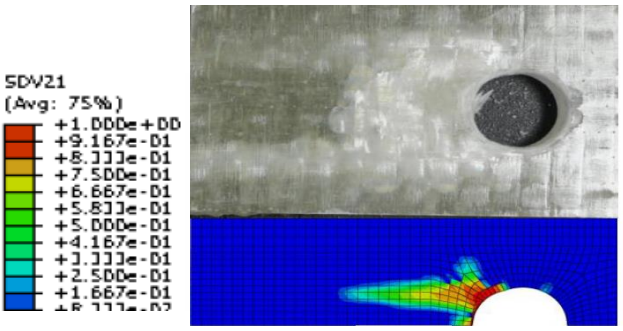

(a) Connection J1

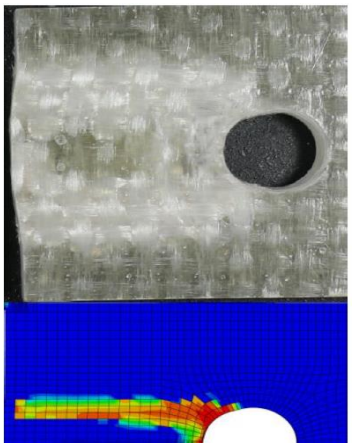

(b) Connection J2

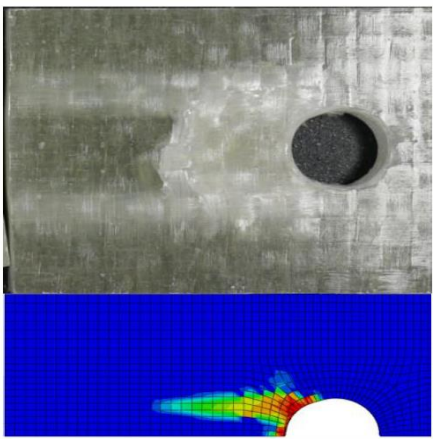

(c) Connection J3

Figure 4.32: Failure modes of single bolted connections

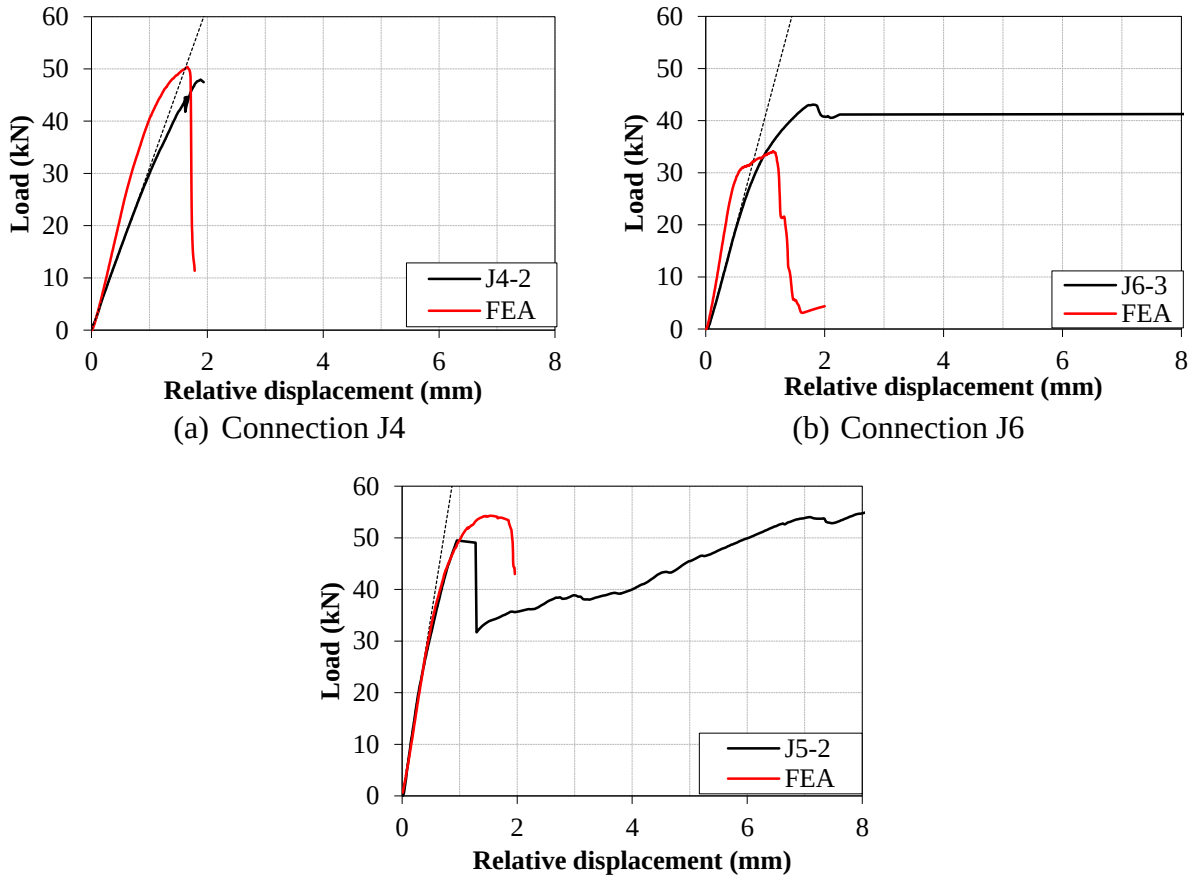

(a) Connection J4

(b) Connection J6

(c) Connection J5

Figure 4.33: Load-displacement relationship of single bolted connection without bolt torque

Figure 4.33 shows the load-displacement relationships of single bolted connections with pin-bearing obtained from the experiment and the numerical analysis. The linear dotted lines show the initial stiffness of the connection of the experiment. Stiffness and ultimate strength of the bearing failure connection J5 found from the numerical analysis are almost the same as those from the experiment. However, stiffnesses of the net-tension and shear failure from the numerical analysis are larger by about 150% than those of the experiment. The net-tension failure strength of the connection J4 is predicted well, but the shear failure strength cannot be predicted by the numerical analysis.

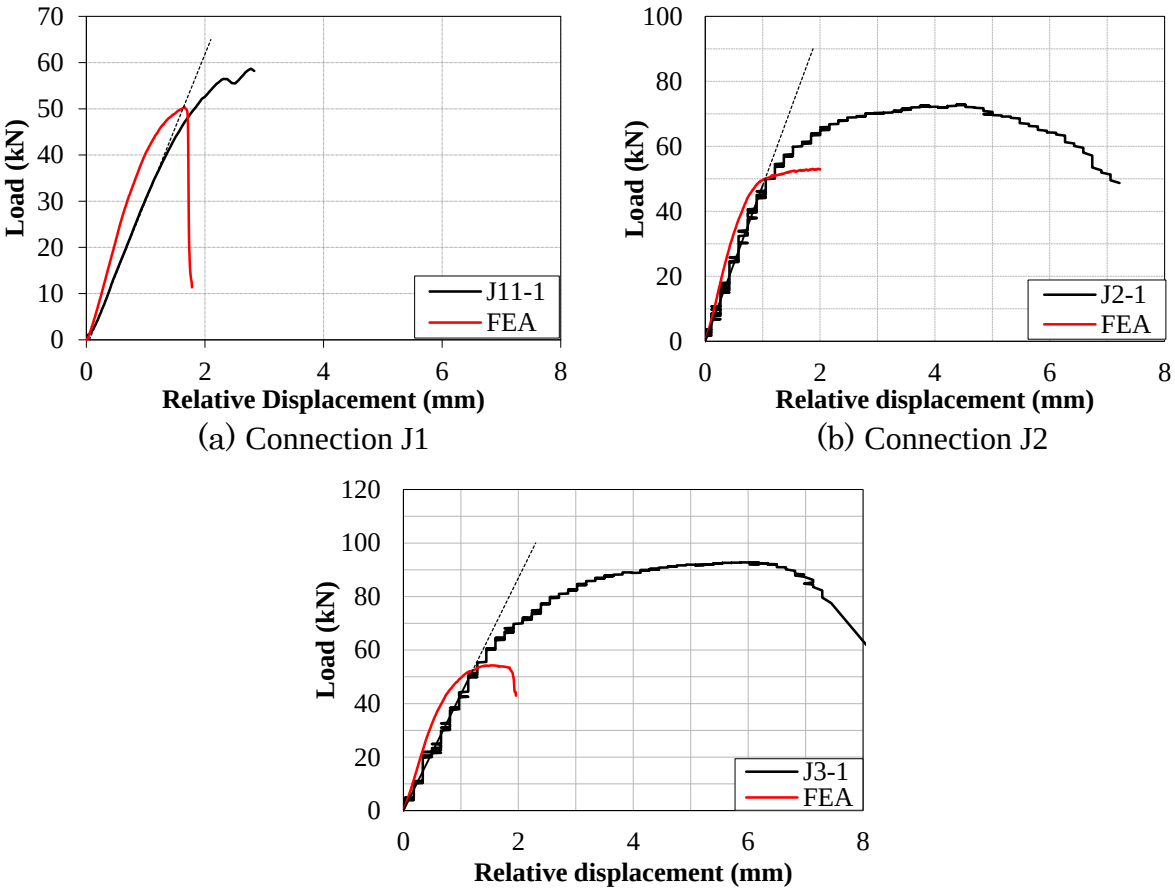

(a) Connection J1

(b) Connection J2

(c) Connection J3

Figure 4.34: Load-displacement relationship of single bolted connection with bolt torque

Figure 4.34 shows the load-displacement relationships of single bolted connections with bolt torque obtained from the experiment and the numerical analysis. The linear dotted lines show the initial stiffness of the connection of the experiment. Stiffnesses of the connections from the numerical analysis are larger by about 150% than those of the experiment. The failure strengths of the connections are lower by about 14% for net-tension failure, by 26% for shear failure, and by 43% for bearing failure than those from the experiment.

4.6 Summary

A series of tensile, compression and shear tests were conducted in this chapter to obtain the material properties of GFRP laminates with thickness of 6, 9, and 12 mm.

Twenty sets of single bolted connections with different parameters were investigated in

this chapter. Three basic failure modes net-tension, shear and bearing failure were observed in the single bolted connection. The bearing and shear failure showed the large displacement before failure of the connection. Whereas, the net-tension failure mode showed a catastrophic failure.

By changing the cover plate from 6-mm steel to 12-mm GFRP, connection strength did not change. However, when the 6-mm steel cover plate was changed to 6-mm GFRP cover plate, the strength decreased by about 26% for the bearing failure and by about 8% for shear failure. Therefore, connections with a cover plate thickness half of the main plate may not be appropriate in the single bolted connection.

The two basic geometric parameters, *w/d* and *e/d*, were changed to determine the effect of geometric parameters. The net-tension failure changed to the bearing failure when the *w/d* ratio increased from 2 to 4, and the shear failure changed to the bearing failure when the *e/d* ratio changed from 1.5 to 4.

Connections with or without 3 N-m bolt torque were tested to determine the effect of bolt torque. The ultimate bearing strength increased by about 93% due to the bolt torque for the connection with a *w/d* ratio of 4 and the ultimate shear strength increased by about 30% for the connection with a *e/d* ratio of 2.

As the effect of confinement by washers, the strength was found to increase by about 18% in the shear failure and by about 93% in the bearing failure.

The ultimate bearing strength of the pin-bearing connection is predicted well by the ASCE LRFD Pre-standard and CNR –DT 205/2007. However, the strength of the connection with bolt torque from the experiment is about 1.9 times the predicted one. The ultimate tensile strength is larger than the strength predicted by the ASCE LRFD Pre-standard and lower than the strength predicted by the CNR –DT 205/2007. The shear strength is much larger than the strength predicted by the ASCE LRFD Pre-standard and CNR-DT 205/2007.

The numerical analysis can predict the failure modes of the connections. Strength and

stiffness were predicted well by the numerical analysis for the pin-bearing connection. However, the strength and stiffness the connection with bolt torque were not predicted well.

CHAPTER 5 EXPERIMENTAL STUDY ON MULTI-ROW BOLTED CONNECTIONS

5.1 Introduction

A comprehensive experimental program was conducted to study and determine the behavior of bearing-type multi-row bolted connections with a double-lap configuration fabricated from woven fabric GFRP composite material. The investigation examined the effect of different parameters on the strength and failure mode of the multi-row bolted connections including cover plates stiffness, width, pitch distance and edge distance. The test program and test results are presented in detail in this chapter.

5.2 Connection Specimens

5.2.1 Parameters

An experimental study was conducted to examine multi-row bolted connections with a double-lap configuration fabricated from woven fabric GFRP composite material. The materials discussed in Section 4.2 were also used for multi-row bolted connections. In the multi-row bolted connection, 12-mm GFRP plate is used as a main plate. The four different stiffness of cover plates have been studied in this study, are 6, 9, and 12 mm for GFRP cover plates, and 6 mm for steel cover plates, which corresponds to stiffness ratios of two cover plates to the main plate of about 1.0, 1.5, and 2.0 for GFRP cover plates and about 8.0 for a steel cover plate, respectively. Each set has three samples of connection.

In this investigation, the three basic geometric parameters have also been studied: the width of the member, w, the pitch distance, p, and the edge distance, e. The width, pitch distance, and edge distance are varied to obtain different values for the width to bolt diameter ratio, w/d, the pitch distance to bolt diameter ratio, p/d, and the edge distance to bolt diameter

ratio, *e/d*. To obtain the different failure modes in the connection, the values of the width, pitch distance, and edge distance were selected. The geometric parameters tested in this study are given in Table 5.1, 5.2, and 5.3. To designate each connection geometry, a connection ID is used in this study. A connection ID consists of a number of bolt rows, connection type, cover plate material, and cover plate thickness as shown in Figure 2.2. Connection type represents a set of geometric parameters.

Table 5.1: Two-row bolted connection parameters

ID	*n*	*w/d*	*p/d*	*e/d*	*Cover plate*	ID	*n*	*w/d*	*p/d*	*e/d*	*Cover plate*
2BF6	2	4.0	4.0	2.0	6-mm GFRP	2QF9	2	6.0	2.5	2.0	9-mm GFRP
2BS6	2	4.0	4.0	2.0	6-mm steel	2QS6	2	6.0	2.5	2.0	6-mm steel
2LF6	2	4.0	5.0	3.5	6-mm GFRP	2XF6	2	6.0	5.0	4.0	6-mm GFRP
2LS6	2	4.0	5.0	3.5	6-mm steel	2XF12	2	6.0	5.0	4.0	12-mm GFRP
2NS6	2	3.0	5.0	3.5	6-mm steel	2XS6	2	6.0	5.0	4.0	6-mm steel

Table 5.2: Three-row bolted connection parameters

ID	*n*	*w/d*	*p/d*	*e/d*	*Cover plate*	ID	*n*	*w/d*	*p/d*	*e/d*	*Cover plate*
3BF6	3	4.0	4.0	2.0	6-mm GFRP	3SF9	3	9.0	2.5	3.0	9-mm GFRP
3BS6	3	4.0	4.0	2.0	6-mm steel	3TF9	3	9	2.5	4.0	9-mm GFRP
3JF6	3	5.0	5.0	3.5	6-mm GFRP	3US6	3	9.0	3.0	2.0	6-mm steel
3JF9	3	5.0	5.0	3.5	9-mm GFRP	3VS6	3	9.0	4.0	2.0	6-mm steel
3JS6	3	5.0	5.0	3.5	6-mm steel	3YF12	3	9.0	5.0	4.0	12-mm GFRP
3KF6	3	5.0	6.0	3.5	6-mm GFRP	3YF6	3	9.0	5.0	4.0	6-mm GFRP
3LS6	3	4.0	5.0	3.5	6-mm steel	3YS6	3	9.0	5.0	4.0	6-mm steel
3MS6	3	6.0	5.0	3.5	6-mm steel	3AaF6	3	9.0	5.0	2.0	6-mm GFRP
3OF6	3	5.0	5.0	4.5	6-mm GFRP	3AaF12	3	9.0	5.0	2.0	12-mm GFRP
3PS6	3	7.0	5.0	3.5	6-mm steel	3AaS6	3	9.0	5.0	2.0	6-mm steel
3RF6	3	9.0	2.5	2.0	9-mm GFRP	3AbF12	3	9.0	5.0	3.0	12-mm GFRP
3FF9	3	9.0	2.5	2.0	9-mm GFRP	3AbS6	3	9.0	5.0	3.0	6-mm steel
3RS6	3	9.0	2.5	2.0	9-mm GFRP						

Table 5.3: Four-row bolted connection parameters

ID	*n*	*w/d*	*p/d*	*e/d*	*Cover plate*	ID	*n*	*w/d*	*p/d*	*e/d*	*Cover plate*
4BF6	4	4.0	4.0	2.0	6-mm GFRP	4MF6	4	6.0	5.0	3.5	6-mm GFRP
4BF9	4	4.0	4.0	2.0	9-mm GFRP	4MS6	4	6.0	5.0	3.5	6-mm steel
4BS6	4	4.0	4.0	2.0	6-mm steel	4NS6	4	3.0	5.0	3.5	6-mm steel

It should be noted that the above parameters listed in Table 5.1 are not the only factors that could influence the behavior of bolted connections. Some of the other factors include the amount of clearance between the bolt and bolt hole, the amount of bolt torque or axial force in the bolt, the size of the washer, and bending effects caused by a single-shear connection. In this investigation, standard washers with 16 mm A2-72 stainless steel (SUS 304) structural bolts were used. The diameter of a bolt hole, d_h, is 17 mm, resulting in a clearance of 1 mm. This clearance was chosen according to CNR DT 205/2007 (National Research Council, 2007) and kept constant throughout this study. The finger tight torque of 3 N-m, was introduced and kept constant for all the multi-row bolted connections.

5.2.2 Connection Fabrication

The fabrication process was described in the previous chapter. Dimensions of the three-row bolted connection plate are shown in Figure 5.1. In the main plate and cover plate of multi-row bolted connection, L_1= 150 mm is considered for the grip of the connection. The multi-row bolted connection, one GFRP main plate and two cover plates either GFRP or steel were used.

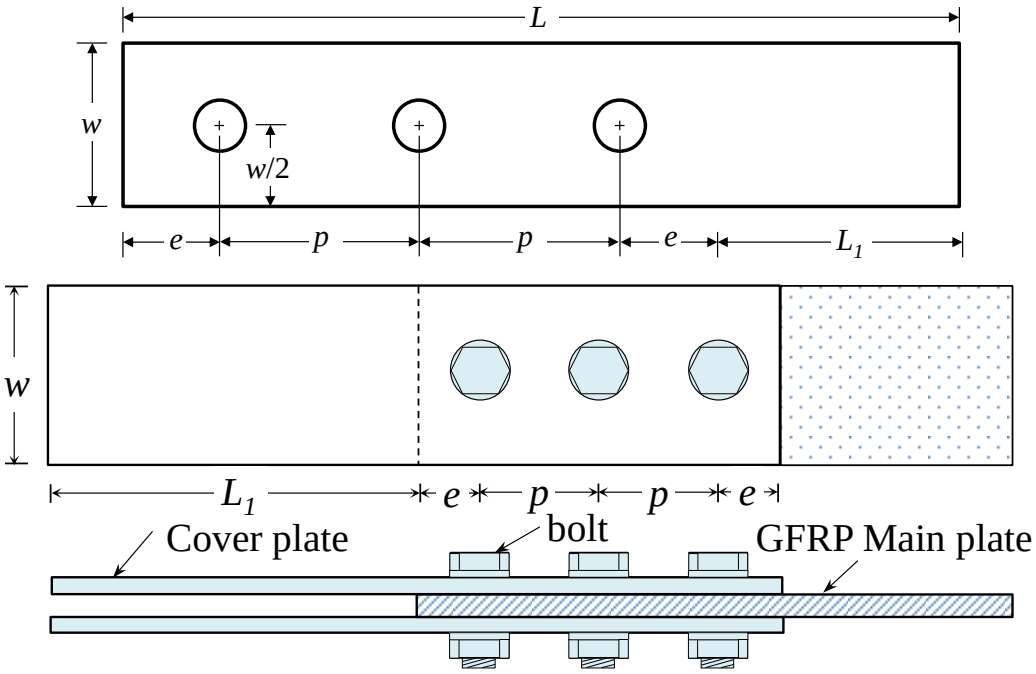

Figure 5.1: Connection plate of multi-row bolted connection

5.3 Test Set-up

In this study, double-lap connections with two to four rows of bolts were tested. The single bolted connections are described in the chapter 4. The typical multi-row bolted connection configurations are shown in Figure 5.2. The finger tightening torque of 3 N-m was applied of the bolts by the torque wrench for clamping the connection plates through the standard washers. A universal testing machine with a capacity of 500 kN was used to perform the test. The main plate was gripped at the top, and cover plates with a 12-mm steel spacer were gripped at the bottom. An effect of gripping configuration is examined by using strain gauges on cover plates closer to the spacer. It was observed that the change of strain in the inner and outer sides of the cover plate was insignificant. Therefore, it was concluded that this gripping configuration will not affect the strength and failure mode. The tensile load was applied to the specimen. Displacements were measured by using four transducers described in Chapter 4. The setting of the displacement transducers is illustrated in Figure 5.2.

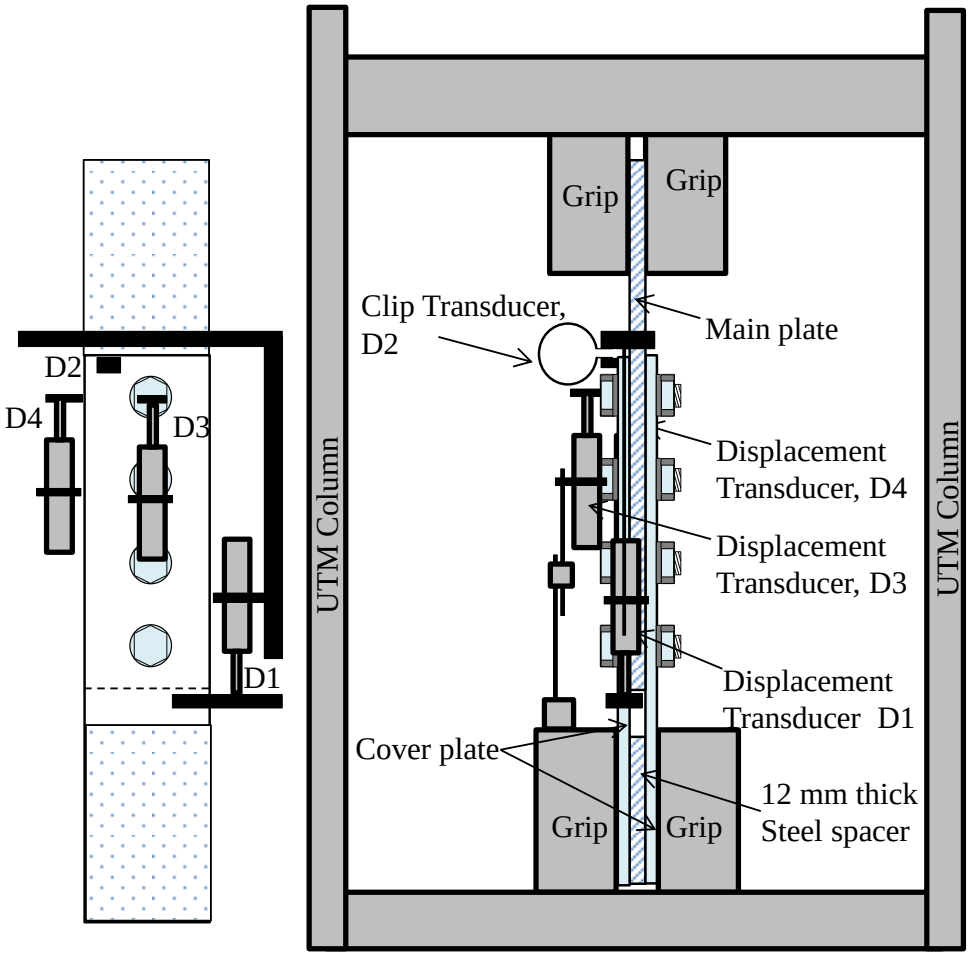

Figure 5.2: Test set-up of multi-row bolted connection

5.4 Results and Discussions

The ultimate strengths and failure modes for all the multi-row bolted connections from the experiments are summarized in Table 5.4, 5.5, and 5.6. The ultimate strength is the total capacity of the connection based on the failure either the main plate or cover plates of the connection. The variation of ultimate load of each set of connections was below 5% except the connection 4BS6. The variability of the ultimate strength within the range of material variability. The damage initiation strength is also shown in the table. The damage initiation was explained in the Section 4.5. The variation of damage initiation strength is larger when compared with ultimate strengths. For about 40% of the connections, the coefficient of variation is greater than 10%. The experimental results are discussed in the following sections.

Table 5.4: Strengths and failure modes of two-row bolted connections

ID	*n*	*w/d*	*p/d*	*e/d*	Average ultimate strength (kN)	COV (%)	Failure mode	Damage initiation strength (kN)	COV (%)
2BF6	2	4.0	4.0	2.0	111	4.1	ES	58	6.1
2BS6	2	4.0	4.0	2.0	130	3.1	B*	66	4.2
2LF6	2	4.0	5.0	3.5	139	2.4	NT	77	19.6
2LS6	2	4.0	5.0	3.5	143	2.9	NT	96	3.9
2NS6	2	3.0	5.0	3.5	111	2.4	NT	77	29.3
2QF9	2	6.0	2.5	2.0	111	4.6	S	60	6.3
2QS6	2	6.0	2.5	2.0	109	2.6	S	53	2.0
2XF6	2	6.0	5.0	4.0	169	2.1	B	104	4.9
2XF12	2	6.0	5.0	4.0	180	1.9	B	105	7.7
2XS6	2	6.0	5.0	4.0	180	2.9	B	99	3.2

Note: NT= Net-tension failure, B = Bearing failure, B* = bearing failure with shear at end of plate, S = Shear Failure, ES = Shear at ends of the main plate and cover plate

Table 5.5: Strengths and failure modes of four-row bolted connections

ID	*n*	*w/d*	*p/d*	*e/d*	Average ultimate strength (kN)	COV (%)	Failure mode	Damage initiation strength (kN)	COV (%)
4BF6	4	4.0	4.0	2.0	141	3.5	NT	124	10.2
4BF9	4	4.0	4.0	2.0	154	1.8	NT	107	15.0
4BS6	4	4.0	4.0	2.0	143	6.3	NT	108	6.0
4MF6	4	6.0	5.0	3.5	201	2.7	NT	145	5.9
4MS6	4	6.0	5.0	3.5	209	1.1	NT	137	6.2
4NS6	4	3.0	5.0	3.5	111	4.4	NT	92	19.3

Note: NT= Net-tension failure, B = Bearing failure, B* = bearing failure with shear at end of plate, S = Shear Failure, ES = Shear at ends of the main plate and cover plate

Table 5.6: Strengths and failure modes of three-row bolted connections

ID	*n*	*w/d*	*p/d*	*e/d*	Average ultimate strength (kN)	COV (%)	Failure mode	Damage initiation strength (kN)	COV (%)
3BF6	3	4.0	4.0	2.0	134	2.7	NT	121	6.2
3BS6	3	4.0	4.0	2.0	143	1.6	NT	90	14.9
3JF6	3	5.0	5.0	3.5	166	0.9	NT	104	14.5
3JF9	3	5.0	5.0	3.5	174	1.6	NT	129	6.5
3JS6	3	5.0	5.0	3.5	167	2.4	NT	107	15.9
3KF6	3	5.0	6.0	3.5	165	2.7	NT	103	12.3
3LS6	3	4.0	5.0	3.5	151	2.3	NT	111	6.8
3MS6	3	6.0	5.0	3.5	197	2.0	NT	132	13.1
3OF6	3	5.0	5.0	4.5	162	2.0	NT	83	24.8
3PS6	3	7.0	5.0	3.5	251	1.0	NT	145	6.8
3RF6	3	9.0	2.5	2.0	156	2.7	S	76	10.7
3RF9	3	9.0	2.5	2.0	152	0.5	S	83	3.9
3RS6	3	9.0	2.5	2.0	160	2.9	S	85	0.9
3SF9	3	9.0	2.5	3.0	180	3.3	S	101	5.8
3TF9	3	9	2.5	4.0	199	1.8	S	108	10.7
3US6	3	9.0	3.0	2.0	187	2.9	S	114	8.8
3VS6	3	9.0	4.0	2.0	218	2.9	S	117	6.5
3YF6	3	9.0	5.0	4.0	257	2.0	B	103	7.9
3YF12	3	9.0	5.0	4.0	280	2.8	B	138	12.3
3YS6	3	9.0	5.0	4.0	182	1.5	B	160	3.8
3AaF6	3	9.0	5.0	2.0	208	1.6	B*	91	5.5
3AaF12	3	9.0	5.0	2.0	232	3.1	B*	106	9.0
3AaS6	3	9.0	5.0	2.0	235	3.8	B*	123	8.4
3AbF12	3	9.0	5.0	3.0	257	2.4	B*	136	3.1
3AbS6	3	9.0	5.0	3.0	252	2.9	B*	135	3.7

Note: NT= Net-tension failure, B = Bearing failure, B* = bearing failure with shear at end of plate, S = Shear Failure, ES = Shear at ends of the main plate and cover plate

5.4.1 Failure Mode

In the experimental study, three basic failure modes were observed in the multi-row bolted connections as shown in Table 5.4, 5.5, and 5.6. Net-tension, shear, and bearing failure modes, which are shown in Figure 5.3. The net-tension failure occurs at the cross-section through the first bolt hole as shown in Figure 5.3(a). The net-tension is found for two-row bolted connections with *w/d* ratios of 3 and 4 (2BF6, 2BS6, 2LF6, 2LS6, and 2NS6), for three-row bolted connections with *w/d* ratios of 4, 5, 6, and 7 (3BF6, 3BS6, 3JF6, 3JF9, 3JS6, 3KF6, 3LS6, 3MS6, 3OF6, and 3PS6), and for four-row bolted connections with *w/d* ratios of 3, 4, and 6 (4BF6, 4BF9, 4BS6, 4MF6, 4MS6, and 4NS6). The net-tension failure caused by the small *w/d* ratio with respect to the maximum tensile force exerted in the section. In some of the net-tension failure cases (3MF6, 3MS6, and 3PS6), bearing damage occurred in the bolt holes before failure of the net-tension.

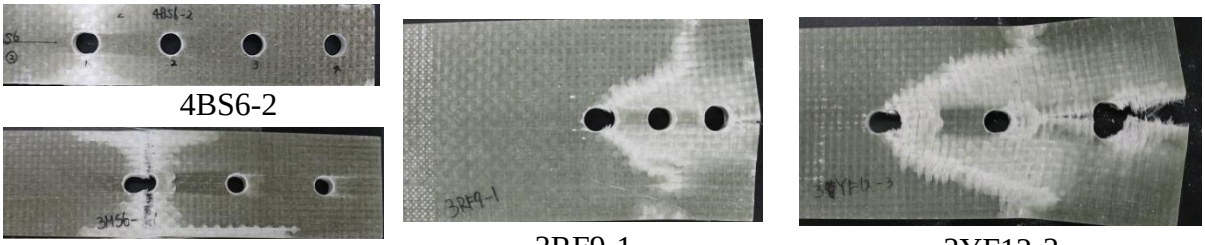

4BS6-2

3MS6-1

3RF9-1

3YF12-3

(a) Tension failure (b) Shear failure (c) Bearing failure

Figure 5.3: Failure modes of multi-row bolted connections

The shear failure occurs at a 45^{o} angle with the loading direction as shown in Figure 5.3(b). The shear failure was found in of the connections of 2QF9, 2QS6, 3RF6, 3RF9, and 3RS6 due to the small *p/d* and *e/d* ratios. The shear failure was initiated in the matrix in the direction parallel to the loading direction beside the bolt holes. The significant shear failure started from the first bolt hole because the maximum tensile force exerted around the first bolt hole. In the shear failure cases, cleavage failure would occur at the final stage of the failure. The cleavage failure was also found in the bearing failure mode, where bearing damage

occurred first then shear failure propagated at a 45^{o} angle with the loading direction from the first hole, and finally cleavage failure occurred in the connection of 2XF6, 2XF12, 2XS6, 3YF6, 3YF12, and 3YS6. The cleavage failure is caused by the transverse force in the plate. The mechanism of cleavage failure is described in Figure 5.4. The bearing force at hole exerted to the loading direction and then the force transfer to the transverse direction. The tensile force acts in the perpendicular direction to the shear failure line Therefore, tensile force exerted in the transverse direction of the plate and as a result cleavage failure.

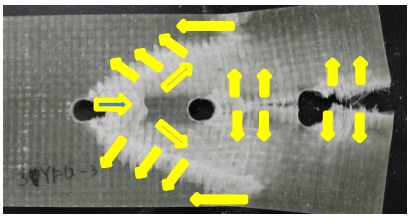

Figure 5.4: Force mechanism of cleavage failure

The minimum requirements of connection geometry by ASCE LRFD Pre-Standard (ASCE, 2010) are w/d = 4, p/d = 4, and e/d =2. Two to four-row bolted connections with those parameters are examined to see the meaning of the minimum requirements. Net-tension failure occurred in the three and four-row bolted connections with steel and GFRP cover plates (3BF6, 3BS6, 4BF6, and 4BS6), whereas, bearing damage in the first hole occurred initially and end shear damage occurred at the end of the GFRP main plate, and finally net-tension failure occurred in the two-row bolted connection with steel cover plate (2BS6). However, end shear failure occurs in the main and cover plates of the two-row bolted connection with 6 mm GFRP cover plates (2BF6). It indicates that the geometry of the connection, which is a minimum requirement of the LRFD Pre-standard (ASCE, 2010), is not sufficient to achieve the bearing failure for those cases even though they satisfy the minimum requirements.

End shear also occurred in the connections of 3AaF6, 3AaF12, and 3AaS6 due to the

small end distance (*e/d* = 2.0). In the connection of 3AaF6 which was 6-mm GFRP cover plates, bearing failure occurred in the intermediate row, and end shear occurred at the ends of the main plate and the cover plates as shown in Figure 5.5(a), while the connections of 3AaF12 and 3AaS6 that have 12-mm GFRP and 6-mm steel cover plates, bearing failure occurred in the first and second holes, and end shear occurred at the end of the main plate and finally shear and cleavage failure occurred as shown in Figure 5.5 (b) and Figure 5.5 (c).

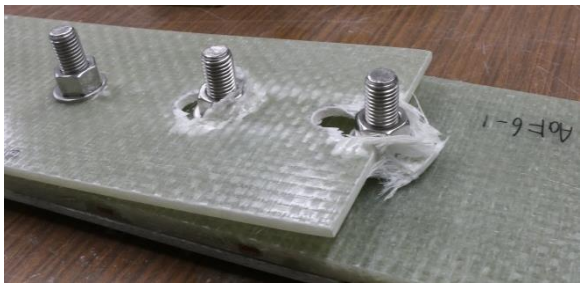

3AaF6-1

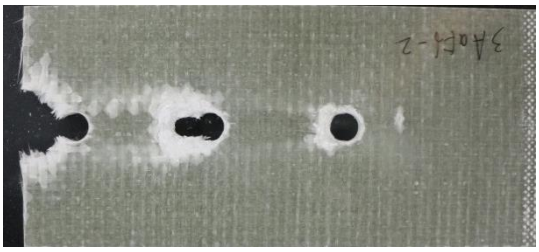

3AaF6-2

(a) Connection with 6-mm FRP cover plates (3AaF6)

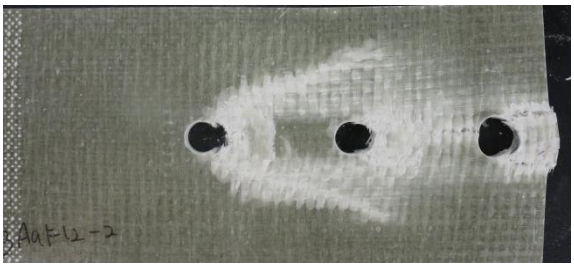

(b) Connection with 12 mm GFRP cover plates (3AaF12-2)

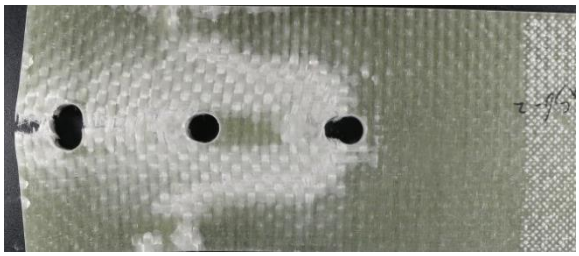

(c) Connection with 6 mm steel cover plates (3AaS6-2)

Figure 5.5: Failure mode of connections with a small end distance (*e/d*=2)

5.4.2 Load-Displacement Relationship

Typical load-relative displacement relationship of the three basic failure modes (net-tension, shear and bearing) are shown in Figure 5.6. A relative displacement of the main plate to the cover plate was measured at the end of the cover plate. The relative displacement was measured by using the clip transducer D2. The initial relative displacement due to slip was subtracted from the measured displacement. Therefore, curves in Figure 5.6 start from

zero relative displacement.

The load linearly increases with the relative displacement before onset of the material nonlinearity. After that the slope decreases slightly due to the material nonlinearity and then suddenly net-tension failure occurred in the connection. There was no sufficient warning before net-tension failure of the connection, and the net-tension failure is a catastrophic failure. In some of net-tension failure cases, bearing damage occurred before the net-tension failure. In such cases, the failure was not as sudden as the pure net-tension failure as shown in Figure 5.7.

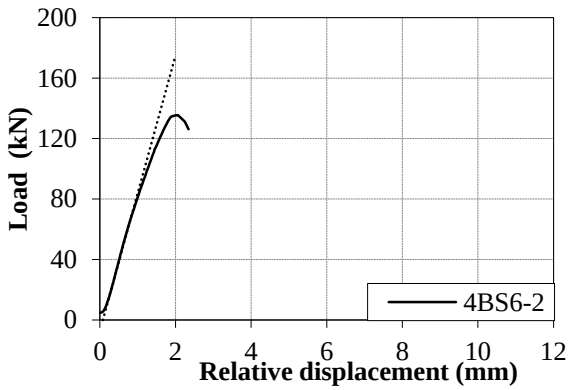

(a) Net-tension failure

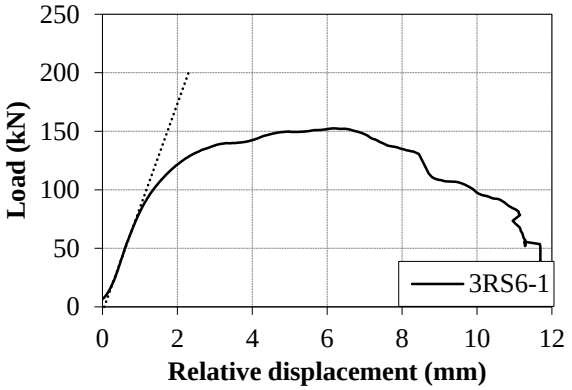

(b) Shear failure

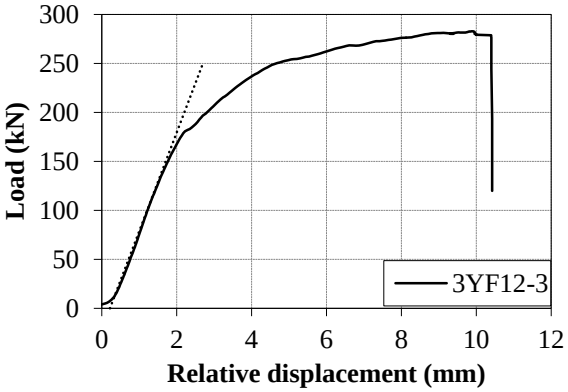

(c) Bearing failure

Figure 5.6: Load-relative displacement of multi-row bolted connections

For the shear failure case, the load-relative displacement relationship is linear before the

onset of shear damage in the connection as shown in Figure 5.6(b). The slope of the curve gradually decreases after the initiation of the shear damage. The load reaches at the ultimate level and then gradually decreases. The shear damage gradually occurs in the matrix, and at the ultimate stage, a significant shear deformation occurs in the main plate and the fibers gradually tear, resulting in the reduction of resisting force in the connection. The shear failure mode shows large displacement before failure. Therefore, the shear failure mode is not a catastrophic failure.

For the bearing failure case, the load-relative displacement relationship is also linear before the onset of bearing damage in the connection as shown in Figure 5.6(c). The slope gradually decreases as bearing damage progresses. The slope of the curve is almost zero at the ultimate level and then a sudden failure occurs due to either cleavage or tension failure. Before failure of the connection, a large displacement occurs due to the elongation of bolt holes. The bearing failure mode is not going to be the final failure mode, and it would net-tension failure or shear failure at the first bolt hole with cleavage failure at the end of plate.

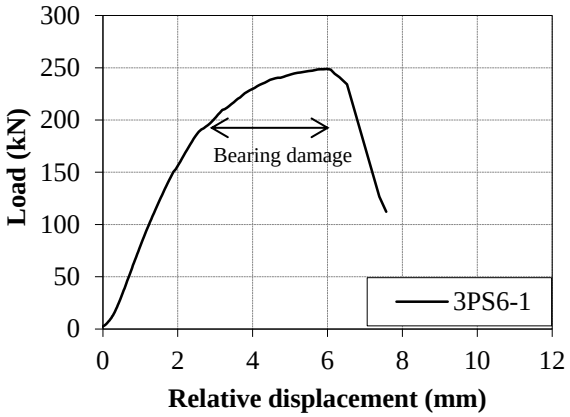

Figure 5.7: Bearing damage before tension failure of connection

5.4.3 Strength of Connections

In the multi-row bolted connections, 41 sets of connections were tested in total to

determine the effect of different parameters on the strength and failure mode of a connection. The ultimate strength, failure mode, and damage initiation strength are shown in Table 5.4, 5.5, and 5.6.

The strengths and failure modes of the connections are also evaluated by the current design guidelines of ASCE LRFD Pre-standard (ASCE, 2010) and CNR-DT 205/2007 (National Research Council, 2007). ASCE LRFD Pre-standard predicts the net-tension strength by using Eq. (5.1), bearing strength by using Eq. (5.2), and shear strength by using Eq. (5.3) for two-row bolted connectoins and Eq. (5.4) for three-row bolted connections.

$$R_{nt} = \frac{wtX_T}{K_{nt}L_{br}\frac{w}{nd} + \frac{K_{op}(1-L_{br})}{1-n\left(\frac{d_h}{w}\right)}} \tag{5.1}$$

where,

$$K_{nt} = \frac{1}{\frac{w}{nd}-1}\left\{1+C_L\left(S_{pr}-1.5\frac{S_{pr}-1}{S_{pr}+1}\Theta\right)\right\},$$

$$\Theta = 1.5-0.5\frac{w}{e} \text{ for } \frac{e}{w} \le 1 \quad , \quad \Theta = 1 \text{ for } \frac{e_1}{w} \ge 1 \quad ,$$

$$S_{pr} = \frac{w}{d}$$

and $K_{op} = 1+C_{op}\left\{1+\left(1-\frac{1}{S_{pr}}\right)^3\right\}$.

$$R_{br} = X_C dt \tag{5.2}$$

$$R_{sh} = 1.4\left(e-\frac{d_h}{2}+s\right)tS_{12} \tag{5.3}$$

$$R_{sh} = 2\{(n-1)s\}tS_{12} \tag{5.4}$$

CNR-DT 205/2007 does not have equations to predict the strength for the multi-row bolted connection. In this study, CNR-DT 205/2007 equations of single bolted connection are extended to derive the equations for multi-row bolted connection. The bearing strength of a

multi-row bolted connection is predicted by using Eq. (5.5).

$$R_{br} = X_C dt \sum C \tag{5.5}$$

where C is load distribution factors of the bolt holes specified by CNR-DT 205/2007.

The net-tension strength of a multi-row bolted connection is predicted by using Eq. (5.6).

$$R_{nt} = (w - d_h) t X_T \tag{5.6}$$

The shear strength of a multi-row bolted connection is predicted by using Eq. (5.7).

$$R_{sh} = 2\left\{ e - \frac{d_h}{2} + (n-1)(p-d) \right\} t S_{12} \tag{5.7}$$

The predicted strengths are presented in Table 5.7 to compare with the experimental results. It can be observed that the failure mode of the connections is predicted correctly for 40 out of 41 connections by the ASCE LRFD Pre-standard, while the CNR-DT 205/2007 predicts for 25 cases out of 41 connections.

Differences between ultimate strengths from the experiment and predicted strengths are shown in Table 5.7. The difference is calculated by (predicted strength – experimental strength)/experimental strength x 100. It can be observed that an error in the ultimate strength is at least 21% for net-tension failure, 35% for shear failure and 26% for bearing failure by the ASCE LRFD Pre-standard. For the CNR-DT 205/2007 case, the ultimate strength is at least 17% lower for net-tension failure, 39% larger for shear failure and 26% larger for bearing failure than the predicted strength.

The ultimate strengths of the connections were affected by the various parameters, and the effect of different parameters on the connection strength is discussed in the following.

Table 5.7: Ultimate strengths and failure modes of multi-row bolted connections

ID	Experimental results			ASCE				CNR-DT 205/2007			
	Failure mode	Average ultimate strength (kN)	Damage initiation strength (kN)	Failure mode	Strength (kN)	Difference (US) (%)	Difference (DIS) (%)	Failure mode	Strength (kN)	Difference (US) (%)	Difference (DIS) (%)
2BF6	ES	111	58	S	68	-38.7	17.2	S	80	-27.9	37.9
2BS6	B*	130	66	S	68	-47.7	3.0	S	80	-38.5	21.2
3BF6	NT	134	121	NT	101	-24.6	-16.5	S	133	-0.7	9.9
3BS6	NT	143	90	NT	98	-31.5	8.9	S	133	-7.0	47.8
4BF6	NT	141	124	NT	104	-26.2	-16.1	NT	181	28.4	46.0
4BF9	NT	154	107	NT	104	-32.5	-2.8	NT	181	17.5	69.2
4BS6	NT	143	108	NT	100	-30.1	-7.4	NT	181	26.6	67.6
2LF6	NT	139	77	NT	99	-28.8	28.6	B	102	-26.6	32.5
2LS6	NT	143	96	NT	99	-30.8	3.1	B	102	-28.7	6.3
2NS6	NT	111	77	NT	75	-32.4	-2.6	B	102	-8.1	32.5
3JF6	NT	166	104	NT	126	-24.1	21.2	B	154	-7.2	48.1
3JF9	NT	174	129	NT	126	-27.6	-2.3	B	154	-11.5	19.4
3JS6	NT	167	107	NT	121	-27.5	13.1	B	154	-7.8	43.9
3KF6	NT	165	103	NT	126	-23.6	22.3	B	154	-6.7	49.5
3LS6	NT	151	111	NT	121	-19.9	9.0	B	154	2.0	38.7
3MS6	NT	197	132	NT	138	-29.9	4.5	B	154	-21.8	16.7
4NS6	NT	111	92	NT	76	-31.5	-17.4	NT	119	7.2	29.3
2QF9	S	111	60	S	49	-55.9	-18.3	S	53	-52.3	-11.7
2QS6	S	109	53	S	49	-55.0	-7.5	S	53	-51.4	0.0
3RF6	S	156	76	S	89	-42.9	17.1	S	80	-48.7	5.3
3RF9	S	152	83	S	89	-41.4	7.2	S	80	-47.4	-3.6
3RS6	S	160	85	S	89	-44.4	4.7	S	80	-50.0	-5.9
3SF9	S	180	101	S	89	-50.6	-11.9	S	80	-55.6	-20.8
3TF9	S	199	108	S	89	-55.3	-17.6	S	80	-59.8	-25.9
3US6	S	187	114	S	107	-42.8	-6.1	S	98	-47.6	-14.0
3VS6	S	218	117	S	142	-34.9	21.4	S	133	-39.0	13.7

Note: NT= Net-tension failure, B = Bearing failure, B* = bearing failure with shear at end of plate, S = Shear Failure, ES = Shear at end of plate, US =Ultimate strength, DIS = Damage initiation strength

Table 5.7: Ultimate strengths and failure modes of multi-row bolted connections (cont'd)

ID	Experimental results			ASCE				CNR-DT 205/2007			
	Failure mode	Average ultimate strength (kN)	Damage initiation strength (kN)	Failure mode	Strength (kN)	Difference (AUS) (%)	Difference (DIS) (%)	Failure mode	Strength (kN)	Difference (AUS) (%)	Difference (DIS) (%)
2XF6	B	169	104	B	102	-39.6	-1.9	B	102	-39.6	-1.9
2XF12	B	180	105	B	102	-43.3	-2.9	B	102	-43.3	-2.9
2XS6	B	180	99	B	102	-43.3	3.0	B	102	-43.3	3.0
3YF6	B	257	103	B	102	-60.3	-1.0	B	102	-60.3	-1.0
3YF12	B	280	138	B	102	-63.6	-26.1	B	102	-63.6	-26.1
3YS6	B	182	160	B	102	-44.0	-36.3	B	102	-44.0	-36.3
3AaF6	B*	208	91	B	154	-26.0	69.2	B	154	-26.0	69.2
3AaF12	B*	232	106	B	154	-33.6	45.3	B	154	-33.6	45.3
3AaS6	B*	235	123	B	154	-34.5	25.2	B	154	-34.5	25.2
3AbF12	B*	257	136	B	154	-40.1	13.2	B	154	-40.1	13.2
3AbS6	B*	252	135	B	154	-38.9	14.1	B	154	-38.9	14.1

Note: NT= Net-tension failure, B = Bearing failure, B* = bearing failure with shear at end of plate, S = Shear Failure, ES = Shear at end of plate, US =Ultimate strength, DIS = Damage initiation strength

5.4.4 Effect of Cover Plate

To illustrate the effect of cover plates, the ultimate strengths of the connections are plotted against the width to bolt diameter ratio in Figure 5.8 for the tension failure mode, for the bearing failure mode, the ultimate strengths of the connections are plotted against the number of bolt rows in Figure 5.9, and for the shear failure mode, the ultimate strengths of the connections plotted against the half of shear length (L_s) to bolt diameter ratio in Figure 5.10. The shear length was measured from the end of the first hole to the end of the plate as shown in Figure 5.11.

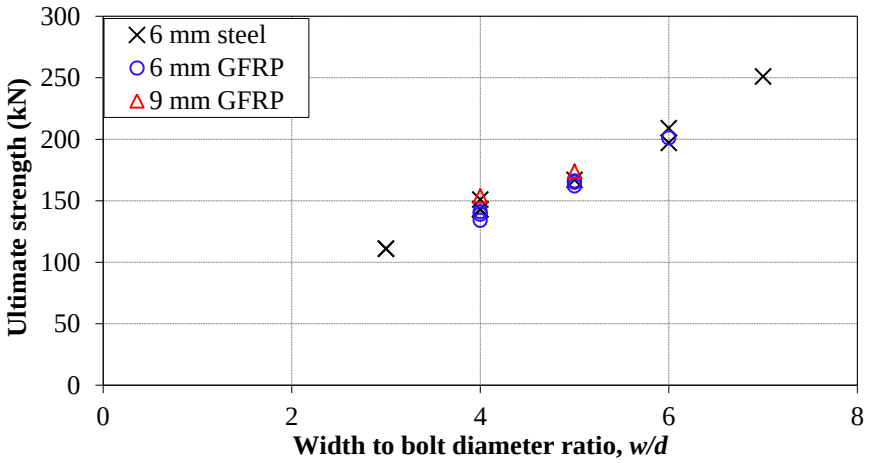

Figure 5.8: Effect of cover plate for tension failure mode

It can be observed from Figure 5.8 that the ultimate strength of net-tension failure is linearly increased with the *w/d* ratio, and the effect of cover plate on the ultimate tensile strength of the connections is not significant. The load carrying capacities of the connections with 9 mm GFRP cover plates (3JF9, and 4BF9) are a little bit higher than the connections with 6 mm steel cover and 6 mm GFRP cover plates (3JF6, 3JS6, 4BF6, and 4BS6). The connection with 6-mm steel cover plates carries almost the same strength to the connection with 6 mm GFRP cover plates.

Table 5.8: Statistical value of ultimate tensile strength

w/d	Average ultimate strength (kN)	Standard deviation (kN)	COV (%)
3.0	111.2	3.2	3.0
4.0	144.4	6.9	5.0
5.0	164.8	3.3	2.0
6.0	202.4	6.2	3.0
7.0	251.3	2.5	1.0

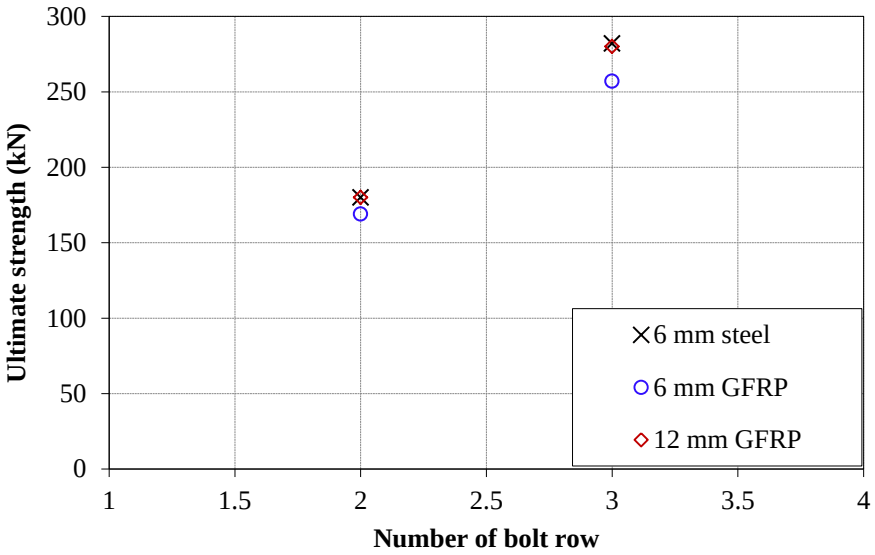

Figure 5.9: Effect of cover plate for bearing failure mode

It can be observed that the ultimate strength of bearing failure is also linearly increased with the number of bolt rows, and the effect of cover plates on the ultimate strength of the bearing failure is not significant either. The connections with 6-mm steel and 12-mm GFRP cover plates carry almost the same strength. However, the connections with 6 mm cover plates could carry lower strengths by about 6% for two row bolted connection and by about 8% for three-row bolted connection than connections with 6-mm steel or 12-mm GFRP cover plates. It is because the cover plates are damaged due to little confinement by the washer.

It is seen in Figure 5.10 that the ultimate strength of shear is also linearly increased with the L_s/d ratio, and the effect of cover plates on the ultimate strength of the shear failure mode is also not significant. The connections with 6-mm steel cover plates carry slightly larger strengths than the connections with 9-mm GFRP cover plates. The connection with 6-mm GFRP cover plates carries almost the same load as the connection with 6-mm steel cover plates.

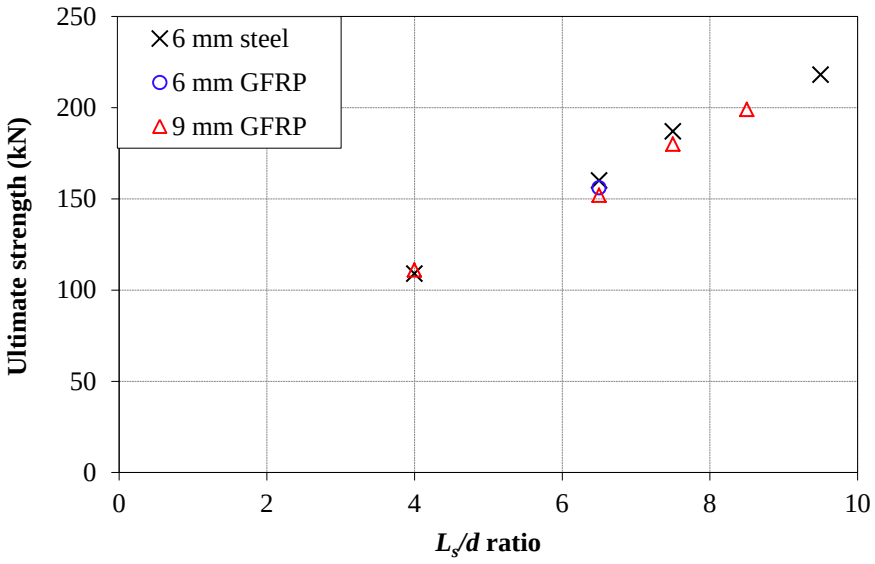

Figure 5.10: Effect of cover plate for shear failure mode

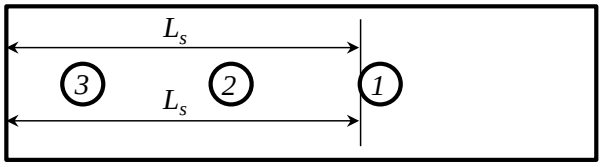

Figure 5.11: Measurement of shear length in a plate

5.4.5 Effect of Width

The width of the members in a connection largely influences the capacity of a connection as well as the corresponding failure mode. The ultimate strength of the connections with respect to the width to bolt diameter ratio, *w/d*, are shown in Figure 5.12 for the sufficient *p/d* and *e/d* ratios to resist the shear failure. In the figure, failure modes are represented as “NT” for net tension and "B" for bearing, and the combined modes of them represented by hyphenated letters. It can be observed that the ultimate strength is increased with the *w/d* ratio for these specimens. The ultimate strength is linearly increased with the increase of *w/d* ratio up to a combined failure bearing and net-tension. Slope of the net-tension strength with *w/d* ratio for the different number of bolt rows is almost the same because the change of net-tension strength is not significant with the change of number of bolts. It can be observed in Figure 5.8, Figure 5.12, and Figure 5.15 (a). In the bearing failure

case, the ultimate strength may not increase with the *w/d* ratio because the bearing area does not change by changing the *w/d* ratio.

It can be observed that the failure modes change with the change of the *w/d* ratio. The net-tension failure switch to the bearing failure when the *w/d* ratio changes from 3 to 6 for the two-row bolted connections (2NS6, 2XF6, 2XF12, and 2XS6), and from 5 to 9 for the three-row bolted connections (3BF6, 3BS6, 3YF6, 3YF12, and 3YS6). The net-tension failure occurs in the four-row bolted connections up to *w/d* ratio of 6 (4MF6 and 4MS6). The combined failure, bearing damage followed by the net-tension failure, occurs in the two-row bolted connection with a *w/d* ratio of 4.0 (2LF6 and 2LS6) and three-row bolted connections with a *w/d* ratios of 6 and 7 (3MS6, 3OF6, and 3PS6).

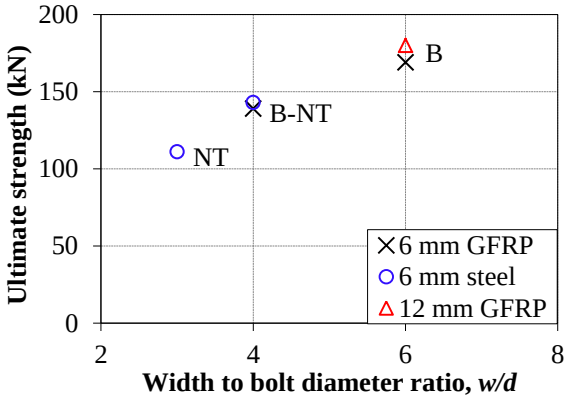

(a) Two-row bolted connection

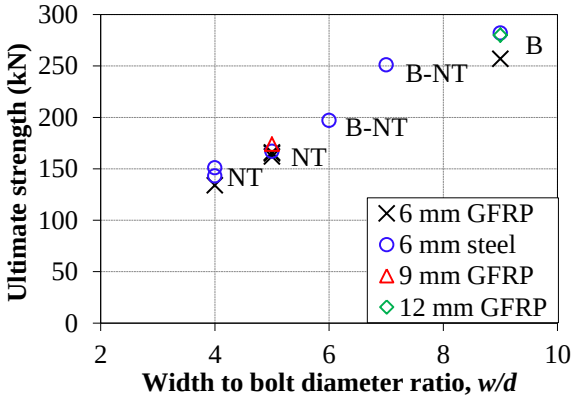

(b) Three-row bolted connection

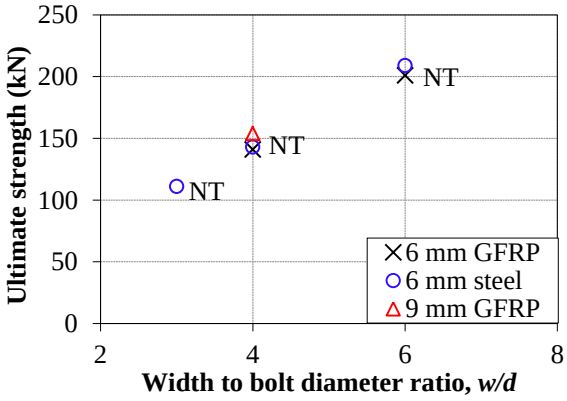

(c) Four-row bolted connection

Figure 5.12: Effect of width to bolt diameter ratio, *w/d*

5.4.6 Effect of Pitch Distance

To illustrate the effects of pitch distance on the connection strength, the ultimate strengths of the connections are plotted with respect to the pitch distance to bolt diameter ratio, *p/d*, in Figure 5.13 for the connections with a large *w/d* ratio to avoid the net-tension failure in the connections. Therefore, the connections with shear and bearing failure are used in the figure. Failure modes are represented as “S” for shear failure and "B" for bearing failure, and the combined mode is represented by hyphenated letters. It can be observed that the failure mode changes with the change of the *p/d* ratio. The shear failure changes to the bearing failure when the *p/d* ratio is changed from 3 to 5. The combined failure, bearing damage followed by shear failure, occurs in the connection for the *p/d* ratio of 4.0.

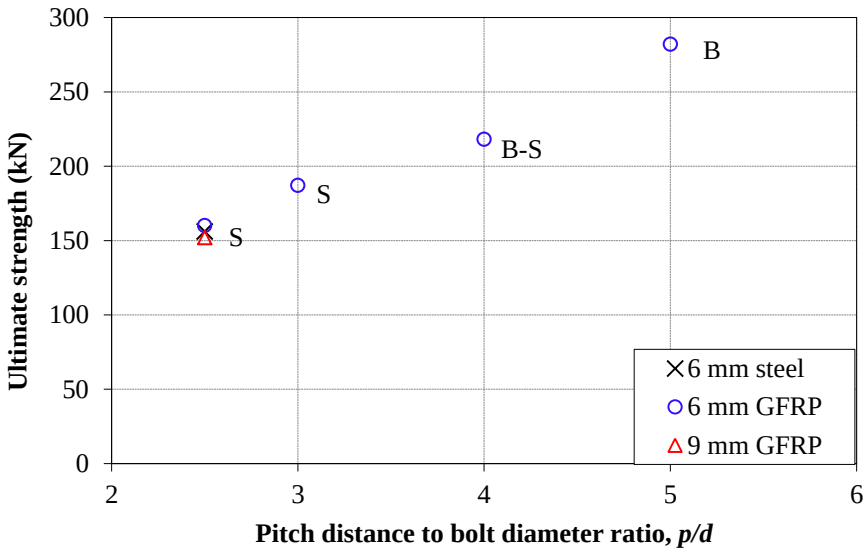

Figure 5.13: Effect of pitch distance to bolt diameter ratio, *p/d*

5.4.7 Effect of Edge Distance

To illustrate the effects of edge distance on the connection strength, the ultimate strengths of the connections are presented with respect to the edge distance to bolt diameter ratio, *e/d*, in Figure 5.14 for connection with a large *w/d* ratio to avoid the tension failure. Therefore, connections of shear and bearing failures are used in the figure. It can be observed

that the ultimate strength is linearly increased with the *e/d* ratio for bolt low and large *p/d* ratio. The ultimate strength has increased by about 9% when the *e/d* ratio is changed from 2 to 3 and 3 to 4 for the connection with *p/d* = 5.0. For the *p/d* = 5.0, the connections with 12 mm GFRP and 6-mm steel cover plates carry almost the same strength. However, the connections with 6 mm GFRP cover plate carry a lower load by about 10% for *e/d* of 2.0 and by about 8% for *e/d* of 4.0 than those connections with 12-mm GFRP and 6-mm steel cover plates.

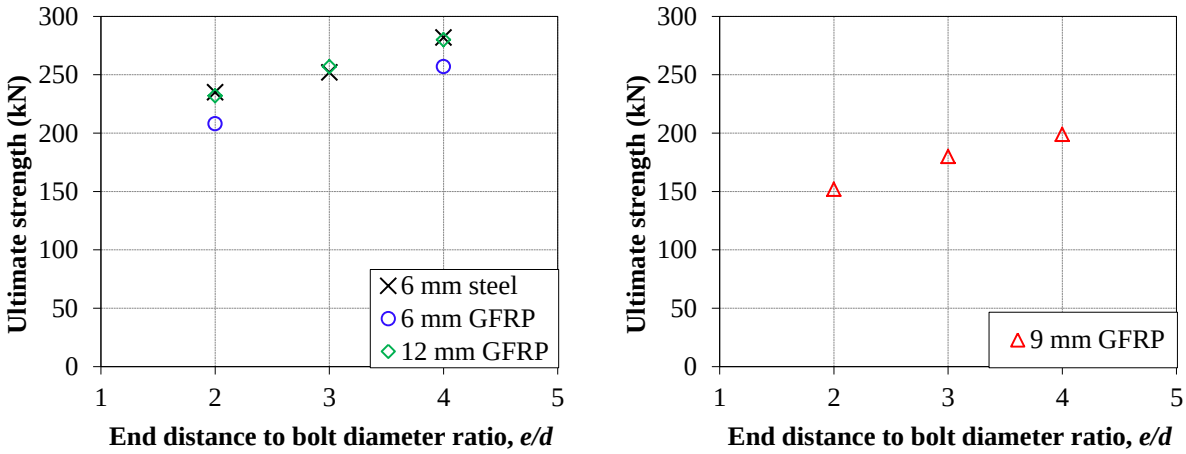

(a) p/d = 5.0 *(b) p/d = 2.5*

Figure 5.14: Effect of end distance to bolt diameter ratio, *e/d*

5.4.8 Effect of Number of Bolt Row

The effects of number of bolt row on the ultimate strengths of the connections are presented in Figure 5.15 for the different failure modes. It can be observed that the ultimate strength of the net-tension failure is affected by the number of bolt rows. The ultimate strength of the shear failure may not be affected by the number of bolt rows because the shear failure load is linear with the shear length. The ultimate load of bearing failure is significantly affected by the number of bolt rows because the bearing area is proportional to the number of bolt rows. The bearing strength increases about 100 kN by increasing bolt rows from 2-rows to 3-row which is almost equal to the ultimate strength of bearing of a single bolted connection.

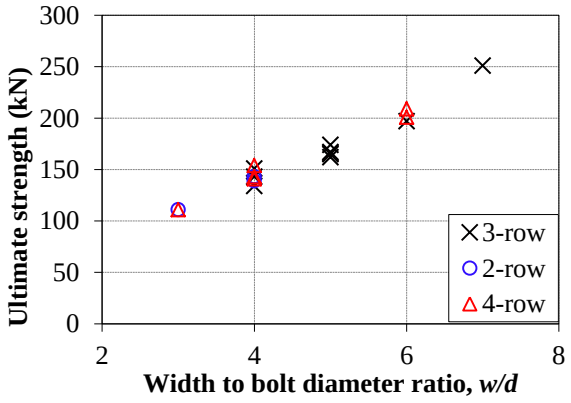

(a) Net-tension failure

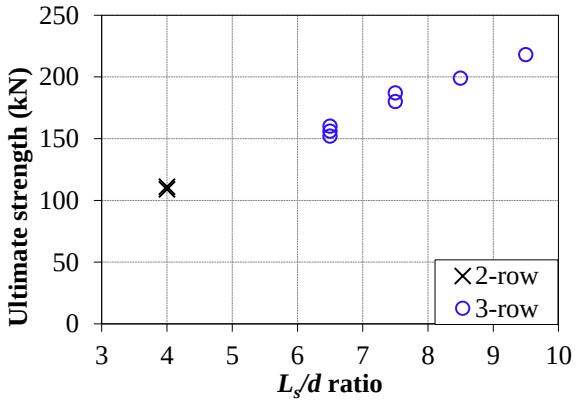

(b) Shear failure

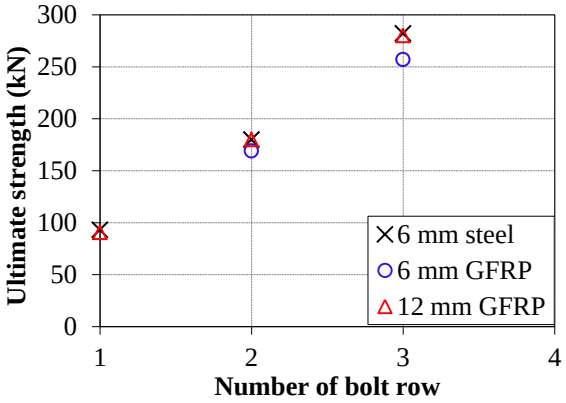

(c) Bearing failure

Figure 5.15: Effect of number of bolt row

5.4.9 Strength Predicted by Design Codes for Multi-Row Bolted Connections

The strength predicted by the design codes with respect to failure mode observed in experiment is compared with that obtained in the experiment. Strength ratio defined as a ratio of experimental strength to strength predicted by the design code is shown in Figure 5.16 and Figure 5.17.

Figure 5.16 shows the ratio of the damage initiation strength to strength predicted by the design codes, r_i. It can be observed that the ASCE LRFD Pre-standard can predict the damage initiation strength well. Average strength ratios and coefficient of variations are 0.96 and 15% for the net-tension failure, 0.86 and 15% for the bearing failure, and 1.01 and 16% for the shear failure. On the other hand, CNR-DT 205/2007 can predict the damage initiation strength

of the bearing and shear failure well, it cannot predict the damage initiation strength for the net-tension failure. Average strength ratios and coefficient of variations are 0.52 and 22% for the net-tension failure, 0.86 and 15% for the bearing failure case, and 0.99 and 13% for the shear failure case.

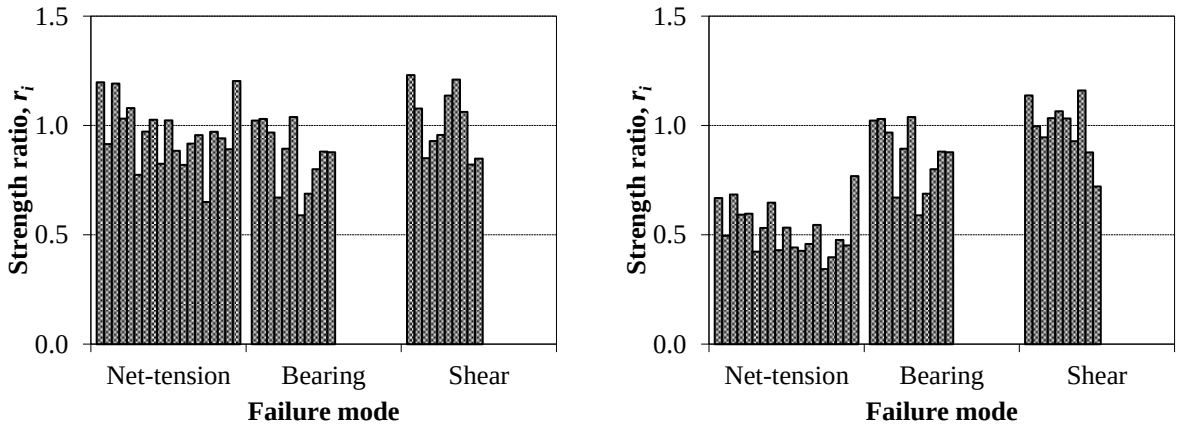

(a) ASCE LRFD Pre-Standard (b) CNR-DT 205/2007

Figure 5.16: Damage initiation strength to predicted strength

Figure 5.17 shows the ratio of the ultimate strength to the strength predicted by the design codes, r_u. It can be observed that the ultimate strength is larger than the strength predicted by the ASCE LRFD Pre-standard. Average strength ratios and coefficient of variations are 1.4 and 7% for the net-tension failure, 1.59 and 12% for the bearing failure, and 1.89 and 14% for the shear failure case. On the other hand, the ultimate strength is lower for net-tension failure and larger for the bearing and shear failures than the strength predicted by the CNR-DT 205/2007. Average strength ratios and coefficient of variations are 0.75 and 12% for the net-tension failure, 1.59 and 12% for the bearing failure case, and 1.85 and 12% for the shear failure case, when the CNR-DT 205/2007 is used.

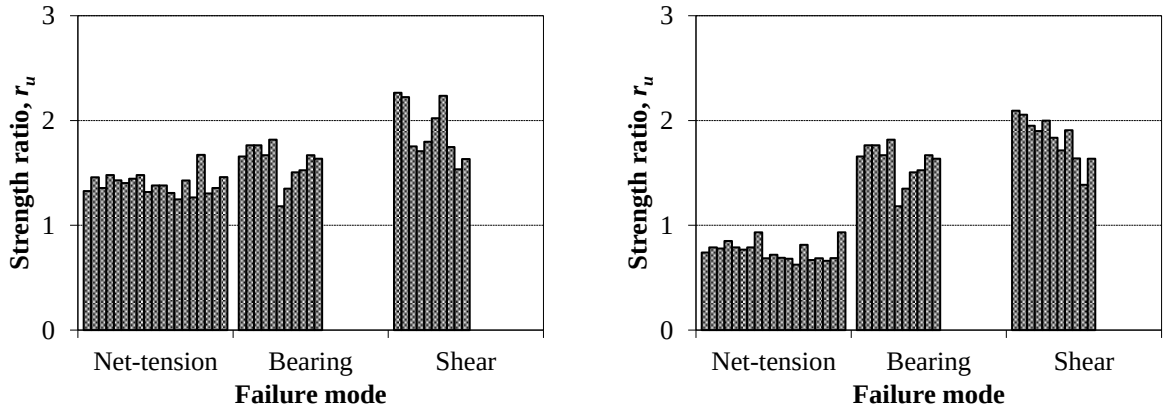

(a) ASCE LRFD Pre-Standard (b) CNR-DT 205/2007

Figure 5.17: Ultimate strength to predicted strength

5.4.10 Numerical Analysis of Multi-Row Bolted Connection

Progressive damage analysis was performed of the connections experimented in this study. The material properties described in Section 4.2 were used in the analysis. Load-displacement relationship, failure mode, and ultimate strength of the connections were evaluated from the progressive analysis. The results are compared with the experimental results in Table 5.9, 5.10, and 5.11. It is observed that the bearing and shear failure modes were predicted well, but the net-tension failure mode was not predicted by the numerical analysis. The ultimate strengths from the experiment in any mode of failure are very different from the ultimate strength in the numerical analysis. The percentage of difference is determined as (numerical analysis strength – experimental strength)/experimental strength. The difference is about 30% to 45% for the bearing, shear, and mixed mode failure (B*) connections. However, the difference is very much changed for the strength of net-tension connections, because the failure mode of the connections found in the numerical analysis is bearing failure.

Figure 5.18 shows the failure modes from the numerical analyses and experiments of Connections 2NS6, 2QS6, and 2XS6. Contour plot in the figure shows the extent of damage in the connection plates. It can be observed that failure modes are not predicted well by the

numerical model. The connection 2NS6 showed net-tension failure in the experiment. However, the numerical analysis found the failure mode of the connection 2NS6 to be a bearing failure mode. This discrepancy is casued by the fact that the confinement effect is not considered in the numerical model and the bearing failure strength in the numerical analysis is lower than that in the experiment. Therefore, bearing failure occurs before net-tension failure.

The connections 2QS6 and 2XS6 showed shear and bearing failures in the experiment, respectively, and the same failure modes were found in the numerical analysis. However, ultimate failure lines in the experiment are different from those of the numerical analysis. For the connection with the shear failure mode, initial damage occurs in parallel to the bolt hole in both the experiment and numerical analysis, but ultimate damage occurs at 45^{o} angle to the loading direction and finally cleavage failure occurs at end of the plate in the experiment, which was not predicted by the numerical analysis. For the connection with bearing failure mode, a significant bearing damage occurs in the bolt holes in both the experiment and numerical analysis, but the ultimate damage occurs at 45^{o} angle to the loading direction and finally cleavage failure occurs at the end of the plate in the experiment, which was not predicted by the numerical analysis.

Table 5.9: Comparison of experimental and numerical strength of two-row bolted connection

ID	Experiment		Numerical Analysis		Difference (%)
	Failure mode	Ultimate strength (kN)	Failure mode	Ultimate strength (kN)	
2BF6	ES	111	S	84	-24.1
2BS6	B*	130	B*	85	-35.0
2LF6	NT	139	B	104	-25.4
2LS6	NT	143	B	100	-30.1
2NS6	NT	111	B	98	-11.9
2QF9	S	111	S	74	-33.4
2QS6	S	109	S	74	-32.5
2XF6	B	169	B	105	-37.8
2XF12	B	180	B	106	-41.3
2XS6	B	180	B	102	-43.4

Table 5.10: Comparison of experimental and numerical strength of three-row bolted connection

ID	Experiment		Numerical Analysis		Difference (%)
	Failure mode	Ultimate strength (kN)	Failure mode	Ultimate strength (kN)	
3BF6	NT	134	B	119	-11.4
3BS6	NT	143	B	129	-9.8
3JF6	NT	166	B	152	-8.3
3JF9	NT	174	B	151	-13.3
3JS6	NT	167	B	139	-17.0
3KF6	NT	165	B	151	-8.7
3LS6	NT	151	B	133	-11.6
3MS6	NT	197	B	143	-27.4
3OF6	NT	162	B	150	-7.7
3PS6	NT	251	B	146	-41.9
3RF6	S	156	S	101	-35.0
3RF9	S	152	S	108	-29.2
3RS6	S	160	S	111	-30.9
3SF9	S	180	S	129	-28.6
3TF9	S	199	S	131	-34.3
3US6	S	187	S	130	-30.5
3VS6	S	218	S	130	-40.4
3YF12	B	257	B	156	-39.2
3YF6	B	280	B	158	-43.7
3YS6	B	282	B	150	-47.0
3AaF6	B*	208	B*	124	-40.4
3AaF12	B*	232	B*	141	-39.4
3AaS6	B*	235	B*	134	-42.8
3AbF12	B*	257	B*	154	-40.0
3AbS6	B*	252	B*	154	-38.8

Table 5.11: Comparison of experimental and numerical strength of four-row bolted connection

ID	Experiment		Numerical Analysis		Difference (%)
	Failure mode	Ultimate strength (kN)	Failure mode	Ultimate strength (kN)	
4BF6	NT	141	B	163	15.5
4BF9	NT	154	B	173	12.2
4BS6	NT	143	B	168	17.5
4MF6	NT	201	B	123	-38.7
4MS6	NT	209	B	170	-18.8
4NS6	NT	111	B	160	44.1

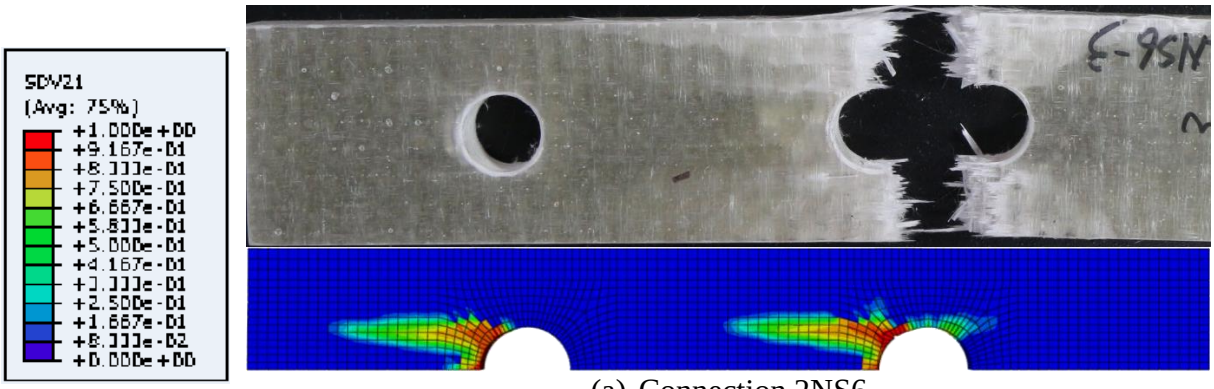

(a) Connection 2NS6

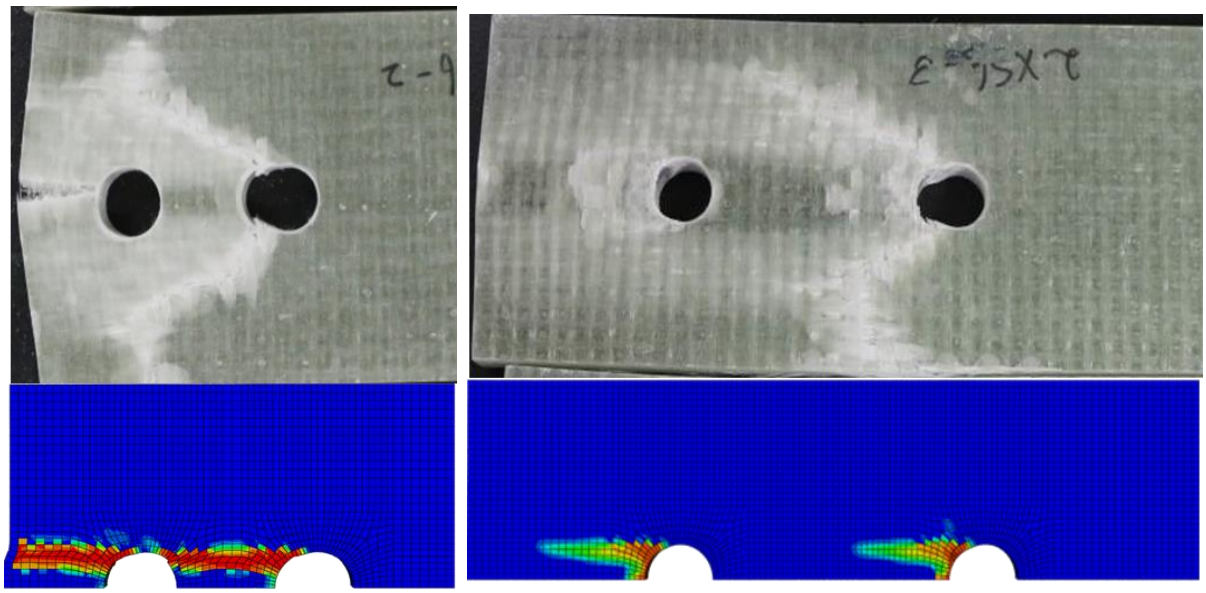

(a) Connection 2QS6 (b) Connection 2XS6

Figure 5.18: Failure modes of multi-row bolted connections

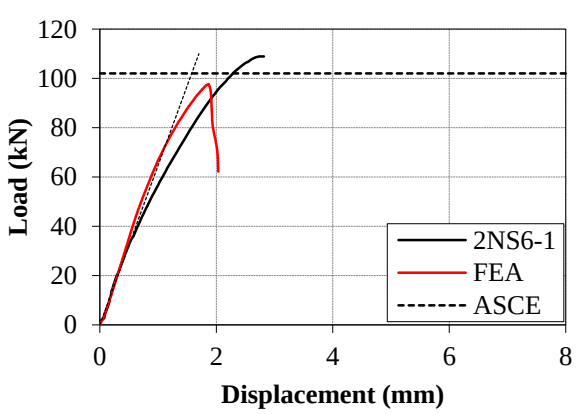

(a) Connection 2NS6-1

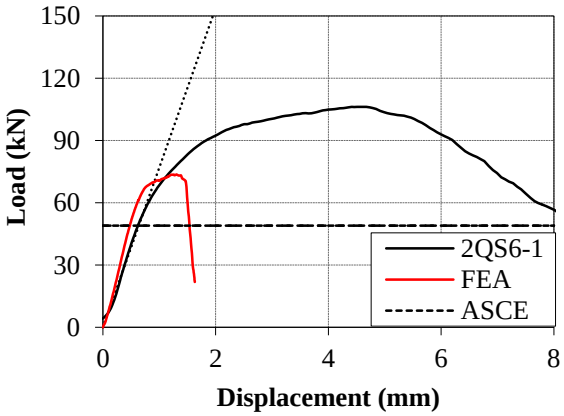

(b) Connection 2QS6-1

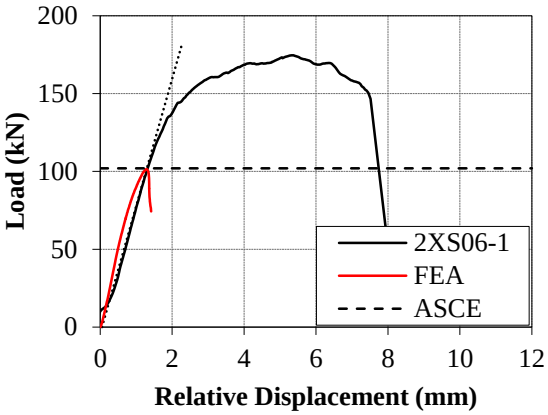

(c) Connection 2XS6-1

Figure 5.19: load-displacement relationship of multi-row bolted connection

Figure 5.19 shows the load-displacement relationships of multi-row bolted connections (2NS6, 2QS6, and 2XS6) obtained from the experiment and the numerical analysis. The linear dotted lines show the average initial stiffness of the connection in the experiment.

It can be observed that stiffness and ultimate strength of the connection are not predicted well by the numerical analysis. For the connection 2NS6 in Figure 5.19(a), the ultimate strength in the numerical analysis is lower than the experiment because the bearing failure occurs in the numerical analysis while the net-tension failure occurs in the experiment. For the connection 2QS6 in Figure 5.19(b), the ultimate shear strength in the numerical analysis is also lower than the experiment. Although the initial shear failure occurs in parallel to the bolt holes for both the experiment and the numerical analysis, the final shear failure occurs at 45^{o} angle to the loading direction in experiment due to the existence of the fibers at 90^{o} angle

while the final failure in the numerical analysis occurs in parallel to the bolt holes. Therefore, shear strength of the experiment is larger than that of the numerical analysis.

For the connection 2XS6 in Figure 5.19(c), the ultimate bearing strength in the numerical analysis is also lower than the experiment. As was explained in Chapter 4 for single bolted connections, this difference in the bearing strength was caused by the confinement effect which is not included in the numerical model. The numerical analysis strength and the strength predicted by the ASCE LRFD Pre-standard are found to be in good agreement for the net-tension and bearing failure modes.

5.5 Summary

In this chapter, strength tests of 41 sets of multi-row bolted connection test were conducted to investigate the effect of cover plate, number of bolt rows, width to bolt diameter ratio, *w/d*, pitch distance to bolt diameter ratio, *p/d*, and end distance to bolt diameter ratio, *e/d*, on strength and failure mode of a connection.

Three basic failure modes were found: net-tension, bearing and shear failure. Cleavage failure was also found at the ultimate stage of the shear and bearing failure modes.

For connections that satisfy the minimum requirement of LRFD Pre-standard, net-tension failure occurred of the three and four-row bolted connections with steel and GFRP cover plates. However, end shear failure occurs in the main and cover plates of the two-row bolted connection with the GFRP cover plate having a half of the main plate thickness. Therefore, the geometry which is satisfied with the minimum requirement of LRFD Pre-standard is not appropriate geometry to get desirable bearing failure mode.

Load-displacement relationship of the connections showed that the net-tension failure is a catastrophic failure. The failure occurs suddenly without any deformation. However, the bearing and shear failure show a large deformation before failure of the connection.

A variation of the ultimate load was within 5%, while that of the damage initiation load

was very large. The damage initiation load was predicted better by ASCE LRFD Pre-standard than CNR-DT 205/2007. However, in many cases, the difference between the damage initiation load and strength predicted by design code is very large.

The effect of cover plate stiffness on the ultimate load was found to be not significant, although the load and load distribution among bolts are significantly affected by the cover plate stiffness as shown in chapters 2 and 3, and reported by the design guidelines (ASCE, 2010; National Research Council, 2007). The connection with the GFRP cover plate having a half of the main plate thickness carries lower loads by about 6% for two-row bolted connection and by about 8% for three-row bolted connection than the connections with the steel cover plate and thickness GFRP cover plates with a larger thickness for the bearing failure case.

The effect of width to bolt diameter ratio, *w/d*, on the ultimate load of the connection is significant. The load is linearly increased with the *w/d* ratio. The net-tension failure switches to the bearing failure by changing the *w/d* ratio from 3 to 6 for the two-row bolted connection, and from 5 to 9 for three-row bolted connection.

The effect of pitch distance to bolt diameter ratio, *p/d*, on the ultimate load of the connection is also significant. The load is increased with the *p/d* ratio. The shear failure switches to the bearing failure by changing the *p/d* ratio from 3 to 5.

The effect of end distance to bolt diameter ratio, *p/d*, on the ultimate load of the connection is also significant. The load is linearly increased with the *e/d* ratio. For three-row bolted connection with a *p/d* of 5.0, the ultimate load has increased by about 9% to increase the unit *e/d* ratio.

The effect of the number of bolt rows on the net-tension and shear failure loads was found to be not significant. However, the ultimate load of bearing failure is significantly affected by the number of bolt rows and the bearing load increases by almost the same amount as the bearing strength of a single bolted connection when one bolt row is increased in

a connection.

ASCE LRFD Pre-standard can predict failure modes and damage initiation strength of any failure mode of the connections. The ultimate strengths are larger than the strength predicted by the ASCE LRFD Pre-standard. On the other hand, CNR-DT 205/2007 can predict damage initiation strength of bearing and shear failure modes only.

CHAPTER 6 EMPERICAL EQUATIONS FOR CONNECTION STRENGTH

6.1 Introduction

This chapter discusses an analytical model proposed to describe the behavior of bolted connection fabricated from GFRP composite material. The model is based on the results of the experimental program conducted in this investigation. Test results show that there are three primary modes of failure for the bolted connections. The first is net-tension, which occurs typically in connections with a small width and a relatively large pitch and a large end distance. The second is shear failure that occurs in connections with a small pitch and a small end distance. The third is bearing failure that occurs in connections with a large width, a large pitch distance and a large end distance. The model in this study consists of three basic failure criteria to determine the ultimate strength and the failure mode of a connection.

The first criterion the net tension failure mode of the connection. Many researchers (Rosner, 1992, Hassan, 1995, Mottram, 2010) have predicted the ultimate tensile strength based on the theory presented by Hart-Smith (1980). The theory accounts for the elastic stress concentrations at a loaded hole in an elastic and isotropic material. For FRP composite material, Hart-Smith introduced a correlation coefficient that relates the elastic stress concentration factor of elastic materials to that of FRP composite materials for a connection of the same geometry based on experimental tests. The theory shows that the tensile strength not only depends on the width but also on the end distance. Mottram (2010) included the effect of load distribution coefficient of the first row in the Hart-Smith criterion. However, the experimental results in this study showed that the end distance as well as the load distribution do not affect the ultimate strength significantly. Therefore, the present study introduces a simple method using stress concentration factor to predict the ultimate tensile strength of a

connection.

The second criterion describes the shear failure mode of the connection. The experimental results in this study showed that the ultimate shear strength linearly increases with the shear length which was defined in Figure 5.11. Therefore, a simple model with a shear strength factor is proposed to determine the ultimate shear strength.

The third criterion describes the bearing failure mode of the connection. The experimental results in this study showed that the ultimate bearing strength linearly increases with the number of bolt rows. The ultimate bearing strength is that load when a connection is failed due to bearing by the load. A simple model with a bearing strength factor is proposed to determine the ultimate bearing strength of a single bolted connection. Based on the ultimate strength of a single bolted connection, the ultimate strength of a multi-row bolted connection is predicted by multiplying the strength of a single bolted connection the number of rows.

6.2 Net-Tension Failure

Stress distribution along the net-section of a connection plate is not uniform. The stress distribution along the net-section is shown in Figure 6.1. Stress concentration occurs at the edge of the hole. Therefore, an average tensile strength of the connection is found to be lower than with the material tensile strength. The average tensile strength is a ratio of tensile load of a connection to the net cross-sectional area of the plate. The stress concentration factor, k_{tc}, can be calculated by using the following equation:

$$k_{tc} = \frac{(w - d_h)tX_T}{P_{ut}} \tag{6.1}$$

where P_u is ultimate tensile strength, w is width of plate, d_h is a diameter of hole, t is a thickness of plate, and X_T is the tensile strength of material.

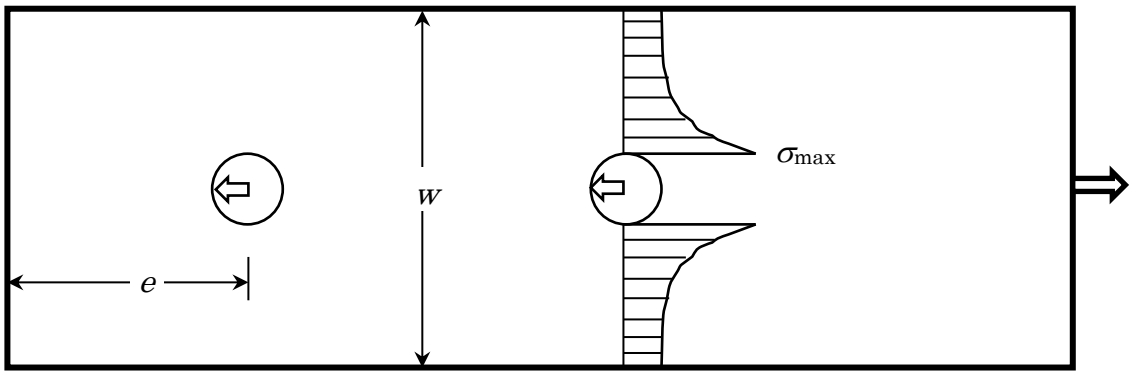

Figure 6.1: Stress distribution along net-section

In this study, stress concentration factors base on Eq. (6.1) for the net-tension failure connections described in Chapters 4 and 5 are shown in Figure 6.2. The stress concentration factor increases with the net-section area. However, the relationship is not linear, and, for $(w\text{-}d_h)/d > 5$, the stress concentration factor does not increase any more. For the stress concentration factor of the connection with net-tension to bolt diameter ratio 5.93 (3PS6) is decreased to compare with the connection with 4.93. In this case only one set of connection has been tested.

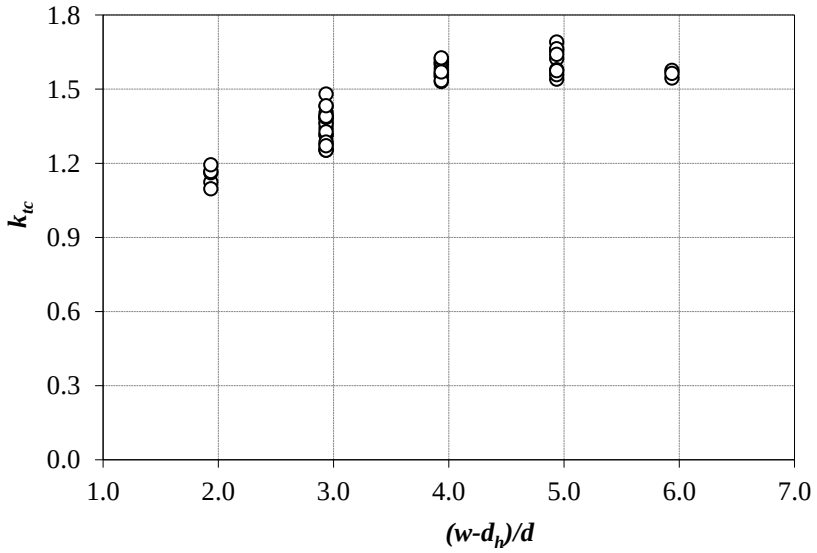

Figure 6.2: Stress concentration factor of net-tension failure connection

The stress concentration factors of each net-section are summarized in Table 6.1. The K-S test was performed to obtain a goodness of fit for statistical distribution. The data are found to fit with a normal distribution as shown in Figure 6.3.

Table 6.1: Statistical value of stress concentration factor

w/d	$(w-d_h)/d$	Average	Standard deviation
3.0	1.93	1.15	0.03
4.0	2.93	1.36	0.60
5.0	3.93	1.58	0.03
6.0	4.93	1.61	0.05

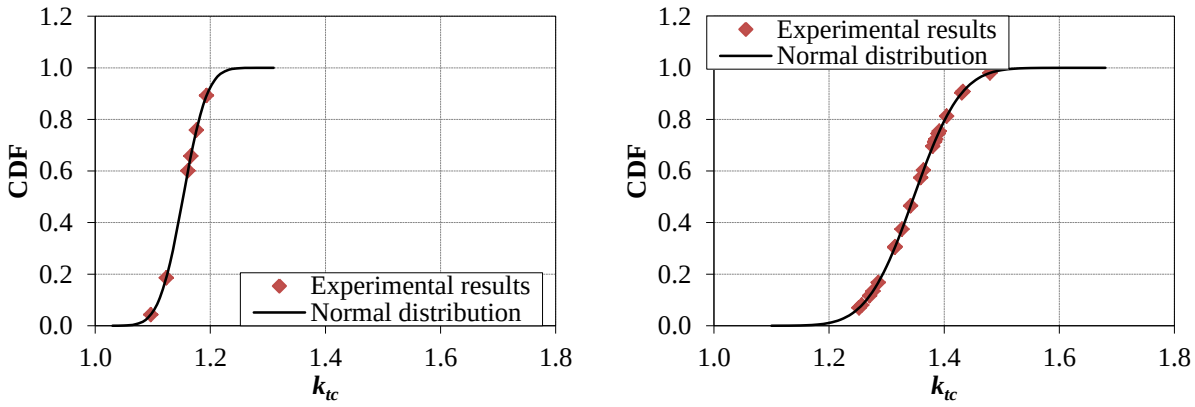

(a) $(w-d_h)/d$ = 1.93 (b) $(w-d_h)/d$ = 2.93

(c) $(w-d_h)/d$ = 3.93 (d) $(w-d_h)/d$ = 4.93

Figure 6.3: Distribution of stress concentration factor with net-section connection

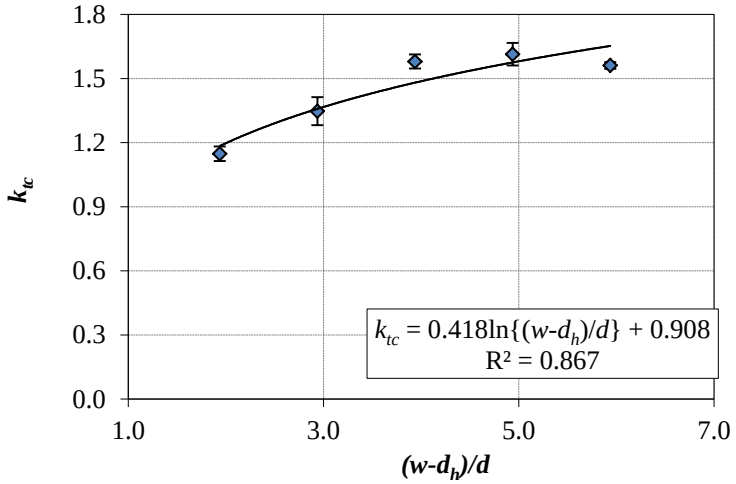

Figure 6.4: Stress concentration factor correlates with net-section

The average stress concentration factors are used to correlate with the net-section of the connection shown in Figure 6.4. The standard deviation is also shown in the figure. Using a trendline, the stress concentration factor is tried to correlate with the net-section to diameter ratio. The stress concentration factor, k_{tc}, can be expressed by the following equation:

$$k_{tc} = 0.418\ln\left(\frac{w-d_h}{d}\right)+0.908 \tag{6.2}$$

By using Eq. (6.2), one can easily determine the stress concentration factor as well as the ultimate net-tension strength of a connection. The ultimate tensile strength, P_{ut}, can be evaluated by using the following equation:

$$P_{ut} = \frac{(w-d_h)tX_T}{k_{tc}} \tag{6.3}$$

6.3 Shear Failure

The experimental results showed that the shear strength linearly increases with the shear length. The shear length is considered to be twice the distance from the end of the first bolt hole to the end of the plate in the direction parallel to the loading as described in Section 5.4, although the final shear failure was observed to occur at a 45^o angle to the loading direction. The assumption is made because the shear failure initiates parallel to the bolt holes, which is influenced the ultimate shear strength.

Shear strength factor, S_F, for the shear failure is proposed to evaluate the shear strength. The shear strength factor can be determined by using the following equation:

$$S_F = \frac{2L_s t S_{12}}{P_{us}} \tag{6.4}$$

where, P_{us} is the ultimate shear strength, L_s is half of shear length, S_{12} shear strength of the material.

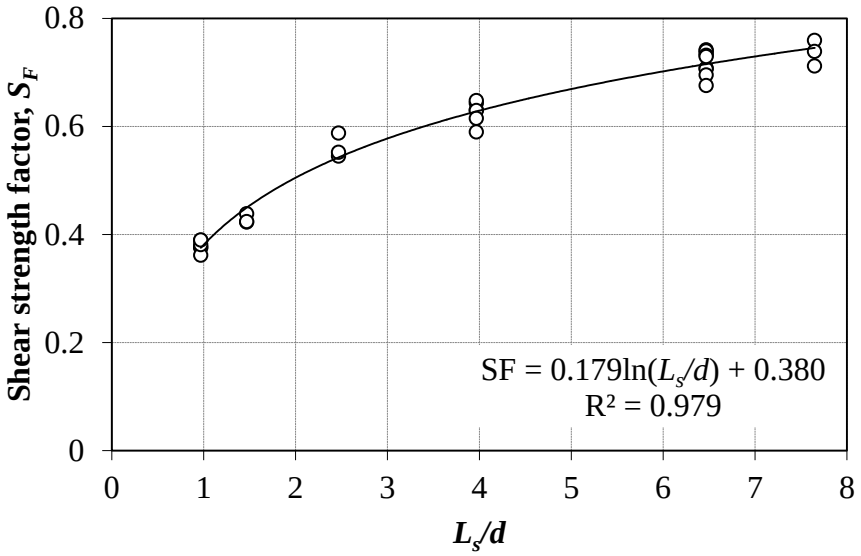

Figure 6.5: Shear strength factor correlates with L_s/d

The shear strength factor from the connections that actually showed shear failure are shown in Figure 6.5. The shear strength factor increases with the L_s/d ratio. However, the increasing rate is decreased with the L_s/d ratio.

In Figure 6.5 shows the trend line between the shear strength factor and L_s/d ratio, which is expressed by the following equation:

$$S_F = 0.179 \ln\left(\frac{L_s}{d}\right) + 0.380 \tag{6.5}$$

By using Eq. (6.5), one can easily determine the shear strength factor as well as the ultimate strength of a connection. The ultimate tensile strength, P_{us}, can be evaluated by using the following equation:

$$P_{us} = \frac{2L_s t S_{12}}{S_F} \tag{6.6}$$

6.4 Bearing Failure

From the experimental results, it is observed that the bearing strength is linearly increased with the number of bolt rows in a connection. in this study, bearing strength factor, B_F, of a connection with bearing failure is defined as the following equation:

$$B_F = \frac{ntdX_C}{P_{ub}} \tag{6.7}$$

where, P_{ub} is the ultimate bearing strength, and X_C is bearing strength of the material.

The bearing strength factors from the experiments are shown in Figure 6.6. The bearing strength factor does not change with the change of number of bolt row. Shown the average values each number of rows. The bearing strength factor is about 0.55. Experimental results of the connections with 6-mm GFRP cover plates are not included due to the cover plates are damaged and connections carry lower load than the other connections.

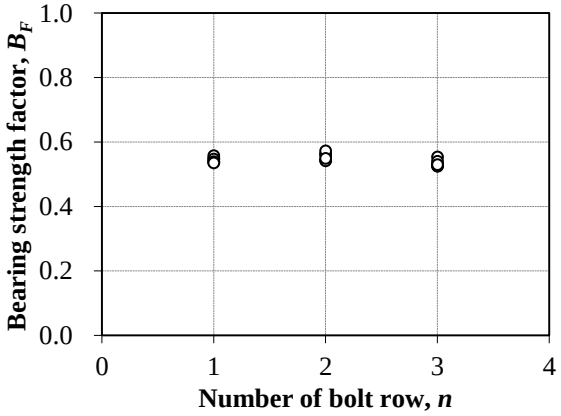

Figure 6.6: Bearing strength factor correlates with number of bolt row

By using the bearing strength factor, one can easily determine the ultimate bearing strength of a connection. The ultimate tensile strength, P_{ub}, can be evaluated by using the following equation:

$$P_{ub} = \frac{ntdX_C}{0.55} \tag{6.8}$$

When n = 1, then the bearing strength is a single bolted connection strength, $P_{usingle}$. The bearing strength of multi-row bolted connection can be evaluated by multiplying $P_{usingle}$ by the number of bolt rows as shown in Eq. (6.9):

$$P_{ub} = nP_{usingle} \tag{6.9}$$

6.5 Design of Connection

Prediction of strength and failure mode of a connection is an important task for the design of a connection. Strength can be predicted by using Eqs. (6.3), (6.6), (6.8), and (6.9). Failure mode can be the smallest strength of those calculated by the equations. Strengths and failure modes predicted by the procedure in this chapter are compared with the ultimate strengths and failure modes from the single bolted connection teste in Table 6.2. It can be observed that the strength and failure mode are predicted with high accuracy for the connections with 3 N-m torque. The difference between the measured and predicted strength almost 5% or lower than that value for the bearing and shear failure modes. However, the tensile strength and the strength of the pin-bearing connections and the strength of connections with 6-mm GFRP cover plates were not predicted well. First of all, the design equations are expressed for the connection with 3 N-m bolt torque. The results from the experiment of the connections with 6-mm GFRP cover plate which are failure in cover plate are not included to develop the design equations.

Table 6.2: Comparison between the experimental and predicted strength and failure mode of single bolted connection

ID	Experiment		Prediction					Difference (%)
	Failure mode	Ultimate strength (kN)	Net-tension failure (kN)	Shear failure (kN)	Bearing failure (kN)	Failure mode	Strength (kN)	
J1	B	84.2	108	100	91	B	91	7.3
J2	S	76.3	143	79	91	S	79	3.3
J3	B	93.1	143	100	91	B	91	-2.4
J4*	NT	45.7	70	100	91	NT	70	35.0
J5*	B	48.2	143	100	91	B	91	47.0
J6*	S	45.7	143	57	91	S	57	19.3
J7	S	59.2	143	57	91	S	57	-4.5
J8	S	44.5	143	45	91	S	45	0.7
J9	NT	75.5	90	100	91	NT	90	15.8
J10*	B	52.1	176	100	91	B	91	42.7
J11	NT	56.8	70	100	91	NT	70	19.2
J12	NT	57.4	70	100	91	NT	70	18.4
J13	S	44.2	143	45	91	S	45	1.3
J14	B	90.7	143	100	91	B	91	0.2
J15*	B	20	70	100	91	NT	70	71.6
J16*	S	17.4	143	45	91	S	45	61.2
J17*	B	17.9	143	100	91	B	91	80.3
J18	NT	59.3	70	100	91	NT	70	15.7
J19	S	41	143	45	91	S	45	8.5
J20	B	69.2	143	100	91	B	91	23.9

Note: NT= Net-tension failure, B = Bearing failure, S = Shear Failure, *Connection with pin-bearing

The predicted strengths and failure modes for the multi-row bolted connections are compared with those obtained in the experiment in Table 6.3, Table 6.4, and Table 6.5. It is observed that the strengths and failure modes of the multi-row bolted connection are predicted well. The connection with small end distance, failure mode cannot predict well because the equations were developed based on the pure failure mode. Combined failure mode is not included in the equation. The difference between the measured and predicted strength is almost 7% or below. It is observed that most of the cases the predicted strength is lower than the measured strength of the connections.

Table 6.3: Comparison between the experimental and predicted strength and failure mode of two-row bolted connection

ID	Experiment		Prediction					Difference (%)
	Failure mode	Ultimate strength (kN)	Net-tension failure (kN)	Shear failure (kN)	Bearing failure (kN)	Failure mode	Strength (kN)	
2BF6	ES	111	143	138	182	S	138	19.8
2BS6	B*	130	143	138	182	S	138	6.1
2LF6	NT	139	143	184	182	NT	143	2.7
2LS6	NT	143	143	184	182	NT	143	-0.1
2NS6	NT	111	104	184	182	NT	104	-6.6
2QF9	S	111	207	110	182	S	110	-1.2
2QS6	S	109	207	110	182	S	110	0.6
2XF6	B	169	207	192	182	B	182	7.0
2XF12	B	180	207	192	182	B	182	1.0
2XS6	B	180	207	192	182	B	182	1.0

Note: NT= Net-tension failure, B = Bearing failure, B* = bearing failure with shear at end of plate, S = Shear failure, ES = Shear at ends of the main plate and cover plate

Table 6.4: Comparison between the experimental and predicted strength and failure mode of four-row bolted connection

ID	Experiment		Prediction					Difference (%)
	Failure mode	Ultimate strength (kN)	Net-tension failure (kN)	Shear failure (kN)	Bearing failure (kN)	Failure mode	Strength (kN)	
4BF6	NT	141	143	276	364	NT	143	1.3
4BF9	NT	154	143	276	364	NT	143	-7.8
4BS6	NT	143	143	276	364	NT	143	-0.1
4MF6	NT	201	207	347	364	NT	207	2.9
4MS6	NT	209	207	347	364	NT	207	-0.9
4NS6	NT	111	108	347	364	NT	108	-2.7

Note: NT= Net-tension failure, B = Bearing failure, B* = bearing failure with shear at end of plate, S = Shear failure, ES = Shear at ends of the main plate and cover plate

Table 6.5: Comparison between the experimental and predicted strength and failure mode of three-row bolted connection

ID	Experiment		Prediction					Difference (%)
	Failure mode	Ultimate strength (kN)	Net-tension failure (kN)	Shear failure (kN)	Bearing failure (kN)	Failure mode	Strength (kN)	
3BF6	NT	134	143	210	273	NT	143	6.2
3BS6	NT	143	143	210	273	NT	143	-0.1
3JF6	NT	166	176	268	273	NT	176	5.5
3JF9	NT	174	176	268	273	NT	176	1.0
3JS6	NT	167	176	268	273	NT	176	5.0
3KF6	NT	165	176	300	273	NT	176	6.1
3LS6	NT	151	143	268	273	NT	143	-5.7
3MS6	NT	197	207	268	273	NT	207	4.9
3OF6	NT	162	176	284	273	NT	176	7.8
3PS6	NT	251	237	268	273	NT	237	-5.7
3RF6	S	156	296	157	273	S	157	0.5
3RF9	S	152	296	157	273	S	157	3.1
3RS6	S	160	296	157	273	S	157	-2.0
3SF9	S	180	296	175	273	S	175	-3.0
3TF9	S	199	296	192	273	S	192	-3.4
3US6	S	187	296	175	273	S	175	-7.0
3VS6	S	218	296	210	273	S	210	-4.0
3YF12	B	257	296	157	273	S	157	0.5
3YF6	B	280	296	276	273	B	273	5.7
3YS6	B	282	296	276	273	B	273	-2.7
3AaF6	B*	208	296	276	273	B	273	-3.4
3AaF12	B*	232	296	243	273	S	243	14.5
3AaS6	B*	235	296	243	273	S	243	4.6
3AbF12	B*	257	296	243	273	S	243	3.4
3AbS6	B*	252	296	260	273	S	260	1.0

Note: NT= Net-tension failure, B = Bearing failure, B* = bearing failure with shear at end of plate, S = Shear failure, ES = Shear at ends of the main plate and cover plate

6.6 Summary

Design equations to predict the ultimate strength of a connection were proposed based on the results of the experimental program for three basic failure modes of net-tension, shear and bearing failures.

It was shown that the proposed equations can predict the strength of the net-tension, shear and bearing failure mode. Based on the strength, failure mode can be determined.

CHAPTER 7 CONCLUSIONS AND RECOMMENDATIONS

7.1 Conclusions

The structural integrity and the capacity of structures fabricated from FRP composite materials are largely controlled by the performance of the connections. Bolted connections are the most practical connection type in civil structural applications of FRP, since they are easily assembled and disassembled, and usually cost-effective when compared to other types of connections. Therefore, an understanding of the behavior of bolted connections is required to utilize the full potential of this material in civil structural applications.

The present study focuses on bearing-type multi-row bolted connections where load does not distribute uniformly among the bolt rows due to the relative displacement of the cover plates to the main plate. Relative stiffness of the cover plate to the main plate is an important factor of the load distribution which may affect the strength of a bolted connection. Therefore, experimental and numerical investigations were conducted to understand the effect of cover plate stiffness on the load distribution among the bolts as well as strength of connections made of hand layup woven fabric GFRP material. The following remarks can be made as conclusions of this research.

7.1.1 Load Distribution of Multi-Row Bolted Connection

A series of 3D elastic finite element analyses were performed to understand the effect of cover plate stiffness on the load distribution among the bolt rows. The effect of geometric parameters was also investigated. Based on the obtained load distribution, efficiency as well as capacity of the connections was determined by assuming the material is linearly elastic until failure and it fails in a very brittle manner. The following conclusions can be made on the load distribution in a multi-row bolted connection.

(a) In bearing-type multi-row bolted connections of FRP structural members, load distribution coefficients are affected by cover plate stiffness. Coefficients of the first and the last rows are affected significantly with the change of cover plate stiffness, while those of intermediate rows are insensitive. However, when the stiffness ratio of cover plates to the main plate becomes greater than 7, load distribution coefficients do not change any more. Therefore, for a connection with steel cover plates, the load distribution is insensitive to the cover plate thickness.

(b) Efficiency of a connection is significantly affected by the cover plate stiffness. The efficiency of two, three and four-row bolted connections with steel cover plates having a half of main plate thickness are equal to 0.72, 0.53 and 0.40, respectively, whereas the efficiency of two, three, and four-row bolted connections with the same thickness of FRP cover plates as that of steel cover plates are equal to 1.00, 0.90 and 0.77, respectively.

(c) Capacity of a connection also largely depends on the cover plate stiffness. An increase in the number of rows more than three in a connection with steel cover plate does not result in a significant capacity increase.

(d) The effect of geometric parameters on the load distribution is not affected significantly the change of cover plate stiffness.

7.1.2 Progressive Damage Analysis of Multi-Row Bolted Connection

A progressive damage model of FRP materials was implemented in the commercial finite element software to simulate material behavior after the damage initiation. By using the model, a series of 3D nonlinear finite analysis were performed to evaluate the strength and failure mode of bolted connections. Based on the progressive damage analysis, the following conclusions can be made:

(a) The progressive damage model is based on a 3D failure criterion and compliance matrix for the damaged material, which is implemented through a user subroutine UMAT in

Abaqus. The stiffness of material is gradually decreased after material failure and a viscous regularization is included so that the model can significantly reduce the convergence problem and prevent the analysis from stopping prematurely.

(b) A connection with FRP cover plates offers a larger strength than that with steel ones. For the two, three, and four-row bolted connections, the strength can be increased by 6%, 19%, and 35%, respectively, by using FRP cover plates in place of steel cover plates having a half of the main plate thickness.

(c) A multi-row bolted connection with FRP cover plates requires a larger end distance than steel cover plates and almost the same end distance as that of a single bolted connection to avoid the shear failure at the end, although current design codes specify a smaller end distance for multi-row bolted connections with FRP cover plates than that for single bolted connections.

7.1.3 Experimental Investigation of Single Bolted Connection

A series of tensile, compression and shear tests were conducted to obtain the material properties of GFRP laminates with thicknesses of 6, 9, and 12 mm. The obtained material properties are used to predict the strength of single and multi-row bolted connections.

Twenty sets of single bolted connections with a double-lap configuration fabricated from woven fabric GFRP are tested to failure. Based on the experimental results, the following remarks can be made:

(a) Three basic failure modes of net-tension, shear and bearing failure are observed in the single bolted connection. The bearing and shear failure showed large displacement before failure of the connection, whereas the net-tension failure mode showed a catastrophic failure.

(b) Connection strength did not change for the change of 6-mm steel cover plate to 12-mm GFRP cover plate. However, when the 6-mm steel cover plate was changed to 6-mm

GFRP cover plate, the connection strength decreased by about 26% for the bearing failure and by about 8% for shear failure because FRP cover plates would fail first before the main plate. Therefore, connections with the cover plate thickness a half of the main plate may not be a choice in the bearing failure mode is desired.

(c) The Failure mode switched from net-tension failure to the bearing failure when the *w/d* ratio was increased from 2 to 4, and from the shear failure to the bearing failure when the *e/d* ratio changed from 1.5 to 4. Therefore, $w/d = 4$, $e/d = 4$ may be the minimum requirements for the bearing failure.

(d) Due to introduction of 3 N-m bolt torque, which is equivalent to a finger tight condition, the ultimate bearing strength increased by about 93% for the connection with a *w/d* ratio of 4, and the ultimate shear strength also increased by about 30% for the connection with a *e/d* ratio of 2.

(e) Due to the lateral confinement by washers the strength increased by about 18% in the shear failure and by about 93% in the bearing failure.

7.1.4 Experimental Investigation of Multi-Row Bolted Connection

Forty one sets of multi-row bolted connections with different parameters were tested to failure. The following conclusions can be made based on the experiment.

(a) Three basic failure modes were found in this investigation. The failure modes are net-tension, bearing and shear failure. Cleavage failure mode was also found at the ultimate stage of the shear and bearing failure modes. Load-displacement relationship of connections showed that the net-tension failure is a catastrophic failure. The failure occurs suddenly without any deformation. However, the bearing and shear failure show a large deformation before a total failure of the connection.

(b) For connections that satisfy the minimum requirement of ASCE LRFD Pre-standard, tensile failure occurred in the three and four-row bolted connections with steel and GFRP

cover plates, while end shear failure occurred in the main and cover plates of the two-row bolted connection with the GFRP cover plate having a half of the main plate thickness. Therefore, the connection geometry which satisfies the minimum requirement of LRFD Pre-standard is not sufficient geometry to obtain desirable bearing failure mode for a connection of woven fabric GFRP.

(c) A coefficient of variation of the ultimate strength found to be within 5%, while that of the damage initiation strength was very large.

(d) The damage initiation strength was predicted better by ASCE LRFD Pre-standard than CNR-DT 205/2007. However, in many cases, the difference between the damage initiation strength and the strength predicted by design codes is not small.

(e) The effect of cover plate stiffness on the ultimate strength was found to be not significant, although the load distribution among bolt rows are significantly affected by the cover plate stiffness as discussed in Chapters 2 and 3, and specified by the design guidelines (ASCE, 2010; National Research Council, 2007). The connection with the GFRP cover plate having a half of the main plate thickness could carry lower strengths by about 6% for two-row bolted connection and by about 8% for three-row bolted connection than the connections with the steel cover plate and GFRP cover plates with a larger thickness for the bearing failure case.

(f) The effect of width to bolt diameter ratio, *w/d*, on the ultimate strength of the connection is significant. The strength is linearly increased with the *w/d* ratio for the case of net-tension failure. The net-tension failure switches to the bearing failure by changing the *w/d* ratio from 3 to 6 for the two-row bolted connection, and from 5 to 9 for three-row bolted connection.

(g) The effect of pitch distance to bolt diameter ratio, *p/d*, on the ultimate strength of the connection is also significant. The strength is increased with the *p/d* ratio for the case of shear failure. The shear failure switches to the bearing failure by changing the *p/d* ratio

from 3 to 5.

(h) The effect of end distance to bolt diameter ratio, *e/d*, on the ultimate strength of the connection is also significant. The strength is linearly increased with the *e/d* ratio for the case of shear failure. For three-row bolted connection with a *p/d* of 5.0, the ultimate strength has increased by about 9% to increase the *e/d* ratio by 1.0.

(i) The effect of the number of bolt rows on the net-tension and shear failure strengths was found to be not significant. However, the ultimate strength of bearing failure is significantly affected by the number of bolt rows, and the bearing strength increases by almost the same amount as the bearing strength of a single bolted connection when one bolt row was added in a connection.

7.1.5 Development of Design Methodology

Based on the experimental results, a design procedure was proposed to predict the ultimate strength and failure modes of bolted connections in FRP composite, where bolts are assumed to be finger tighten. The following conclusions can be made on the design of bolted connection:

(a) The proposed design equations for the strength of a connection are very simple, and one can easily calculate a connection strength. It was showed the proposed equations can predict the strength and failure mode of the tested connections with high accuracy where the difference between the measured and the predicted strength was less than 10%.

7.2 Recommendations for Future Study

To develop design guidelines of bearing-type multi-row bolted connections of FRP members, A further investigation may be required. The following topics are recommended for future study based on the results of this study.

(a) The parametric study should be extended to include more connections that fall

within the transition zones of various failure modes to study the behavior of combined failure.

(b) The experimental program should be conducted for connections with different types of materials such as GFRP various stacking sequences and pultruded GFRP.

(c) The experimental program may be extended to include different thicknesses of the main plate, different diameter of bolt, and number of bolts per row with different geometric parameters.

(d) Combined bolted and bonded connections may be investigated to study the general behavior as well as the load distribution between the bolts and the adhesive.

(e) Connections with FRP bolts may be investigated to understand the behavior FRP bolts in a connection.

(f) The numerical study may be extended to include the third direction effect in nonlinear finite element model.

REFERENCES

Abd-El-Naby, S. F. M., and Hollaway, L. (1993). The experimental behaviour of bolted joints in pultruded glass/polyester material. Part 1: Single-bolt joints. *Composite, 24*, 531-538.

American Society of Civil Engineers (ASCE). (2010). *Pre-Standard for Load and Resistance Factor Design of Pultruded Fiber Reinforced Polymer Structures*.

BSI (2006) BS EN 1993-1-4 : Eurocode 3: Design of steel structures - part 1.4: General rules and supplementary rules for stainless steels. CEN; 2006.

Camanho P. P., and Dávila, C. G. (2002). Mixed-mode decohesion finite elements for the simulation of delamination in composite materials. *NASA/TM-2002-211737*, 1-37.

Camanho, P.P., and Matthews, F.L. (1999). A progressive damage model for mechanically fastened joints in composite laminates. *Journal of Composite Materials, 33*(24), 2248-2280.

Chang, F.K., and Lessard, L. B. (1991). Damage tolerance of laminated composites containing an open hole and subject to compressive loadings: part I – analysis. *Journal of Composite Materials, 25*(1), 2-43.

Civil Engineering Research Foundation. (1994). *Materials for Tomorrow Infrastructures.* CERF Reports 94-5011, Washington D. C.

Clarke, J. L. (Eds.). (1996). *Structural Design of Polymer Composites, EUROCOMP Design Code and Handbook.* London, UK.

Cooper, C., and Turvey, G. J. (1995). Effects of joint geometry and bolt torque on the structural performance of single bolt tension joints in pultruded GRP sheet material. *Composite Structures, 32*, (1-4), 217-226.

Dano, M. L., Gendron, G., and Picard, A. (2000). Stress and failure analysis of mechanically fastened joints in composite laminates. *Composite Structures, 50*(3), 287-296.

Dassault Systèms. (2011). *Abaqus 6.11 documentation*.

DiNicola, A. J., and Fantle, S. L. (1993). Bearing strength behaviour of clearance fit fastener holes in toughened graphite/epoxy laminates. *In: Camponeshi Jr. ET (Ed.), Composite Materials: Testing and Design (Eleventh Volume), ASTM STP 1206. American Society for Testing and Materials, Philadelphia,* . 220-237.

Duvaut, G., and Lions, J.L. (1976). *Inequalities in mechanics and physics*. Springer, Berlin.

Feo, L., Marra, G., and Mosallam, A. S. (2012). Stress analysis of multi-bolted joints for FRP pultruded composite structures. *Composite Structures, 94*(12), 3769-3780.

Godwin, E. W., and Matthews, F. L. (1980). A review of the strength of joints in fibre-reinforced plastics. Part 1. Mechanically fastened joints. *Composites, 11*(3), 155-160.

Hart-Smith, L. J. (1980). Mechanically-fastened joints for advanced composites phenomenological considerations and simple analyses. *Proc. 4th Conf. on Fibrous Compos. in Struct. Des., Plenum Publishing Corp.*, New York, N.V.

Hart-Smith, L. J. (1980). Mechanically-fastened joints for advanced composites - phenomenological considerations and simple analyses. *Proceedings of the Fourth Conference on Fibrous Composites in Structural Design*, San Diego, California, New York, 543-574.

Hashin, Z. (1980). Failure criteria for unidirectional fiber composites. *Journal of Applied Mechanics, 47*(2), 329-334.

Hassan, N. K. (1995). *Multi-bolted connections for fiber reinforced plastic structural members*, PhD thesis, Ain-Shams Univ., Cairo, Egypt.

Hassan, N. K., Mohamedien, M. A., and Rizkalla, S. H. (1995). Finite element analysis of bolted connections for PFRP composites. *Composites Part B: Engineering, 27*(3-4), 339-349.

Hill, R. (1948) A theory of the yielding and plastic flow of anisotropic Metals. *Proceedings of*

the Royal Society of London 1948, 193(1033), 281-297.

Hyer, M. W., Hung, C. L., and Cooper, D. E. (1987). Effects of pin elasticity, clearance and friction on the stresses in a pin-loaded orthotropic plate. *Journal of Composite Materials*, 21(3), 190-206.

Johnson, M., and Matthews, F. L.(1979). Determination of safety factors for use when designing bolted joints in GRP. *Composites, 10*(2), 73-76.

Karbhari, V. M., and Zhao, L. (2000). Use of composites for 21st century civil infrastructure. *Computer Methods in Applied Mechanics and Engineering* , *185*, 433-454.

Khashaba, U. A., Sallam, H. E. M., Al-Shorbagy, A. E., and Seif, M. A. (2006). Effect of washer size and tightening torque on the performance of bolted joints in composite structures. *Composite Structure, 73*(3), 310-317.

Khashaba, U. A., Sebaey, T. A., Mahmoud, F. F., Selmy, A. I., and Hamouda, R. M. (2013). Experimental and numerical analysis of pinned-joints composite laminates: Effects of stacking sequences. *Journal of Composite Materials, 47*(27), 3353-3366.

Kishore, A.N., Malhotra, S.K., and Prasad, N.S. (2009). Failure analysis of multi-pin joints in glass fibre/epoxy composite laminates. *Composite Structures, 91*, 266-277.

Kriz, R. D., and Stinchcomb, W. W. (1979). Elastic moduli of transversely isotropic graphite fibers and their composite. *Journal of Experimental Mechanics, 19*, 41-49.

Lapczyk, I., and Hurtado, J.A. (2007). Progressive damage modeling in fiber-reinforced materials. *Composites Part A: Applied Science and Manufacturing, 38*(11), 2333-2341.

Matzenmiller, A., Lubliner, J., and Taylor, R.L. (1995). A constitutive model for anisotropic damage in fiber-composites. *Mechanics of Materials, 20*, 125-152.

McCarthy, C. T., McCarthy, M. A., and Lawlor V. P. (2005). Progressive damage analysis of multi-bolt composite joints with variable bolt-hole clearances. *Composites Part B: Engineering*, 36(4), 290-305.

McCarthy, M. A., Lawlor, V. P., Stanley, W. F., and McCarthy, C. T. (2002). Bolt-hole

clearance effects and strength criteria in single-bolt, single-lap, composite bolted joints. *Composites Science and Technology*, 62(10-11), 1415-1431.

McKay, M. D., Conover, W. J., and Beckman, R. J. (1979). A comparison of three methods for selecting values of input variables in the analysis of output from a computer code. *Technometrics*, 21(2), 239-245.

Mottram, J. T. (2005). Friction and load transfer in bolted joints of pultruded fibre reinforced polymer section. *Proc., 2nd Int. Conf. on FRP Composites in Civil Engineering*, Taylor and Francis, London, 845-850.

Mottram, J. T. (2010). Prediction of net-Tension strength for multirow bolted connections of pultruded material using the Hart-Smith semiempirical modeling approach. *Journal of Composites for Construction*, 14(1), 105-114.

Mottram, J. T., Lutz, C., and Dunscombe, G. C. (2004). Aspects on the behaviour of bolted joints for pultruded fibre reinforced polymer profiles. Proc. 2nd Inter. Conf. on Advanced Polymer Composites for Structural Applications in Construction (ACIC04). University of Surrey, UK, 20–22 April 2004. Cambridge:Woodhead Publishing Limited, 384-391.

Mottram, J. T., and Turvey G. J. (2003). Physical test data for the apptaisal of design procedures for bolted joints in pultruded RP structural shaps and systems. *Progress in Structural Engineering and Materials*, 5 4, 195-222.

Mottram, J. T., and Zafari, B. (2011). Pin-bearing strengths for bolted connections in fibre-reinforced polymer structures. *Proceedings of the Institution of Civil Engineers Structures and Buildings, 164* (SB5): 291-305.

National Research Council (CNR). (2007). *Guide for the Design and Construction of Structures Made of FRP Pultruded Elements*, CNR-DT 205/2007, Rome.

Olmedo, Á., and Santiuste, C. (2012). On the prediction of bolted single-lap composite joints. *Composite Structures, 94*(6), 2110-2117.

Rosner, C. N. (1992). *Single-bolted connections for orthotropic fiber reinforced composite*

structural members, MS thesis, Univ. of Manitoba, Winnipeg, Manitoba, Canada.

Stockdate, J. H., and Matthews, F. L. (1976). The effect of clamping pressure on bolt bearing loads in glass fibre reinforced plastics. *Composite, 9,* 34-38.

Thoppul, S. D., Finegan, J., and Gibson, R. F. (2009). Mechanics of mechanically fastened joints in polymer-matrix composite structures - A review. *Composites Science and Technology, 69,* 301-329.

Tsai, S. W., and Wu, E. M. (1971). A general theory of strength for anisotropic materials. *Journal of Composite Materials1971, 5*(1), 58-80.

Van Der Meer, F.P., and Sluys, L.J. (2009). Continuum models for the analysis of progressive failure in composite laminates. *Journal of Composite Materials, 42*(20), 2131-2156.

Vasarhelyi, D. D., and Chang, W. N. (1965). Misalignment in bolted joints. *Journal of the Structural Division, Proceedings of the American Society of Civil Engineers, 91(ST4)*: 1-15.

Zhang, J., Liu, F., Zhao, L., Chen, Y., and Fei, B. (2014). A progressive damage analysis based characteristic length method for multi-bolt composite joints. *Composite Structures, 108*, 915-923.

APPENDIX A FAILURE MODE OF CONNECTIONS IN THE EXPERIMENT

A.1 Single Bolted Connections

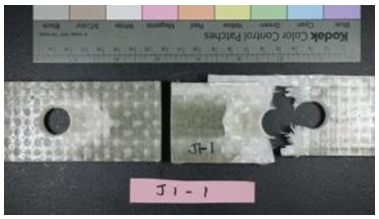

(a) Connection J1

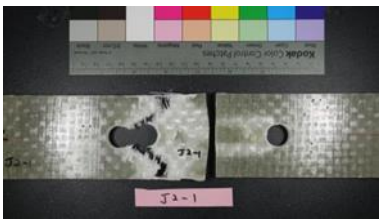

(b) Connection J2

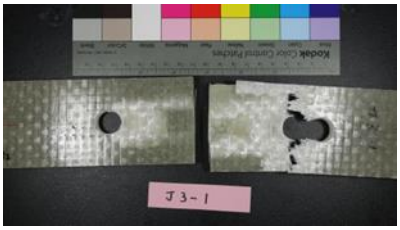

(c) Connection J3

(d) Connection J4

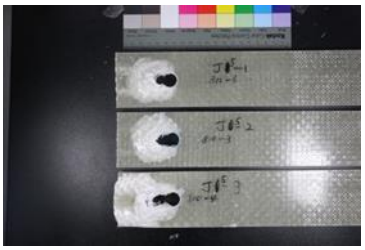

(e) Connection J5

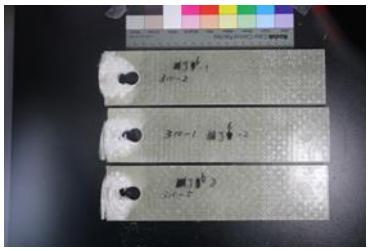

(f) Connection J6

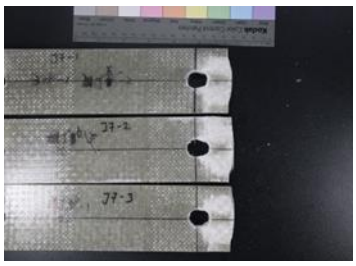

(g) Connection J7

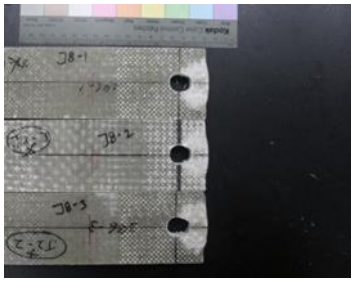

(h) Connection J8

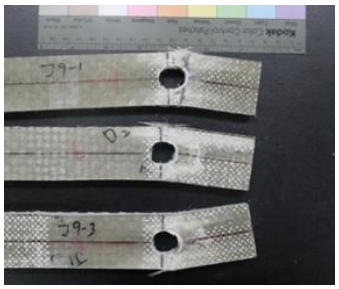

(i) Connection J9

(j) Connection J10

(k) Connection J11

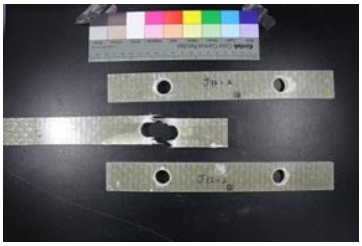

(l) Connection J12

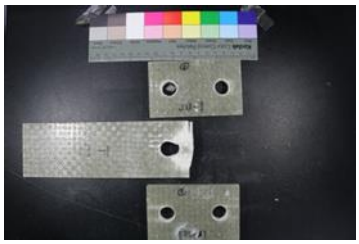

(m)Connection J13

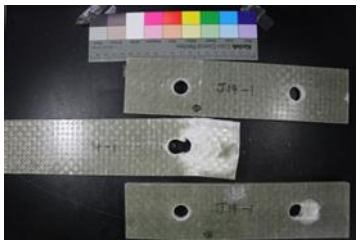

(n) Connection J14

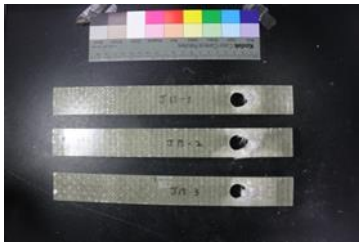

(o) Connection J15

Figure A.1: Failure mode of single bolted connection

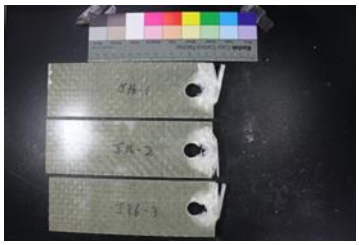

(p) Connection J16

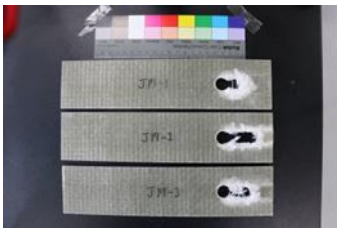

(q) Connection J17

(r) Connection J18

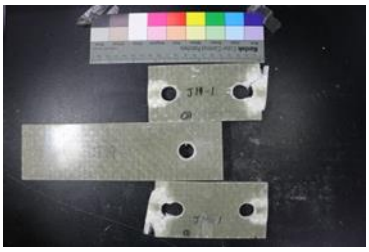

(s) Connection J19

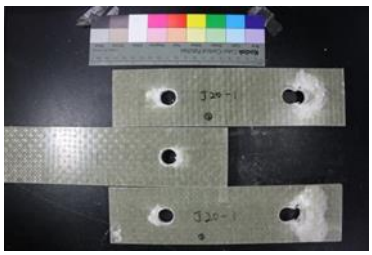

(t) Connection J20

Figure A.1: Failure mode of single bolted connection (cont'd)

A.2 Multi-Row Bolted Connections

A.2.1 Net-Tension Failure Geometric Parameter Specimens

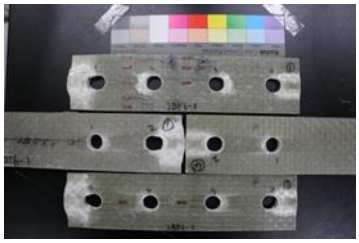

(a) Connection 2BF6

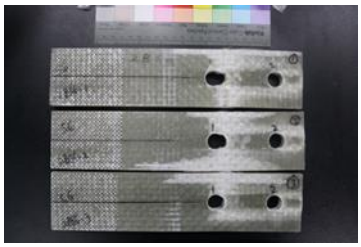

(b) Connection 2BS6

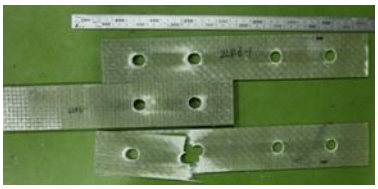

(c) Connection 2LF6

(d) Connection 2LS6

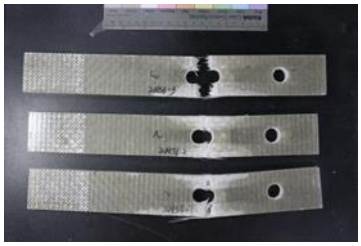

(e) Connection 2NS6

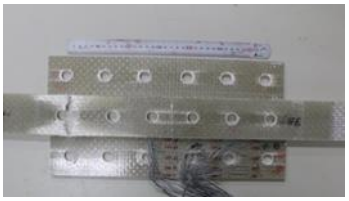

(f) Connection 3BF6

Figure A.2: Failure mode of multi-row bolted connection with net-tension failure geometric parameters

(g) Connection 3BS6

(h) Connection 3JF6

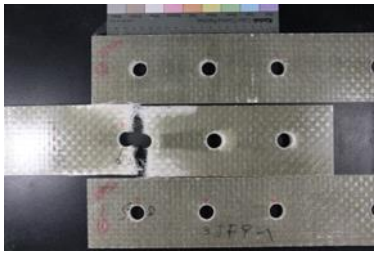

(i) Connection 3JF9

(j) Connection 3JS6

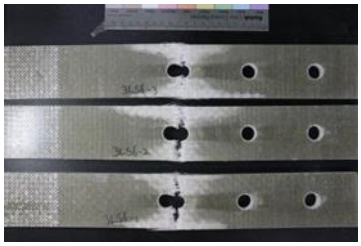

(k) Connection 3LS6

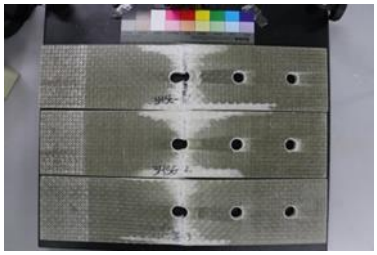

(l) Connection 3MS6

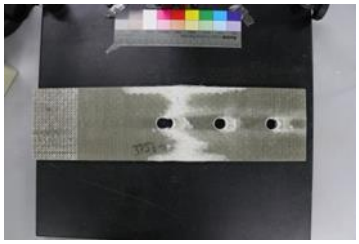

(m)Connection 3PS6

(n) Connection 4BF6

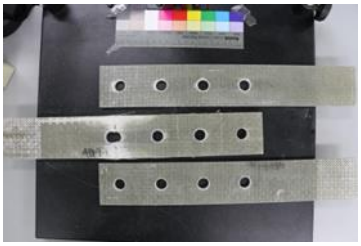

(o) Connection 4BF9

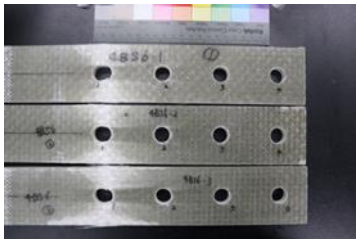

(p) Connection 4BS6

(q) Connection 4MF6

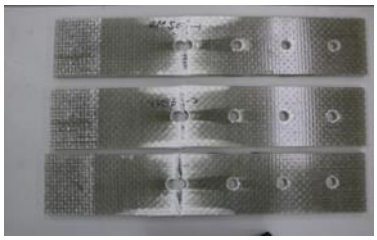

(r) Connection 4MS6

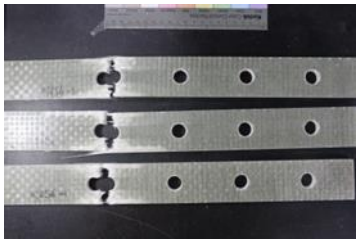

(s) Connection 4NS6

Figure A.2: Failure mode of multi-row bolted connection with net-tension failure geometric parameters (cont'd)

A.2.2 Shear Failure Geometric Parameter Specimens

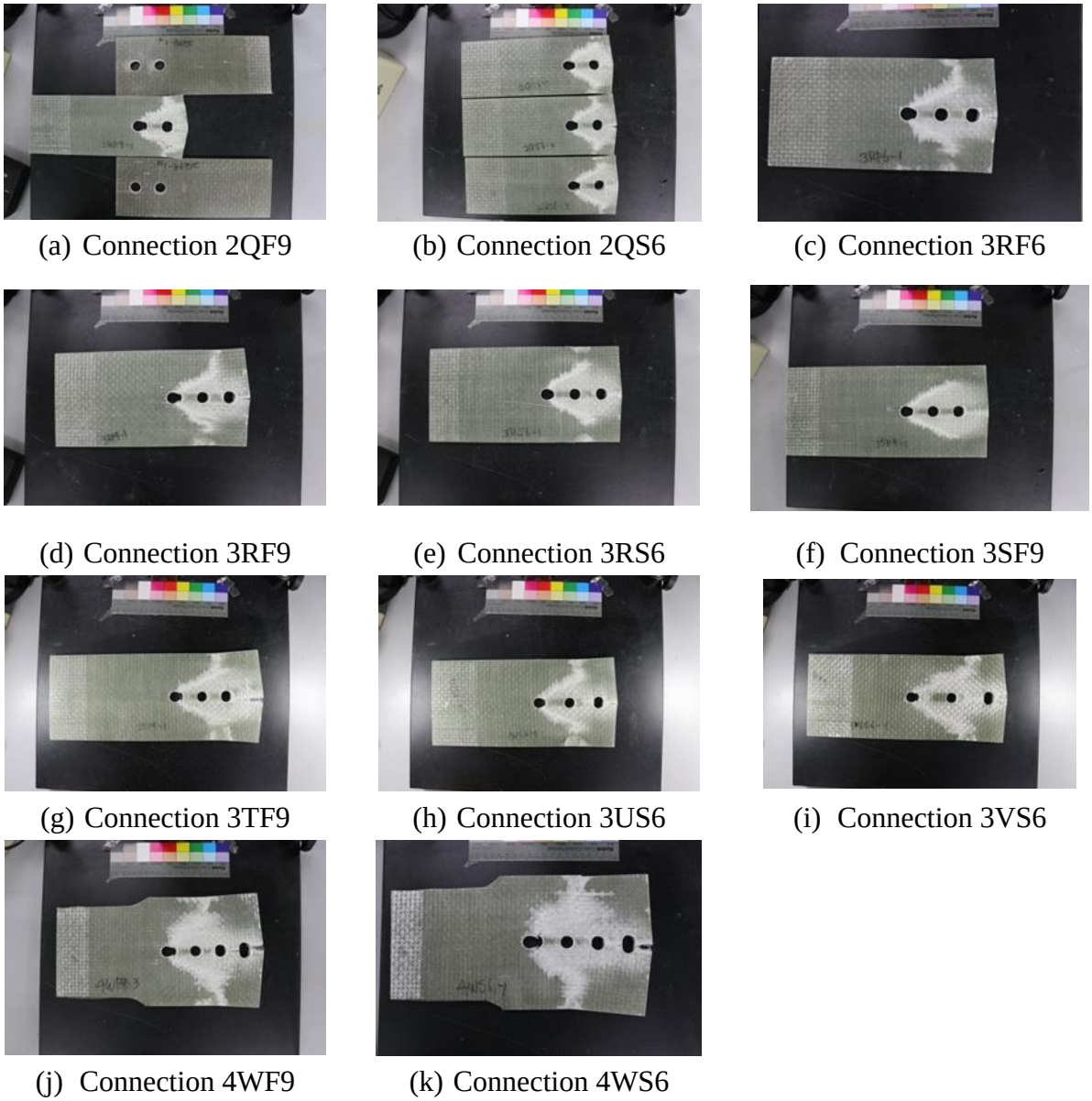

(a) Connection 2QF9 (b) Connection 2QS6 (c) Connection 3RF6

(d) Connection 3RF9 (e) Connection 3RS6 (f) Connection 3SF9

(g) Connection 3TF9 (h) Connection 3US6 (i) Connection 3VS6

(j) Connection 4WF9 (k) Connection 4WS6

Figure A.3: Failure mode of multi-row bolted connection with shear failure geometric parameters

A.2.3 Bearing Failure Geometric Parameter Specimens

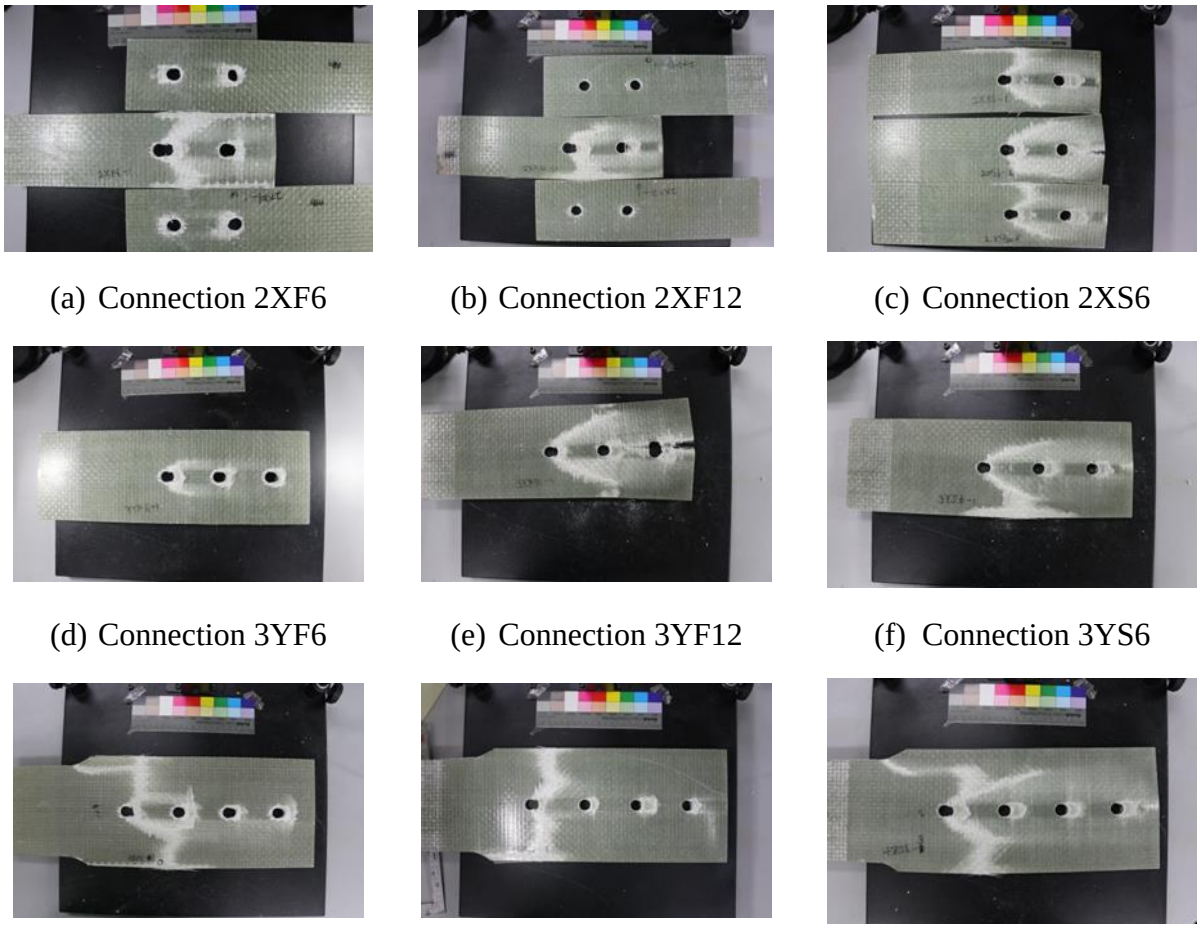

(a) Connection 2XF6 (b) Connection 2XF12 (c) Connection 2XS6

(d) Connection 3YF6 (e) Connection 3YF12 (f) Connection 3YS6

(g) Connection 4ZF6 (h) Connection 4ZF12 (i) Connection 4ZS6

Figure A.4: Failure mode of multi-row bolted connection with bearing failure geometric parameters

A.2.4 End Shear Failure Geometric Parameter Specimens

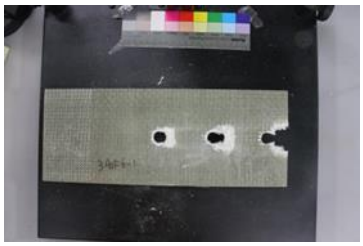

(a) Connection 3AaF6

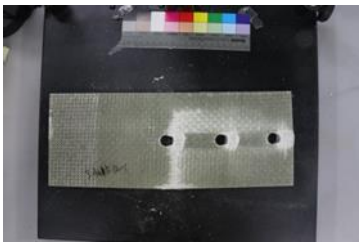

(b) Connection 3AaF12

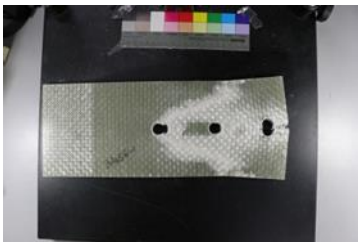

(c) Connection 3AaS6

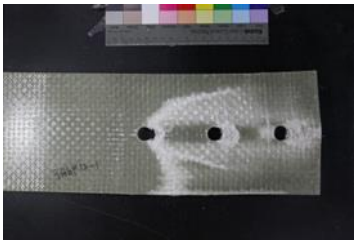

(d) Connection 3AbF12

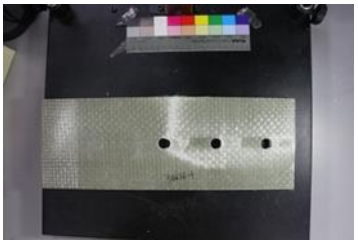

(e) Connection 3AdS6

Figure A.5: Failure mode of multi-row bolted connection with end shear failure geometric parameters

APPENDIX B LOAD-DISPLACEMENT RELATIONSHIP FROM THE EXPERIMENT

B.1 Single Bolted Connections

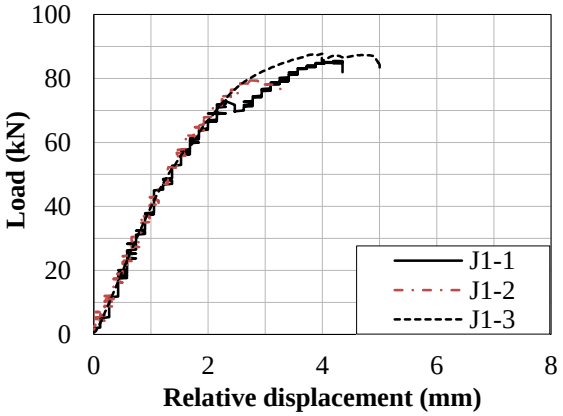

(a) Connection J1

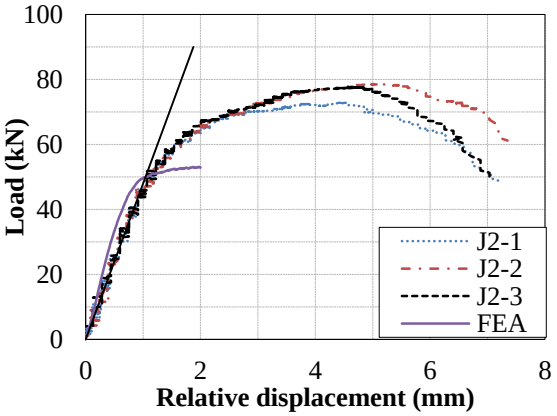

(b) Connection J2

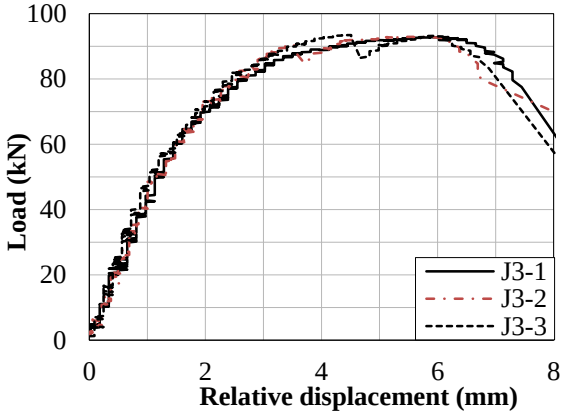

(c) Connection J3

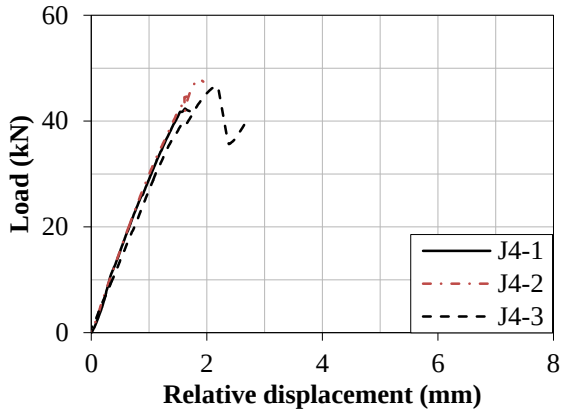

(d) Connection J4

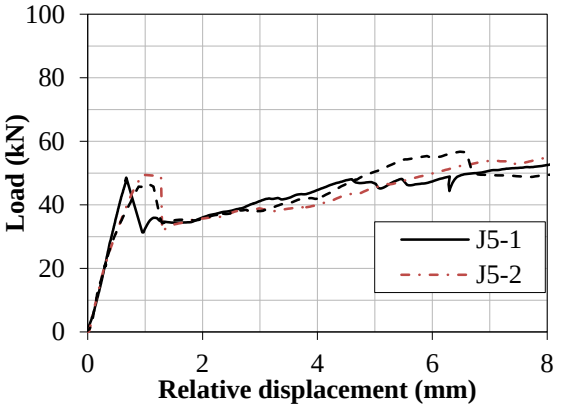

(e) Connection J5

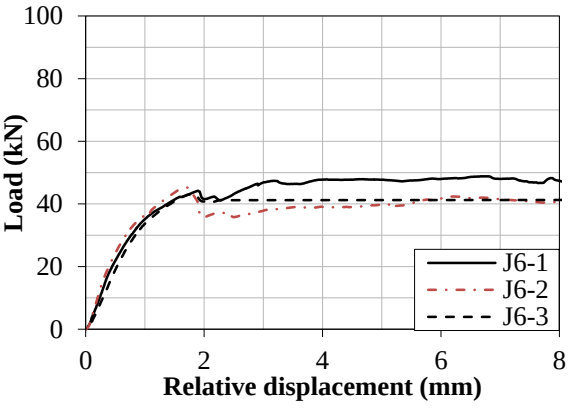

(f) Connection J6

Figure B.1: Load-displacement relationship of single bolted connection

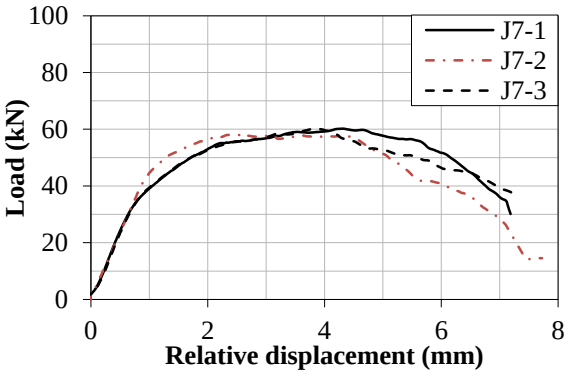

(g) Connection J7

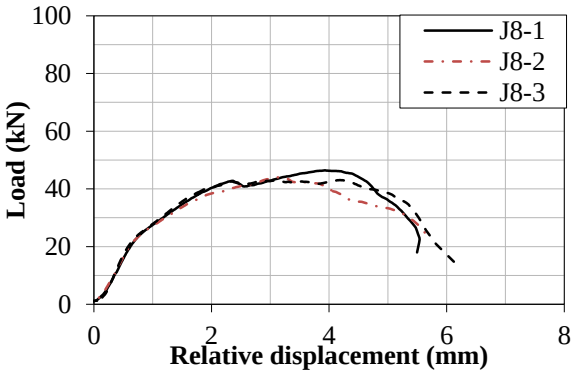

(h) Connection J8

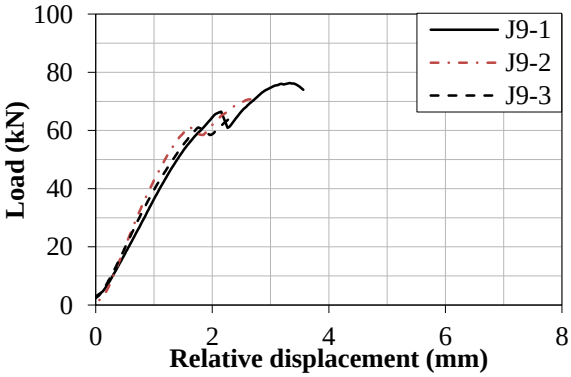

(i) Connection J9

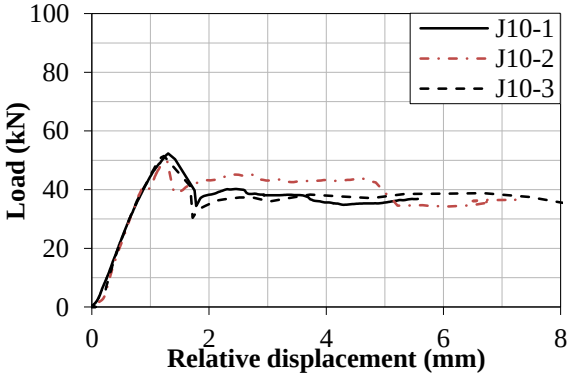

(j) Connection J10

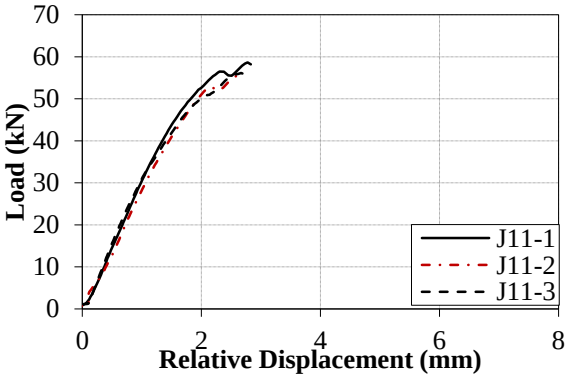

(k) Connection J11

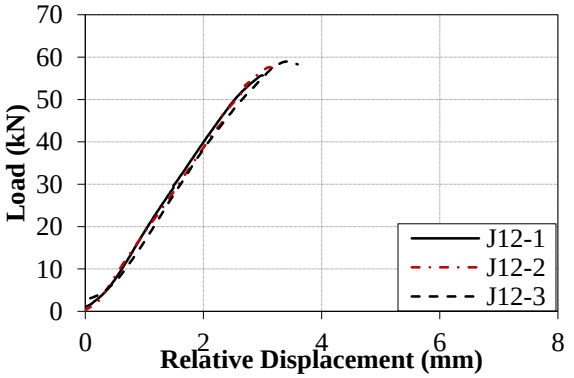

(l) Connection J12

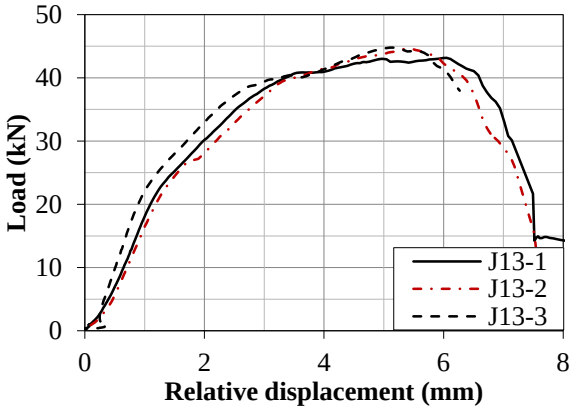

(m)Connection J13

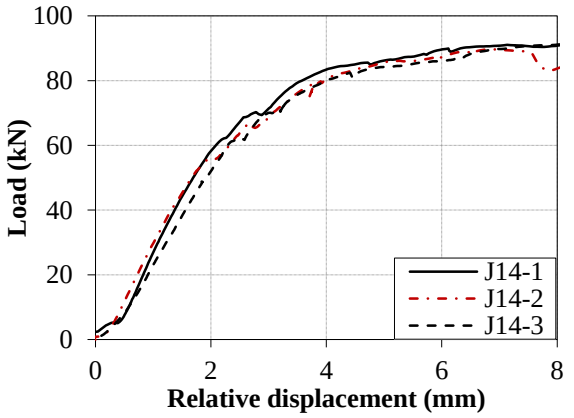

(n) Connection J14

Figure B.1: Load-displacement relationship of single bolted connection (cont'd)

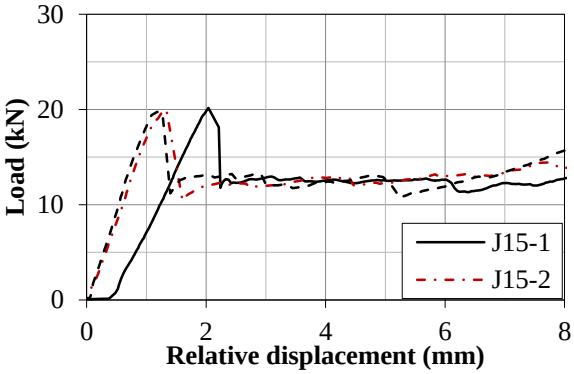

(o) Connection J15

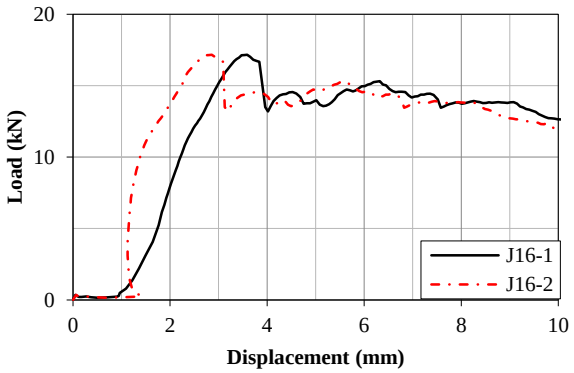

(p) Connection J16

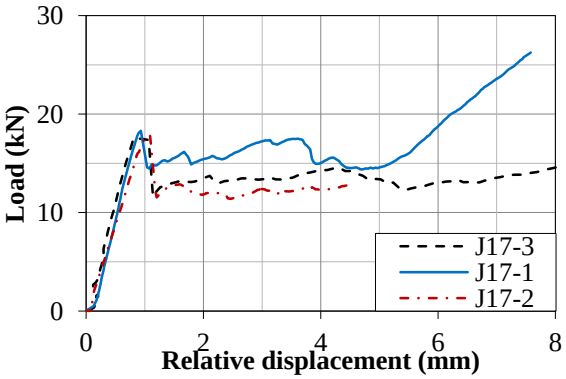

(q) Connection J15

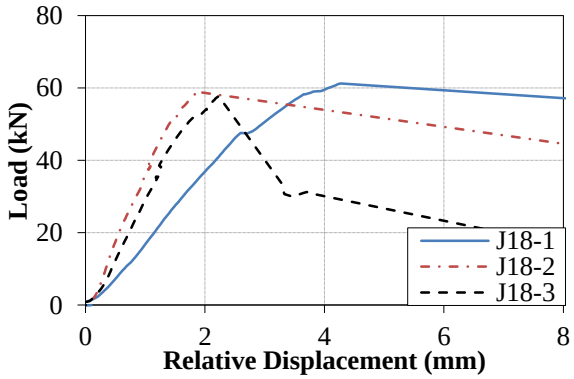

(r) Connection J16

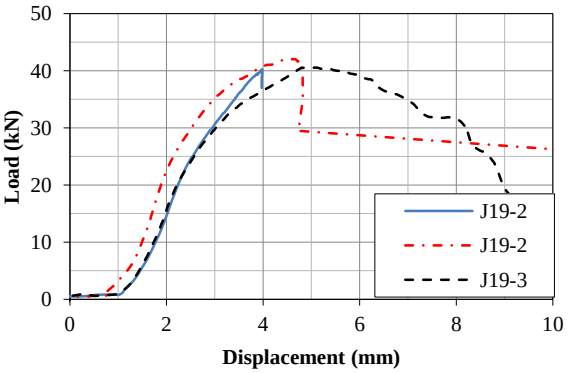

(s) Connection J15

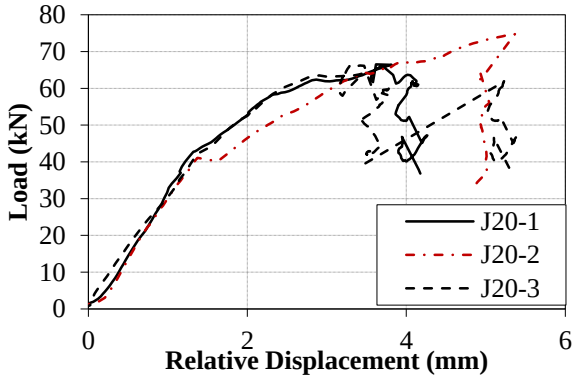

(t) Connection J16

Figure B.1: Load-displacement relationship of single bolted connection (cont'd)

B.2 Two-Row Bolted Connections

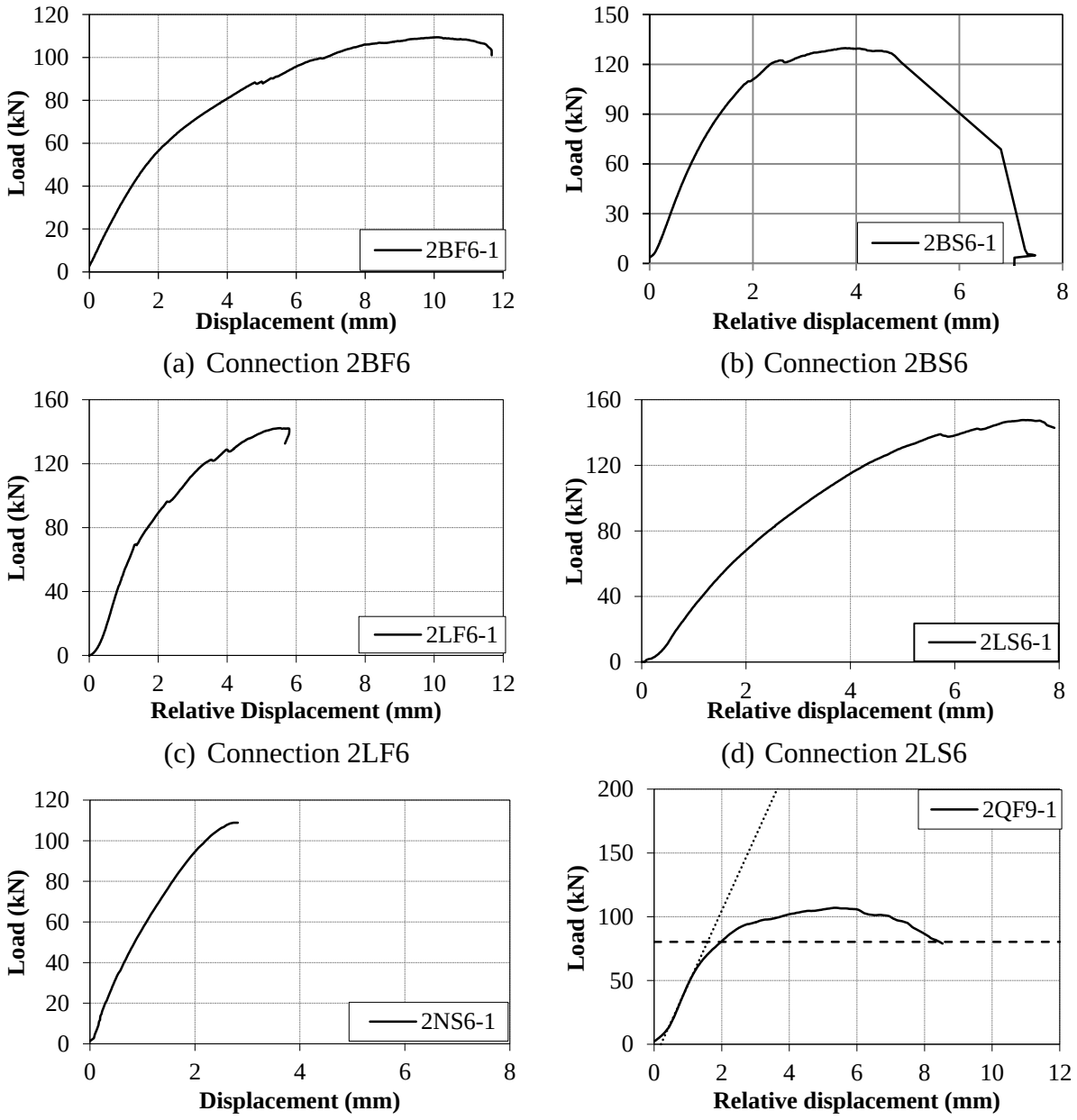

(a) Connection 2BF6 (b) Connection 2BS6

(c) Connection 2LF6 (d) Connection 2LS6

(e) Connection 2NS6 (f) Connection 2QF9

Figure B.2: Load-displacement relationship of two-row bolted connection

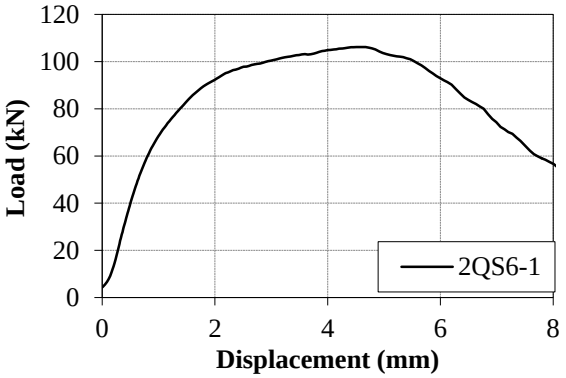

(g) Connection 2QS6

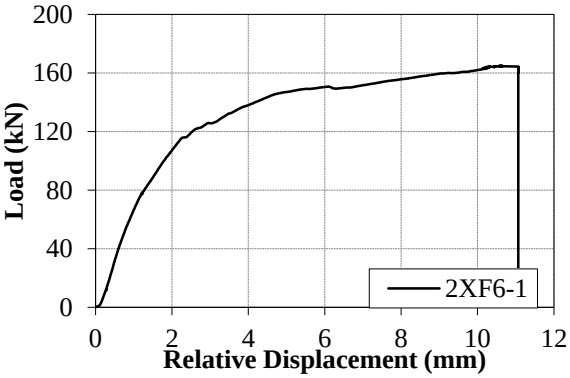

(h) Connection 2QS6

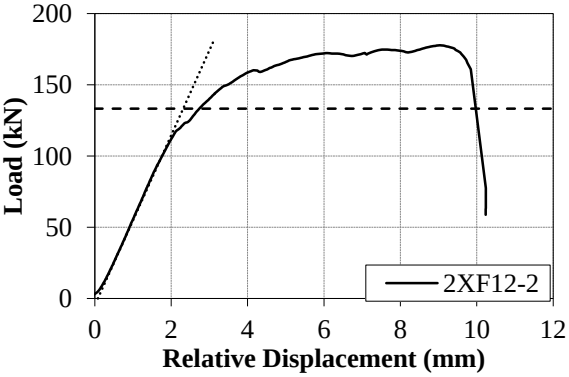

(i) Connection 2XF12

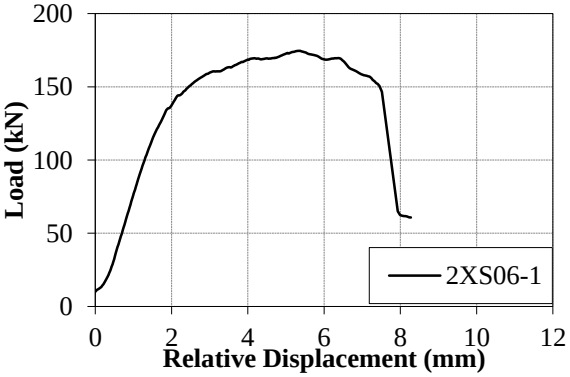

(j) Connection 2XS6

Figure B.2: Load-displacement relationship of two-row bolted connection (cont'd)

B.3 Three-Row Bolted Connections

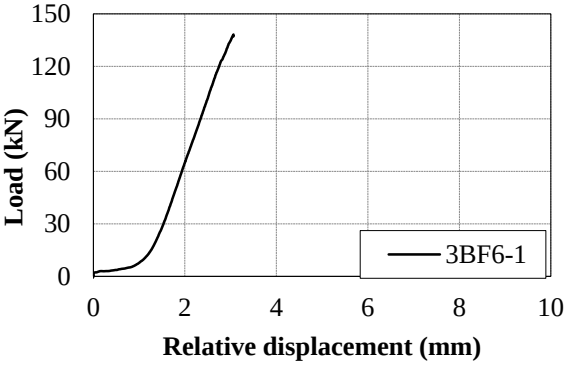

(a) Connection 3BF6

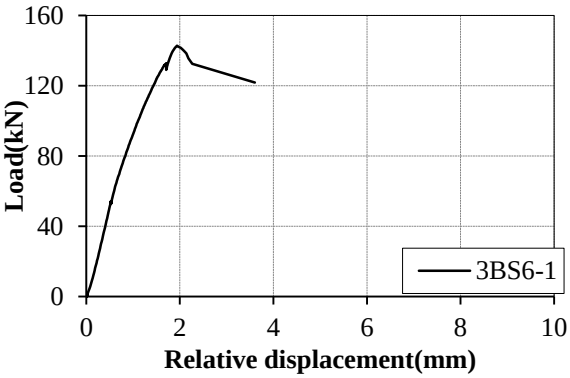

(b) Connection 3BS6

Figure B.3: Load-displacement relationship of three-row bolted connection

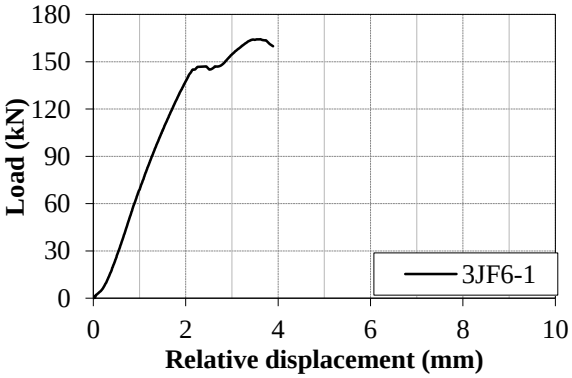

(c) Connection 3JF6

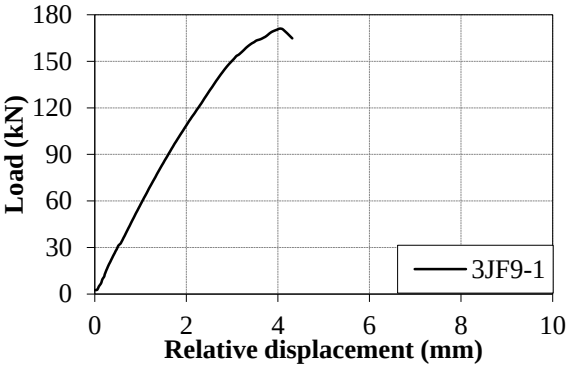

(d) Connection 3JF9

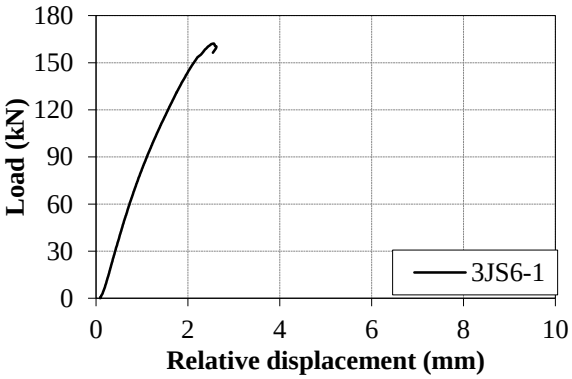

(e) Connection 3JS6

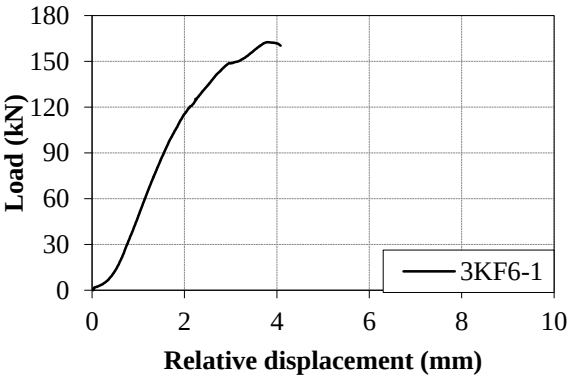

(f) Connection 3KF6

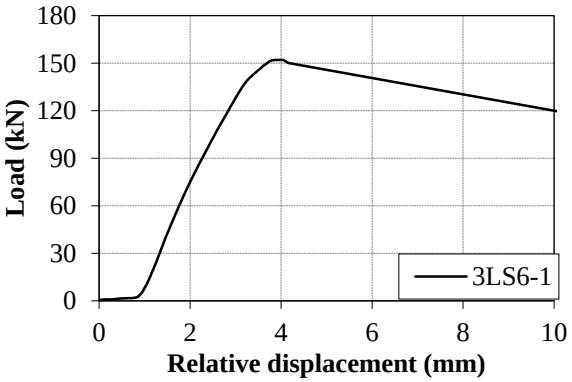

(g) Connection 3LS6

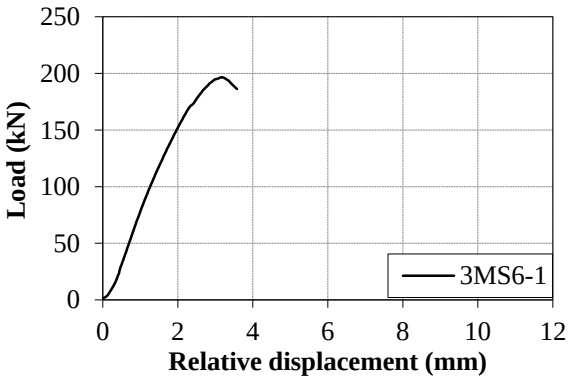

(h) Connection 3MS6

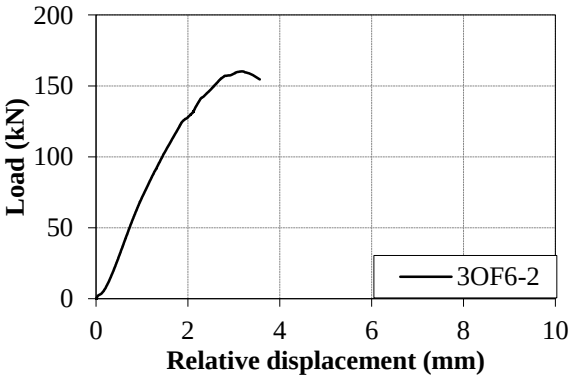

(i) Connection 3OF6

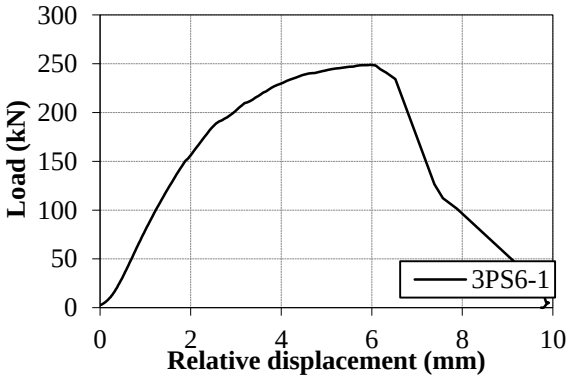

(j) Connection 3PS6

Figure B.3: Load-displacement relationship of three-row bolted connection (cont'd)

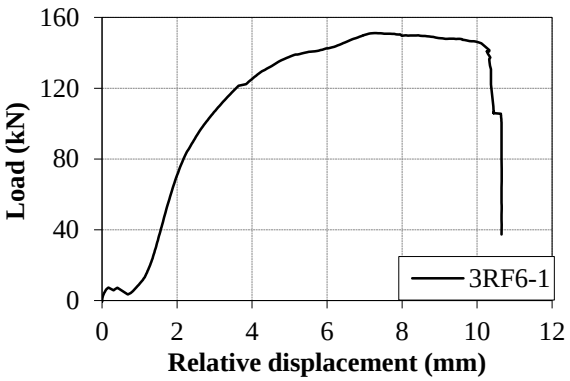

(k) Connection 3RF6

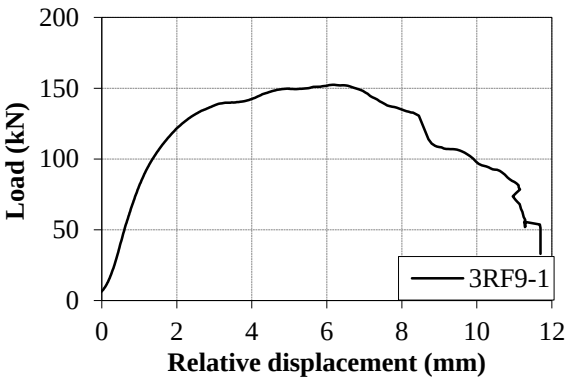

(l) Connection 3RF9

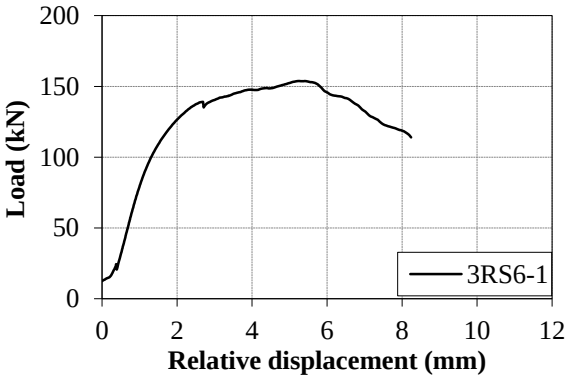

(m)Connection 3RS6

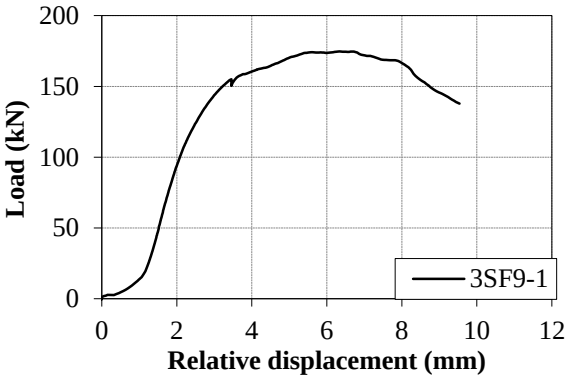

(n) Connection 3SF9

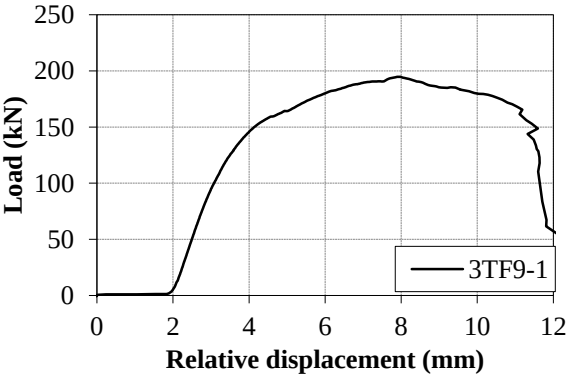

(o) Connection 3TF9

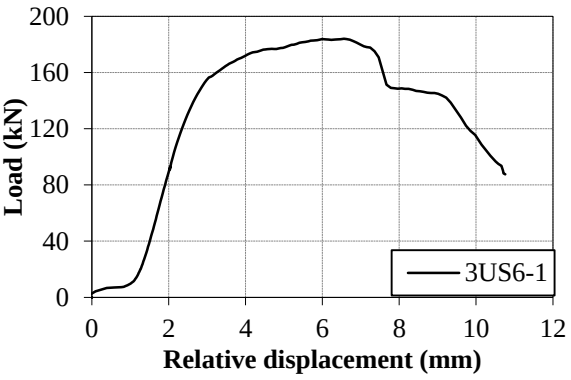

(p) Connection 3US6

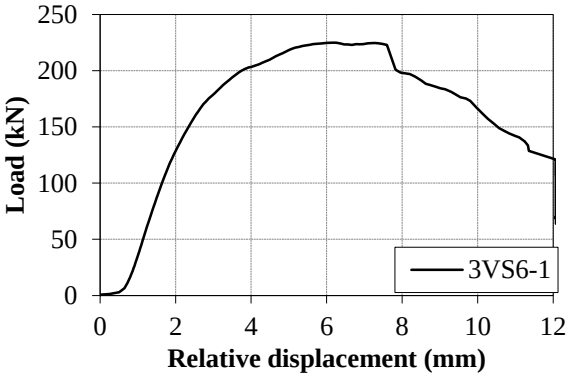

(q) Connection 3VS6

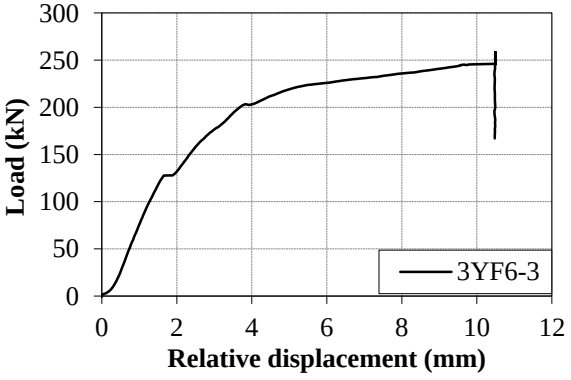

(r) Connection 3YF6

Figure B.3: Load-displacement relationship of three-row bolted connection (cont'd)

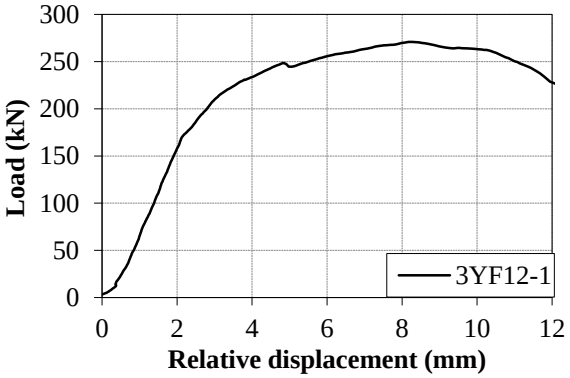

(s) Connection 3YF12

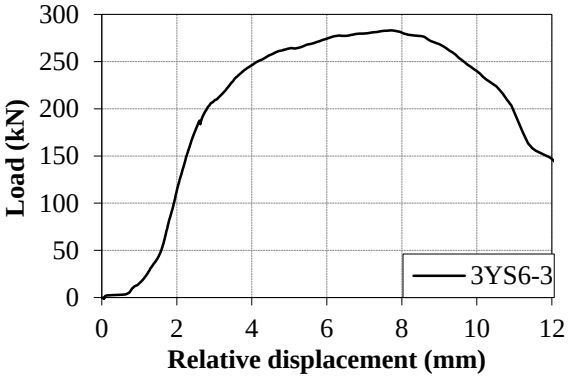

(t) Connection 3YS6

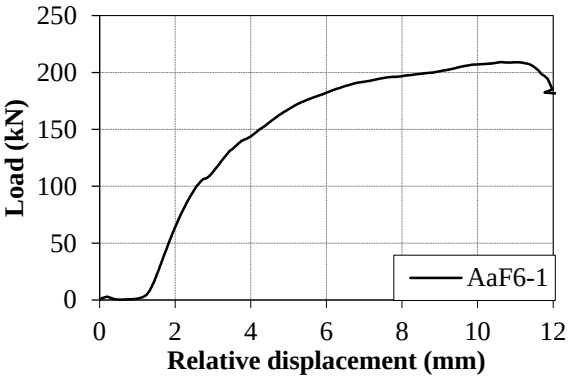

(u) Connection 3AaF6

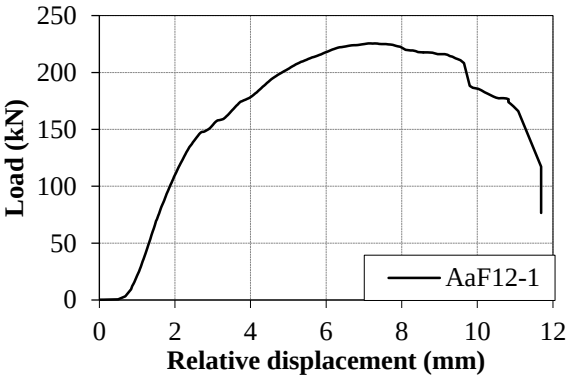

(v) Connection 3AaF12

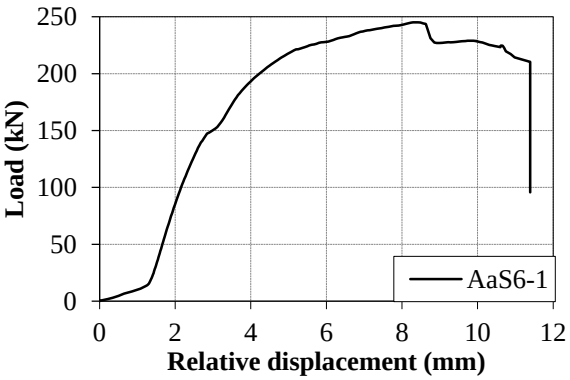

(w) Connection 3AaS6

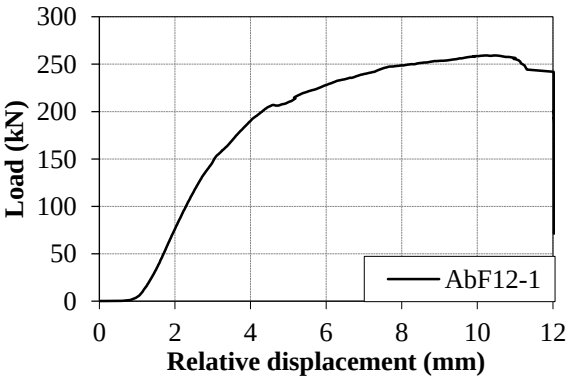

(x) Connection 3AbF12

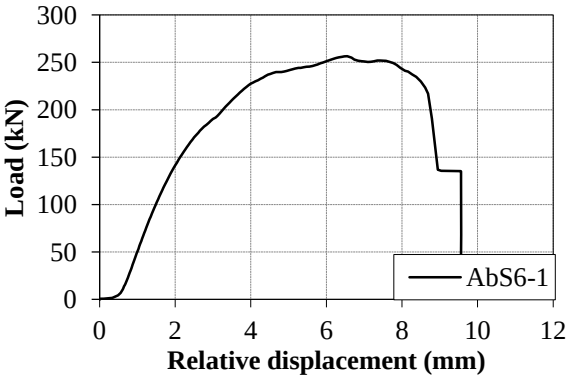

(y) Connection 3AbS6

Figure B.3: Load-displacement relationship of three-row bolted connection (cont'd)

B.4 Four-Row Bolted Connections

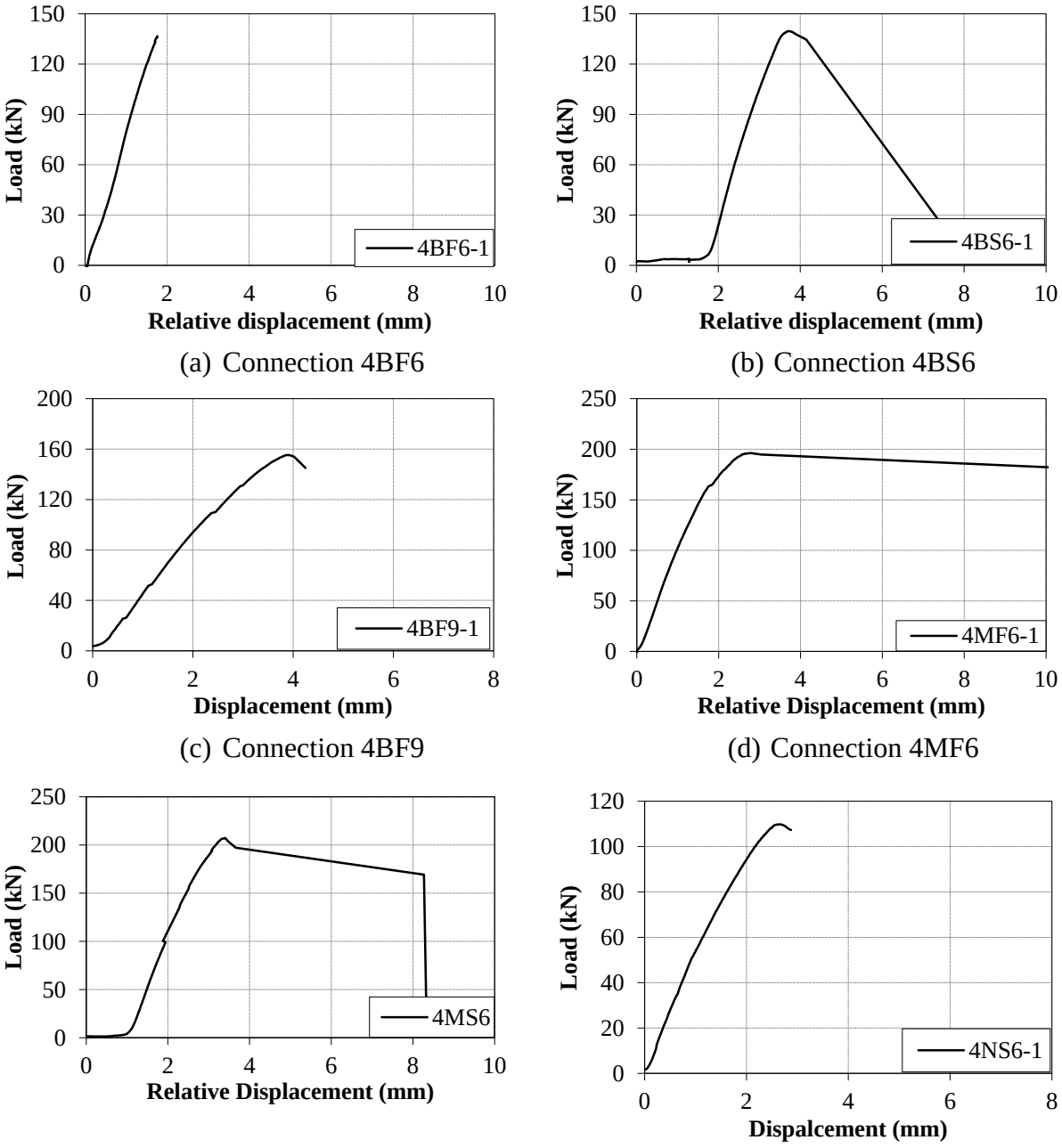

(a) Connection 4BF6 (b) Connection 4BS6

(c) Connection 4BF9 (d) Connection 4MF6

(e) Connection 4MS6 (f) Connection 4NS6

Figure B.4: Load-displacement relationship of four-row bolted connection